



LUMPED-PARAMETER MODELLING OF CARDIOVASCULAR SYSTEM
DYNAMICS UNDER DIFFERENT HEALTHY AND DISEASED CONDITIONS

by

Yubing Shi

A thesis submitted in partial fulfilment of
the requirements for the degree of
PhD by Publication

Academic Supervisor: Professor Rodney Hose

Department of Cardiovascular Science,
Faculty of Medicine, Dentistry and Health,
University of Sheffield

July, 2013

Abstract

Cardiovascular disease is the most common cause of death in the modern society, and research into the diagnosis and treatment of cardiovascular diseases is an urgent task. Lumped-parameter mathematical modelling as an efficient and effective research technique has been extensively applied in the cardiovascular dynamics research, and has achieved enormous success in assisting the cardiovascular physiology study. This thesis reports a coherent work of lumped-parameter cardiovascular modelling based on some selected works that the author has conducted and published in the past several years. After a critical and comprehensive review of the concurrent lumped-parameter modelling technique, an improved lumped-parameter model that effectively describes the important cardiovascular features of heart valve dynamics and atrial-ventricular septum motion is presented. The model is then adapted to study several application cases of typical heart failure condition with ventricular assist device support, and extension of the lumped-parameter modelling for the optimisation of a pulsatile bioreactor in cardiovascular tissue engineering study. Some on-going works and future directions are also introduced. The reported modelling studies are useful for the cardiovascular physiology research and design optimisation of cardiovascular prosthetic organs.

Acknowledgments

I would like to express my sincere gratitude to my advisor Prof. Rodney Hose, for the continuous support to me during my PhD candidature and my postdoctoral research, for his patience, motivation, enthusiasm, and immense knowledge. I could not have imagined having a better advisor for my PhD study.

My sincere thanks also go to my personal tutor, Dr. Martina Daly, for the support and help to me in the procedure from PhD application, registration, thesis writing-up and revision, to final submission.

I want to thank Dr Sheila Francis, the Department of Cardiovascular Science, and the University of Sheffield, who gave me the opportunity and support to work on this PhD degree.

I also want to thank Prof. Patricia Lawford, Prof David Barber, Dr Andrew Narracott, and Dr John Fenner, for the help, encouragement, and support to me during my working in the Medical Physics group.

I would like to thank my former Postdoctoral supervisor, Prof. Theodosios Alexander for the support during my working on OD modeling.

I am also grateful to my colleagues in the Medical Physics group, Department of Cardiovascular Science, for the helps to me and the enjoyable time we have had in the last four years.

Last but not the least, I would like to thank my parents for supporting me spiritually throughout my life, and my wife Hongyi for her understanding and support during my working on the thesis.

Table of Contents

Chapter 1 Commentary	1
1.1 Cardiovascular physiology	2
1.2 Cardiovascular research	3
1.3 Modelling in cardiovascular research	5
1.4 0D cardiovascular modelling	9
1.4.1 Models of the systemic vasculature	10
1.4.2 Models of the heart	18
1.4.3 Models of the heart valves	20
1.4.4 Nonlinear effects and external interactions	21
1.4.5 Integrated cardiovascular system models	28
1.4.6 Commentary on the 0D model developed in this thesis	29
1.4.7 Applications of 0D models	32
1.4.8 Commentary on 0D modelling applications reported in this thesis	34
1.4.9 Multi-scale modelling	44
1.5 Structure of the thesis and authors' contributions to the papers included in each chapter	45
Chapter 2 Development of a Lumped Parameter Model for the Human Cardiovascular System Including Heart Valve Dynamics and Atrio-ventricular Interaction	49
2.1 Introduction	49
2.2 Method	53
2.2.1 MRI Measurement of Cardiac Dynamics	53
2.2.2 Conceptual Illustration of General Cardiac Response	56
2.2.3 Mathematical Model	59
2.2.4 System Parameters	67
2.3 Results	71

2.3.1	Response of the Simplified Model.....	72
2.3.2	Response with Combined Effect of Atrio-ventricular Interaction and Atrial Contraction.....	75
2.3.3	Response with Heart Valve Dynamics Alone	84
2.3.4	Response with All Features.....	90
2.4	Discussion.....	96
2.5	Conclusions	101
Chapter 3 Computational Modelling and Evaluation of Cardiovascular Response under Pulsatile Impeller Pump Support		
		103
3.1	Introduction	103
3.2	Materials and Methods.....	108
3.2.1	Numerical model of the System	108
3.2.2	Strategy for the optimisation of pump motion	109
3.2.3	Evaluation of cardiovascular performance.....	110
3.2.4	System Parameters.....	114
3.2.5	Procedure of numerical study.....	114
3.3	Results	115
3.3.1	Cardiovascular Response in Healthy and Left Ventricular Failure Conditions and with Baseline Impeller Pump Support	117
3.3.2	Searching for VAD motion to produce satisfactory cardiovascular response including arterial pressure pulsation	121
3.4	Discussion.....	127
3.5	Conclusions	130
Chapter 4 Physiological Control of an In-series Connected Pulsatile VAD: Numerical Simulation Study.....		
		133
4.1	Introduction	133
4.2	Materials and Methods.....	137

4.2.1	Model of the Native Cardiovascular System	137
4.2.2	Model of Pulsatile VAD pumping action and motion	139
4.2.3	Physiological Controller Design.....	140
4.2.4	Test Case of VAD Control.....	143
4.2.5	System Parameters.....	144
4.2.6	Simulation Procedure.....	145
4.3	Results.....	146
4.3.1	Cardiovascular Response without VAD Control and Physiological Disturbance	147
4.3.2	Cardiovascular Response under VAD Control and Physiological Disturbance	153
4.4	Discussion	155
4.5	Conclusions	158
Chapter 5 Numerical Simulation of Global Hydro-dynamics in a Pulsatile Bioreactor for Cardiovascular Tissue Engineering.....		161
5.1	Introduction	161
5.2	Methods.....	163
5.2.1	Basic configuration of the pulsatile bioreactor	163
5.2.2	Numerical model of the pulsatile bioreactor	164
5.2.3	Boundary conditions	167
5.2.4	Parameter settings.....	168
5.3	Results and Discussion	171
5.4	Conclusion.....	174
Chapter 6 Conclusion and Future Works.....		175
6.1	Conclusions	175
6.2	Limitations of lumped-parameter modelling.....	176
6.3	On-going works	177

6.4 Future works..... 181

List of figures

<i>Number</i>	<i>Page</i>
Figure 1-1 Circulation system	2
Figure 1-2 Different scales of modelling	6
Figure 1-3 Mono-compartment models for the vessel network	12
Figure 1-4 A sample multi-compartment model	16
Figure 1-5 A sample complete circulatory system model.....	28
Figure 2-1 Short axis MRI slice in diastolic phase.....	55
Figure 2-2 SolidEdge images of the lower portions of ventricle geometries in diastole, reconstructed from MRI measurements.....	55
Figure 2-3 Volume change of left ventricle measured from MRI data	55
Figure 2-4 Illustration of the systemic loop response of the cardiovascular system during a typical healthy heart cycle	57
Figure 2-5 Schematic of the circulation system model.....	59
Figure 2-6 Elastance change in the left ventricle and left atrium during a typical heart cycles.....	60
Figure 2-7 Forces acting on the KG diaphragm in the vicinity of the mitral valve.....	63
Figure 2-8 Illustration of typical forces acting on a heart valve leaflet	65
Figure 2-9 Response with the simplified model.....	74
Figure 2-10 Response with modelling of the atrial contraction alone	77
Figure 2-11 Response with modelling of the KG diaphragm motion alone	79
Figure 2-12 Resultant motion of the KG diaphragm in the left heart when both KG diaphragm dynamics and atrial contraction are considered	79
Figure 2-13 Elastance change in the left heart when both KG diaphragm dynamics and atrial contraction are considered.....	79

Figure 2-14 Response with modelling both KG diaphragm motion and atrial contraction	81
Figure 2-15 Resultant change of heart valve leaflet angular position (opening) in the simplified model	85
Figure 2-16 Resultant change of heart valve leaflet angular position (opening) with valve dynamics modelling alone.....	86
Figure 2-17 Response with heart valve dynamics modelling alone	88
Figure 2-18 Comparison of KG diaphragm motion in left heart when all the features of atrial contraction, KG diaphragm motion and heart valve dynamics are considered with that under combined influence of KG diaphragm motion and atrial contraction	90
Figure 2-19 Comparison of changes of heart valve leaflet angular position (opening) when all the features of atrial contraction, KG diaphragm motion and heart valve dynamics are considered with those of heart valve dynamics modelling alone	91
Figure 2-20 Response when all the features of atrial contraction, KG diaphragm motion and heart valve dynamics are considered	93
Figure 2-21 Phase lag between left atrial and left ventricular pressures in end diastole	94
Figure 3-1 Illustration of cardiovascular system with impeller pump VAD.....	107
Figure 3-2 Conceptual drawing of pump characteristics for Berlin Heart INCOR® impeller pump.....	108
Figure 3-3 Legends for impeller pump speed change.....	109
Figure 3-4 System response of cardiovascular model in different simulation cases ...	117
Figure 3-5 Illustration of change in cardiac output under different situations of pulsation ratio	118
Figure 3-6 Performance indexes for the characteristic cardiovascular variables	126
Figure 3-7 Cardiovascular response for the chosen optimal case (Phase shift = 200 degree, Pulsation ratio = 0.4).....	127
Figure 4-1 System configuration	138
Figure 4-2 Schematic of the reciprocating valve pump type VAD	138
Figure 4-3 Pumping action profiles of the LVAD.....	139

Figure 4-4 Change of arterial resistance in a simulated exercise condition.....	142
Figure 4-5 System response of cardiovascular model with and without VAD support	149
Figure 4-6 Cardiac response under arterial resistance change and without VAD control	151
Figure 4-7 Cardiac response under arterial resistance change and with VAD control	152
Figure 4-8 Comparison of VAD mean variables.....	153
Figure 5-1 Schematics of the pulsatile bioreactor.	163
Figure 5-2 Equivalent circuit description of the hydro-dynamic characteristics for the pulsatile bioreactor.....	164
Figure 5-3 Driving pressure in the air chamber.....	168
Figure 5-4 Simulated pressure and flow-rate changes generated in the tissue construct position.....	170
Figure 5-5 Simulated motion profile of the silicon diaphragm.....	170
Figure 5-6 Comparison of pressure and flow-rate changes in different positions of the system.....	171
Figure 6-1 Circulatory model with coronary loop and several important branches	178
Figure 6-2 Schematic of the integrated cardiovascular/pharmaceutical model	179
Figure 6-3 Coupled 0D/3D modelling, with 0D model providing the boundary conditions for the 3D CFD study.....	180

List of tables

<i>Number</i>	<i>Page</i>
Table 1-1 Comparison of animal experiments and mathematical modelling techniques in cardiovascular research	4
Table 1-2 Comparison of modelling techniques for cardiovascular dynamics studies....	8
Table 1-3 Comparison of distributed-parameter models and lumped-parameter models for cardiovascular applications	8
Table 1-4 Four typical vessel segment models as building blocks of multi-compartment description of the vessel network.....	15
Table 1-5 Comparison of various 0D models for the systemic vasculature.....	17
Table 1-6 Typical applications of 0D model.....	32
Table 1-7 Comparison of the two traditional types of VADs	35
Table 2-1 Parameters for the Heart.....	68
Table 2-2 Parameters for the Blood Vessels	69
Table 2-3 Parameters for KG diaphragm motion modelling.....	70
Table 2-4 Parameters for variable valve opening model.....	71
Table 2-5. Additional Parameters	71
Table 3-1. Physiological variables and the corresponding membership functions constructed in assess the cardiovascular response	112
Table 3-2 Changes of cardiovascular variables and index values under different phase shift and pulsation ratio values	119
Table 4-1. VAD motion control parameters.....	144
Table 5-1 Parameter settings for the bioreactor.....	168

Nomenclature

List of symbols

A	Sectional area
AR	Area ratio
C	Compliance
CO	Cardiac output
CQ	Flow coefficient
CV	Flow coefficient
D	Characteristics of one-way flow in the valves, like a diode
E, e	Elastance
I	Inertial moment of rotating
K, k	Coefficient
L	Inertance
l	Displacement
m	Mass
P	Pressure
Q	Flow rate
R	Resistance
r	Radius
T	Heart period
t	Time
u	Voltage
V	Volume
v	Velocity
X, x	Stroke, displacement
w	Wall thickness
ϕ	Phase difference
Δ	Difference, variation
Δt	Time step
θ	Rotating angle of valve leaflet, ventricular wall stress
τ	Valve opening
ω	Rotating speed of the pump

List of subscripts

0	Initial value; offset value; value for unstressed condition
a	Amplitude, air
ao	Aortic valve
atm	Atmospheric

<i>bm</i>	Velocity effect on the valve dynamics, due to blood motion
<i>ci</i>	Inlet to the media chamber
<i>cl</i>	Lower media chamber
<i>co</i>	Outlet to the media chamber
<i>ct</i>	Tissue construct in the media chamber
<i>cu</i>	Upper media chamber
<i>d</i>	Diastolic phase
<i>e</i>	Elastance action
<i>ea</i>	Elastance of atrium
<i>ev</i>	Elastance of ventricle
<i>f</i>	Frictional action
<i>fr</i>	Frictional effect on the valve dynamics, due to resistance of neighbouring tissue
<i>i</i>	Inlet
<i>la</i>	Left atrium
<i>lv</i>	Left ventricle
<i>lvf</i>	Left ventricular failure
max	Maximum value
<i>mi</i>	Mitral valve
min	Minimum value
<i>o</i>	Outlet
<i>p</i>	Pulse; effect of pressure force
<i>par</i>	Pulmonary arterioles
<i>pas</i>	Pulmonary artery sinus
<i>pat</i>	Pulmonary artery
<i>pav</i>	Right heart annulus fibrosus
<i>pcp</i>	Pulmonary capillary
<i>po</i>	Pulmonary valve
<i>pr</i>	Pressure effect on the valve dynamics
<i>pvn</i>	Pulmonary vein
<i>pwb</i>	Beginning of P wave in ECG
<i>pww</i>	Duration of P wave in ECG
<i>ra</i>	Right atrium
<i>rv</i>	Right ventricle
<i>s</i>	Systolic phase
<i>s1</i>	Peak of systolic phase
<i>s2</i>	End of systolic phase
<i>sar</i>	Systemic arterioles
<i>sas</i>	Systemic aortic sinus
<i>sat</i>	Systemic artery
<i>sav</i>	Left heart annulus fibrosus
<i>scp</i>	Systemic capillary
<i>ss</i>	Effect of shear stress on the valve dynamics
<i>st</i>	Strain action
<i>svn</i>	Systemic vein

<i>T1</i>	Beginning instance of T wave in ECG signal
<i>T2</i>	Ending instance of T wave in ECG signal
<i>ti</i>	Tricuspid valve
<i>twb</i>	Beginning of T wave in ECG signal
<i>twe</i>	End of T wave in ECG signal
<i>tww</i>	Duration of T wave in ECG signal
<i>U2</i>	Ending instance of U wave in ECG signal
<i>v</i>	Vascular
<i>vad</i>	Ventricular assist device
<i>vo</i>	Vortex effect on the valve dynamics
<i>vpi</i>	Inflow conduit for the VAD
<i>vpo</i>	Outflow conduit for the VAD
<i>vvi</i>	Inlet port of the VAD
<i>vvo</i>	Outlet port of the VAD

Chapter 1 Commentary

Cardiovascular disease is the most common cause of death in the UK, costing millions of pounds of NHS resources every year (£140m in 1999/00 and £187m in 2008/09, according to the Office of National Statistics, UK (UK National Statistics 2013)). The prognosis for patients with cardiovascular diseases is often poor, and research into the diagnosis and treatment of cardiovascular diseases is an urgent task.

During the past decades, researchers have invested huge effort in the study of cardiovascular physiology and pathology, using various types of research techniques. These studies have contributed enormously to the ever-improving clinical diagnosis and treatment of cardiovascular diseases (Aaronson *et al.* 1999, Bergel 1972, Fung 1984, Guyton 2006, van de Vosse 2003). However, due to the complexity of the disease mechanisms, many problems remain unsolved. Among the various types of research methods applied, mathematical modelling as a mature engineering tool has been extensively used in the cardiovascular studies and achieved impressive success (Bassingthwaite *et al.* 2009, Formaggia 2009, Li 2000, van de Vosse 2003, Westerhof *et al.* 2009). This thesis focuses on the lumped-parameter (also called 0D, or concentrated-parameter) mathematical modelling of the cardiovascular system. The thesis starts with a comprehensive review of the previous and concurrent 0D cardiovascular models, and then introduces an improved 0D cardiovascular system developed by the current author, followed by some application studies. Specifically, this chapter is presented as a commentary to tie together the research papers submitted as the body of this thesis. Following a brief introduction to set the context for the research it seeks to combine a comprehensive literature review with an analysis of the challenges that are addressed by the specific works included in this thesis and thus of the contribution of the work to the domain knowledge. This chapter draws extensively on the author's recently published review of the field (Shi *et al.* 2011b).

1.1 Cardiovascular physiology

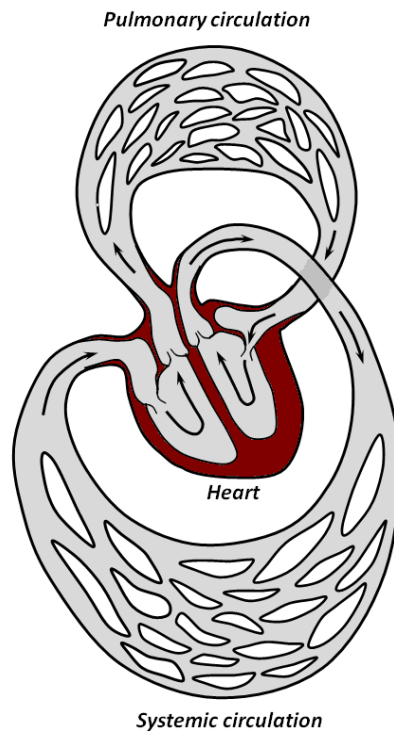


Figure 1-1 Circulation system

(Adapted from(Marieb 2003))

The cardiovascular system is the vehicle for the transport of blood throughout the body, conveying nutrients to the body tissues and organs and removing some waste products (Levick 2003). The circulatory system comprises the four chamber heart (including the four heart valves), the systemic vessels that deliver the blood to and collect the blood from the peripheral organs, and the pulmonary vessels that transport the blood through the lung for exchange of oxygen and carbon dioxide (Guyton 2006, Levick 2003, Marieb 2003). Figure 1-1 illustrates the structure of the circulatory system. The heart contracts to pump the blood into the systemic and pulmonary vasculature for circulation around the whole body. The four heart valves maintain the direction of the flow. The systemic and pulmonary vessels each can be divided into aorta/pulmonary artery, main and small arteries, arterioles, capillaries, venules, veins, and vena cava/pulmonary vein. From the aorta to the arteries, arterioles, and on into the capillaries, the vessel branches into a tree-like structure, with vessel diameters decreasing, overall vessel luminal area increasing and the vessel wall becoming stiffer for every consecutive generation of branching. The aorta and the larger arteries are

quite elastic, and they act as reservoirs that buffer the pulsatility of the flow from the heart. There is active control, in that the arterioles changed their vessel calibre under neuro-regulation and various bio-chemical regulations, to adjust the pressure and flow of blood to the peripheral organs. Capillaries are where the exchange of nutrients and metabolites take place. From the capillaries to venules, veins and vena cava, the vessels are merging along the flow direction to form an inverse tree-like structure, with greater compliance in the larger vessels. The vena cava and the larger veins are the most elastic vessels and they serve as a reservoir to accommodate the redistribution of blood volume during transitions between different physiological conditions. Some veins such as those in the lower extremity have venous valves to aid the directionality of the blood flow, and they are also subjected to the compression action of the surrounding muscles, providing a secondary pumping action returning blood to the right side of the heart. Some other veins, such as those in the lung, collapse when their intra-luminal pressure is lower than the extra-luminal tissue pressure.

1.2 Cardiovascular research

As in any other field of study, cardiovascular research involves experimental studies and mathematical modelling studies (Bergel 1972, Fung 1984, Guyton 2006). The experimental studies can be classified into *in vitro* studies that are executed on mock cardiovascular systems and *in vivo* studies that are carried out in animal and human bodies (Bergel 1972). In *in vitro* studies, mechanical and electrical components are assembled into an artificial system to conceptually mimic the cardiovascular functioning, which is useful for the fundamental study of blood flow physics. Examples of this type of research include pulse wave dynamics simulations (Alastruey *et al.* 2011, Bessems *et al.* 2008, Borlotti *et al.* 2012, Khir and Parker 2002, Khir *et al.* 2007, Li and Khir 2011, Swalen and Khir 2009) and evaluation of cardiac assist devices for mechanical circulation support (Biglino *et al.* 2012, Biglino *et al.* 2010, Ferrari *et al.* 2011, Fresiello *et al.* 2013, Khir 2011, Khir *et al.* 2005, Khir *et al.* 2006, Koenig *et al.* 2004, Kresh *et al.* 1990, Tuzun *et al.* 2011). Due to device limitations *in vitro* studies often over-simplify the upstream and downstream loading conditions to the research objects. More realistic and sophisticated experimental studies are often implemented *in vivo* using animal and human subjects and the derived cell lines. In these studies, various cardiac, biochemical and haemodynamic parameters are measured for the investigation of mechanisms of pathogenesis of cardiovascular disease (Aarnoudse *et*

al. 2004, Beyar *et al.* 1987, Borlotti *et al.* 2012, Borlotti *et al.* 2010, Bowman *et al.* 2004, Cohen *et al.* 1995, Enriquez-Sarano *et al.* 1993, Hollander *et al.* 2004, Khir 2010, Khir *et al.* 2001, Khir and Parker 2005, Khir *et al.* 2004, Kilner *et al.* 2000, Li *et al.* 2011, Merckx *et al.* 2013, Schampaert *et al.* 2013b, Sharp *et al.* 2000, van T. Veer *et al.* 2009, Verberne *et al.* 2007) and the effects of drug/device intervention (Frazier *et al.* 2004, Khir 2010, Khir *et al.* 2003, Kresh *et al.* 1990, Loerakker *et al.* 2008).

Table 1-1 Comparison of animal experiments and mathematical modelling techniques in cardiovascular research

<p><i>in vivo</i> experiment</p>	<ul style="list-style-type: none"> • Causes pain and death to experimental subjects. Needs to be regulated by Home Office Licence and ethical approval • There are differences in the physiological response between the human and the animals; some of these are significant and many are poorly understood. • Probes inserted into animal/human bodies may change the native physiological condition. • Not all signals are measurable. • The response in the animal/human body is often induced by multiple factors. It is difficult to identify the individual contribution of each factor from the overall response. • Expensive, time consuming, and laborious.
<p>Computer simulation</p>	<ul style="list-style-type: none"> • No ethical issues involved in the construction of generic models based on general principles and/or on published literature. • Ethical issues are associated with only the collection and use of human data, governed generally by the principle of informed consent wherever possible and, depending on its nature, by data protection legislation, and overseen by local medical ethics committees. Often, subject to these constraints, clinical data can be re-used effectively to support modelling with no adverse implications for the subject. • Models can be easily adapted to simulate response in either human or animal. • Depending on the modelling accuracy required, theoretically response in any body part can be simulated. • The researchers can choose a balance between accuracy and the modelling effort; any signal of interest can be simulated. • Each physiological factor can be manipulated to identify its individual contribution, as well as the overall contribution. • Economic, rapid. Once the model is developed and validated, it can be run repeatedly to study similar physiological conditions for an unlimited number of times.

In recent years, with the development of mathematic science and computer technology, mathematical modelling has developed into a mature research technique, and it is seeing ever-increasing applications to reduce/replace *in vivo* and *in vitro* studies in cardiovascular medicine (Bassingthwaighte *et al.* 2009, Formaggia 2009, van de Vosse 2003). In contrast to experimental studies, mathematical modelling studies explore the mathematical equations that describe the bio-physical and bio-chemical changes in the living system for the description and prediction of cardiovascular response in different healthy and diseased conditions. Like engineering systems, the human/animal body also follows the bio-physical and bio-chemical laws. By deriving the governing equations underneath the physical and chemical laws corresponding to the physiological/pathological procedures and calibrating the equations with realistic human/animal data, the healthy/diseased responses in the human/animal body can be accurately duplicated and effectively predicted (Fung 1984, van de Vosse 2003, Westerhof *et al.* 2009). The mathematical modelling approach can not only predict the physiological responses (like arterial pressure and cardiac index) that are measurable *in vivo*, but also provide wider ranges of information (including venous pressure and flow, vascular impedance etc.) that are important but difficult or impossible to measure in the human/animal body, thus enabling the reduction, refinement and replacement of *in vivo* experiments in cardiovascular medicine (Fung 1984, van de Vosse 2003). Table 1-1 compares the mathematical modelling and the *in vivo* experimental techniques in cardiovascular medicine.

1.3 Modelling in cardiovascular research

Like all fluid systems, blood flow in the cardiovascular system obeys the laws of mass conservation, momentum conservation and energy conservation (Fung 1984, van de Vosse 2003). Unlike more traditional engineering piping networks, the vessels are comparatively flexible, and the constitutive equations of the vessel walls provide additional constraints that strongly influence the blood flow dynamics. Furthermore the mechanical propulsion is provided by the muscle of the heart, governed by its own constitutive equations including active components.

Modelling of cardiovascular dynamics can be classified into time domain or frequency domain studies. Frequency domain representations of the cardiovascular system (Burattini and Campbell 2000, Burattini and Natalucci 1998, John 2004, Quick *et al.*

1998, Quick *et al.* 2006) are based on linearisation of the governing equations, achieved by neglecting the convective acceleration terms. The simplified equations are then solved in the frequency domain using Fourier or Laplace transformation. Frequency domain analysis permits fast and effective solution methods, but due to the linearization process it is more suitable for analysing problems in which the system is only slightly perturbed from a reference state. For a broader range of problems in which the nonlinear terms cannot be neglected, time domain methods must be employed.

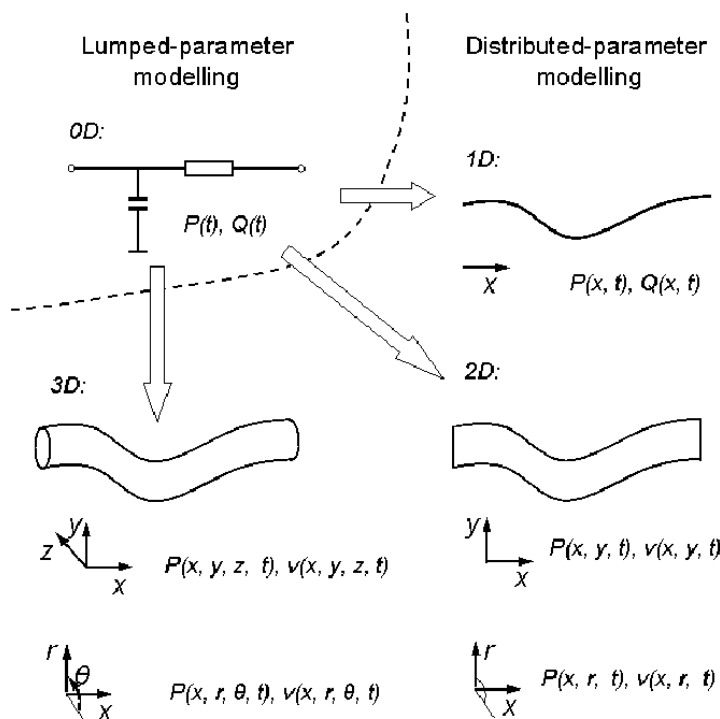


Figure 1-2 Different scales of modelling

The selection of the appropriate dimensionality in a model representation, from 0D though to 3D, depends on the aims and the required accuracy of the research study. Zero dimensional (0D), or lumped-parameter, models assume a uniform distribution of the fundamental variables (pressure, flow and volume) within any particular compartment (organ, vessel or part of vessel) of the model at any instant in time, whilst the higher dimensional models recognise the variation of these parameters in space. This is illustrated in Figure 1-2. For convenience of description, in the following the vocabularies of 0D model and lumped-parameter model are used interchangeably.

0D models give rise to a set of simultaneous ordinary differential equations (ODEs): in representations of the vasculature there are often two ODEs for each compartment, representing conservation of mass and conservation of momentum, complemented by

an algebraic equilibrium equation relating compartment volume to pressure. System models constructed from 0D components generally feature the major components of the system, such as the heart, the heart valves and compartments of the vasculature, and are suitable for examination of global distributions of pressure, flow and blood volume over a range of physiological conditions, including study of interactions between the modelled components. Distributed-parameter models (1D, 2D and 3D) give rise to a series of partial differential equations describing conservation of mass and momentum (the Navier-Stokes equations), again complemented by equilibrium equations. In the context of cardiovascular mechanics, 1D models have the important facility to represent wave transmission effects within the vasculature: these are important in the aorta and larger systemic arteries. However, it should be noted that a 1D model can be effectively approximated with a series of 0D components, with each 0D component representing a control segment in the 1D model, when the convective effect in the 1D model can be neglected (Formaggia and Veneziani 2003, van de Vosse and Stergiopoulos 2011). One example is the blood flow in a segment of healthy artery, in which the pulse wave velocity is much higher than the flow velocity and there is no sudden change of vessel diameter. 3D solutions are required to compute complex flow patterns, for example in the ventricles, around heart valves, near vessel bifurcations, or in any region with vortical or separated flows. In the context of the vasculature, there is a place for 2D models which can represent the radial variation of velocity in an axisymmetric tube. Due to the often enormous computing resource involved, distributed-parameter models are eminently suited to study of local haemodynamics in a certain cardiovascular organ or in a segment of vessel, where local blood flow changes have little influence on other parts of the circulatory system. Table 1-2 summarises the dimensionality of the fluid mechanics representations and their broad ranges of applications in the study of cardiovascular dynamics. Table 1-3 further compares the distributed-parameter models and lumped-parameter models for cardiovascular applications from the aspects of modelling purpose, mathematical tools used, results presentation etc. The lumped-parameter models and the distributed-parameter models are developed for different research purposes, and each has its own advantages and disadvantages. Increasingly the research community is seeking to develop integrated multi-scale models to enjoy the benefits of both.

Previously van de Vosse has reviewed the concurrent mathematical modelling of the cardiovascular system (van de Vosse 2003), covering different scales of model studies. van de Vosse and Stergiopoulos further reviewed the cardiovascular modelling works on pulse wave propagation (van de Vosse and Stergiopoulos 2011), which was mainly focused on 1D models but also covered other scales of modelling. As a supplementary work to these two studies, this chapter specifically reviews the 0D cardiovascular modelling studies.

Table 1-2 Comparison of modelling techniques for cardiovascular dynamics studies

Method of study		Suitable research target	
Time domain study	0D (lumped parameter) model	Global cardiovascular dynamics in the whole circulation system; general pressure and flow-rate changes in a local circulation loop; interaction between different cardiovascular organs, or between the native circulation system and the cardiovascular artificial organs (such as artificial heart); possibly to provide boundary conditions for local 3D models	
	Distributed parameter model	1D	Pulse wave transmission in artery or artery network; improved boundary conditions for 3D local models, capable of capturing systemic wave reflection effects
		2D	Local haemodynamic flow field study in axisymmetric domains; further improvement of boundary conditions for local 3D models, but limited applicability
		3D	Local haemodynamic flow field study in full 3D domains
Frequency domain study		Frequency response analysis of cardiovascular system after linearization	

Table 1-3 Comparison of distributed-parameter models and lumped-parameter models for cardiovascular applications

	Distributed-parameter models	Lumped-parameter models
Target of study	Blood flow in a vessel segment or in a specific cardiovascular organ in different healthy and diseased conditions.	System level cardiovascular response in different healthy and diseased conditions.
Purpose of study	To obtain simulated spatial distributions of pressure, velocity, shear stress, vorticity etc. in the organs studied, for the evaluation of features such as pressure gradients across stenoses or of mechanical damage to blood cell and endothelia.	To calculate the temporal changes of pressure, flow, volume, vascular impedance, cardiac augmentation index, ejection fraction etc. in the circulatory system, for the evaluation of perfusion to important organs and the circulatory interaction between

		different cardiovascular organs.
Typical diseases studied	Aneurysms, atherosclerosis, valve incompetence etc.	Hypertension, heart failure, stroke, haemorrhage etc.
Dimension of study	Three dimensional, two dimensional, or one dimensional.	Zero dimensional.
Mathematical tools used	Solution of partial differential equation with finite volume method, finite element method, or finite difference method.	Time marching solution of a group of nonlinear ordinary differential equations.
Results presentation and clinical relevance	Results are presented as distribution of pressure, velocity, shear stress etc. in the organ studied. The clinical interpretation of these results in a biological context can be difficult, particularly in prognosis for an individual, partly because there is a paucity of data and partly because such data as exists is often contradictory and conflicting.	Results are presented as changes of pressure and flow etc. versus time. This presentation can often be compared directly with clinical measurements and thus are much easier to interpret in the clinical context.
Computer resources involved	Computational intensive, requires high performance super-computer and long computing time.	Normal desktop computer is sufficient for the computing task, and the computation takes only several seconds to finish.

1.4 0D cardiovascular modelling

0D models are developed to simulate the global haemodynamics in the whole circulation system. In carrying out 0D modelling, the concept of a hydraulic-electrical analogue is often applied (Westerhof *et al.* 2009). Generally, there are strong similarities between blood flow in the circulatory system and electric conduction in a circuit: blood pressure gradient in the circulatory loop drives the blood to flow against the hydraulic impedance; similarly, voltage gradient in a circuit drives current to flow against the electric impedance. Hydraulic impedance represents the combined effect of the frictional loss, vessel wall elasticity and blood inertia in the blood flow, whilst electric impedance represents the combination of the resistance, capacitance and inductance in the circuit. Blood flow is described by the continuity equation for mass conservation, Poiseuille's Law for the steady state momentum equilibrium, and the Navier-Stokes equation for the unsteady state momentum balance; similarly the electric flow in the circuit is governed by Kirchhoff's current law for current balance, and Ohm's law for the steady state voltage-current relation, and the transmission line

equation for the high frequency voltage-current relation. Thus by representing the blood pressure and flow-rate with voltage and current, describing the effects of friction and inertia in blood flow and of vessel elasticity with resistance R , inductance L and capacitance C in the electric circuit respectively, the well-established methods for analysis of electric circuits can be borrowed and applied to the investigation of cardiovascular dynamics.

0D cardiovascular system analysis started with the modelling of arterial flow using the famous Windkessel model. This was subsequently expanded to cover the modelling of other organs such as the heart, heart valves, and veins.

1.4.1 Models of the systemic vasculature

There is a wide range of 0D systemic vasculature models to simulate the intra-luminal pressure and flow changes, from the simplest Windkessel model which models the vasculature as a single capacitance C connected in parallel with a single resistance R , to the most comprehensive Guyton model (Guyton *et al.* 1972) in which most of the main circulatory branches from arteries to veins were specifically represented as well as some autonomic and hormone regulation effects. These models can be divided into two subgroups, namely single- or mono-compartment models, in which increasing levels of sophistication are used to capture systemic response, and multi-compartment models, in which separate parts of the vasculature are represented as different compartments (often with similar electrical components but with different particular values of frictional loss coefficient, inertia and vessel compliance).

1.4.1.1 Mono-compartment descriptions

In a mono-compartment description, the whole vessel network is described with a single resistance-compliance-inductance (RLC) combination (although there might be more than one of each component). The simplest and the first mono-compartment description is the famous two-element Windkessel model, which was first proposed by Stephen Hales in 1733, and later formulated mathematically by Otto Frank in 1899 (Li 2000). The Windkessel model consists of two parallel elements, a capacitor C that describes the storage properties of large arteries and a resistor R that describes the dissipative nature of small peripheral vessels including arterioles and capillaries, as illustrated in Figure 1-3 (a). This model was developed to represent the elementary characteristics of the systemic artery network, while the veins were neglected and

represented as a far field zero pressure. Although it appears to be very crude compared with the more sophisticated models developed later, the two-element Windkessel model provides a simple way of representing the pressure decay in the aorta over the period of diastole. Even today, this simple RC combination model is still used in clinical practice for the estimation of total arterial compliance when peripheral resistance and the aortic pressure pulse waveform are known (Levick 2003, Li 2000). Despite the obvious restriction that this model has only a single time constant, and therefore cannot capture the high frequency components associated with pressure reflections in the artery network, it is nevertheless often used in cardiovascular modelling to provide a simple representation of the after-load on the heart.

Extending the Windkessel model for the simulation of arterial characteristics, Landes (Landes 1943) introduced an extra resistance element R_c , connected in series with the RC Windkessel model, as shown in Figure 1-3 (b). This model has been extensively studied by Westerhof and co-workers (Westerhof *et al.* 1971), and is sometimes called the Westkessel model, or RCR model. The second resistance R_c represents the characteristic impedance of the arterial network, defined as the ratio of the oscillatory pressure and the oscillatory flow when no reflective waves are present (Nichols and O'Rourke 1990). The overall resistance R_c+R equals the total systemic vascular resistance in the previous RC model, and the capacitance C represents the elasticity effect of the arterial network (Westerhof *et al.* 1971). Despite its simplicity, the introduction of the proximal R_c greatly improves the high frequency performance of the model (Westerhof *et al.* 1971). *In vivo* and numerical studies have indicated that the RCR model provides, subjectively, a good representation of after-load in the context of prediction of stroke volume, stroke work, and systolic and diastolic aortic pressure (Burkhoff *et al.* 1988). It is widely used in cardiovascular simulations as the after-load for the evaluation of cardiac function under various physiological and pathological conditions. However, *in vivo* studies have also indicated that the RCR model significantly underestimates peak aortic flow, slightly underestimates mean arterial pressure, and does not provide realistic aortic pressure and flow waveforms, when compared to a realistic arterial impedance model under the same simulated ventricular action (Burkhoff *et al.* 1988).

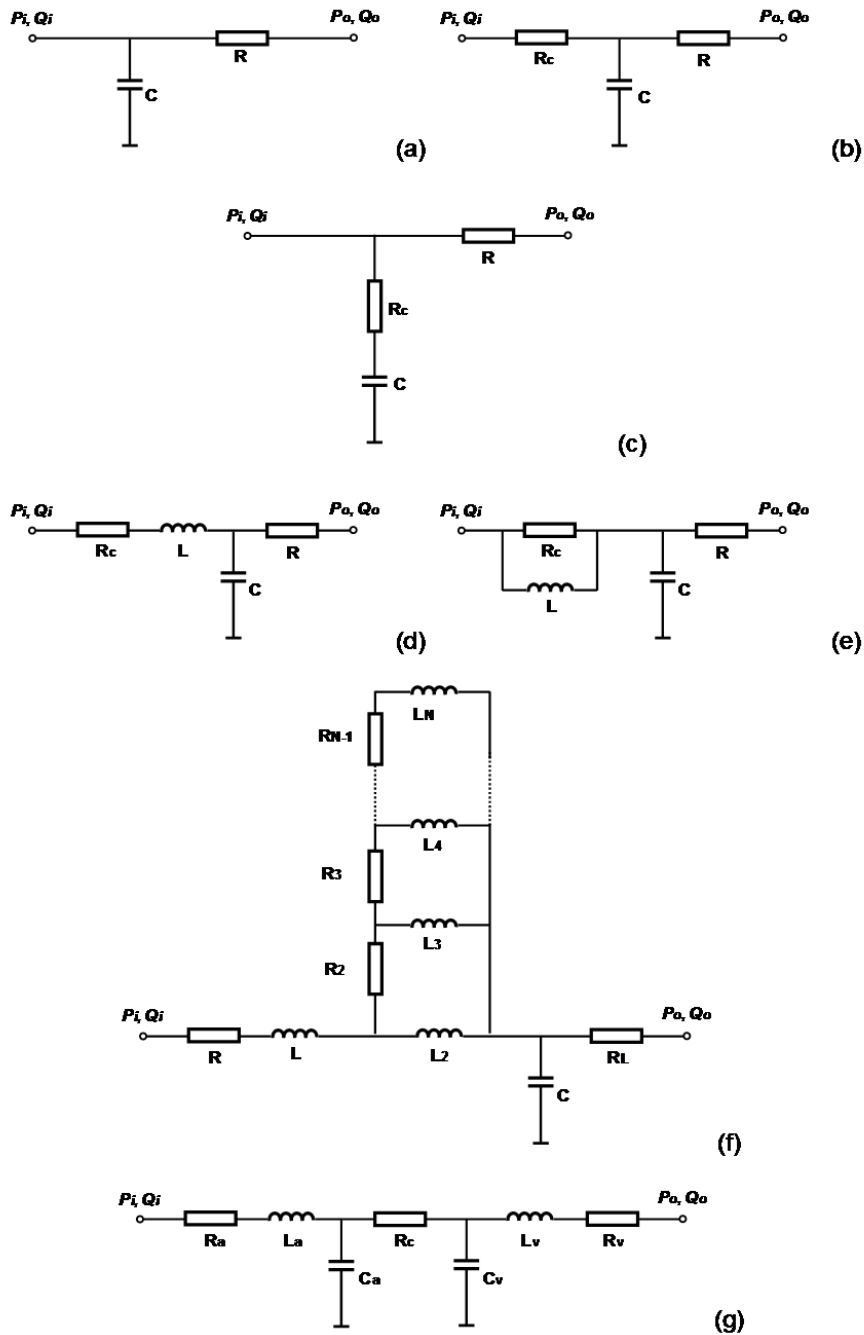


Figure 1-3 Mono-compartment models for the vessel network

(a) RC Windkessel model; (b) RCR Westkessel model; (c) RCR2 model; (d) RLCR1 model; (e) RLCR2 model; (f) RLCR1 model with sleeve effect; (g) RLCRCLR model)

In parallel to the Westkessel RCR model, Burattini and Natalucci (Burattini and Natalucci 1998) developed a different configuration of the three element RCR model to describe the arterial characteristics, in which the a small resistance R_c was placed in series with the capacitor C instead of in series with the RC combination, as shown in Figure 1-3 (c). In this configuration the small resistance R_c was conceptually coupled

with the capacitor C to describe the visco-elastic property of the vessel wall, in contrast to its use to capture grossly the wave reflection response in Westerhof *et al.*'s RCR model.

Landes (Landes 1943) further extended the RCR arterial model by incorporating the inertial effect of blood flow, forming a model configuration of RLRC1 as shown in Figure 1-3 (d). Westerhof *et al.* also added the inertial effect of blood flow in the RCR model and proposed another four-element arterial model of RLRC2 (Jager *et al.* 1965, Stergiopoulos *et al.* 1999), as illustrated in Figure 1-3 (e). Inclusion of the inertial term L helps to further improve the modelling accuracy of vessel impedance in the middle frequency range. Several *in vivo* studies have been carried out to compare the modelling accuracy of the RC, RCR, RLRC1 and RLRC2 models, and it has been demonstrated that the RLRC1 model best reproduces the character of the vascular impedance data (Deswysen *et al.* 1980, Sharp *et al.* 2000). However, with more elements included, identification of model parameters becomes a difficulty. For this reason the RLRC1 and RLRC2 model are not so widely used as the RCR and RC models.

To further improve the arterial modelling, Westerhof *et al.* have also extended the RCR model by including more R and L components, configured as illustrated in Figure 1-3 (f), to simulate the laminar oscillatory flow impedance, the so called sleeve effect (Jager *et al.* 1965). This model is excellent for test cases representing Womersley's solutions for axisymmetric flow in a straight cylindrical tube, but has less relevance to complex vascular networks. Later on, Huberts *et al.* (Huberts *et al.* 2009) further developed this concept by proposing a four-element model, in which a Womersley number dependent resistor and an inductor was connected in parallel to describe the combined response of viscous boundary layer and inertia dominated flow core. Westerhof *et al.*'s original model was relatively complicated, and accurate resolution of the radial distribution of velocity/flow can be better achieved through 2D or 3D computational fluid dynamics studies. As a result this model has been relatively unexploited by other researchers in the field.

The above RC, RCR and RLRC1 models were mainly developed to describe the pressure and flow characteristics in the aorta, and they were also applicable to arterial pressure/flow modelling in general vessel branches where the pressure and pressure pulsation in the venous side of the vessel beds are negligible, and this is the case for

most of the applications. However, for some circulation beds such as coronary and pulmonary circulations, there are significant pulsatile components in the venous pressure and flow and thus the venous side contribution to the overall haemodynamics is not negligible (Frasch *et al.* 1996, Rose and Shoukas 1993). To rectify the problem, more complex 5, 6 and 7 element vascular models (RCRCR, RCRCR and RLCRCR models) have been derived in which extra R, C and L elements were included to account for the dynamic characteristics of the veins. Figure 1-3 (g) shows a 7 element RLCRCR model. Originally the 7 element RLCRCR model was proposed as a mono-compartment model to describe the characteristics of the complete systemic vasculature, but it can also be interpreted as a series connection of an RLC model for the arterial subsystem, a resistance model for the capillaries, and another RLC model for the venous subsystem. In this sense it can also be considered as a multi-compartment model as discussed in the next section.

1.4.1.2 Multi-compartment descriptions

In the mono-compartment models discussed above, the whole systemic vasculature is treated as a single block, and thus the internal distribution of pressure and flow-rate in the different segments of the vessel network is not computed (although, depending on the problem formulation, some spatial information might be computed as internal compartment variables). Multi-compartment models have been developed to address these shortcomings. In these models the systemic vasculature is partitioned into a number of segments, and each segment, or compartment, is described by its own resistance R, compliance C and inductance L, depending on the local vessel characteristics. The vessel segments are connected together to form the complete model of the whole vessel network. Depending on the specific aims of any particular study, and the requirement for modelling accuracy, the systemic vasculature can be appropriately partitioned to provide detail in the region(s) of interest, whilst other segments can reasonably be lumped together using less sophisticated model elements. This flexible and simple description of the systemic vasculature is a powerful tool for cardiovascular simulation.

In constructing the multiple compartment models for the vessel network, it is necessary to first derive suitable RLC models for the vessel segment, as a building block in the development of the whole vessel network model. Formaggia and Veneziani (Formaggia

and Veneziani 2003) and Milisic and Quarteroni (Milisic and Quarteroni 2004) provided detailed derivations of four typical compartment model configurations appropriate for the description of a vessel segment. The four compartmental configurations were labelled as L network element, inverted L network element, T element and π element as illustrated in Table 1-4. Each is most appropriately used with particular combinations of boundary conditions. Among these configurations, the inverted L network element uses the inlet flow and the outlet pressure as boundary conditions, and solves for the inlet pressure and the outlet flow. This is consistent with the common practice of using upstream velocity and downstream pressure as boundary conditions in 2D and 3D computational fluid dynamics studies.

Table 1-4 Four typical vessel segment models as building blocks of multi-compartment description of the vessel network

(After (Formaggia and Veneziani 2003, Milisic and Quarteroni 2004))

Network element	Circuit model	Corresponding boundary conditions
Inverted \mathcal{L} element		Upstream flow-rate Q_i and downstream pressure P_o
\mathcal{L} element		Upstream pressure P_i and downstream flow-rate
T element		Upstream and downstream pressures P_i and P_o
π element		Upstream and downstream flow-rates Q_i and Q_o

Using these network elements as building blocks, several multi-compartment models of the systemic vasculature have been developed, with various levels of complexity, from the single branch models upwards. Most researchers take the approach of partitioning the systemic vasculature into segments representing aorta, artery, arteriole, capillary,

and vein (Beyar *et al.* 1987, Burkhoff and Tyberg 1993, Santamore and Burkhoff 1991, Ursino 1999, Ursino *et al.* 1996, Zacek and Krause 1996), characterising the network element to suit local flow features, and then connecting the segments to form the circulation loop. In the aorta and the main arteries the blood vessels are quite elastic, and the blood flow is pulsatile, thus the full resistance, compliance and inductance effects (RLC combination) need to be considered. In the arterioles and capillaries, the vessel wall is relatively rigid, the flow is steady and frictional loss is the dominant factor, thus the local flow dynamics is adequately described by a pure resistance element. The general veins and vena cava are compliant and the blood flow is relative steady, thus the inertial effect is often neglected and an RC combination is considered sufficient to describe their flow characteristics. Figure 1-4 illustrates a sample multiple compartment model for the systemic vasculature developed by Shi *et al.* (Shi *et al.* 2010). Some researchers have also built multi-branched multi-compartment models (Chen *et al.* 2008, Heldt *et al.* 2002, Lu *et al.* 2001, Noordergraaf *et al.* 1963, O'Rourke and Avolio 1980, Olansen *et al.* 2000, Pennati *et al.* 1997a, Snyder and Rideout 1969, Sun *et al.* 1997, Ursino 1998, Ursino and Magosso 2000a, Ursino and Magosso 2003, Werner *et al.* 2002) to investigate blood flow distribution and pressure/flow characteristics in each simulated vessel branches. Noordergraaf *et al.* (Noordergraaf *et al.* 1963), Avolio (Avolio 1980), and O'Rourke and Avolio (O'Rourke and Avolio 1980) have constructed full models for the systemic arterial network. O'Rourke and Avolio's model bore a close relationship to Noordergraaf *et al.*'s model, but was claimed to be more realistic in its representation of the vascular bed, particularly that in the upper part of the body (O'Rourke and Avolio 1980). These three complex models have been directly applied or slightly adapted for usage as the reference arterial tree model in plenty of later studies (Alastruey *et al.* 2011, John 2004, Matthys *et al.* 2007, Mynard and Nithiarasu 2008, Reymond *et al.* 2009, Segers and Verdonck 2000, Sheng *et al.* 1995, Sherwin *et al.* 2003, Wang and Parker 2004).

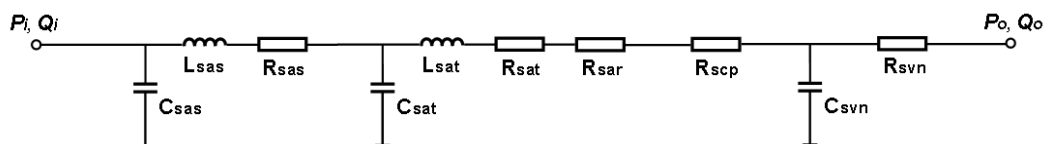


Figure 1-4 A sample multi-compartment model

(Refer to nomenclature for symbol meanings.)

1.4.1.3 Summary of properties and attributes of systemic vasculature models

As a summary, the vessel models described above are compared in Table 1-5.

Table 1-5 Comparison of various 0D models for the systemic vasculature

Model configuration		Advantages	Disadvantages		
Mono-compartment model	RC model	Reveals the general storage properties of large arteries and the dissipative nature of small peripheral vessels with the simplest model structure	Cannot simulate the effect of high frequency components in the arterial impedance, cannot accurately match the aortic pressure and flow-rate waveforms	Venous pressure is assumed to be zero and thus venous pressure fluctuation cannot be described	Cannot describe the pressure and flow-rate changes in specific segments of the vasculature; cannot simulate the pulse wave transmission effect
	RCR model	Simple, and gives a better description of the high frequency components in the arterial impedance than the RC model	Cannot describe the features of the secondary maximum and a discrete minimum in the medium frequency range of the arterial impedance.		
	RLCR model	Simple, and offers improved description of the secondary maximum and a discrete minimum in the medium frequency range of the arterial impedance than the RCR model	Parameter setting is more difficult than for the RCR and RC models, which limited its applications.		
	RLCRCLR model	Simplest model that accounts for venous pressure fluctuations	The model structure is complex compared with RC, RCR and RLCR models, thus parameter setting is more difficult.		
Multiple compartment model		Flexible combination of RLC network elements to describe the vessel characteristics to whatever level of detail required. Captures, within the limitations of the model, pulse wave	More complex to implement than the mono-compartment models. Difficult to determine appropriate RLC parameters when the model includes many vessel segments.		

1.4.2 Models of the heart

1.4.2.1 Isolated chamber models

There have been numerous studies on quantitative characterisation of the heart as a pump. Leefe and Gentle (Leefe and Gentle 1995) discussed the characteristics of the left ventricle, exploring whether it was better described as a pressure or as a flow source: of course in truth it is a combination of the two. In the 1970s, Suga *et al.* (Suga *et al.* 1973) proposed a varying elastance model for the ventricle. In this model, the ventricular pressure is presented as a function of the ventricular elastance and the change of the ventricular volume from its unstressed value. The change of ventricular volume is determined by the blood flow into and out of the ventricular chamber, and the ventricular elastance is defined as a time-varying function based on the *in vivo* measurement of the ventricular activity over the cardiac cycle. This model is easy to understand and to implement, and it has been widely adopted by researchers such as (Barnea *et al.* 1990, Beyar *et al.* 1987, Lu *et al.* 2001, Migliavacca *et al.* 2001, Pennati *et al.* 1997a, Pennati *et al.* 1997b, Santamore and Burkhoff 1991, Ursino 1999, Ursino *et al.* 1996, Yaku *et al.* 1991).

Various alternatives to the varying elastance model have been developed. Žáček and Krause (Zacek and Krause 1996) derived a heart model in which heart muscle mechanics were based on Hill's three parameter model. The ventricular pressure was calculated from the computed muscle force and the volume calculated from the change of muscle length. Werner *et al.* (Werner *et al.* 2002) proposed equations to calculate the myocardial wall tension in systole and diastole by using Hill's model and considering the Frank-Starling effect, and then calculated the ventricular pressure based on the Laplace law by assuming the heart chamber to be spherical in shape. Bovendeerd *et al.* (Bovendeerd *et al.* 2006) and Diaz-Zuccarini and LeFevre (Diaz-Zuccarini and LeFevre 2007) calculated the ventricular pressure in a similar way. Specifically Bovendeerd *et al.* (Bovendeerd *et al.* 2006) described the chamber pressure as a function of the muscle fibre contraction in the ventricle, and called this model single fibre model. Another simpler model for the heart is to use an exponential equation to define the cardiac output as a function of the atrial pressure, with ventricular dynamics details completely

neglected (Cavalcanti *et al.* 2006, Cavalcanti and Di Marco 1999). Nevertheless, due to its concise model structure and clear physical meaning, the varying elastance model remains the most popular. In addition to its original usage as a descriptor of left ventricle performance, the variable elastance model has also been extended for applicability to the simulation of atrial dynamics (Beyar *et al.* 1987, Lu *et al.* 2001, Migliavacca *et al.* 2001, Pennati *et al.* 1997b, Santamore and Burkhoff 1991, Sun *et al.* 1997). Yaku *et al.* extended the variable elastance model further to study ventricular fibrillation, assigning different parameters to the normal and diseased cardiac muscles (Yaku *et al.* 1991). However, some researchers (Vandenberghe *et al.* 2006) argued that the varying elastance model is not valid in applications where the failing heart is mechanically supported with ventricular assist devices, since the derived elastance variation deviates much from that in the isolated heart. In such situations, other models such as the single fibre model may be adopted as a better description of the cardiac dynamics.

1.4.2.2 Models of Chamber Interactions

Various interactions including atrial-ventricular interaction (Korakianitis and Shi 2006a, Korakianitis and Shi 2006b), ventricular interaction (Beyar *et al.* 1993, Beyar *et al.* 1987, Chung *et al.* 1997, Maughan *et al.* 1987, Olansen *et al.* 2000, Santamore and Burkhoff 1991, Santamore *et al.* 1990, Slinker *et al.* 1987, Slinker and Glantz 1986, Sun *et al.* 1997), and the effect of the pericardium on the cardiac dynamics (Beyar *et al.* 1987, Chung *et al.* 1997, Olansen *et al.* 2000, Santamore *et al.* 1990, Sun *et al.* 1997) have also been studied and reported in the literature. Noting that the atrial-ventricular septum (annulus fibrosus) undergoes large displacements during the heart cycle, and that the septum motion contributes about 10% of the cardiac output, Korakianitis and Shi (Korakianitis and Shi 2006a, Korakianitis and Shi 2006b) have derived detailed equations to model the septum motion. Ventricular interaction was also considered to be important in cardiovascular dynamics studies by some researchers (Beyar *et al.* 1993, Beyar *et al.* 1987, Chung *et al.* 1997, Maughan *et al.* 1987, Olansen *et al.* 2000, Santamore and Burkhoff 1991, Santamore *et al.* 1990, Slinker *et al.* 1987, Slinker and Glantz 1986, Sun *et al.* 1997). The left and right ventricles are separated by a ventricular septum. During diastole, the imbalance of pressure in the two ventricular chambers produces septum motion, thus causing an interaction in the filling of the two ventricles. In systole the septum also contracts and contributes to the cardiac output. To

model this process the variable elastance model has been further developed to account for the specific response of the left and right ventricular free walls and the ventricular septum. Another interaction extension is to include the effects of the enclosure of the heart in pericardium, recognising that the volume change in one heart chamber would affect the pressure value in the pericardial sac, and thus that the pressure-volume relation in the other three chambers would inevitably be affected. To model this feature, an exponential pressure-volume relation was assumed in the sac, and applied in the calculation of pressure-volume relations in the four heart chambers (Beyar *et al.* 1987, Chung *et al.* 1997, Olansen *et al.* 2000, Santamore *et al.* 1990, Sun *et al.* 1997).

1.4.3 Models of the heart valves

There are four heart valves in the normal heart, the mitral, tricuspid, aortic and pulmonary valves. The valves prevent backflow of blood from the ventricles to the atria during systole (mitral and tricuspid valves) or from the aorta and pulmonary arteries into the ventricles during diastole (the aortic and pulmonary valves). These valves close and open passively under various external effects of pressure gradient across the valve, vortex flow near the valve (Bellhouse 1972, Yacoub *et al.* 1996), shear force acted on the valve leaflet surfaces etc. Extensive analytical, numerical and experimental studies (de Hart *et al.* 2003b, Hose *et al.* 2006, McQueen *et al.* 1982) have been carried out to investigate valve dynamics in three dimensions, but the fundamental mechanics of opening and closure remain difficult to characterise.

The simplest models of the heart valve used in 0D studies featured the valve as a diode plus a linear or nonlinear resistance (Drzewiecki *et al.* 1996, Heldt *et al.* 2002, Pennati *et al.* 1997b, Vollkron *et al.* 2002). The valve has little resistance to the flow when the pressure gradient across it is positive, while the flow is totally stopped when the pressure gradients across it is negative. This idealised description ignores the more complex features of valve dynamics. The complexity of valve motion has been demonstrated *in vivo*: for example, Leyh *et al.* (Leyh *et al.* 1999) conducted trans-thoracic and trans-oesophageal echocardiographic studies on 20 human subjects after different surgical interventions for repair of aortic valves, and found that the valve undergoes a three-stage motion pattern: a rapid early systolic opening, a slow middle systolic closing, and a rapid early diastolic closing movement. Clinical observation has also revealed that the mitral valve has a regression motion that causes the leaflet to

return to the fully open position before the rapid early diastolic closing (Berne and Levy 1981, Levick 2003).

It is clear that real valve motion is a more complex procedure than a simple change of status between open and closed as described by the idealised diode model. Žáček and Krause (Zacek and Krause 1996) considered the change of heart valve resistance during valve motion by using the concept of a time-dependent drag coefficient. In their work the drag coefficient was a prescribed function of the valve open area, and it approached infinity when the valve was closed. The drag coefficients were added to the losses of the conduit in which the valve was situated. Werner *et al.* (Werner *et al.* 2002) described the valve behaviour by including the volume of the reverse flow during the closure phase: in their study this was referred to as the ‘dead space volume’, which was a function of the valve leaflet opening angle and became zero when the valve was fully closed. Shi *et al.* (Shi *et al.* 2004) modelled the valve dynamics by considering the local flow resistance and the blood inertial effect. The valve was described with an orifice model, and the valve opening change was prescribed based on previous experimental observations. To further improve the valve dynamics modelling, Korakianitis and Shi (Korakianitis and Shi 2006c) proposed a more advanced heart valve model, in which the valve dynamics were described by an ordinary differential equation that considered the different effects of pressure gradient across the valve, vortex flow near the valve, shear force acted on the valve leaflet surfaces etc. In this model, the relative importance of these factors was determined by referring to the results of previous two dimensional and three dimensional computational fluid dynamics studies. With these improvements, the model could effectively simulate the valve opening and closing procedures, and the numerical results agreed well with the published results on *in vivo* measurement of valve motions with echo-cardiography (Berne and Levy 1981, Levick 2003, Leyh *et al.* 1999).

1.4.4 Nonlinear effects and external interactions

Although the electrical-hydraulic analogue has been widely used to study cardiovascular dynamics it should be noted that, in contrast to the electrical system, the cardiovascular system can exhibit strong nonlinearities. These nonlinear effects include sympathetic/parasympathetic neuro-regulation, auto-regulation in cerebral and coronary circulation loops, cardio-pulmonary interaction, collapse of vessels due to

environmental pressure, effect of venous valves, and pressure-dependent vessel compliance in the artery etc.

1.4.4.1 Neuro-regulation

The nervous system has an important influence on the cardiovascular changes, through the sympathetic and para-sympathetic nerves. There are baroreceptors in the aortic arch, carotid artery and atrium, which are continuously monitoring blood pressure and blood oxygen levels. When these physiological variables are out of the normal ranges, the baroreceptors trigger the nervous system so that sympathetic and/or parasympathetic nerves are stimulated and regulate cardiovascular response. The sympathetic nerves can trigger arteriole contraction and thus cause an increase in resistance to blood flow and a concomitant decrease in the rate of blood flow through the tissues. Similarly it can decrease the unstressed volume of veins and thus push more blood into the heart for circulation: this in turn causes an increase in heart rate and an increased cardiac pressure and cardiac output. In contrast, action of the parasympathetic nerves causes a marked decrease in heart rate and a slight decrease in heart muscle contractility. Through these mechanisms the nervous system controls the circulation by redistributing blood flow to different areas of the body, increasing or decreasing pumping activity by the heart, and, especially, providing very rapid control of systemic arterial pressure (Guyton 2006). Thus in some physiological conditions, such as posture change or tilting, hypoxia, response to gravitational acceleration, effect of intra-thoracic pressure variation etc., the effect of neuro-regulation on the cardiovascular system becomes too important to be neglected.

Ursino *et al.* have developed an analytical model of neuro-regulation, and combined this model with a multiple compartment cardiovascular model for the simulation of physiological and pathological responses under various conditions of isocapnic hypoxia (Ursino and Magosso 2000a, Ursino and Magosso 2000b), haemorrhage (Ursino 1998), hypercapnia and hypocapnic hypoxia (Magosso and Ursino 2001) and carotid occlusion (Ursino *et al.* 1996). Lu *et al.* (Lu *et al.* 2001) derived detailed models for a fast vagal pathway and three slow sympathetic pathways for the control of heart rate, myocardial contractility and vasomotor tone, and combined the neuro-control model with a cardiovascular system model and a lung mechanics model for the simulation of the cardiopulmonary response under the Valsalva manoeuvre. Green and Miller (Green and

Miller 1973), using an RCR model to describe the systemic vasculature, adopted a simple linear equation to model the neuro-regulation effect of systemic compliance based on arterial pressure, and simulated cardiovascular response to acceleration stress. Melchior *et al.* (Melchior *et al.* 1992) produced a comprehensive review of the mathematical modelling of the human cardiovascular system for the simulation of orthostatic response, including neuro-regulation.

1.4.4.2 Auto-regulation

In any tissue of the body, an acute increase in arterial pressure causes an immediate rise in blood flow. Within less than a minute, however, the blood flow in most tissues returns almost to the normal level, even when the arterial pressure remains elevated. This restoration of flow towards the normal state is called auto-regulation. In contrast with neuro-regulation, which is under the control of the central nervous system, auto-regulation is a local biochemical procedure. The detailed underlying mechanism of auto-regulation is unknown, but the metabolic requirement of the organ and the myogenic response of the vascular smooth muscle are considered to be two of the main causes (Guyton 2006). Auto-regulation has an important influence on the blood flow in several local circulation loops, including the cerebral, renal, and hepatic circulations, and is a requisite component of any model of these subsystems.

Lodi and Ursino (Lodi and Ursino 1999) have published a circulation loop model for the simulation of cerebral circulation dynamics. Based on the metabolic requirement theory for the auto-regulation effect, a sigmoidal auto-regulation curve was developed to relate the pial artery compliance to the cerebral blood flow, and the pial artery resistance was regulated indirectly by the changes in its volume associated with its compliance. Similarly Jeays *et al.* (Jeays *et al.* 2007) developed a model based on myogenic response for the modelling of gut blood flow regulation and postprandial hyperaemia. Cornelissen *et al.* (Cornelissen *et al.* 2002, Cornelissen *et al.* 2000) modelled the auto-regulation effect in coronary circulation by considering the myogenic, flow-dependent, and metabolic flow controls. However, because the underlying mechanisms governing the auto-regulation effect are still under investigation, these modelling efforts are mostly based on incomplete assumptions.

1.4.4.3 Interaction between the cardiovascular system and the respiratory system

The main organs of the cardiovascular system and those of the respiratory system are all situated in the thoracic cavity. For this reason strong interaction exists between the two systems. In modelling the interaction between the cardiovascular system and the respiratory system, Bai *et al.* (Bai *et al.* 1998) developed a combined model for the simulation of cardio-pulmonary response in step-leap respiration exercise for the treatment of cor pulmonale. To account for the respiratory effect on the pulmonary circulation, the volumes of the pulmonary artery and veins were modelled using an exponential function of the intra-thoracic pressure. Lu *et al.* (Lu *et al.* 2001) combined a neuro-control model, a cardiovascular system model and a lung mechanics model for the simulation of cardiopulmonary response under the Valsalva manoeuvre. This model included specific consideration of the effects of pleural pressure on the intra-cardiac pressure and the pressures within the large intra-thoracic blood vessels, and the effect of lung air volume change on the capillary resistance in the pulmonary blood vessels. Lazzari *et al.* (de Lazzari *et al.* 2006) built a cardiovascular model to study the interaction of a ventricular assist device and artificial ventilation, in which the influence of intra-thoracic pressure on the blood flow in the heart, systemic thoracic veins, and pulmonary vessel network was adequately considered.

1.4.4.4 Venous collapse due to environmental pressure

Large veins usually have little resistance to blood flow when they are distended. However, due to the compression action of surrounding tissues and organs, and to the rest state of intra-abdominal and intra-thoracic pressures, veins are usually at least partially collapsed. In these situations, the large veins do usually offer some resistance to blood flow (Guyton 2006). The majority of published cardiovascular studies have focused on the cardiac and arterial systems, whilst veno-dynamics has received less attention,

Fung (Fung 1984) produced a detailed analysis of venous collapse, and derived the detailed analytical formulations that govern the behaviour of the veins in the collapse phase. In the context of lumped-parameter modelling of venous collapse, Lu *et al.* (Lu *et al.* 2001) used an exponential pressure-volume relation for the modelling of the capacitance of systemic veins, with nonlinear and/or piecewise linear equations to

describe the compliance and the resistance of the vena cava as functions of luminal blood volume. Zervides *et al.* (Zervides *et al.* 2008) derived pressure-dependent venous resistance, compliance and inductance. Beyar *et al.* (Beyar *et al.* 1987) modelled the venous resistance as linear function of the difference between the peripheral and central vena cava pressures when the peripheral venous pressure is less than zero, and as a constant value when the peripheral venous pressure is greater than zero. Ursino *et al.* (Ursino 1999, Ursino *et al.* 1996) modelled the pressure-volume relation of the peripheral and venous vessels as a nonlinear exponential function. In simulating venous circulation, Snyder and Rideout (Snyder and Rideout 1969) applied a higher compliance value (by twenty times) for the collapsed veins compared with that for un-collapsed ones, determining the current state by comparison of the current volume of a venous segment with its unstressed volume. Peterson *et al.* (Peterson *et al.* 2002) applied a similar model in the simulation of the influence of gravity and posture on cardiac performance. In simulating the interaction between the native cardiovascular system with an intra-aortic balloon pump, Barnea *et al.* (Barnea *et al.* 1990) represented the pressure-volume relation of systemic veins by a fifth order polynomial approximation.

1.4.4.5 Effect of venous valves

The valves in the veins are arranged so that the direction of blood flow (except for local and temporary changes due to venous compliance) can be only towards the heart. Every time a person moves the legs or even tenses the leg muscles, a certain amount of venous blood is propelled toward the heart. Thus valves in the veins have an important role in countering the tendency of some changes in posture (and associated gravitational changes) to cause flow away from the heart (Guyton 2006). Zervides *et al.* (Zervides *et al.* 2008) modelled the venous valve as a diode to allow no backflow, and also reported on the effects of simple modifications to account for swept-volume flow reversal and for a leaky valve. Beyar *et al.* (Beyar *et al.* 1987) simulated the venous valve by assigning different resistance values to the valve subjected to positive or negative pressure gradients. Similarly, Snyder and Rideout (Snyder and Rideout 1969) simulated the venous valve by a two diode configuration in which the resistance to the reverse flow was different from that for the forward flow.

1.4.4.6 Pressure-dependent constitutive equations and vessel properties

Most often in the 0D model descriptions and solution methods, the component values (R, L and C) are taken to be constant. However, since these represent real physical parameters they are subject to the same nonlinearities as any other description of vascular mechanics, namely geometrical and material nonlinearities. As the vessel diameter changes under changes of pressure, its compliance will change as will its resistance to flow. The vessel wall exhibits a nonlinear stress-strain curve (Fung 1993), meaning that the compliance C is also a function of the luminal pressure. Furthermore the vessel wall material is visco-elastic. However, given that the diameter changes in the arterial system are relatively small (order of 10%), and that the range of arterial pressures over the cardiac cycle is such that the material tends to operate in a relatively linear region of the stress-strain curve, it is possibly justifiable to neglect the pressure dependence of the arterial properties. This is not so for the veins, at least when they enter a collapsed state.

To address the pressure-dependence of the constitutive equations for vessels, several researchers have proposed models based on *in vivo* measurements or on theoretical derivations. Ursino *et al.* (Ursino 1999, Ursino *et al.* 1996) used a linear pressure-volume relationship to model the arteries in the simulation of carotid baro-regulation of pressure pulsation. Fogliardi *et al.* (Fogliardi *et al.* 1996) carried out *in vivo* experimentation to further test the linear and nonlinear formulation of the RCR model, and based on the experimental results commented that no additional physiological information was gained when a pressure-dependent compliance throughout the heartbeat was incorporated in the three-element Windkessel, compared with that using a constant compliance. They also reported that the nonlinear model did not significantly improve the approximation of diastolic pressure in the presence of an evident oscillation. In contrast, Li *et al.* (Berger and Li 1992, Li *et al.* 1990) adopted an exponential variation of arterial compliance with pressure changes, applied the proposed relation in a three element RCR vessel model, and came to the conclusion that a pressure-dependent compliance could more accurately predict aortic and stroke volume. Cappello *et al.* (Cappello *et al.* 1995) developed a one-step computational procedure for estimating the parameters of the nonlinear RCR model of the arterial system incorporating a pressure-dependent compliance.

Coronary vessels are subject to a different mechanical environment compared with that of other arterial vessels, associated with the large myocardial stresses generated in systole. For the simulation of coronary vessels Geven *et al.* (Geven *et al.* 2004) modelled the resistance of the coronary capillary bed as a linear function of left ventricular pressure in systole, and as a constant value in diastole. Bovendeerd *et al.* (Bovendeerd *et al.* 2006) used 20 times larger values for the coronary arterial, coronary myocardial and coronary venous resistances in normoxia compared to those in hyperemia. Barnea *et al.* (Barnea *et al.* 1990) modelled the coronary arterial resistance as a linear function based on the pressure difference between the aortic pressure and venous pressure and the pressure difference between the aortic and ventricular pressure. Smith *et al.* (Smith *et al.* 2002) modelled the resistance and the compliance of the coronary arterioles, capillary and venules as function of both arteriolar and venular pressures. Spaan *et al.* (Spaan *et al.* 1981) developed a model for the coronary loop in which the resistances of the coronary arteriole and veins changed under auto-regulation, and the same group (Cornelissen *et al.* 2002, Cornelissen *et al.* 2000) added myogenic, flow-dependent, and metabolic flow control to coronary flow modelling. The developed model has been validated (Kolyva *et al.* 2008, Verberne *et al.* 2007) through *in vivo* measurements.

In summary, it might be deemed necessary to consider the pressure-dependent vascular properties in the coronary vessels and in the veins, but the argument for their usage in other arteries is less compelling.

1.4.5 Integrated cardiovascular system models

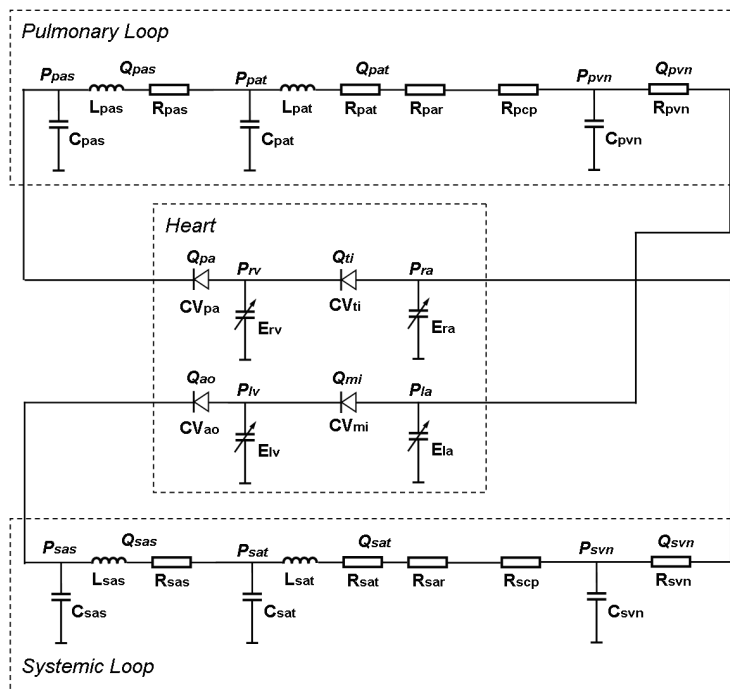


Figure 1-5 A sample complete circulatory system model

(Refer to nomenclature table for name of each component in the figure)

Numerous 0D integrated system models have been developed by assembling component models of the vasculature, the heart and the heart valve, according to the needs of particular studies. The simplest system models represent the whole vasculature as two element (RC) or three element (RCR) Windkessels (Berger and Li 1992, Cavalcanti and Belardinelli 1996, Diaz-Zuccarini and LeFevre 2007, Drzewiecki *et al.* 1996, Green and Miller 1973) whilst more comprehensive models feature multiple vascular compartments (Beyar *et al.* 1987, Burkhoff and Typerg 1993, Santamore and Burkhoff 1991, Ursino 1999, Ursino *et al.* 1996, Zacek and Krause 1996), sometimes with the important local branches represented individually (Chen *et al.* 2008, Heldt *et al.* 2002, Lu *et al.* 2001, Olansen *et al.* 2000, Pennati *et al.* 1997a, Snyder and Rideout 1969, Sun *et al.* 1997, Ursino 1998, Ursino and Magosso 2000a, Ursino and Magosso 2003, Werner *et al.* 2002). The most common model of the heart in an integrated system model is the varying elastance model and the most common heart valve model is a simple diode. Figure 1-5 shows a typical integrated cardiovascular system model developed by Shi and Korakianitis (Shi and Korakianitis 2006).

A special case of 0D modelling is that of the specific study of the local circulation characteristics in some important vascular subsystem, such as cerebral, coronary, renal or lower extremity, where often multiple compartment models have been designed to include such features as complex anastomoses, auto-regulation effects and sometimes collapsible vessels and internal valves. Most commonly these detailed local simulations have not included a heart model, and usually flow rates and/or pressures are directly applied as boundary conditions. Examples of these types of models are those proposed by (Bovendeerd *et al.* 2006, Geven *et al.* 2004, Lodi and Ursino 1999, Manor *et al.* 1994, Pennati *et al.* 1997a, Snyder and Rideout 1969, Ursino 1991, Ursino and Giulioni 2003, Ursino *et al.* 1995, Ursino *et al.* 2000).

1.4.6 Commentary on the 0D model developed in this thesis

Plenty of 0D cardiovascular models have been developed and published over the past decades, as introduced above. Each of these models was developed to address a specific research question, and there is no universally optimal model that perfectly suits every application case. The researcher's task is not just to develop the model, but also to keep a balance between accuracy and efficiency in model construction.

There are several specific challenges that are addressed in the work collected in this thesis. The aim has been to develop a model, or series of models, of appropriate complexity to study circulatory response under some typical disease conditions such as systemic/pulmonary hypertension, heart failure and haemorrhage. For this purpose the current author considered the following features to be important:

1. To describe the general cardiovascular response observed in clinical practice, including the cardiac, cardio-pulmonary, and systemic changes, the model should have both the systemic loop and the pulmonary loop, and the four chamber heart;
2. To investigate the blood pressure changes in different parts of the vessel, the blood vessel should be modelled as a multi-segment configuration for both the systemic and pulmonary loops;
3. Heart valve opening and closing processes contribute significantly to the circulatory response, but these were not simulated in previous models. The heart valve dynamics should be modelled in the new model to be developed;

4. Atrial contraction promotes the ventricular filling, especially in the exercise condition. This feature was neglected in more than half of previous models, and should be included in the new model to be developed;
5. There is a hypothesis (Korakianitis 2003) that the atrial-ventricular septum works as an auxiliary pump in the circulation system and contributes to the overall cardiac output, although this effect had not been quantified. To investigate this effect, MRI measurements of cardiac dynamics were conducted in a healthy volunteer. The data obtained appeared to confirm the hypothesis (Roditi 2004). This is a new feature which deserves to be considered in cardiovascular modelling.

Based on these considerations, the author developed an improved circulatory system model, as presented in (Korakianitis and Shi 2006a, Korakianitis and Shi 2006b) and detailed in Chapter 2 of this thesis. The model has three main parts: heart; systemic circulation loop; and pulmonary circulation loop. The heart is modelled as a four chamber pump with variable elastance and four heart valves that control the blood flow direction. The systemic and pulmonary circulation loops are each separated into aortic sinus/pulmonary artery sinus, artery, arteriole, capillary and vein segments. In every segment the individual component is modelled by considering the local resistance to blood flow, elasticity of blood vessels, and inertia of blood. The ventricles are modelled with the varying elastance model, while the left and right atriums are modelled in the similar way but with different timing for elastance variation to simulate the atrial contraction in end diastole. The four heart valves are modelled with differential equations describing the momentum balance on the valve leaflet due to actions of pressure, shear stress, vortex, blood kinetics etc. The atrial-ventricular septum motion is simulated by considering the force balance on the septum, including the forces of cardiac muscle stretching, septum gravity, and pressure difference.

Deriving the governing equations formed the skeleton of the model, while to make the model work another important task is to properly set the model parameters. This is not straightforward because there are a number of model parameters to be decided, while there are limited clinical data to support the evaluation of these model parameters. Previous researchers have shared their experience and published their choice of model parameters (Cappello *et al.* 1995, Deswysen *et al.* 1980, Fogliardi *et al.* 1996, Grant and Paradowski 1987, Li *et al.* 1990, Liu *et al.* 1986, Lucas *et al.* 1988, Quick *et al.*

1998, Stergiopoulos *et al.* 1995, Wesseling *et al.* 1993, Westerhof *et al.* 2009, Yoshigi and Keller 1997). These provide a good starting point. However, in comparing these previous parameter settings it was observed that there were much discrepancy and contradiction among these data. In facing this situation, the author's strategy was first to collect as much clinical data as possible from the literature, and then used reverse-deduction to find the reasonable ranges of model parameters. The deduced parameter ranges were then compared with the data adopted by previous researchers. This process supported the selection of a set of parameters that were most consistent with the underlying physiology and with the wider literature, and thus were considered most reliable. The author then used these more reliable parameters as the starting point and conducted a series of numerical experiment to tune his own model, finally found the optimal parameter combination that produced the results best matching the clinically observed responses.

The improved model was first tested by comparing the simulated typical cardiovascular response with the clinical data reported in the open literature. Not only the trends of the simulated response curves including the atrial pressure, cardiac flow, and atrial/ventricular volumes matched the clinical observations, but also the ranges/amplitudes of the simulation data agreed well with the clinical data. Besides these fundamental agreements, the improved model also effectively simulated the cardiovascular features of E/A ratio in mitral flow, the dicrotic notch in aortic pressure, and the a wave in the atrial pressure, which had been mostly neglected in previous models. The model also revealed that the motion of the atrial-ventricular septum contributes about 10% of extra cardiac output compared to the situation when the septum motion was not considered. Such comparison suggested that inclusion of new modelling features of heart valve dynamics, atrial contraction, and atrial-ventricular septum motion had contributed positively to the improvement and refinement of the simulation quality.

As an initial application study and also for further validation, the developed model was used to study the cardiovascular response under valve disease conditions (Korakianitis and Shi 2006c). Two representative cases of mitral stenosis and aortic regurgitation were investigated and the simulation results were compared with the clinical data. The developed model not only duplicated the changes in atrial/arterial pressures, mitral/aortic flows and atrial/ventricular volumes, but also the three-stage heart valve

motion pattern of fast opening-slow opening-fast closing as observed in the clinical ultra-sound examination, while this three-stage valve motion pattern has never been simulated by previous researchers.

Overall, the author’s model achieved a good balance between accuracy and efficiency, and satisfactorily simulated the previously identified cardiovascular features.

1.4.7 Applications of 0D models

0D models are widely used in various areas of cardiovascular studies, from basic cardiovascular physiology research to astronautic medicine and design analysis of cardiovascular artificial organs. Typical applications of 0D cardiovascular models are summarised in Table 1-6.

Table 1-6 Typical applications of 0D model

Application	Model feature	Examples
Analysis of the systemic arterial flow characteristics	Only the arterial network is modelled	<p>Characteristics of the three- and four-element Windkessel models (Jager <i>et al.</i> 1965, Noordergraaf 1978, Noordergraaf <i>et al.</i> 1963, Segers <i>et al.</i> 2008, Stergiopoulos <i>et al.</i> 1999, Toorop <i>et al.</i> 1987, Westerhof <i>et al.</i> 1969, Westerhof <i>et al.</i> 1971);</p> <p>Advantages and disadvantages of using the three element RCR model as aortic input impedance (Burkhoff <i>et al.</i> 1988);</p> <p>Comparison of different configurations of three element and four element models as the embryonic aortic impedance (Yoshigi and Keller 1997);</p> <p>Investigation of aortic input impedance in infants and children by curve fitting to two, three and four element Windkessel models (Sharp <i>et al.</i> 2000);</p> <p>Study of the linear and nonlinear formulations of the three element Windkessel model by considering the pressure-dependent capacitance effect in the arterial network (Cappello <i>et al.</i> 1995, Fogliardi <i>et al.</i> 1996, Li <i>et al.</i> 1990);</p> <p>Two port analysis to extend the Windkessel models by considering the venous side flow pulsations in the systemic loop (Frasch <i>et al.</i> 1996, Rose and Shoukas 1993);</p> <p>Ventricular-systemic arterial coupling (McIlroy and Targett 1988).</p>
Hemodynamic response in the	Complete description of	Cardiovascular response in normal healthy subjects (Zacek and Krause 1996);

<p>native cardiovascular system under various healthy and diseased conditions</p>	<p>the native cardiovascular system</p>	<p>Study of the ventricular interaction effect (Santamore and Burkhoff 1991).</p> <p>Modelling the dysfunction in regional stunned myocardium of the left ventricular (Drzewiecki <i>et al.</i> 1996) ;</p> <p>Modelling of cardiac muscles in the study of mechanics and energetics of fibrillating ventricle (Yaku <i>et al.</i> 1991);</p> <p>Study of changes in pulmonary venous pressure after the onset of left ventricular dysfunction (Burkhoff and Typerg 1993).</p>
<p>Hemodynamic changes under various surgical and therapeutical interventions.</p>	<p>The native cardiovascular system was partly changed.</p>	<p>Circulation dynamics in the presence of the bidirectional cavopulmonary anastomosis in children with a uni-ventricular heart (Pennati <i>et al.</i> 1997b);</p> <p>Rest and exercise hemodynamics in patients with total cavopulmonary connection (Magosso <i>et al.</i> 2002);</p> <p>Modelling the hemodynamic characteristics in patients with hypoplastic left heart syndrome after the palliative Norwood operation (Migliavacca <i>et al.</i> 2001);</p> <p>Study of the cardiovascular response in patients with right ventricular bypass and uni-ventricular circulation support (Kresh <i>et al.</i> 1990);</p> <p>Modelled the cardiovascular control adaptations in chronic renal failure patients (Lerma <i>et al.</i> 2004);</p> <p>Modelling of the hemodynamic response to hemodialysis induced hypovolemia (Cavalcanti and Di Marco 1999).</p> <p>Modelling of the cardio-pulmonary response under step-leap respiration exercise for the treatment of patients with Cor Pulmonale (Bai <i>et al.</i> 1998).</p>
<p>Ventricular assist device support for heart failure</p>	<p>The native cardiovascular system was in heart failure condition, and a VAD model is coupled.</p>	<p>Studies of cardiovascular response in the heart failure condition supported with various types of VADs (Choi <i>et al.</i> 2001, Cox <i>et al.</i> 2009, de Lazzari <i>et al.</i> 2006, Ferrari <i>et al.</i> 2013, Giridharan and Skliar 2002, He <i>et al.</i> 2005, Pekkan <i>et al.</i> 2005, Shi and Korakianitis 2006, Vandenberghe <i>et al.</i> 2002, Vollkron <i>et al.</i> 2002);</p> <p>Studies of cardiovascular response in the heart failure condition supported with intra-aortic balloon pumps (Barnea <i>et al.</i> 1990, Fresiello <i>et al.</i> 2013, Khir <i>et al.</i> 2005, Schampaert <i>et al.</i> 2013a);</p> <p>Comparison of the assistance action of different types of VAD and VAD motion profiles (Shi <i>et al.</i> 2007);</p> <p>Study of the effect of the inlet and outlet cannulation sites for connecting the VADs to the native cardiovascular system (Korakianitis and Shi 2007);</p>

		Study of the physiological control of pulsatility gradient in rotary blood pump (Arndt <i>et al.</i> 2008, Shi <i>et al.</i> 2010).
Study of cardiovascular response under neuro-regulation	The native cardiovascular system was coupled with the models for the nervous system	<p>Simulate the cardiovascular responses under neuro-regulation in various conditions of isocapnic hypoxia (Ursino and Magosso 2000a, Ursino and Magosso 2000b), haemorrhage (Ursino 1998), hypercapnia and hypocapnic hypoxia (Magosso and Ursino 2001), carotid occlusion (Ursino <i>et al.</i> 1996);</p> <p>Simulation of cardiopulmonary response in Valsalva manoeuvre (Lu <i>et al.</i> 2001);</p> <p>Simulation of circulation system response to acceleration stress (Green and Miller 1973);</p> <p>Simulation of the cardiovascular response to orthostatic stress (Heldt <i>et al.</i> 2002).</p>
Study of special and local circulation loops in the cardiovascular system.	Only the local circulation loop was modelled, and arterial pressure or flow-rate was applied as upstream boundary condition.	<p>Simulation of human foetal cardiovascular system (Pennati <i>et al.</i> 1997a);</p> <p>Studies of cerebral auto-regulation effect (Ursino 1991, Ursino and Giulioni 2003), cerebral vasospasm (Lodi and Ursino 1999), acute brain damage (Ursino <i>et al.</i> 1995), and cerebral hemodynamics during arterial and CO₂ pressure change (Ursino <i>et al.</i> 2000);</p> <p>Modelling of coronary local circulation loop (Manor <i>et al.</i> 1994);</p> <p>Study of dependence of intra-myocardial pressure and coronary flow on ventricular loading and contractility (Bovendeerd <i>et al.</i> 2006, Geven <i>et al.</i> 2004);</p> <p>Study of venous valves in pressure shielding in the lower extremity (Zervides <i>et al.</i> 2008);</p> <p>Simulation of venous circulation in lower extremities (Snyder and Rideout 1969).</p>
As boundary condition in multi-scale simulation of cardiovascular dynamics	The 0D circulation system model was coupled with the distributed parameter models (1D, 2D or 3D).	Multi-scale simulation of the cardiovascular dynamics (Formaggia <i>et al.</i> 2006, Liang <i>et al.</i> 2009, Migliavacca <i>et al.</i> 2006, Pontrelli 2004, Watanabe <i>et al.</i> 2004).

1.4.8 Commentary on 0D modelling applications reported in this thesis

The author has applied his 0D model to study the cardiovascular response in a number of application cases (Korakianitis and Shi 2006c, Korakianitis and Shi 2007, Shi 2008,

Shi *et al.* 2011a, Shi and Hose 2009, Shi and Korakianitis 2006, Shi *et al.* 2007, Shi *et al.* 2010, Shi *et al.* 2011c). Chapters 3 to 5 of the thesis reported three selected cases.

1.4.8.1 Case study 1: Modelling of cardiovascular response under pulsatile impeller pump support

This study is presented in Chapter 3. In recent years, there has been strong interest in the study of circulatory response under the heart failure condition with artificial heart support (Mahmood *et al.* 2000). The main driving force behind this is the ever-increasing number of heart failure patients. Changes of life style and food structure in the modern society, together with increasing longevity, enormously increase the occurrence of cardiovascular diseases including heart failure. For those end stage heart failure patients whose cardiac muscles are so compromised that they are not responsive to pharmaceutical stimulations (Birks *et al.* 2006, Frazier *et al.* 2004), the only long-term treatment option is cardiac transplantation. However, the number of donor hearts available is always far less than required. During the long waiting period for the donor hearts, the blood circulation of the patient needs to be supported with ventricular assist devices (VAD). In principle, VAD is a mechanical blood pump that works alongside and bypasses the patient's native heart, so that the blood circulation in the patient is mainly driven by the VAD instead of the diseased heart.

Table 1-7 Comparison of the two traditional types of VADs

Displacement pump	Impeller pump
First generation of VAD design, has longer history	New generation of design
Bulky, has more moving parts, and thus has more chances to develop mechanical failure	Small size, has less moving parts, and thus has less chance to develop mechanical failure
Produces pulsatile blood flow, similar to that in the physiological condition	Produces steady flow (no pressure/flow pulse)
Less likely to cause damage to blood cells	More likely to cause damage to blood cells due to high rotating speed of the rotor
More chances of infection	Less chances of infection
Expensive	Relatively cheap

Current VAD related studies cover several directions, from the fundamental device characteristics study (Bourque *et al.* 2001, Chou *et al.* 2001, Gobel *et al.* 2001), to the assistance effects of the VAD (Biglino *et al.* 2010, Biglino *et al.* 2008, de Lazzari *et al.*

1994, Ferrari *et al.* 2011, Fresiello *et al.* 2013, Khir 2010, Khir 2011, Khir *et al.* 2005, Khir *et al.* 2003, Khir *et al.* 2006, Schampaert *et al.* 2013a, Schampaert *et al.* 2011), physiological VAD control (Abe *et al.* 1998, Arndt *et al.* 2008, Barnea *et al.* 1992, Bullister *et al.* 2002, Casas *et al.* 2007, Drzewiecki *et al.* 1990, Giridharan and Skliar 2003, Hsu 2004, Nakata *et al.* 1999, Ohuchi *et al.* 2004, Olegario *et al.* 2003, Waters *et al.* 1999, Wu *et al.* 2003) and VAD clinical application studies (Ei-Banayosy *et al.* 2000, Frazier *et al.* 2004, Stevenson and Rose 2003). Engineering and medical researchers are both active in the area.

Currently there are two types of commercial VAD products available on the market for middle to long term patient support. One is the displacement pump, and the other is the impeller pump (also called rotary pump) (Mahmood *et al.* 2000). The displacement pump VAD design was developed to resemble the working of the human native heart. In the pump there are two mechanical heart valves equipped at the inlet and outlet of the pump flow channels to keep the one-way flow direction. The main VAD working area is an elastic chamber whose wall was driven by either a mechanical or a pneumatic mechanism to produce a periodic volume change in the chamber, to simulate the contraction and relaxation of the human native heart chamber in a heart cycle. The alternative design of impeller pump VAD is quite similar to the impeller pump used for delivering water or oil in industrial applications, in which a rotor is continuously rotating inside a stator chamber and driving the blood from the pump inlet to the outlet against a pressure difference of about 100mmHg. Table 1-7 compares these two types of VADs. Generally each of these two traditional VAD designs has its advantages and disadvantages (Takatani 2001). Compared to the displacement pump, the impeller pump has the advantages of compactness, no valves, a simpler control system, lower power consumption and reduced cost, thus giving it greater market potential. However, the impeller pump is designed to work under the constant rotating speed mode, and thus produces no pressure pulse in the patient body. Besides these two types of VADs for middle to long term usage, there is another type of VAD called intra-aortic balloon pump (IABP), developed specifically for short term circulatory support. IABP is a balloon type device inserted to the ascending aorta of the patient through the femoral artery, and the balloon is inflated and deflated periodically in phase to the contraction of the patient native heart, to assist the diseased heart in pumping more blood to the peripheral organs. Khir and co-workers (Biglino *et al.* 2012, Biglino *et al.* 2010,

Biglino *et al.* 2008, Ferrari *et al.* 2011, Fresiello *et al.* 2013, Khir 2010, Khir 2011, Khir *et al.* 2005, Khir *et al.* 2003, Khir *et al.* 2006) had worked extensively on experimental and numerical studies of cardiac response with IABP support, and specifically studied the influence of patient posture on the IABP functioning.

While the discussion on the physiological importance of the pressure pulse in maintaining normal blood perfusion to the human body has continued for many years, a major part of the arguments were about whether the pressure pulse is important in maintaining the normal cardiovascular physiology in patients supported with VAD (Chow *et al.* 1997, Ei-Banayosy *et al.* 2000, Isoyama *et al.* 2000, Khir *et al.* 2006, Koenig *et al.* 2004, Potapov *et al.* 2000, Qian 1996, Qian *et al.* 2000, Sezai *et al.* 1999, Undar 2003, Undar 2004, Undar *et al.* 1999, Undar *et al.* 1998). In recent years some researchers (Sezai *et al.* 1999, Undar 2004) claimed that pressure pulse has an important effect on cardiovascular physiology: it promotes kidney and liver perfusion, and promotes microcirculation at the cell level which is important in the early treatment of acute heart failure. Also some clinical evidence (Frazier *et al.* 2004, Undar 2003) seemed to suggest that patients supported with impeller pumps has more chances to develop cerebral complications than patients supported with displacement pumps, given other clinical conditions being same.

In such a situation, some researchers (Chou *et al.* 2001, Gobel *et al.* 2001, Qian 1996, Vandenberghe *et al.* 2005) proposed to generate the pressure pulse in the patient body by periodically modulating the rotating speed in the impeller pump in each heart cycle, with the hope to enjoy the benefits of both types of VADs. They have worked along this line and reported their initial successful *in vitro* results. In reviewing their works, it is apparent that there were some negative response data to which the authors, perhaps surprisingly, provided no comments. For example, significant regurgitant pump flow was identified in (Qian 1996, Qian *et al.* 2000) (Vandenberghe *et al.* 2005); strong negative pressure was developed at the pump inlet in (Gobel *et al.* 2001). These are all deleterious effects that should be avoided in VAD applications.

To validate the idea of producing pulsatile cardiac flow by modulating the pump speed in impeller pump, the current author adapted his model for the 0D analysis of this procedure (Shi *et al.* 2011a, Shi *et al.* 2010). The study is reported in Chapter 4 of this thesis. The author started by investigating the HeartMate® III impeller pump (Thoratec Corp, CA, USA). This pump was chosen because HeartMate® is a well-established

brand, and the detailed pressure-flow characteristics of the pump are available in the open literature (Bourque *et al.* 2001). In carrying out the study, the author used a polynomial to fit the pressure-flow curves of the pump. In the study the pump inlet was cannulated to the left ventricular apex and the outlet to the ascending aorta. A sinusoidal change with horizontal offset was specified as the motion profile in the pump. The horizontal offset determined the mean pump flow so that the general pump output approximates the normal cardiac output of $5L/min$, and the sinusoidal speed variation was chosen because this causes minimal mechanical impact in the pump. Both the amplitude of the sinusoidal change and the phase lag between the sinusoidal change and the native ventricular contraction were changed to observe the cardiovascular response under different pump speed modulation conditions. The physiological variables of atrial pressure, arterial pressure, ventricular pressure, ventricular volume, and cardiac output etc. were observed and compared for different study cases. Generally the results shows that it is impossible to find a proper motion profile for the HeartMate® III impeller pump so that the pump speed can be effectively manipulated to produce physiologically meaningful arterial pressure pulsation (as suggested by the literature, a minimum arterial pressure pulsation of 15mmHg is considered as physiological meaningful). In a small number of conditions a pressure pulsation of 15mmHg can be purposely induced in the pump, but at the same time strong flow regurgitation also developed in the pump, which enormously decreases the pump efficiency and would cause undesirable complications of pulmonary hypertension, thus these situations should be avoided.

The conclusion with the HeartMate® III impeller pump cannot be directly extrapolated to other impeller pumps, as the cardiovascular response is closely related to the specific pumps in use. Having examined the HeartMate® III pump, the author extends the same study to the Berlin Heart InCor® impeller pump (Berlin Heart GmbH, Berlin, German). To standardise and quantify the comparison of different cardiovascular conditions, in Chapter 3 the author constructed a performance index to reflect the deviation of the cardiovascular response from that of the ideal healthy condition. The performance index was defined as a weighted average of the important cardiovascular variables including the cardiac output, atrial pressure, arterial pressure, ventricular pressure, ventricular volume, ejection fraction etc. The same pump speed modulation strategy used in HeartMate® study was applied in the Berlin Heart InCor® study. Results for

the Berlin Heart InCor® pump supported the same conclusion as that for the HeartMate® III pump. Overall, the evidence collected so far does not support the idea of producing physiologically meaningful arterial pressure pulsation by modulating the pump speed in the impeller pump.

1.4.8.2 Case study 2: Physiological control of VAD

This study is elaborated in Chapter 4. The majority of end stage heart patient patients need to live with VAD support for a long period of time during their waiting for donor heart available (Reul and Akdis 2000). During the waiting period, patients go back home and lead normal family lives. They will experience different physiological conditions, from rest to taking up some mild exercise, and emotional variations etc. Such changes in the physiological conditions are usually accompanied by variations in cardiovascular response. How to adapt the VAD support to match the variations of cardiovascular needs is an important issue to consider. Current commercial VAD products all require human intervention in such situations. During transition of physiological conditions the VADs need to be tuned manually by experienced technicians, or the patients are trained to adjust the VAD working by themselves (Reul and Akdis 2000). Such manual tuning is inefficient and unsafe. It is highly imperative for some automatic control algorithms to be implemented in the VAD control unit, to automatically tune the VAD working to suit the changes of body needs in different physiological conditions.

The fundamental aim of VAD control is to deliver the tailored amount of cardiac output to suit the oxygen and nutrients demands in the patient body in different physiological conditions, and at the same time maintaining the normal level of arterial pressure so that the important peripheral organs receive proper blood perfusion at all times. The arterial pressure approximately equals the product of the cardiac output and the vascular impedance. Since the blood vessels in the patient body often have different degrees of dilation or contraction in response to the disease condition, which already changes the vascular impedance, it is impossible to accurately control both the cardiac output and the arterial pressure in the patient body to match that of the healthy condition. At best, only one of these two is precisely controlled while the other is maintained within a reasonable range.

Besides the fundamental control aim above, there are advanced aims to be addressed in VAD control. These include: 1) to meet further metabolic requirements of the patient body by maintaining physiological variables of heart rate, ejection fraction, arterial pressure, blood oxygen saturation level, blood pH level, partial pressure of carbon dioxide in the blood etc. all in the normal range; 2) to make the patient feel comfortable during the transition of the physiological condition, 3) to monitor the VAD working for fault detection, auto diagnosis and auto correction; and 4) to minimise the energy consumption of the VAD during its working. These requirements are difficult to meet at the same time, and some of them are even hard to quantify with clearly defined physical variables. The majority of published research focuses only on the fundamental aim of controlling either the cardiac output (Abe *et al.* 1998, Choi *et al.* 2001, He *et al.* 2005, Hsu 2004, Klute *et al.* 1992, Saito *et al.* 1999, Yoshizawa *et al.* 1992) or the arterial pressure (Barnea *et al.* 1992, Bullister *et al.* 2002, He *et al.* 2005, Kosaka *et al.* 2003, Wu *et al.* 2003).

The current author started his research on VAD control by choosing the new VAD design of reciprocating valve pump as the object of study (Shi *et al.* 2011c). The detailed study is presented in Chapter 4 of this thesis. The reciprocating valve pump has several advantages over the traditional VAD designs in that it causes no damage to the cardiac muscle and no fusion of the heart valve (Shi and Korakianitis 2006, Shi *et al.* 2007), while these two problems are common in patients implanted with either the displacement pump or the impeller pump. The mean arterial pressure was selected as the target variable because this helps to simplify the control algorithm design. In using the cardiac output as the control target, it is necessary to prescribe the optimal cardiac output that corresponds to each specific physiological condition (rest or exercise). While by maintaining a constant mean arterial pressure, the cardiac output produced will be automatically regulated by the vascular impedance change in the patient body.

For the implementation of the VAD control, the author used the pressure at the VAD outlet as the surrogate for the arterial pressure, and adopted the proportion-integration-differentiation (PID) control law to control the stroke of the VAD based on the arterial pressure feedback. Previous researchers have used PID control as well as some other more complex control algorithms such as optimal control (Barnea *et al.* 1992, He *et al.* 2005, Klute *et al.* 1992), fuzzy logic (Choi *et al.* 2001, Hsu 2004), or modern linear feedback control (Kitamura and Gross 1990) in their studies. Compared to these more

complex control algorithms PID control, although simple, has been applied in industrial practice for decades and has proven to be more efficient, more robust, and a more reliable control law in dealing with all kinds of strong non-linearity in the systems. More important is that PID control can be implemented without knowing the accurate mathematical model of the system. By enhancing the traditional PID algorithm with a simple online tuning capability, the parameters for the PID controller can be automatically determined through analysing the response in a limited number of trial conditions. During system operation, if the environment conditions change significantly, the online tuning module can also automatically tune the PID parameters to suit the changed situation and still maintain the optimal response in the system.

In the research the PID control algorithm was tested against a representative case of transition between the rest condition and mild exercise condition. The corresponding results were compared with that has no VAD control. Results proved that the controller design could satisfactorily regulate the VAD motion to suit the change of physiological conditions. Following this initial success, in the next stage effort needs be made to construct a more comprehensive control index, to address some of the advanced control aims whilst maintaining the arterial pressure or the cardiac output.

In implementing the VAD control system, some researchers (Ayre *et al.* 2000) proposed the idea of using the intrinsic VAD voltage or current signals for the estimation of arterial pressure or cardiac output changes, in order to save the usage of transducers. This is an attractive idea, but with some limitations. VAD voltage or current signal is influenced by both the pre-load and the after-load to the VAD. Arterial pressure and cardiac output are related only to the after-load of the VAD. From the change in VAD voltage or current signal alone it is difficult to judge whether the change is due to pre-load or after-load variation. Thus the current author thinks it is still preferable to use a physical transducer to measure the arterial pressure changes.

1.4.8.3 Case study 3: Design optimisation of cardiovascular bioreactor

This study is detailed in Chapter 5. Lumped-parameter modelling is a generic research method. Any engineering, biological or social system, whose dynamics can be described by a group of mixed algebraic and ordinary differential equations, can be effectively studied with the lumped-parameter modelling technique.

In the past decades, tissue and cell level cardiovascular research are receiving ever increasing attention among researchers, with the expectation that regenerative medicine and molecular biology will revolutionise medical practice in the future (Basu and Ludlow 2012, Fisher *et al.* 2013). In tissue engineering studies, the bioreactor is the indispensable equipment that is used to provide the suitable biological environment during the tissue or cell growing (Sodian *et al.* 2002). Over the years the bioreactor design has experienced enormous changes (Barron *et al.* 2003, Chen and Hu 2006, Martin *et al.* 2004, Martin and Vermette 2005, Portner *et al.* 2005). Early designs of bioreactors focused on providing the necessary nutrients, pH level, temperature, and humidity environment to the growing tissue and cells. In such designs, the growing tissue or cells are immersed in a liquid growing medium, and the growing medium is routinely replenished or replaced to meet the required biochemical and physical conditions for tissue/cell growing. Later on, it was recognised that pressure and shear stress have important regulation effects on the tissue and cell growth. To mimic the shear stress stimulation on the growing tissue and cells, the second generation of bioreactors designs were proposed and put into usage, in which either the growing medium chamber was sloshing periodically, or a water pump was used to circulate the growing medium at a constant speed inside the bioreactor. These improved designs still suffer the constraint that the shear stress and pressure cannot be accurately controlled to reproduce the periodic variations representative of the physiological condition. More sophisticated third generation designs were developed in recent years. These advanced bioreactor designs function like a mock circulation system rig enhanced with biochemical (pH level, nutrients) and environmental condition (temperature, humidity) controls, using mechanical and electric components assembly to produce periodic pulsatile flows to mimic the pressure and shear stress stimulus needed during tissue and cell growth. The biochemical and environmental condition control (i.e., nutrients, pH level, temperature etc.) part were generally similar to that in previous designs, while the more complex motion control part in these sophisticated bioreactor designs demands more careful design considerations. To achieve prescribed periodic pressure and shear stress variations representative of that in the human body, not only the geometry of the growing chamber needs to be optimised, but also the motion control mechanism and the motion profile need to be carefully chosen and evaluated. Such a procedure is not intuitive and requires several repetitions of the design-evaluation-revision cycle. This is an area in which numerical simulation can play an important part for the optimisation

of the system design. However, up to now relatively few experimental studies of bioreactor design have been reported in the open literature (Narita *et al.* 2004, Sodian *et al.* 2002, Sodian *et al.* 2001), and there is no system level modelling has been conducted to optimise the bioreactor system dynamics.

In filling the gap, this author applied the 0D modelling technique to study a typical bioreactor design proposed by previous researchers. The bioreactor design has much similarity to a simplified human circulation system supported with a displacement pump type VAD. The upper and lower medium chambers as well as the tissue construct behave like a weakened heart chamber. A silicon diaphragm pump activated by a pneumatic source produces volume and pressure variations in the medium chambers, just like a pneumatically activated VAD supports the weakened ventricle in the human body. Two one-way valves maintain the flow direction in the same way as the heart valves. Silicon connecting tubes and a medium reservoir function as the vessel network, to form a closed loop and to store the mass fluid for circulation. As the system dynamics is dominated by the transformation and conversion between the kinetic energy and the potential energy, due to the effects of frictional loss, component elasticity, and medium fluid inertia in the system, the hydraulic-electric analogue concept in 0D cardiovascular modelling can be applied to analyse the bioreactor system dynamics. By deriving the governing equations for the mass and momentum balance in the bioreactor system, a 0D model was constructed for the analysis of the system level hydro-dynamics in the bioreactor. The model parameters were assigned to match those in the experimental design in the literature. Simulation results agreed well with that in the previous experimental studies of (Narita *et al.* 2004, Sodian *et al.* 2002, Sodian *et al.* 2001).

Modelling of hydro-dynamics in pulsatile bioreactors concerns both system level lumped-parameter study and component level distributed-parameter study. System level study is implemented using 0D modelling and is used for the evaluation of pressure and flow profiles in the reactor. This main aim of such study is to decide the optimal system configuration and ensure that the expected pressure changes can be realised in the system. Based on the simulated flow change and the geometry of the tissue construct and medium chamber, 0D modelling can also provide an initial estimation of the shear stress level in the system. The component level study is based on CFD calculation in the local area of the tissue construct for the investigation of

velocity and shear stress distributions, as implemented in (Davidson *et al.* 2003, Dubey *et al.* 2006, Singh *et al.* 2007, Williams *et al.* 2002, Zeng *et al.* 2006). This type of study is mainly applied to evaluate the flow distribution related effects on the tissue/cell growth, for example: 1) to evaluate the mechanical damage to the growing tissue or cells based on the predicted shear stress distribution; or 2) to identify the under-perfused zones in the tissue construct caused by flow stagnation, based on the predicted velocity distribution. Such information can be used as reference for further optimisation of the bioreactor geometry. When combined with mass transportation modelling and empirical equations for tissue/cell growth, this study can also predict the flow modulated tissue/cell growing process in the bioreactor. Due to the computing expense involved, this study is not suitable for simulating the pressure profile as predicted by the system level 0D modelling. These two levels of studies should be applied in combination to provide a comprehensive simulation analysis of the hydro-dynamics in the bioreactor. This is also part of this author's plan for the next stage of bioreactor modelling.

1.4.9 Multi-scale modelling

The cardiovascular system is a closed network, and there are strong interactions between its components. Emphasis on either only the global circulation dynamics or only the local flow features can provide only partial information of the whole cardiovascular response. In recent years there have been rapid developments in the application of multi-scale modelling techniques, in which 0D models are coupled with 1D, 2D and/or 3D models to form complete representations of the cardiovascular system, as reviewed by van de Vosse in (van de Vosse 2003). Typically local haemodynamics is computed in an anatomically realistic detailed 3D model of the organ or region of interest, and boundary conditions for this domain are provided by coupled or uncoupled 0D or 1D system models. Quarteroni (Quarteroni 2001) reviewed the development of cardiovascular system modelling, and gave a basic introduction of the concept of multi-scale modelling. When coupling 0D and 1D models, pressure and flow can be directly exchanged at the interface of the two types of models (Pontrelli 2004) (Formaggia *et al.* 1999). A special issue that arises when coupling 0D/1D models to 2D/3D models is that of dealing with the problem of defective boundary conditions: the lack of distribution information makes the flow-rate description in 0D/1D models insufficient to be applied as conditions for 2D/3D models. Possible solutions include

mapping of flow-rates from 0D/1D models to a velocity distribution based on Womersley's solutions (Womersley 1955, Womersley 1957) for transient flows in a long tube (Formaggia *et al.* 2001). Based on these coupling strategies, multi-scale has experienced enormous development in recent years, and has been extensively applied in the numerical simulation of aortic flow (Formaggia 2009, Formaggia *et al.* 2001, Formaggia *et al.* 2006, Formaggia *et al.* 1999, Formaggia and Veneziani 2003, Kim *et al.* 2009, Kroon *et al.* 2012, Liang *et al.* 2009, Migliavacca *et al.* 2006, Milisic and Quarteroni 2004, Olufsen 1999, Stergiopoulos *et al.* 1998, Taylor *et al.* 2010, Taylor *et al.* 2001, Wan *et al.* 2002), coronary flow (Formaggia 2009, Formaggia *et al.* 2006, Formaggia *et al.* 1999, Smith *et al.* 2004), and cerebral flow (Kroon *et al.* 2012, Mulder 2011, Mulder *et al.* 2011).

1.5 Structure of the thesis and authors' contributions to the papers included in each chapter

This thesis reports a series of 0D cardiovascular modelling studies selected from the author's previous works in the area. These studies form a coherent description of the author's previous 0D modelling works with applications to cardiovascular related research, while each chapter also stands on its own and focuses on a specific sub-direction within the overall framework. This chapter introduces the background knowledge of cardiovascular circulation, reviews the concurrent 0D cardiovascular modelling research, and comments on the works reported in the following chapters. Chapter 2 introduces the development of an improved lumped-parameter cardiovascular model that includes the effects of atrial contraction, atrial-ventricular septum motion, and heart valve dynamics. Chapter 2 is based on the following two papers:

- Korakianitis T., Shi Y., A Concentrated Parameter Model for the Human Cardiovascular System Including Heart Valve Dynamics and Atrio-ventricular Interaction, *Medical Engineering & Physics*, 28(7), pp613-628, 2006
- Korakianitis T., Shi Y., Effects of Atrial Contraction, Atrio-ventricular Interaction, and Heart Valve Dynamics on Human Cardiovascular System Response, *Medical Engineering & Physics*, 28(8), pp762-779, 2006

For these two papers, Shi Y designed the study, conducted the research, drafted and revised the papers. Korakianitis T revised and submitted the papers.

Chapters 3 to 5 present three application cases of the 0D cardiovascular modelling, using the model elaborated in Chapter 2. Chapter 3 is about a numerical study of the cardiovascular response under the heart failure condition supported with the varying speed impeller pump type VAD, which is based on the following two papers:

1. Shi Y., Brown A., Arndt A., Nuesser P., Lawford P., Hose R., Numerical Modelling and Evaluation of Cardiovascular Response under Pulsatile Impeller Pump Type VAD Support, *Journal of the Royal Society: Interface Focus*, 1(3), pp320-337, 2011
2. Shi Y., Hose R., Lawford P., Numerical Modelling of Hemodynamics with Pulsatile Impeller Pump Support, *Annals of Biomedical Engineering*, 38(8), pp2621-2634, 2010

For these two papers, Shi Y designed the study, conducted the research, drafted and revised the papers. Shi Y and Hose R worked on the design of a physiological index for the evaluation of cardiovascular response in paper 1. Brown A participated in revision of paper 1. Lawford P revised the papers. Hose R revised the papers and approved submission of paper 1 and 2. Arndt A and Nuesser P provided the pump performance data and approved the submission of paper 1.

Chapter 4 explores the topic of VAD feedback control and is based on the paper:

- Shi Yubing, Shi Yuhui, Korakianitis Theodosios, Physiological Control of an In-series Connected Pulsatile VAD: Numerical Simulation Study, *Computer Methods in Biomechanics and Biomedical Engineering*, 14(11), pp995-1007, 2011

For this paper, Shi Yubing designed the study, conducted the research, drafted, revised and submitted the paper. Shi Yuhui participated in the development of the control algorithm. Korakianitis Theodosios approved the submission.

Chapter 5 extends the 0D modelling technique for the study of the hydraulic response in a cardiovascular bioreactor. This chapter is based on the paper:

- Shi Y., Numerical Simulation of Global Hydro-dynamics in a Pulsatile Bioreactor for Cardiovascular Tissue Engineering, *Journal of Biomechanics*, 41(3), pp953-959, 2008

For this paper, Shi Y designed the study, conducted the research, drafted, revised and submitted the paper.

Chapter 6 summarises the works reported in this thesis, explain the some on-going research as the extension of the reported study, and suggests the future directions for

further research breakthroughs. The last section of this chapter is adapted from the paper:

- Shi Y., Lawford P., Hose R., Review of Zero-D and 1-D Models of Blood Flow in the Cardiovascular System, *Biomedical Engineering Online*, 10:33, 2011

For this paper, Shi Y conducted the review, drafted and revised the paper. Lawford P revised the paper. Hose R overviewed the review work, revised the paper and approved the paper submission.

Chapter 2 Development of a Lumped Parameter Model for the Human Cardiovascular System Including Heart Valve Dynamics and Atrio-ventricular Interaction¹

Numerical modelling of the human cardiovascular system has always been an active research direction since the 19th century. In the past, various simulation models of different complexity were proposed for different research purposes. In this chapter an improved numerical model to study the dynamic function of the human circulation system is proposed. In the development of the mathematical model, the heart chambers are described with a variable-elastance model. The systemic and pulmonary loops are described based on the resistance-compliance-inertia concept by considering local effects of flow friction, elasticity of blood vessels, and inertia of blood in different segments of the blood vessels. As advancement from previous models, heart valve dynamics and atrio-ventricular interaction, including atrial contraction and motion of the annulus fibrosus, are specifically modelled. With these improvements the developed model can predict several important features that were missing in previous numerical models, including regurgitant flow on heart valve closure, the value of E/A velocity ratio in mitral flow, the motion of the annulus fibrosus (called the KG diaphragm pumping action). These features have important clinical meaning and their changes are often related to cardiovascular diseases. Successful simulation of these features enhances the accuracy of simulations of cardiovascular dynamics, and helps in clinical studies of cardiac function.

2.1 Introduction

Numerical simulation of physiological and pathological changes in the human cardiovascular system has its origin in the 19th century (Nichols and O'Rourke 1990),

¹ Adapted from:

- Korakianitis T., Shi Y., A Concentrated Parameter Model for the Human Cardiovascular System Including Heart Valve Dynamics and Atrio-ventricular Interaction, *Medical Engineering & Physics*, 28(7), pp613-628, 2006
- Korakianitis T., Shi Y., Effects of Atrial Contraction, Atrio-ventricular Interaction, and Heart Valve Dynamics on Human Cardiovascular System Response, *Medical Engineering & Physics*, 28(8), pp762-779, 2006

and it has become an active research area in the past decades with the development of computer technology. Various mathematical models have been proposed to study the dynamics of the cardiovascular system. General models in this area can be classified as distributed parameter models and Lumped Parameter models. Distributed parameter models are mostly used in investigations of local dynamics in certain parts of the cardiovascular system, including the heart (Baccani *et al.* 2002), heart valves (Cacciola *et al.* 2000, Shi *et al.* 2003), and blood vessels (Einav *et al.* 1988), with computational fluid dynamics (Baccani *et al.* 2002, Shi *et al.* 2003), finite element analysis (Cacciola *et al.* 2000), transmission line method (Einav *et al.* 1988, Myers and Capper 2002) etc. In contrast, Lumped Parameter models (also called concentrated parameter models) are mostly used to study the global response of the circulation system, and although sometimes a local part is studied, the ultimate target of research with Lumped Parameter models is still the global response of the system.

Lumped Parameter modelling in the cardiovascular system began with the Windkessel model proposed by Otto Frank in 1899 to model the general resistance and capacitance effects of systemic blood vessels (Nichols and O'Rourke 1990, Noordergraaf 1978). Later this evolved into: the modified Windkessel model (for instance (Sharp and Dharmalingam 1999)); nonlinear viscoelastic property study of vessel segments (Barnea *et al.* 1990); pressure-dependent description of veins (Barnea *et al.* 1990, Lu *et al.* 2001); pressure-dependent description of venae cavae (Lu *et al.* 2001); pressure-dependent compliance effect of the arteries (Berger and Li 1992, Li *et al.* 1990); and variable resistance effect of arterioles (Ursino 1998). In recent years several fractal models of the blood vessel have been proposed (Brown 1996, Grasman *et al.* 2003). The early discussion on heart models was on whether the characteristics of the ventricle are better described as a pressure driven or a flow-rate driven phenomenon, as referred to by Leef *et al.* (Leefe and Gentle 1995). In the 1970s Suga *et al.* (Suga *et al.* 1973) proposed a variable elastance model for the ventricle. This model attracted the attention of most researchers, and it has been widely used from then on (Barnea 1994, Barnea *et al.* 1990, Berger and Li 1992, Burkhoff *et al.* 1988, Drzewiecki *et al.* 1996, Heldt *et al.* 2002, Lu *et al.* 2001, Olansen *et al.* 2000, Pennati *et al.* 1997a, Pennati *et al.* 1997b, Santamore and Burkhoff 1991, Sun *et al.* 1997, Thomas *et al.* 1997, Ursino 1998, Ursino *et al.* 1996, Ursino and Magosso 2000a, Ursino and Magosso 2000b, Ursino and Magosso 2003, Vollkron *et al.* 2002, Yaku *et al.* 1991). Some researchers even

extended this model to study the atrial contraction effect (Pennati *et al.* 1997a, Sun *et al.* 1997, Vollkron *et al.* 2002). New activation functions for this model also evolved in recent years (Ottesen and Danielsen 2003). Besides modelling the heart chamber, some researchers also studied intra-ventricular interaction (Chung *et al.* 1997, Olansen *et al.* 2000, Santamore and Burkhoff 1991, Sun *et al.* 2000), postulating that this crosstalk between the two neighbouring ventricles affects the global dynamic response. However, in a critical review Melchior *et al.* (Melchior *et al.* 1992) implicitly questioned the importance of intra-ventricular interaction.

Models of neurological regulation in the cardiovascular system have also been developed. Closed-loop regulation models of the cardiovascular system were proposed in which the pressure signal in the baroreceptor was fed back for combined sympathetic and parasympathetic control of the heart rate, ventricle contractility, arteriole resistance and vein tone (Heldt *et al.* 2002, Lu *et al.* 2001, Sun *et al.* 1997, Ursino 1998, Ursino 1999, Ursino *et al.* 1996, Ursino and Magosso 2000a, Ursino and Magosso 2000b, Ursino and Magosso 2003). These studies have seen promising applications in areas such as orthostatic response in training of astronauts, study of physiological processes like haemorrhagic shock, and so on.

These studies greatly improved our understanding of cardiovascular dynamics, but there are still areas unexplored in the modelling work. One issue is the detailed analysis of heart valve dynamics. In the human heart four heart valves work together to keep the blood flowing in one direction. Heart valve dynamics greatly influence the pressure and flow-rate changes in the heart. In previous investigations these heart valves were mostly modelled as diodes plus a linear or nonlinear resistance (Drzewiecki *et al.* 1996, Heldt *et al.* 2002, Pennati *et al.* 1997a, Pennati *et al.* 1997b, Vollkron *et al.* 2002). This description puts more emphasis on the ideal characteristic of one-way flow in the heart valve, while the more complex aspects of valve dynamics were ignored, so that realistic features of local hemodynamics such as regurgitant flow were not simulated. Žáček and Krause (Zacek and Krause 1996) used the concept of a time-dependent drag coefficient to describe the heart valve in their simulation. In their work the drag coefficient is a function of the valve open area, and it approaches infinity when the valve is closed. The drag coefficients were added to the losses of the conduit where the valve was situated. Werner *et al.* (Werner *et al.* 2002) described the valve dynamics by introducing the concept of dead-space volume, which is the volume of

fluid contained in the valve region. The dead-space volume is a function of the valve leaflet opening angle, and the volume is zero when the valve is fully closed. These two models improved heart valve modelling, but the leaflet motion was prescribed instead of computed, so that the blood-leaflet interaction effect, which dominates the leaflet dynamics, was not considered.

Yacoub *et al.* (Yacoub *et al.* 1996) studied the aortic outflow and the aortic root, and suggested that aortic flow is a tale of dynamism and crosstalk between the blood and the surrounding structures including sinuses of Valsalva, valve cusps, and the contracting ventricle chamber. Besides the contraction motion of the ventricle, the aortic root and valve cusps also have smooth muscles that contribute to the crosstalk. In this complex interaction vortices form in the sinuses of Valsalva. These vortices play an important role in smooth valve opening and closure, and aid coronary flow. This opinion gives a realistic and in-depth description of physiological phenomena in aortic flow.

Due to limitations in research methods and computing facilities, realistic modelling of blood-valve dynamics can only be carried out with considerable simplifications, e.g. by omitting the contraction and elasticity of the valve cusps and aortic root, ignoring the effect of vortices in the sinuses of Valsalva, and considering only the effect of pressure difference and shear stress in the valve. Some research work has been carried out in this direction (de Hart *et al.* 2003a, de Hart *et al.* 2000, de Hart *et al.* 2003b, Kiris *et al.* 1997, Lai *et al.* 2002, Makhijani *et al.* 1996a, Makhijani *et al.* 1996b, Makhijani *et al.* 1997, Shi *et al.* 2003).

In the current research such distributed-parameter description for the valve function is adapted and included within the concentrated-parameter study for the overall dynamic model of the circulation system. This helps to simulate the aortic notch in aortic pressure, and the regurgitant flow on valve closure, which are important features in revealing pathological and physiological changes in clinical diagnoses. In comparison to previous models that treated the heart valves as diodes combined with resistances, or modelled the valve dynamics but used prescribed leaflet motion, the proposed model improves the accuracy of the simulations

Another issue is the atrio-ventricular interaction effect, which was analysed and termed the KG diaphragm by Korakianitis and Grandia (Korakianitis and Grandia 2003),

because it acts as a diaphragm pump (as opposed to a dividing septum like the atrial septum). Kilner *et al.* (Kilner *et al.* 2000) briefly discussed the role of this atrio-ventricular interaction in their research of asymmetric redirection of flow through the heart. Power (Power 1979) modelled this effect with a first order differential equation in his numerical simulation of systemic circulation. However, in Power's analysis only the pressure difference and the elastic force in the septum were considered, while the active stretching actions of the atrial and ventricular chamber walls were ignored. With Power's model, in the systolic phase the KG diaphragm would bulge into the atrial chamber due to increased ventricular pressure. This result is exactly contrary to what happens under the physiologic systole condition, in which the KG diaphragm is pulled into the ventricular chamber due to the active contractile action of the surrounding ventricle wall. In the work reported here, the contribution of the KG diaphragm motion to cardiac dynamics is modelled by including the effect of nearby tissue stress on the KG diaphragm, based on the MRI measurements on a healthy human volunteer.

The current work is a further contribution in cardiovascular system modelling. In this study a numerical model of the whole human circulation system is presented, which includes several phenomena that were not simulated in previous models. The heart chambers are described with the variable-elastance model as proposed by Suga *et al.* (Suga *et al.* 1973). Features of atrial contraction motion, the pumping effect of the motion of the KG diaphragm, and dynamics of the heart valves are specifically included in the proposed model. In the simulations the developed model is solved with a 4-stage Runge-Kutta method to study the system response under the action of these features.

2.2 Method

2.2.1 MRI Measurement of Cardiac Dynamics

As preliminary experimental study of cardiac dynamics for this work, and in order to provide suitable inputs to the numerical models, an MRI measurements of geometric changes in the four heart chambers of a healthy human subject was carried out. The subject was scanned with a 1.5-T Philips Gyroscan ACS-NT MRI system (release 8.1, Philips Medical Systems, Best, The Netherlands) utilizing a 5 element cardiac phased array coil. Vectorcardiographic ECG gating equipment was employed for accurate cardiac synchronisation. Survey images were first obtained, and subsequent breath-hold

balanced fast field echo (steady state free precession) cine images were performed in: left heart 2 chamber; short axis 2 chamber; and horizontal long axis 4 chamber orientations, in order to plan standard planes for cardiac short-axis imaging. In these short-axis measurements 20 slice levels (6mm thick with zero gap) that spanned from the apex of the ventricles to the cardiac base (including the atria) were captured. At each level cine imaging was performed using sensitivity encoding parallel acquisition to allow 30 phases per cardiac cycle in a breath-hold, with a field of view of 420mm and an image matrix of 256×256. The in-plane resolution was 1.6mm. Similar multi-slice, multi-phase cine imaging was performed in trans-axial planes with similar parameters. Corroborative phase contrast quantitative flow imaging for flow curves was performed across both the aortic root and right ventricular outflow tract with retrospective ECG gating and a temporal resolution of 35 cardiac phases per heart cycle.

Post-processing consisted of evaluating volume changes for each chamber with cardiac analysis software (EasyVision release 4.2, Philips Medical Systems, Best, The Netherlands) to delineate the endocardial contours of the chambers. Functional parameters were derived i.e. end-diastolic volume, end-systolic volume, stroke volume and volumetric ejection fraction. The individual images were also saved in TIFF format and exported to a CAD program SolidEdge (version 14.0, Electronic Data System Corporation, Texas, USA) for reconstruction of the three-dimensional geometries of the heart chambers.

The motion trend of the KG diaphragm observed from the MRI measurements provided the basis for qualitative comparison with the results predicted in the current numerical simulation. The maximum and minimum displacements of the KG diaphragm were used for parameter setting in modelling the atrio-ventricular interaction effect. As measurement of the KG diaphragm motion is not currently a standard procedure in clinical practice, point to point tracking of the two-dimensional or reconstructions of the three-dimensional KG diaphragm motion during the heart cycle was not automatically supported in the MRI system. The motion trend of the KG diaphragm was estimated (with computer graphics applications) from the MRI movies, and used for qualitative comparison with the simulation results. This measurement of the KG diaphragm pumping motion and pumping action deserves further investigations in future clinical and modelling research.

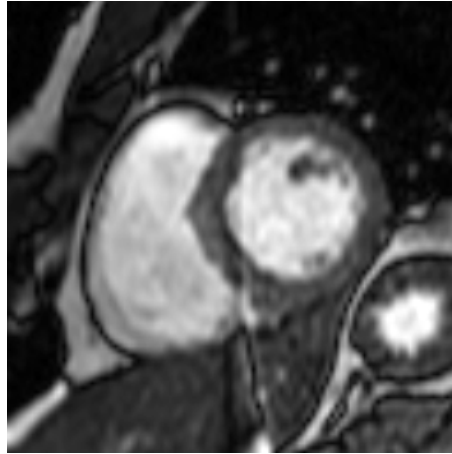


Figure 2-1 Short axis MRI slice in diastolic phase

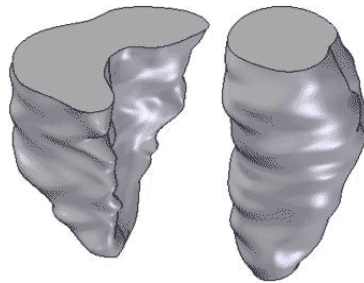


Figure 2-2 SolidEdge images of the lower portions of ventricle geometries in diastole, reconstructed from MRI measurements

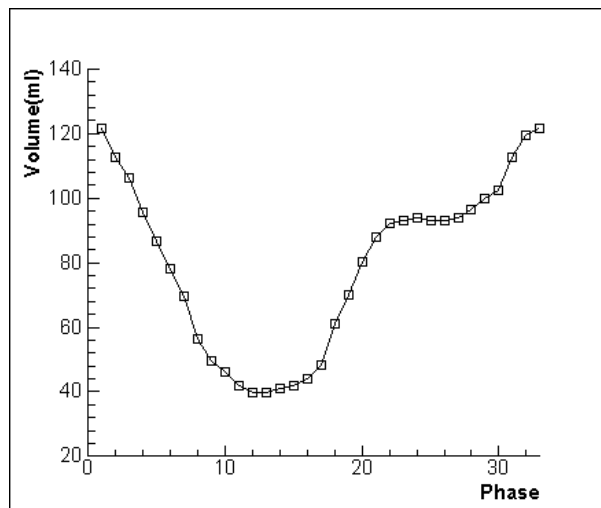


Figure 2-3 Volume change of left ventricle measured from MRI data

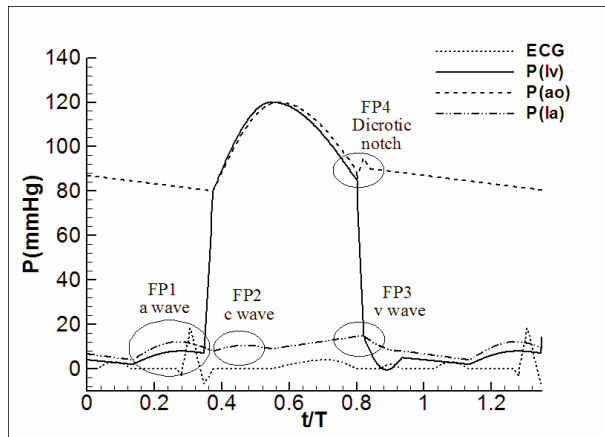
Figure 2-1 shows one of the MRI short axis images in the end diastolic phase. SolidEdge images of the lower portions of the corresponding three-dimensional geometry of the left and right ventricles reconstructed from the MRI image data are shown in Figure 2-2. Figure 2-3 gives the volume change of the left ventricle during a

heart cycle, and agrees very well with other experimental measurements of the volume trace presented, for instance, in (Bowman *et al.* 2004, Chen *et al.* 1997), and that shown in physiology textbooks, for instance (Berne and Levy 1981, Boron and Boulpaep 2003, Guyton 1986, West 1990).

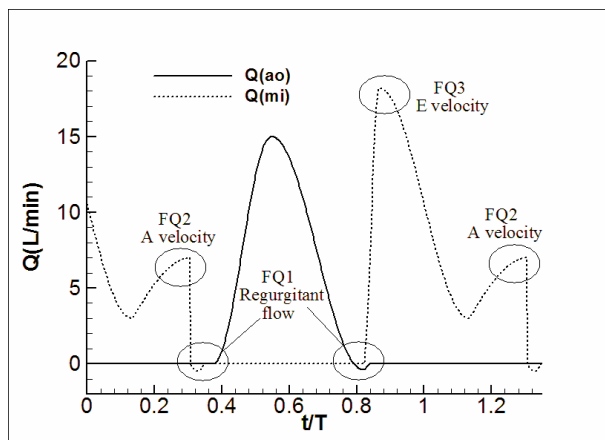
From these the typical volume response is constructed as illustrated in Figure 2-4 (c), which clearly demonstrates local volume increase due to atrial contraction. Figure 2-4 (c) already covers the main features of Figure 2-3, and Figure 2-4 gives other additional details of the pressure and flow-rate changes in a typical heart cycle. Therefore, in the discussion of the results comparisons are made mainly with Figure 2-4, while the volume change in Figure 2-3 and the motion of the KG diaphragm observed in the MRI measurements are also referred to when appropriate. Image sequences in these MRI measurements revealed that due to interaction between the atrium and the ventricle, the KG diaphragm moves along the long axis of the adult heart for about $0.02 \sim 0.03m$ in each heart cycle. The area around the aorta does not move significantly during the heart cycle, and most of the KG diaphragm motion, and corresponding pumping action, is attributed to motion of the annulus fibrosus around the mitral valve. This motion of the mitral-valve annulus fibrosus of the KG diaphragm contributes about $8 \sim 12ml$ to the volume change of each heart chamber, which is more than 10% of the total $70ml$ stroke volume. This pumping action of the KG diaphragm affects the physiological response of the heart, and is specifically modelled in the numerical approach presented in this chapter.

2.2.2 Conceptual Illustration of General Cardiac Response

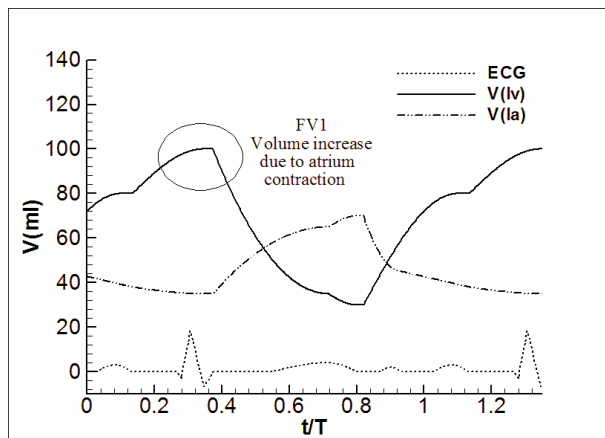
Figure 2-4 shows conceptually the general trends of physiological changes including pressure, flow-rate and volume variations in one heart cycle in the cardiovascular system. These drawings are constructed based on general information on cardiovascular physiology published in textbooks and journals (Berne and Levy 1981, Boron and Boulpaep 2003, Guyton 1986, Nageh *et al.* 1999, Nichols and O'Rourke 1990, Sohn *et al.* 1997, West 1990). Besides the normal trends and parameter ranges, several important features are specifically emphasized in these figures, which are mostly absent in the simulation results of previous research.



(a) Pressure



(b) Flow-rate



(c) Volume

Figure 2-4 Illustration of the systemic loop response of the cardiovascular system during a typical healthy heart cycle

(Important features in the pressure, flow and volume responses are marked in the figure. Refer to the main text for detailed explanations)

In Figure 2-4 (a) illustrating the pressure changes, four features are emphasized:

1. FP1: At the end of diastolic phase, due to the atrial contraction, local peaks exist in both atrial and ventricular pressure response. In atrial pressure, this is called the *a* wave (Guyton 1986). In those previous studies that neglected atrial contraction, the *a* wave is missing.

2. FP2: During the early part of systole, accompanying the rapid contraction in the ventricles is a bulging of the mitral/tricuspid valves towards the atria, which causes a pressure surge in the atria. This pressure surge is called the *c* wave (Guyton 1986). This feature is produced by the elasticity of the mitral and tricuspid valves, and is missing in simulation results that neglected the elasticity effect of the valves. Usually this feature is not so obvious (Perloff 2000, Timmis *et al.* 1997), and it is exaggerated in Figure 2-4 (a) in order to be shown clearly.

3. FP3: During systole, the mitral valve is closed, while blood continuously enters the atrial chamber and accumulates. This process continues until the mitral valve opens at the beginning of the next diastole. This process produces a local pressure peak in the atrium, which is called the *v* wave (Guyton 1986). In previous studies that included the model of the atrium as an elastic chamber this feature might be simulated, while in those studies that neglected atrial compliance this feature is missing.

4. FP4: In the late stage of the systolic phase, accompanying the closure of the aortic and pulmonary valves, there is a pressure surge in the aorta and pulmonary artery, which originates from the closing motion of the leaflets in the aortic and pulmonary valves. This pressure surge is called the “dicrotic notch” (Nichols and O'Rourke 1990). Most previous studies neglected valve closure dynamics, so that this feature is missing from the simulation results.

The flow-rate changes in Figure 2-4 (b) emphasize three characteristic features:

1. FQ1: At the end stages of diastolic and systolic phases, accompanying closing of the mitral and aortic valves, there is corresponding regurgitant flow. Most previous studies neglected valve dynamics, thus the regurgitant flow was not simulated.

2. FQ2 and FQ3: Transmitral flow velocity is an important physiological variable in evaluating heart function. Echocardiography measure of transmitral flow velocity shows that there are two local peaks in mitral flow, early (*E*) and late (*A*) transmitral flow velocity. The *E* velocity peak corresponds to the initial filling flow in early diastole, and the *A* velocity peak is due to atrial contraction. The ratio of early to late

velocities (E/A) is in the range of 1 to 2 (Nageh *et al.* 1999, Sohn *et al.* 1997). In previous studies that neglected atrial contraction, the local peak of flow-rate that corresponds to the A velocity is missing. The E velocity peak is always simulated in previous simulations, however whether the atrium is considered as a chamber with constant or variable elastance will affect the simulation accuracy.

In the volume changes in Figure 2-4 (c), feature FV1 represents the volume jump in late diastolic phase due to atrial contraction, which was also observed in the MRI measurement results illustrated in Figure 2-3.

2.2.3 Mathematical Model

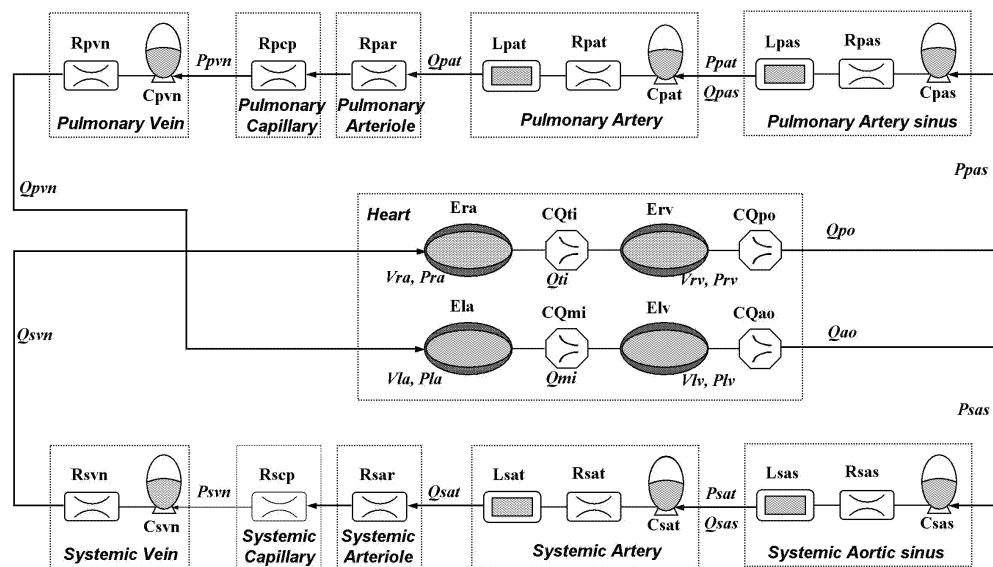


Figure 2-5 Schematic of the circulation system model

(The model includes a four chamber heart with heart valves, a systemic loop and a pulmonary loop each divided into the aorta/pulmonary artery, arteries, arterioles, capillaries, and veins. Refer to the nomenclature table at the front pages of the thesis for the detailed name of each model component.)

Components of the whole circulation system are modelled as illustrated in Figure 2-5 in three main parts: heart; systemic circulation loop; and pulmonary circulation loop. The heart is modelled as a four chamber pump with variable elastance and four heart valves that control the blood flow direction. The systemic and pulmonary circulation loops are each separated into aortic sinus/pulmonary artery sinus, artery, arteriole, capillary and vein segments. In every segment the individual component is modelled by considering the local resistance to blood flow, elasticity of blood vessels, and inertia of blood. The

combined effect of venule, vein and vena cava is modelled as the vein segment. The artery segment represents the general characteristics of both the main and smaller arteries. The aortic sinus is separated from the artery to facilitate estimation of pressure response in the aortic arch.

2.2.3.1 Ventricle

Basic ventricular characteristics are described with the pressure-volume relation with the widely-used Suga *et al.*'s variable elastance model (Suga *et al.* 1973), in which the ventricular pressure is described as a linear function of the chamber volume and the chamber elastance. The chamber volume is decided by the flow-rate difference between the inlet and the outlet of the chamber, while the chamber elastance varies in a heart cycle representing the action of the heart muscle.

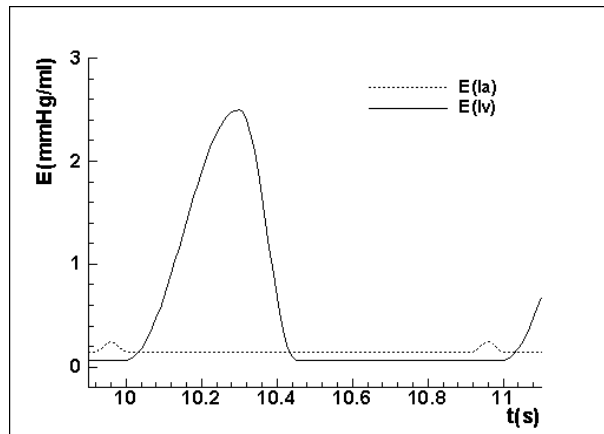


Figure 2-6 Elastance change in the left ventricle and left atrium during a typical heart cycles

The volume change rate in the left ventricle is equal to the flow-rate difference between mitral and aortic valves:

$$\frac{dV_{lv}}{dt} = Q_{mi} - Q_{ao} \quad (2-1)$$

The time-varying ventricle elastance is a function of the characteristic elastance ($E_{lv,s}$ and $E_{lv,d}$) and an activation function $\bar{e}_{lv}(t)$:

$$e_{lv}(t) = E_{lv,d} + \frac{E_{lv,s} - E_{lv,d}}{2} \bar{e}_{lv}(t) \quad (2-2)$$

The activation function $\bar{e}_{lv}(t)$ describes the contraction and the relaxation changes in the ventricular muscle. Ottesen and Danielsen (Ottesen and Danielsen 2003) compared several forms of activation functions in their work and investigated their applicability.

Generally these activation functions have only slight differences in shapes due to different assumptions used in model derivation. A commonly used activation function is adopted here:

$$\bar{e}_{lv}(t) = \begin{cases} 1 - \cos\left(\frac{t}{T_{s1}}\pi\right), & 0 \leq t < T_{s1} \\ 1 + \cos\left(\frac{t - T_{s1}}{T_{s2} - T_{s1}}\pi\right), & T_{s1} \leq t < T_{s2} \\ 0, & T_{s2} \leq t < T \end{cases} \quad (2-3)$$

The left ventricular elastance change in a typical heart cycle obtained using this activation function is illustrated in Figure 2-6. The pressure in the left ventricle is then derived from the instantaneous volume and elastance values in the ventricle:

$$P_{lv} = P_{lv,0} + e_{lv}(V_{lv} - V_{lv,0}) \quad (2-4)$$

The motion of the annulus fibrosus also affects volume changes in the heart, as described in the following sections. The model for the right ventricle is similar to that for the left side, except the values of parameters are different.

2.2.3.2 Atrium

Following the P wave in the ECG signal, the atrium contracts and leads to a rapid rise in the ventricular end-diastolic volume and pressure. This effect is sometimes called the “atrial kick”, which contributes about 20% to 30% of ventricular filling volume and reflects the “booster pump” function of the atrium (Guyton 1986, West 1990). Features FP1, FQ2 and FV1 in Figure 2-4 reflect the influence of this action. In those previous studies that ignored atrial contraction, these features are missing.

In describing the left atrium, the modelling process is very similar to that for the left ventricle. Again Suga *et al.*'s variable elastance model (Suga *et al.* 1973) is adopted, while the values of parameters and the form of the activation function are adapted to represent the dynamic changes in the atrium. To analyse the effect of atrial contraction, the system models both with and without consideration of atrial contraction are adopted. When the atrial contraction effect is ignored, the atrium elastance $e_{la}(t)$ is set to a constant value of $E_{la,min}$. When the atrial contraction effect is considered, the atrium elastance is represented with variable elastance model, as used by (Pennati *et al.*

1997a, Pennati *et al.* 1997b, Thomas *et al.* 1997, Vollkron *et al.* 2002, Zacek and Krause 1996):

$$e_{la}(t) = E_{la,\min} + \frac{E_{la,\max} - E_{la,\min}}{2} \bar{e}_{la}(t) \quad (2-5)$$

in which the atrium activation function is set as:

$$\bar{e}_{la}(t) = \begin{cases} 1 - \cos\left(\frac{t - T_{pwb} + T}{T_{pww}} 2\pi\right), & 0 \leq t < (T_{pwb} + T_{pww} - T) \\ 0, & (T_{pwb} + T_{pww} - T) \leq t < T_{pwb} \\ 1 - \cos\left(\frac{t - T_{pwb}}{T_{pww}} 2\pi\right), & T_{pwb} \leq t < T \end{cases} \quad (2-6)$$

The corresponding elastance change in the left atrium in a typical heart cycle obtained using this activation function is illustrated in Figure 2-6. In the right atrium the governing equations are similar, except the values of parameters can be different.

2.2.3.3 Atrio-ventricular Interaction

The KG diaphragm is a soft tissue which includes the annulus fibrosus and the four heart valves. In the native heart the KG diaphragm undergoes periodic displacement into the atrial or ventricular chambers under the combined action of several forces. Figure 2-7 illustrates a portion of the KG diaphragm and the forces acting on it in the vicinity of the mitral valve. These include: the pressure force $(P_{lv} - P_{la}) \cdot A_{savv}$ which is due to the pressure difference across the valves and surrounding tissue; the tissue strain forces $F_{st,la}$ and $F_{st,lv}$ from both the atrium and the ventricle sides that act on the annulus fibrosus base; the frictional force $K_{f,sav} \cdot dl/dt$ from blood flow; and the elastic force $K_{e,sav} \cdot l$ due to the elasticity of the KG diaphragm (Korakianitis and Grandia 2003). The KG diaphragm displacement l is decided by the balance of all these forces. The MRI measurements of heart kinetics in several heart cycles in an adult native healthy heart show that in the systolic phase the KG diaphragm moves into the ventricular chamber, and in end-diastolic phase it moves into the atrium (due to atrial contraction). The total displacement along the long axis of the heart is about $0.02 \sim 0.03m$.

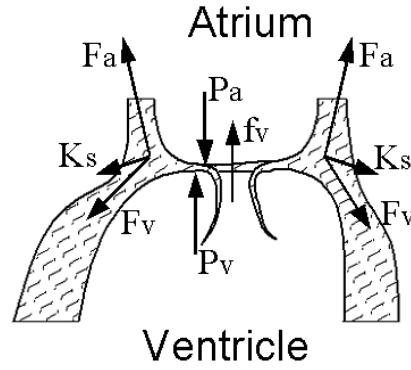


Figure 2-7 Forces acting on the KG diaphragm in the vicinity of the mitral valve

Based on Newton's second law of motion, in the left heart the KG diaphragm dynamics are governed by:

$$M_{sav} \cdot \frac{d^2 l}{dt^2} = F_{st,la} - F_{st,lv} + (P_{lv} - P_{la}) \cdot A_{sav} - k_{f,sav} \cdot \frac{dl}{dt} - k_{e,sav} \cdot l \quad (2-7)$$

Here the diaphragm neutral position is assigned to the location where both the atrium and the ventricle are in their unstressed status, and motion into the atrium is assigned as positive displacement.

Based on the MRI measurements, as a first approximation it is assumed that tissue strain is a linear function of the corresponding elasticity status of the chamber muscle. These effects are modelled by:

$$F_{st,la} = K_{e,la} \cdot e_{la} \quad (2-8)$$

$$F_{st,lv} = K_{e,lv} \cdot e_{lv} \quad (2-9)$$

Thus in the left heart the KG diaphragm dynamic equation is:

$$M_{sav} \cdot \frac{d^2 l}{dt^2} = K_{e,la} \cdot e_{la} - K_{e,lv} \cdot e_{lv} + (P_{lv} - P_{la}) \cdot A_{sav} - k_{f,sav} \cdot \frac{dl}{dt} - k_{e,sav} \cdot l \quad (2-10)$$

It is noted that mitral and tricuspid valves occupy much of the area in the atrio-ventricular septum, which affects the effective area of A_{sav} in equation (2-10) or of A_{pav} for the calculation in right heart. However, since in systole the mitral and tricuspid valves are closed, while in diastole the pressure difference between the atrium and ventricular chambers are small, the term $(P_{lv} - P_{la}) \cdot A_{sav}$ in equation (2-10) still gives a reliable estimation of the pressure force for the calculate of the septum dynamics.

The motion of the KG diaphragm redefines the location of the atrio-ventricular boundary at each time instant and introduces volume changes to the two chambers:

$$V_{lv} = V_{lv} + A_{sav} \cdot l \quad (2-11)$$

$$V_{la} = V_{la} - A_{sav} \cdot l \quad (2-12)$$

In the right heart, KG diaphragm dynamics are modelled in a similar way.

2.2.3.4 Heart Valves

Most prior studies have modelled heart valves as resistance components in the fully open or fully closed position, while the dynamics of the opening and closing processes were not considered. There were some who considered the opening and closing processes, such as Žáček and Krause (Zacek and Krause 1996), and Werner *et al.* (Werner *et al.* 2002), but they used prescribed valve motion, which neglected the blood-leaflet interaction effect, and thus the results were enormously compromised. In those previous works that ignored the heart valve dynamics, features FP4 (dicotic notch) and FQ1 (regurgitant flow in the valves) are missing from the system predicted response.

In the physical system heart valve dynamics are dominated by the blood-leaflet interaction effect (de Hart *et al.* 2003b, Kiris *et al.* 1997, Lai *et al.* 2002, Makhijani *et al.* 1996b, Shi *et al.* 2003). Full description of this effect needs detailed 3-dimensional distributed-parameter modelling of the pulsatile flow field around the valve and the valve-leaflet deformation / motion (such as with CFD studies). Previous studies on the blood-leaflet interaction effect (de Hart *et al.* 2003a, de Hart *et al.* 2000, de Hart *et al.* 2003b, Kiris *et al.* 1997, Lai *et al.* 2002, Makhijani *et al.* 1996a, Makhijani *et al.* 1996b, Makhijani *et al.* 1997, Shi *et al.* 2003) are mostly case specific, and cannot be used for overall dynamic modelling of the whole cardiovascular system as illustrated in Figure 2-5. As a novel contribution, this study makes a compromise between the detailed 3-dimensional study and the simplified diode-like description of the valve, using a concentrated-parameter method to describe the blood-leaflet interaction effect. For this modelling purpose, the heart valve is simplified as follows: a nominal leaflet opening angle is used as an average of the variation of angular position in the different parts of the elastic leaflet; the detailed pressure and velocity distributions in the valve are rounded and replaced with the averaged pressure and flow-rate before and after the

valve. The nominal leaflet opening angle is calculated by solving the governing differential equation for the leaflet dynamics, which takes into account the contribution of the blood flow, while the corresponding leaflet motion also drives the local pressure and flow-rate changes around the valve. This concentrated-parameter model of the blood-leaflet interaction effect is less detailed than 3-dimensional distributed parameter studies, but is an advancement over the diode models, and it satisfies the need of the present study to model the overall cardiovascular system.

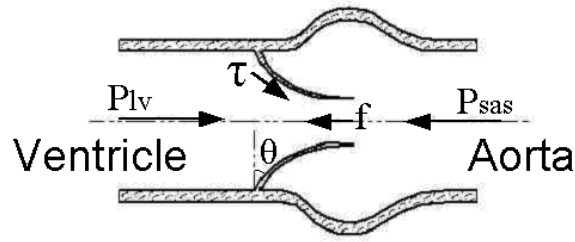


Figure 2-8 Illustration of typical forces acting on a heart valve leaflet

(θ is the nominal leaflet opening angle. The leaflet motion is governed by the balance of momentums on the leaflet due to different factors such as pressure difference, frictional force.)

In the current model the basic pressure-flow relation in the aortic valve is described with an orifice model as usually used in fluid mechanics (Granet 1996):

$$Q_{ao} = \begin{cases} CQ_{ao} \cdot AR_{ao} \sqrt{P_{lv} - P_{sas}}, & P_{lv} \geq P_{sas} \\ CQ_{ao} \cdot AR_{ao} \sqrt{P_{sas} - P_{lv}}, & P_{lv} < P_{sas} \end{cases} \quad (2-13)$$

while the valve opening AR_{ao} is derived in two ways. In the simplified model, like that of most prior studies, the valve opening switches between 0 and 1 corresponding to fully closed and fully open positions, depending on which side of the valve has higher pressure:

$$AR_{ao} = \begin{cases} 1, & P_{lv} \geq P_{sas} \\ 0, & P_{lv} < P_{sas} \end{cases} \quad (2-14)$$

In the current model, the circular valve opening is a function of the angular position of the valve leaflets, as illustrated in Figure 2-8:

$$AR_{ao} = \frac{A_{ao} (1 - \cos \theta)^2}{A_{ao} (1 - \cos \theta_{\max})^2} = \frac{(1 - \cos \theta)^2}{(1 - \cos \theta_{\max})^2} \quad (2-15)$$

In equation (2-15), θ is the leaflet opening angle. Zero (0 degrees) for θ corresponds to the fully closed leaflet position, and the maximum opening angle corresponds to the

fully open leaflet position. θ is computed by considering the various factors that affect the leaflet motion. These include: the moment due to the pressure difference across the valve; the moment generated by the shear stress on the leaflet due to fluid flow; the moment produced by the frictional force; and the moment generated by the vortex near the valve leaflet surface, as shown in Figure 2-8. Based on the CFD results of Hart *et al.* (de Hart *et al.* 2003a, de Hart *et al.* 2000, de Hart *et al.* 2003b) and Shi *et al.* (Shi *et al.* 2003), the shear stress force is much smaller than the pressure force acting on the leaflet, so the shear stress acted on the valve is neglected. The effect of the vortex in the heart valve is an open question and its contribution is still under investigation. Some researchers proposed that the vortices influence the valve closing process (Bellhouse 1972, Yacoub *et al.* 1996), but this argument needs further validation, and it is the subject of future investigations. Thus in this study the vortex effect is also neglected. Based on these considerations the following governing equation for the aortic leaflet motion is derived:

$$I_{ao} \cdot \frac{d^2\theta}{dt^2} = k_{p,ao} \cdot (P_{lv} - P_{sas}) \cdot \cos\theta - k_{f,ao} \cdot \frac{d\theta}{dt} \quad (2-16)$$

The parameters needed in the model are reduced from three (I_{ao} , $k_{p,ao}$, and $k_{f,ao}$) to two ($K_{p,ao}$, and $K_{f,ao}$) by dividing through with I_{ao} and simplifying the equation in the model to:

$$\frac{d^2\theta}{dt^2} = K_{p,ao} \cdot (P_{lv} - P_{sas}) \cdot \cos\theta - K_{f,ao} \cdot \frac{d\theta}{dt} \quad (2-17)$$

The consideration of valve dynamics helps to describe the regurgitant flow in the valve, thus improving the accuracy of the simulation. Modelling of the remaining three valves is implemented in the same way, except the values of model parameters can be different.

2.2.3.5 Blood Circulation Loops

In modelling the various components of systemic circulation, depending on detailed local flow conditions, the frictional loss, elastance, and blood inertia are modelled as resistance, compliance, and inductance effects, following the classical idea of electric-fluid analogue. The systemic circulation loop is divided into five parts: aortic sinus; artery; arterioles; capillary; and vein. The aortic sinus and artery are quite elastic, and the flow is pulsatile in these segments, so that all the resistance, compliance and

inductance effects must be considered. The arterioles and capillaries are dominated by the resistance effect. Veins function to collect and store blood, thus resistance and compliance effects are considered in the vein model.

Pressure and flow-rate oscillations are experienced in the aortic sinus due to the local tissue elastance and result in important flow features related to coronary flow. The pressure is governed by:

$$\frac{dP_{sas}}{dt} = \frac{Q_{ao} - Q_{sas}}{C_{sas}} \quad (2-18)$$

and the flow-rate is:

$$\frac{dQ_{sas}}{dt} = \frac{P_{sas} - P_{sat} - R_{sas} \cdot Q_{sas}}{L_{sas}} \quad (2-19)$$

The pressure and flow-rate changes in the artery are similar to that in the aortic sinus. As arterioles and capillaries are both considered as pure resistance units, their effects are integrated with the artery as resistance units. Thus the pressure equation is:

$$\frac{dP_{sat}}{dt} = \frac{Q_{sas} - Q_{sat}}{C_{sat}} \quad (2-20)$$

and the flow-rate equation is:

$$\frac{dQ_{sat}}{dt} = \frac{P_{sat} - P_{svn} - (R_{sat} + R_{sar} + R_{scp}) \cdot Q_{sat}}{L_{sat}} \quad (2-21)$$

The systemic vein is modelled as a compliance combined with a resistance. In the vein the pressure is:

$$\frac{dP_{svn}}{dt} = \frac{Q_{sat} - Q_{svn}}{C_{svn}} \quad (2-22)$$

and the flow-rate is governed by:

$$Q_{svn} = \frac{P_{svn} - P_{ra}}{R_{svn}} \quad (2-23)$$

The pulmonary loop model is similar to that of the systemic loop, with different values for system parameters.

2.2.4 System Parameters

Values for the physiological parameters are usually difficult to measure, and they change from person to person. This is a common problem in medical and biomedical

studies. To minimize the potential influence of the values of these parameters on the results, first the valid ranges for the values to these physiological variables were identified from widely referred papers and textbooks. Next numerical experiments were carried out to find the optimal parameter combinations within these value ranges, so that the simulated cardiovascular response matches the typical data reported in the open literature.

Table 2-1 Parameters for the Heart

Part	Parameter	Value	Unit
Left heart	CQ_{ao}	350	$ml / (s \cdot mmHg^{0.5})$
	CQ_{mi}	400	$ml / (s \cdot mmHg^{0.5})$
	$E_{lv,s}$	2.5	$mmHg / ml$
	$E_{lv,d}$	0.1	$mmHg / ml$
	$P_{lv,0}$	1.0	$mmHg$
	$V_{lv,0}$	5.0	ml
	$E_{la,max}$	0.25	$mmHg / ml$
	$E_{la,min}$	0.15	$mmHg / ml$
	$P_{la,0}$	1.0	$mmHg$
	$V_{la,0}$	4.0	ml
Right heart	CQ_{po}	350	$ml / (s \cdot mmHg^{0.5})$
	CQ_{ti}	400	$ml / (s \cdot mmHg^{0.5})$
	$E_{rv,s}$	1.15	$mmHg / ml$
	$E_{rv,d}$	0.1	$mmHg / ml$
	$P_{lv,0}$	1.0	$mmHg$
	$V_{lv,0}$	10.0	ml
	$E_{ra,max}$	0.25	$mmHg / ml$
	$E_{ra,min}$	0.15	$mmHg / ml$
	$P_{ra,0}$	1.0	$mmHg$
	$V_{ra,0}$	4.0	ml

Using this technique, chamber elastance values are assigned as shown in Table 2-1, based on the parameter selection in (Heldt *et al.* 2002, Lu *et al.* 2001, Thomas *et al.* 1997, Ursino 1999). Key parameters for the systemic and pulmonary loops are shown in Table 2-2, based on the data reported in (Lu *et al.* 2001, Thomas *et al.* 1997, Ursino 1998, Ursino 1999).

Table 2-2 Parameters for the Blood Vessels

Part	Parameter	Value	Unit
Systemic circulation	C_{sas}	0.08	$ml/mmHg$
	R_{sas}	0.003	$mmHg \cdot s/ml$
	L_{sas}	0.000062	$mmHg \cdot s^2/ml$
	C_{sat}	1.6	$ml/mmHg$
	R_{sat}	0.05	$mmHg \cdot s/ml$
	L_{sat}	0.0017	$mmHg \cdot s^2/ml$
	R_{sar}	0.5	$mmHg \cdot s/ml$
	R_{scp}	0.52	$mmHg \cdot s/ml$
	R_{svn}	0.075	$mmHg \cdot s/ml$
	C_{svn}	20.5	$ml/mmHg$
	V_{lv0}	500	ml
Pulmonary circulation	C_{pas}	0.18	$ml/mmHg$
	R_{pas}	0.002	$mmHg \cdot s/ml$
	L_{pas}	0.000052	$mmHg \cdot s^2/ml$
	C_{pat}	3.8	$ml/mmHg$
	R_{pat}	0.01	$mmHg \cdot s/ml$
	L_{pat}	0.0017	$mmHg \cdot s^2/ml$
	R_{par}	0.05	$mmHg \cdot s/ml$
	R_{pcp}	0.25	$mmHg \cdot s/ml$
	R_{pvn}	0.006	$mmHg \cdot s/ml$
	C_{pvn}	20.5	$ml/mmHg$
	V_{rv0}	400	ml

Coefficients for KG diaphragm motion and heart valve dynamics are estimated based on physiological conditions observed in the MRI measurements in this study and those found in textbooks. In modelling the KG diaphragm motion, the diameter of the annulus fibrosus of the mitral valve is assumed to be $25mm$, and the thickness of the annulus fibrosus is assumed to be $1mm$. Taking the tissue density to be $0.8 \times 10^3 kg/m^3$, the annulus fibrosus has a sectional area of $4.7 \times 10^{-4} m^2$ and a mass of $4.0 \times 10^{-4} kg$. During the heart cycle the annulus fibrosus is under continuous reciprocating motion around its neutral position. The MRI measurements indicate that the annulus fibrosus has a displacement of about $0.02 \sim 0.03m$ during the heart cycle,

and in the diastolic phase the annulus fibrosus is stretched into the atrium chamber with a displacement of about $0.003m$. The coefficients in the governing equations for KG diaphragm motion are then derived, and listed in Table 2-3. The coefficients of the valve dynamics model were estimated by considering the normal flow-rate and pressure loss in the valves and the relative contribution of various factors that affect the valve motion, thus producing near physiological valve motion as described in the literature (de Hart *et al.* 2003a, de Hart *et al.* 2000, de Hart *et al.* 2003b, Kiris *et al.* 1997, Lai *et al.* 2002, Makhijani *et al.* 1996a, Makhijani *et al.* 1996b, Makhijani *et al.* 1997, Shi *et al.* 2003). The corresponding parameter settings are included in Table 2-4.

Other parameters such as duration of systole, the beginning and duration of the P wave, the time step of simulation etc., were chosen based on general information published in physiological textbooks(Guyton 1986, West 1990). Table 2-5 shows values for these parameters.

In solving the governing differential equations, proper initial values need to be assigned to the related variables. Pressures for the vasculature can be set at the normal physiological ranges observed clinically, and the initial volumes of the ventricles are set as listed in Table 2-2.

Table 2-3 Parameters for KG diaphragm motion modelling

Part	Parameter	Value	Unit
Left heart	$K_{st,la}$	2.5	$m/(s^2 \cdot mmHg)$
	$K_{st,lv}$	20.0	$m/(s^2 \cdot mmHg)$
	$K_{f,sav}$	0.0004	$1/s$
	$K_{e,sav}$	9000.0	$1/s^2$
	m_{sav}	0.0004	kg
	A_{sav}	0.00047	m^2
Right heart	$K_{st,ra}$	2.5	$m/(s^2 \cdot mmHg)$
	$K_{st,rv}$	20.0	$m/(s^2 \cdot mmHg)$
	$K_{f,pav}$	0.0004	$1/s$
	$K_{e,pav}$	9000.0	$1/s^2$
	m_{pav}	0.0004	kg
	A_{pav}	0.00047	m^2

Table 2-4 Parameters for variable valve opening model

Part	Parameter	Value	Unit
Systemic part	$K_{p,ao}$	5500	$rad/(s^2 \cdot mmHg)$
	$K_{f,ao}$	50	1/s
	$K_{p,mi}$	5500	$rad/(s^2 \cdot mmHg)$
	$K_{f,mi}$	50	1/s
Pulmonary part	$K_{p,po}$	5500	$rad/(s^2 \cdot mmHg)$
	$K_{f,po}$	50	1/s
	$K_{p,ti}$	5500	$rad/(s^2 \cdot mmHg)$
	$K_{f,ti}$	50	1/s

Table 2-5. Additional Parameters

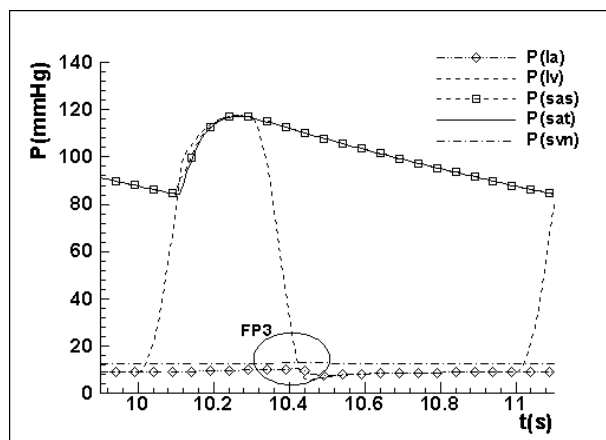
Parameter	Value	Unit
dt	0.0001	s
T	1	s
T_{s1}	0.3	s
T_{s2}	0.45	s
T_{pwb}	0.92	s
T_{pww}	0.09	s

2.3 Results

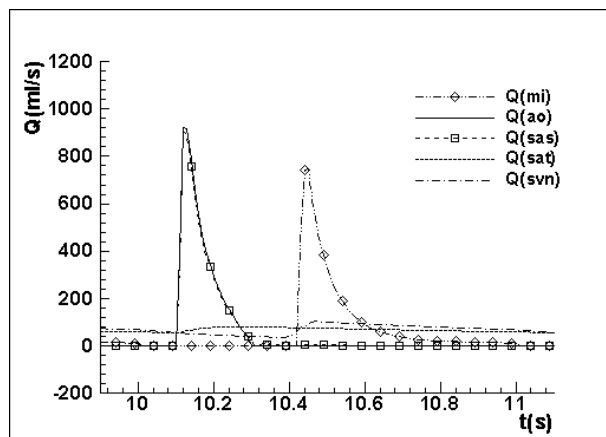
A program is developed in C language to conduct numerical simulations of the dynamic changes in the heart chambers and the blood vessels. The equations are integrated in time with the 4-stage Runge-Kutta method. For ease of comparison of results the heart period is chosen to be 1 second. The simulation reaches periodic solution after 4 to 5 heart cycles. To facilitate discussion of results, in all cases the converged solution of the 11th period, from the 10th to the 11th second, is presented in the figures. In the following details of the pressure, flow-rate and volume traces of the human cardiovascular system are presented, as each feature of atrio-ventricular interaction and heart valve dynamics are included in the model. First the effects of atrio-ventricular interaction and heart valve dynamics are neglected, and the response of the corresponding simplified model is compared with the one that appears in

textbooks, identifying missing features of the predicted response. Next each one of these features are considered in the simulation one by one, and the corresponding response is compared with that of the simplified model to observe the contribution of each part of the model to cardiovascular dynamics. Finally these features are all applied simultaneously to observe their combined effects. This gradual introduction of the model features enables a discussion of what aspects of the system response are affected by the physiology of each part of the model, both in a physiological as well as in a modelling sense.

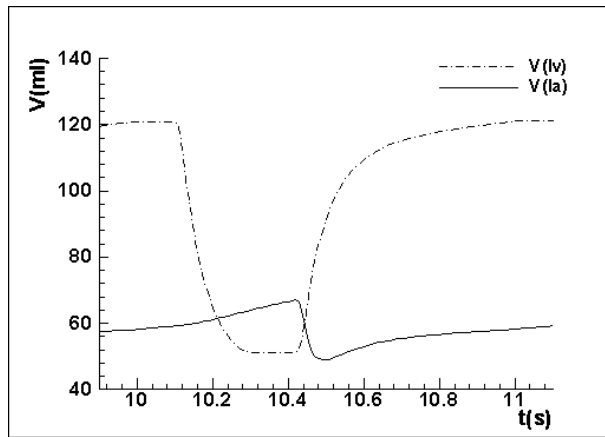
2.3.1 Response of the Simplified Model



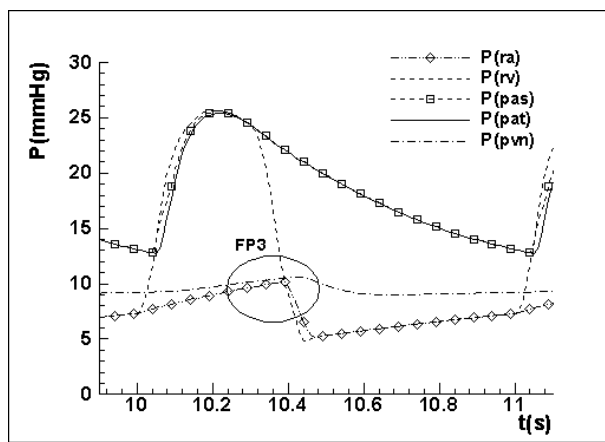
(a) Pressure, left heart



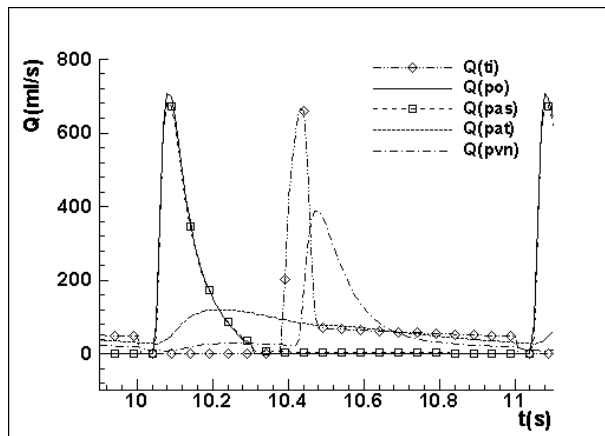
(b) Flow-rate, left heart



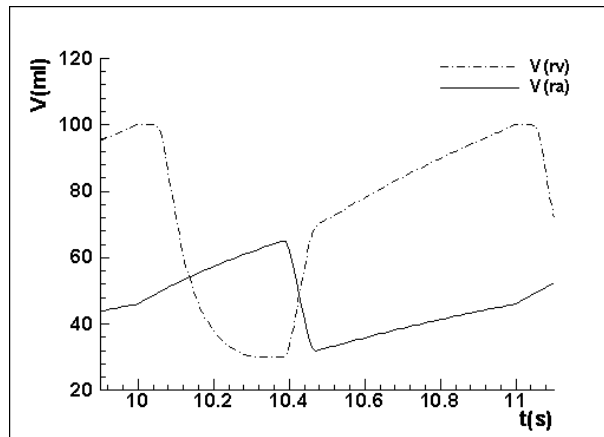
(c) Volume, left heart



(d) Pressure, right heart



(e) Flow-rate, right heart



(f) Volume, right heart

Figure 2-9 Response with the simplified model

First the simulation is carried out using the simplified model. The ventricles are described with variable elastance model in the form of equations (2-1)~(2-4). The systemic and pulmonary loops are modelled with the RLC concept as described by equations (2-18)~(2-23). The atria are treated as constant elastance chambers with atrial elastance set to value of $E_{la,min}$. The KG diaphragm motion is neglected, and heart valves are modelled as a diode with nonlinear resistance effect, described by equations (2-13) and (2-14). In carrying out the simulation, values for the parameters are assigned as discussed previously. The corresponding response of the cardiovascular system, pressure, flow-rate and volume changes in a typical heart cycle in the left and right parts of the heart, is shown in Figure 2-9 (a) to (f).

These results broadly agree (in trends and parameter ranges) with the conceptual drawings in Figure 2-4. The left ventricular pressure is in the range of 0 ~ 120mmHg, and the aortic pressure changes between 80 ~ 120mmHg. Periodic peak flows exist in the mitral and aortic flows, with average flow-rate of about 5l/min. The left ventricular volume change is approximately from 50ml to 120ml, with a stroke volume of 70ml. Even though in this simplified model the atria are modelled as chambers with constant elastance, they still accumulate blood during systole, so feature FP3 for the v wave is observed in the atrial pressure change in Figure 2-9 (a) and (d), but with decreased amplitude due to the decreased elastance in this model. The E velocity peak is present in mitral and tricuspid flow, but as the A velocity peak is absent (due to neglecting atrial contraction), the ratio of early to late velocities (E/A) cannot be evaluated. Also due to neglecting atrial contraction, features FP1 for the a

wave, FP2 for the c wave, FQ2 for the a velocity peak and FV1 for the step volume increase are missing from the system response. Because valve dynamics are not considered in the simplified model, features FP4 for the dicrotic notch in the aortic and pulmonary artery pressure, and FQ1 for valve regurgitant flow, are also missing from the simplified system response.

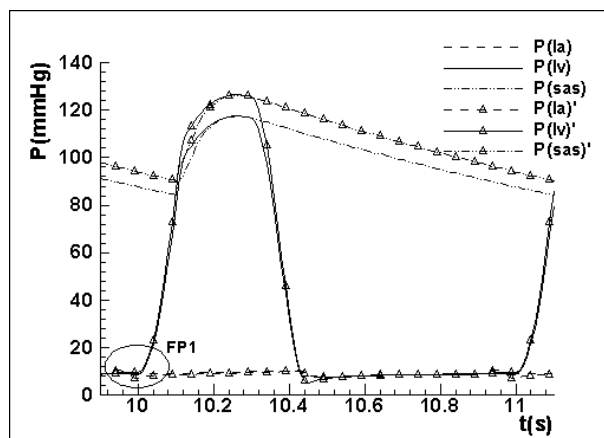
In the following as each one of the new features is included in the simplified model, the new response is compared with the response of the simplified model shown in Figure 2-9. In the comparisons shown in Figure 2-10 and subsequent figures, those trace lines with triangular tick marks and with a prime (') in the legends for pressure, flow-rate and volume traces are the response when the new feature is considered, while those without the triangular marks and the prime in the legends represent the response in the simplified model.

2.3.2 Response with Combined Effect of Atrio-ventricular Interaction and Atrial Contraction

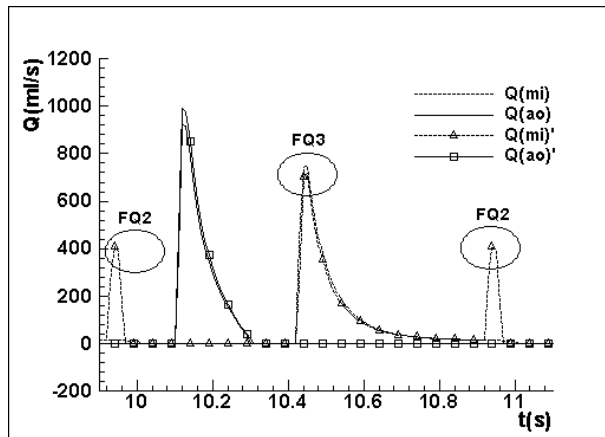
Kilner *et al.* (Kilner *et al.* 2000) and Korakianitis *et al.* (Korakianitis and Grandia 2003) proposed that the KG diaphragm works as an auxiliary mechanism (as an auxiliary pump) in promoting blood flow. In modelling this effect, first the individual effects of atrial contraction and KG diaphragm are investigated one by one, and then their combined effect is studied.

To simulate the effect of atrial contraction alone, the variable elastance model for the atrium is applied. Equations (2-5) and (2-6) for the variable atrial elastance model are used to replace the constant elastance value of $E_{la,min}$ in the simplified model. Comparison of the corresponding system response with that of the simplified model, including pressure, flow-rate and volume changes in a typical heart cycle, are shown in Figure 2-10. As the results for the flow-rate and volume changes in the right side of the heart are similar to those in the left side, they are not illustrated here. Figure 2-10 (a) and (d) compare the corresponding pressure responses in the systemic and pulmonary loops with those of the simplified model. In comparison to the simplified model atrial contraction results in about 10% increase in aortic pressure and left ventricular systolic pressure. The aortic pressure range increases from 80 ~ 120mmHg to 90 ~ 130mmHg, and peak left ventricular pressure increases from 120mmHg to 130mmHg. The pulmonary loop has highly distensible blood vessels, and thus greater compliance,

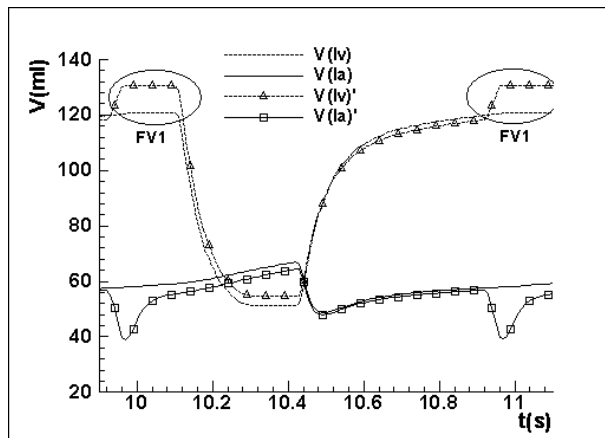
which buffers the pressure pulsation significantly. Therefore the atrial contraction also causes a pressure increase in the right side of the heart, but the change is much smaller as compared to that in the left side of the heart. Atrial contraction also decreases the left atrial pressure during the systolic phase. Also due to the atrial contraction effect, the *a* wave in the atrial pressure response is clearly demonstrated in Figure 2-10 (d), corresponding to feature FP1 in Figure 2-4, while in the systemic circulation feature FP1 is not so obvious (shown in Figure 2-10 (a)). Due to the different peak systolic pressures in the two loops, this local pressure peak is more pronounced in the pulmonary loop than in the systemic loop. Figure 2-10 (b) compares the corresponding flow-rate waveforms. Corresponding to the *A* velocity peak, feature FQ2 is clearly demonstrated in the flow-rate response. Also by referring to feature FQ3 of the *E* velocity, it is observed that *E/A* velocity ratio is about 1.5 in the systemic circulation (in the normal range of 1 ~ 2 (Nageh *et al.* 1999, Sohn *et al.* 1997)). Figure 2-10 (c) compares the corresponding volume changes in left side of the heart. The local increase in ventricular volume and the local trough in atrial volume changes due to atrial contraction can be clearly observed in the graph, corresponding to feature FV1. Comparison shows that in the late diastolic phase, atrial contraction prominently elevates the ventricular volume and decreases the atrial volume. From the figure it is estimated that atrial contraction contributes about 25% of stroke volume. This agrees well with descriptions in textbooks (Guyton 1986, West 1990).



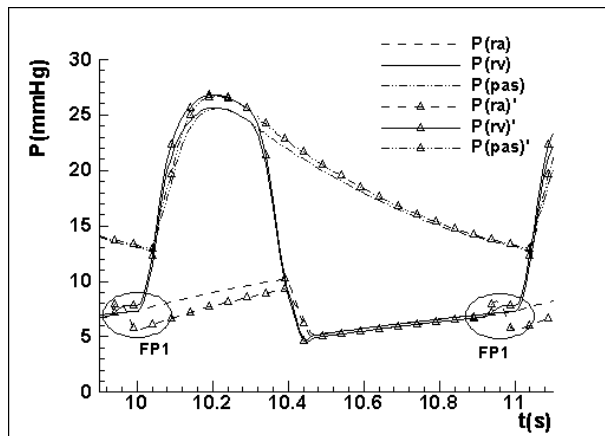
(a) Pressure, left heart



(b) Flow-rate, left heart

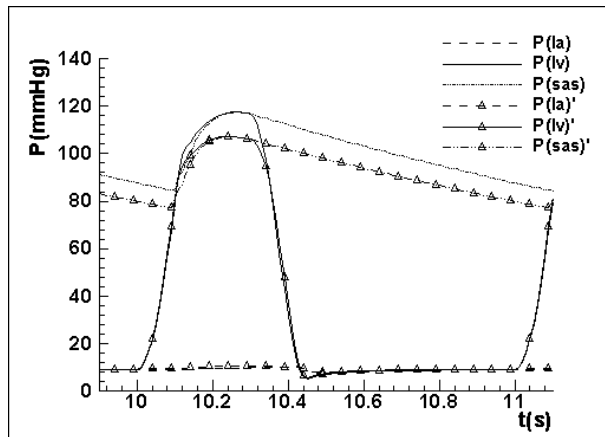


(c) Volume, left heart

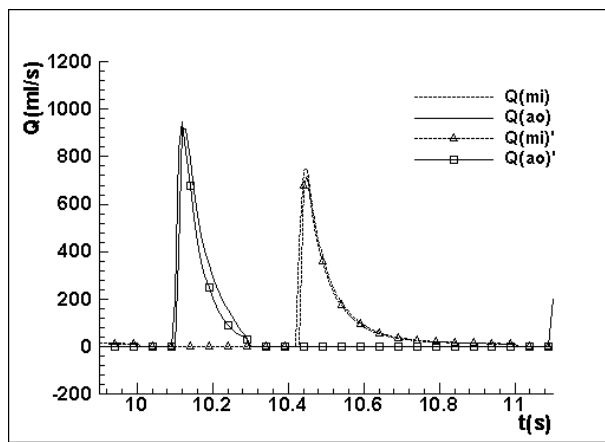


(d) Pressure, right heart

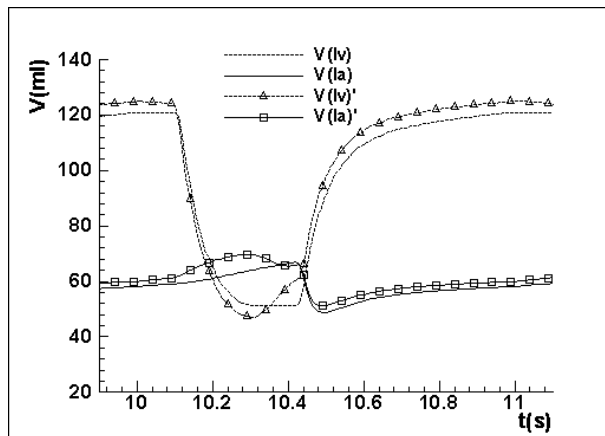
Figure 2-10 Response with modelling of the atrial contraction alone
 (Responses with a prime(') correspond to the condition when the atrial contraction is considered.)



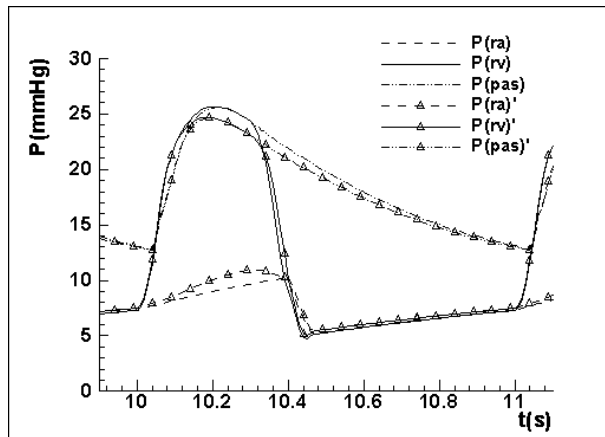
(a) Pressure, left heart



(b) Flow-rate, left heart



(c) Volume, left heart



(d) Pressure, right heart

Figure 2-11 Response with modelling of the KG diaphragm motion alone

(Responses with a prime(') correspond to the condition when the KG diaphragm motion is considered.)

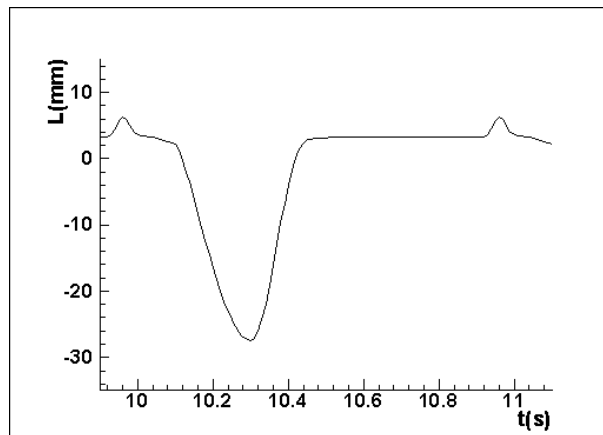


Figure 2-12 Resultant motion of the KG diaphragm in the left heart when both KG diaphragm dynamics and atrial contraction are considered

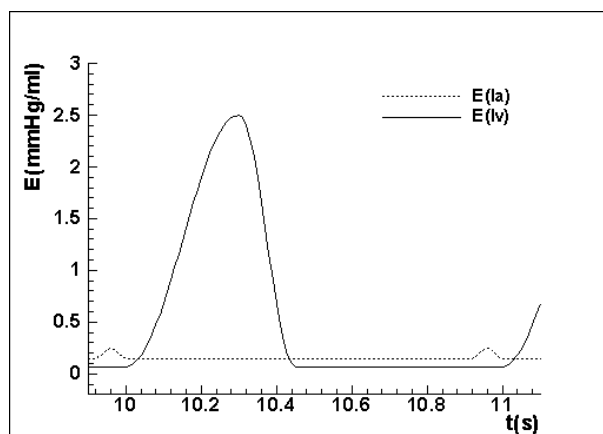
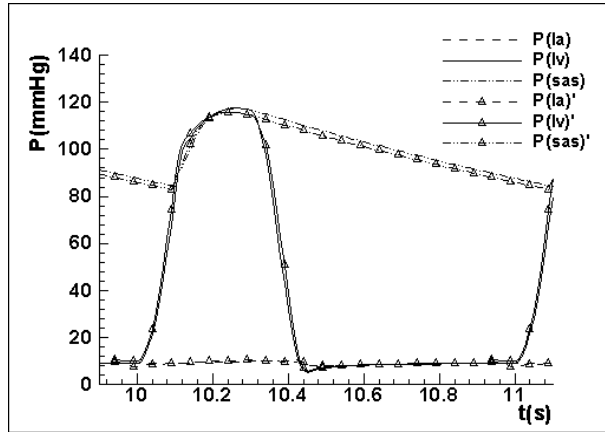
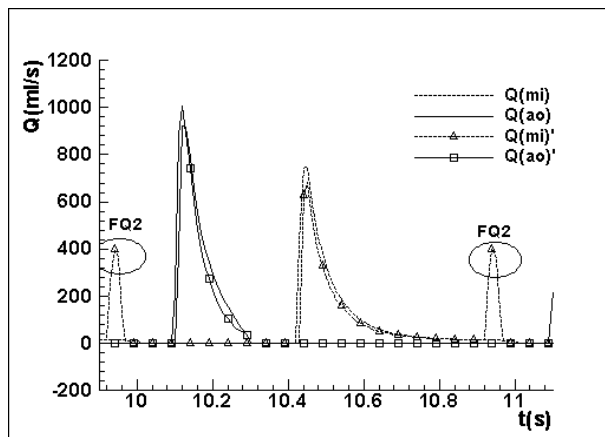


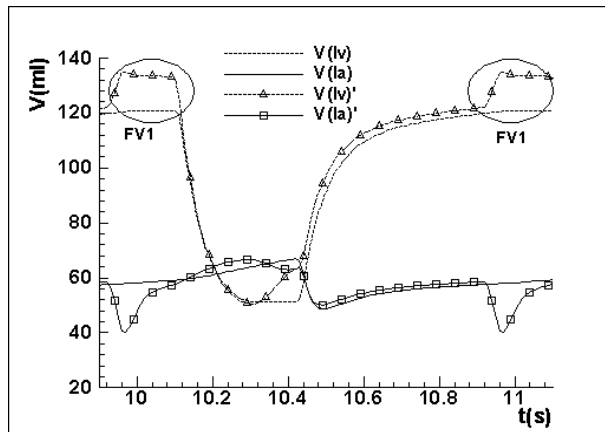
Figure 2-13 Elastance change in the left heart when both KG diaphragm dynamics and atrial contraction are considered



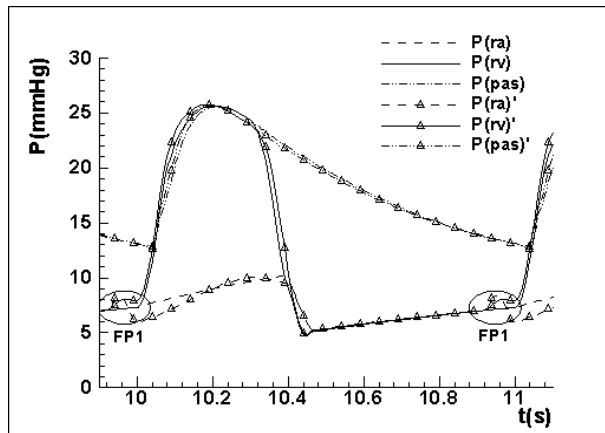
(a) Pressure, left heart



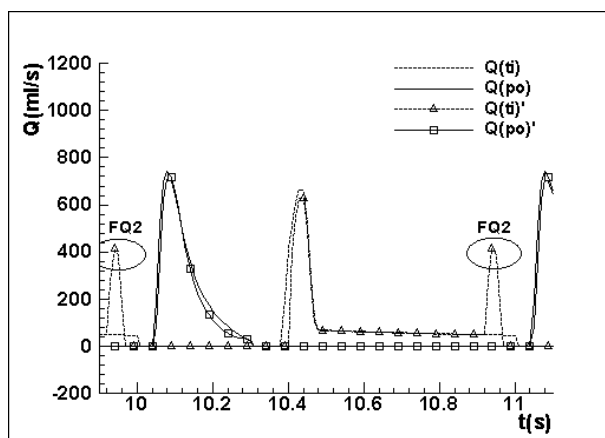
(b) Flow-rate, left heart



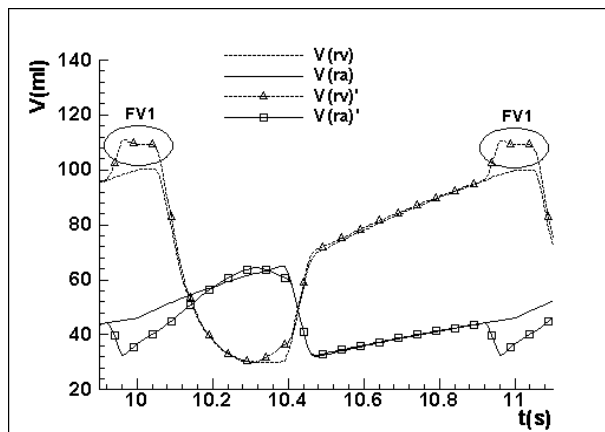
(c) Volume, left heart



(d) Pressure, right heart



(e) Flow-rate, right heart



(f) Volume, right heart

Figure 2-14 Response with modelling both KG diaphragm motion and atrial contraction

(Responses with a prime(') correspond to the condition when both the KG diaphragm motion and the atrial contraction are considered.)

In modelling the atrio-ventricular interaction effect alone, equation (2-10) that describes the motion of the KG diaphragm, and equations (2-11), (2-12) for correction of atrial and ventricular volumes are coupled to the simplified system model.

Comparison of system response with that in the original simplified model in a typical heart cycle is shown in Figure 2-11. Flow-rate and volume changes in the right heart are similar to those in the left heart, so they are omitted here. Figure 2-11 (c) shows that in the systolic phase, motion of the KG diaphragm into the ventricular chamber causes the minimum ventricular volume to decrease from $51.3ml$ to $47.1ml$, while atrial volume is increased from $63.5ml$ to $69.7ml$. The rate of volume change in the ventricle is also affected, and in early systole the ventricular volume drops faster than that in the simplified model. All over the diastolic phase, motion of the KG diaphragm into the atrial side causes the ventricular volume to increase about $5ml$, while atrial volume is increased by about $2ml$, compared with that in the simplified model. The reason is that the prominent volume increase in the atrium during the systolic phase causes more blood to enter the atrial chamber. The effect of this blood build up in the atrium lasts into the diastolic phase, and causes the increase in the atrial volume compared to the simplified model. Compared with that in the simplified model, the KG diaphragm motion increases ventricular stroke volume by about 15%. As shown in Figure 2-11 (a) and (d), accompanying this volume increase due to motion of the KG diaphragm, the systolic atrial pressure is slightly elevated by about $0.9mmHg$ in the left heart and $1.3mmHg$ in the right heart. This pressure difference almost disappears in diastole. In the systolic phase the peak aortic pressure and left ventricular pressure are prominently decreased from $117.2mmHg$ to $107.2mmHg$, while the peak pulmonary pressure and right ventricular pressure are decreased from $25.6mmHg$ to $24.6mmHg$. The elevated aortic/pulmonary pressure lasts from the systolic and into the diastolic phase. The pressure drop in the right ventricle is much smaller than that in the left ventricle. This is the natural consequence of the highly distensible blood vessels, and thus the greater compliance, in the pulmonary loop. The flow-rate response is illustrated in Figure 2-11 (b). Compared with that of the simplified model the peak flows past the heart valves increase slightly, and the aortic/pulmonic flow rates decrease faster.

The motion of the KG diaphragm affects the values, but does not affect the general trend in the pressure, flow-rate and volume changes in the heart, so that when the KG diaphragm alone is modelled most features in the conceptual drawing of cardiovascular response in Figure 2-4 are either missing or are not obvious in the above system response. Based on analysis of the pressure and volume response, it is concluded that

the motion of the KG diaphragm increases ventricular stroke volume by about 15% , while decreasing ventricular pressure. These observations confirm that the KG diaphragm works as an auxiliary pumping mechanism, which greatly reduces the workload of the ventricle.

Atrial contraction changes the preload to the heart, thus affecting details of the function of the KG diaphragm. The combined action of KG diaphragm motion and atrial contraction on the system is then investigated. The resultant motion of the KG diaphragm in the left heart is illustrated in Figure 2-12, and the accompanying elastance changes in the left atrium and ventricle are shown in Figure 2-13. Comparison of system response with that of the original simplified model in a typical heart cycle is shown in Figure 2-14.

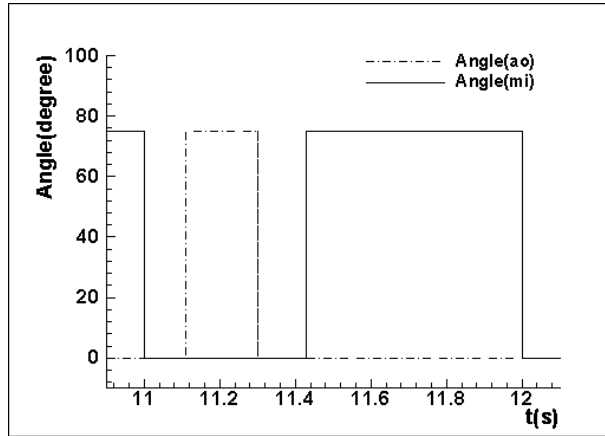
In Figure 2-12 the KG diaphragm displacement refers to the motion of the root of the annulus fibrosus with respect to its neutral position (when the atrium and ventricle are in the unstressed condition). In the systolic phase, along with the increased tissue elastance in the ventricle in Figure 2-13, the KG diaphragm moves towards the apex of the heart, with the peak displacement reaching $-0.0286m$ from the neutral position. In the diastolic phase, along with decrease of ventricular elastance, the KG diaphragm moves back towards the atrium direction. In late diastole, combined with atrial contraction the KG diaphragm reaches the peak displacement of $0.0032m$. The diaphragm motion is affected by several factors: pressure difference across the diaphragm; tissue stress on the diaphragm due to the atrial and ventricular contraction; friction; and elasticity of the diaphragm tissue. By comparing the changes in Figure 2-12 and Figure 2-13, it is observed that in systole motion of the KG diaphragm generally follows the changes of the ventricular elasticity, and thus the corresponding changes in ventricular tissue stress. In end diastole, with the relaxation of the ventricular muscle and the atrial contraction, the KG diaphragm moves towards the atrial direction and reaches the peak displacement in this direction at the instance of the atrial contraction. The phenomena described here agree with the physiological movement of the KG diaphragm (in contrast to the counter-intuitive results of Power (Power 1979), which were mentioned in the introduction.).

Figure 2-11 suggests that the effect of the KG diaphragm alone decreases aortic pressure and systolic ventricular pressure, while Figure 2-10 shows that the effect of atrial contraction alone elevates the aortic pressure and systolic ventricular pressure.

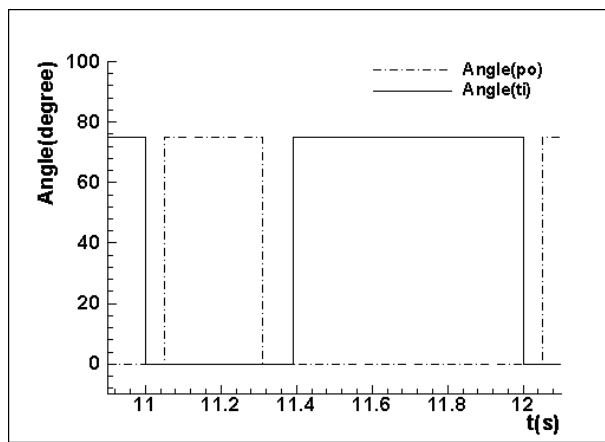
When the two effects interact with each other, atrial contraction reduces the effect of KG diaphragm motion on pressure. Thus under the combined action of KG diaphragm motion and atrial contraction the pressures in atria, ventricles, aorta and pulmonary artery are generally restored to those in the simplified model, as shown in the pressure comparison in Figure 2-14 (a) and (d). Also atrial contraction introduces feature FP1 (the *a* wave) in the atrial pressure response. In the flow-rate response in Figure 2-14 (b) and (e), it is observed that atrial contraction induces feature FQ2, the effect of *A* velocity, in the mitral/tricuspid flow. *E/A* ratios in both left and right sides of the heart are in the normal range of 1 ~ 2. Under the combined action of atrial contraction and KG diaphragm motion, the volume curves of both atria and ventricles in Figure 2-14 (c) and (f) generally match those in the simplified model, except that atrial contraction produces feature FV1 in the volume response, with a step increase (from 120.9ml to 133.6ml in the left heart and from 100.2ml to 109.4ml in the right heart) in ventricular volume, and a local decrease (from 57.9ml to 40.3ml in the left heart and from 45.2ml to 32.8ml in the right heart) in atrial volume in the late diastolic phase, so that the stroke volume is increased by about 20%. Overall the combined action of KG diaphragm motion and atrial contraction increases the volumetric throughput while keeping the pressure at the lower levels of the simplified system response.

2.3.3 Response with Heart Valve Dynamics Alone

To study the effect of heart valve dynamics alone, in the simplified model the valve opening equations in the form of equation (2-14) are replaced with equations of the form of equation (2-15) and (2-17). Thus the valve dynamics are coupled with the simplified model to give a better representation of the valve opening and closing processes. Figure 2-15 shows the valve opening sequences simulated with the simplified model, and Figure 2-16 illustrates the valve opening sequences of the four heart valves when valve dynamics are considered. In Figure 2-15 and Figure 2-16, 0 degree for opening angle corresponds to the fully closed leaflet position, and the maximum opening angle corresponds to the fully open leaflet position. Figure 2-17 compares the system response with inclusion of valve dynamics alone with that in the simplified model.

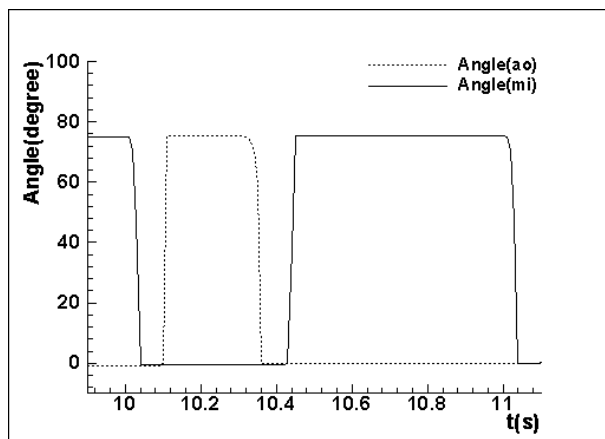


(a) Aortic and mitral valves

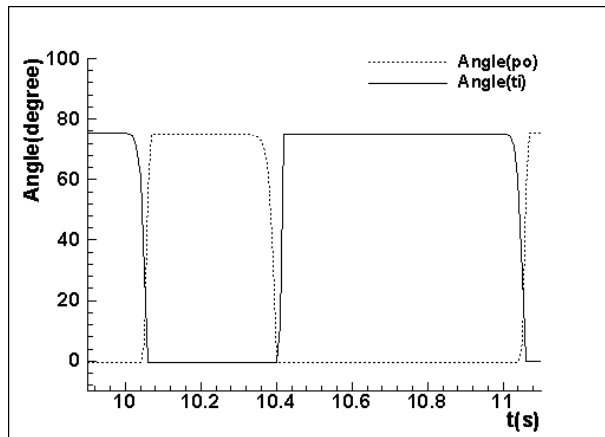


(b) Pulmonary and tricuspid valves

Figure 2-15 Resultant change of heart valve leaflet angular position (opening) in the simplified model

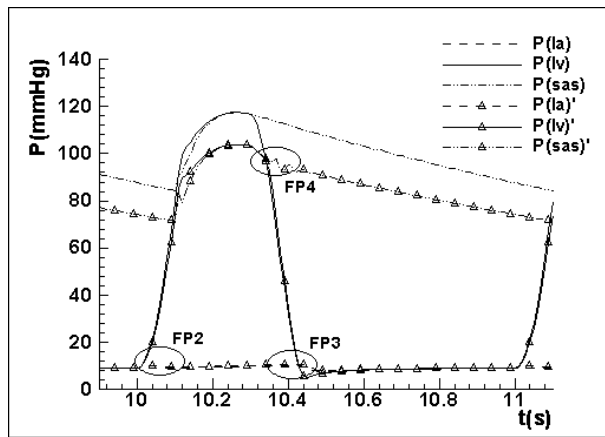


(a) Aortic and mitral valves

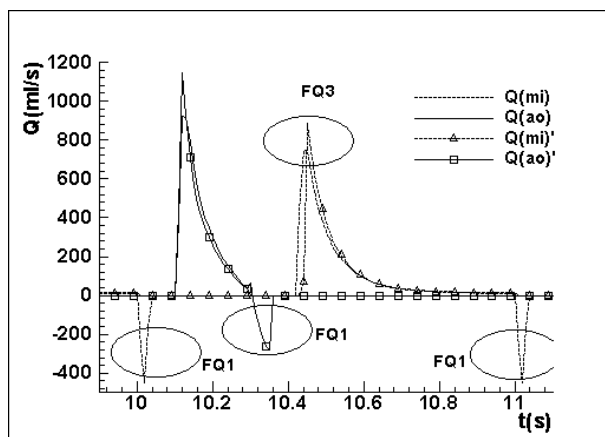


(b) Pulmonary and tricuspid valves

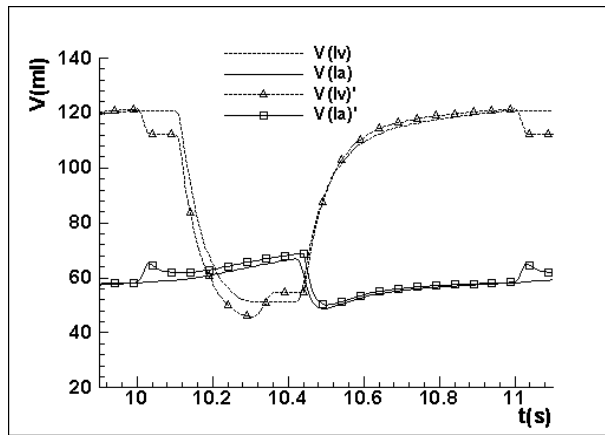
Figure 2-16 Resultant change of heart valve leaflet angular position (opening) with valve dynamics modelling alone



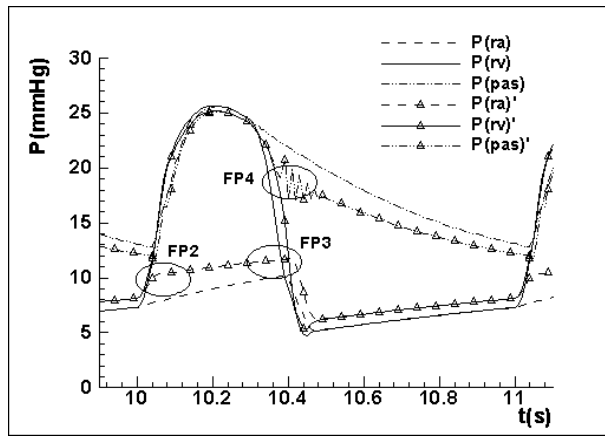
(a) Pressure, left heart



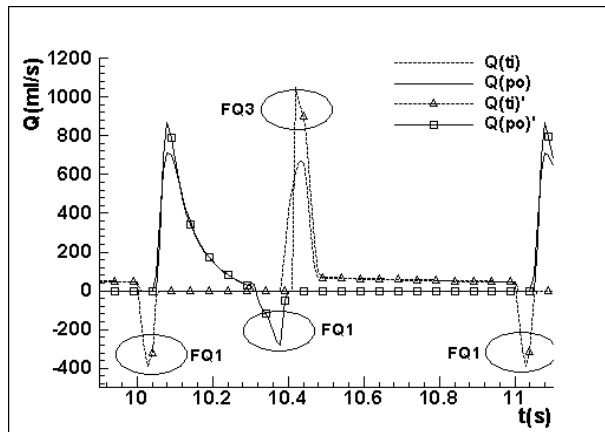
(b) Flow-rate, left heart



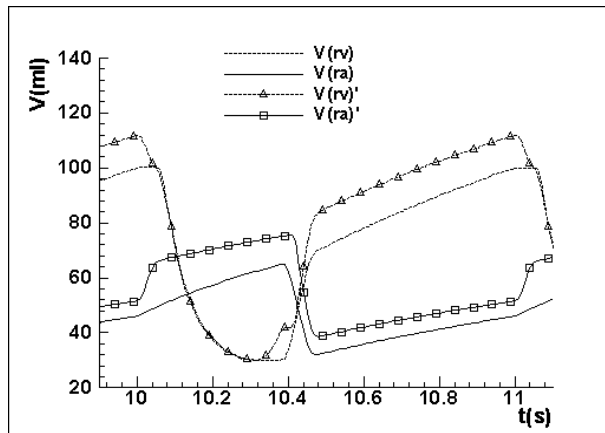
(c) Volume, left heart



(d) Pressure, right heart



(e) Flow-rate, right heart



(f) Volume, right heart

Figure 2-17 Response with heart valve dynamics modelling alone

(Responses with a prime(') correspond to the condition when the heart valve dynamics is considered.)

In the valve opening sequences simulated with the simplified model shown in Figure 2-15, the valves open and close abruptly, driven by the local pressure difference across the valves. In Figure 2-16 the opening sequences become smoother with the introduction of the valve dynamics modelling. The valve opening and closing instances also change, and the effect is more pronounced in the response of the pulmonary and tricuspid valves. From Figure 2-16 it is observed that the valve opening and closing processes take about $0.1s$. Comparing the valve motions in the right heart to that in the left heart, it is found that the pulmonary valve opens about $0.15s$ earlier and closes about $0.1s$ later than the aortic valve, and the tricuspid valve opens about $0.05s$ earlier and closes about $0.05s$ later than the mitral valve. This is closely related to the lower pressure range in the pulmonary loop and the slower pressure change rate in the right ventricle. The atrial pressures in the left and right heart are similar, thus the slower rise in pressure in the right ventricle induces the later closing of the tricuspid valve. The earlier opening the tricuspid and pulmonary valves and the later closing of the pulmonary valve are the results of the combined actions of the lower pressure value in the pulmonary loop, and slower pressure change rate in the right ventricle.

Figure 2-17 (a) and (d) compare the corresponding pressure response when considering the effect of opening and closing dynamics of the four heart valves alone. The most distinguishing feature is FP4, the dicrotic notch, which is more prominent in the pulmonary loop than in the systemic loop. Inclusion of valve dynamics helps to simulate valve regurgitant flow, and therefore it also affects features FP2 and FP3, c

and v waves in the atrial pressure, which are also more obviously demonstrated in pulmonary circulation (because the high to low pressure differences are on a percentage basis larger than in systemic circulation). Due to regurgitant flow in the mitral and tricuspid valves, feature FP3 is elevated to a higher value. Although feature FP2 is exhibited, it is still not prominent. This is partly due to its minor effect in the physiological response, and partly due to neglecting valve elasticity in the system modelling. In the systolic phase, regurgitant flow in mitral/tricuspid valve decrease the work load of the ventricles, so that the peak pressure in the aorta and the left ventricle drop to 103.8mmHg (from 117.4mmHg in the simplified model), and in the pulmonary loop the peak pressure in the pulmonary artery and right ventricle drop from 25.7mmHg to 25.4mmHg . The pressure drop in the pulmonary loop is much smaller than that in the systemic loop in the systolic phase. In the diastolic phase, regurgitant flow in the aortic/pulmonary valve causes a pressure drop of about 16mmHg in the aorta and a pressure drop of about $1 \sim 2.7\text{mmHg}$ in the pulmonary artery, while it also induces negligible increase in the left and right ventricular pressures. The pressure drops in the right heart are much smaller than that in the left heart. This is still the effect of the highly distensible blood vessels (and thus the greater compliance) in the pulmonary loop. Regurgitant flow to the atria also increases the atrial pressure throughout the heart cycle, which is more prominently exhibited in the pulmonary loop.

The most obvious feature in the flow-rate response in Figure 2-17 (b) and (e) is feature FQ1, the regurgitant flows, across the aortic/pulmonary valves (in early diastole) as well as across the mitral/tricuspid valves (in early systole). Regurgitant flow through the mitral and tricuspid valves builds up more blood in the atria, and increases the preload, so that in early diastole the peak flow-rates corresponding to feature FQ3 (E velocity) increases from 746.2ml/s to 848.0ml/s in the mitral valve and from 954.3ml/s to 984.3ml/s in the tricuspid valve. Accompanying this, in early systole the peak aortic flow increases from 879.4ml/s to 1088.6ml/s , and the peak tricuspid flow also increases from 706.6ml/s to 841.1ml/s . In early diastolic phases regurgitant flow in the aortic and pulmonary valves slightly increase the ventricular pressure, thus the peak mitral/tricuspid flow corresponding to feature FQ3 occurs about 0.1s later compared to that in the simplified model.

Comparing to the results in the simplified model, regurgitant flow increases the atrial volume, especially in the systolic phase, as illustrated in Figure 2-17 (c) and (f). This also increases atrial preload, thus naturally increasing the ventricular volume in the diastolic phase. In the systolic phase however, the ventricles contract to a smaller volume due to the mitral/tricuspid regurgitant flow. In the early diastolic phase, the additional volume increase in the ventricles is due to aortic/pulmonary regurgitant flow. Similarly, mitral/tricuspid regurgitant flows cause additional volume drops in the ventricles, and volume increases in the atria in both the late diastolic and the early systolic phases. The regurgitant flows increase the volume load to the ventricles.

2.3.4 Response with All Features

Finally the simplified model is coupled with both the features of atrio-ventricular interaction and heart valve dynamics. In this case, equations (2-5) and (2-6) for variable atrial elastance are used to replace the constant atrial elastance value of $E_{la,min}$ in the simplified model; equation (2-10) for KG diaphragm dynamics and equations (2-11), (2-12) for correction of atrial and ventricular volumes are combined in the modelling; equation (2-14) in the simplified model is replaced with equations (2-15) and (2-17) to consider the heart valve dynamics. Results for KG diaphragm displacement, heart valve angle changes and corresponding pressure, flow-rate and volume changes in a typical heart cycle are illustrated in Figure 2-18 to Figure 2-20.

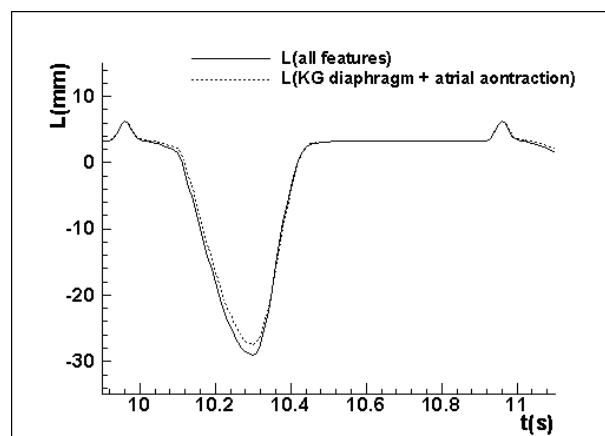
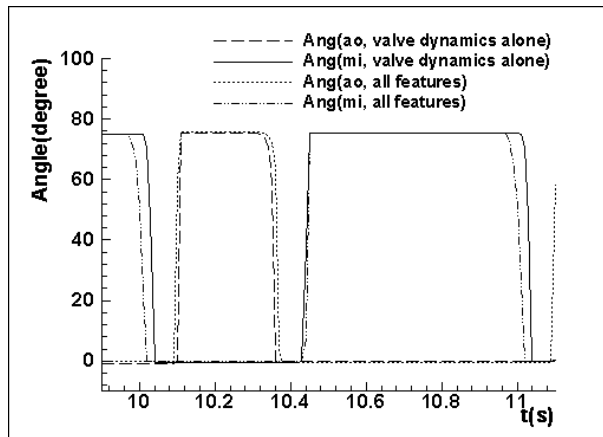
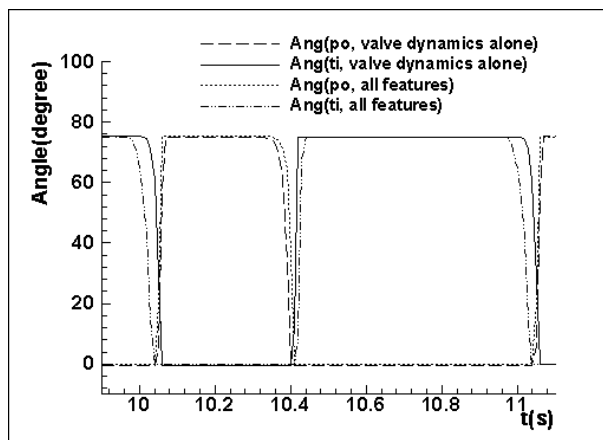


Figure 2-18 Comparison of KG diaphragm motion in left heart when all the features of atrial contraction, KG diaphragm motion and heart valve dynamics are considered with that under combined influence of KG diaphragm motion and atrial contraction



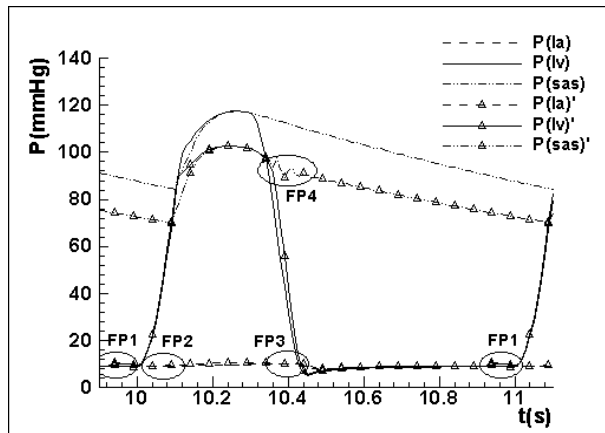
(a) Aortic and mitral valves



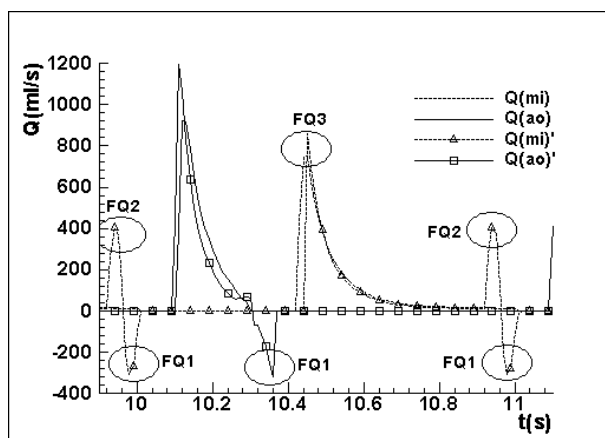
(b) Pulmonary and tricuspid valves

Figure 2-19 Comparison of changes of heart valve leaflet angular position (opening) when all the features of atrial contraction, KG diaphragm motion and heart valve dynamics are considered with those of heart valve dynamics modelling alone

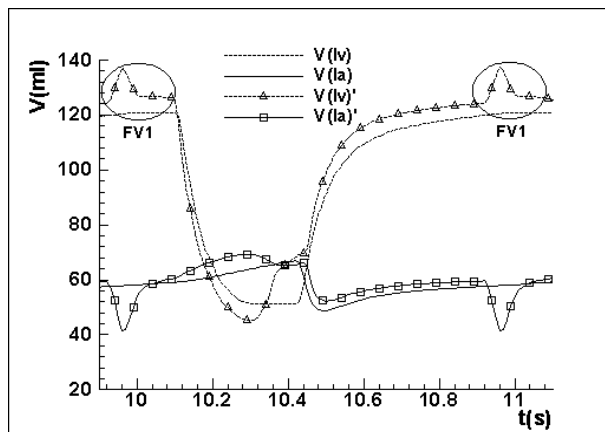
Figure 2-18 compares the KG diaphragm displacement changes in the left heart in a typical heart cycle in the two situations. The dotted line represents the response when the KG diaphragm motion and atrial contraction effects are modelled. The solid line represents the response when all the features of atrial contraction, KG diaphragm motion and heart valve dynamics are considered. The extra contribution of heart valve dynamics helps to stretch the KG diaphragm further into the ventricle for about $0.002 \sim 0.004m$ during systole. A possible reason is that due to mitral regurgitation, the left ventricle contracts to a smaller volume during systole, thus stretching the KG diaphragm towards the apex direction for a few extra millimetres. The same situation occurs in the right heart.



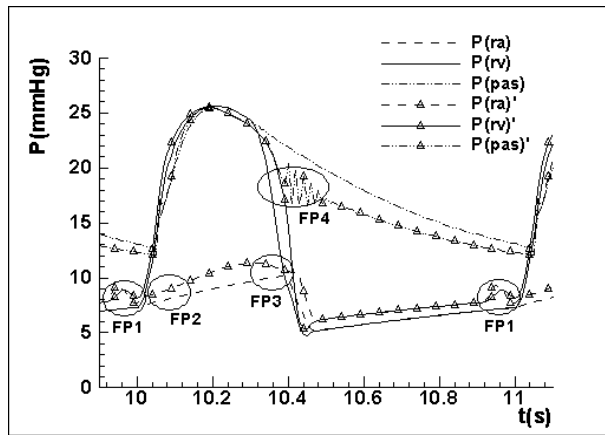
(a) Pressure, left heart



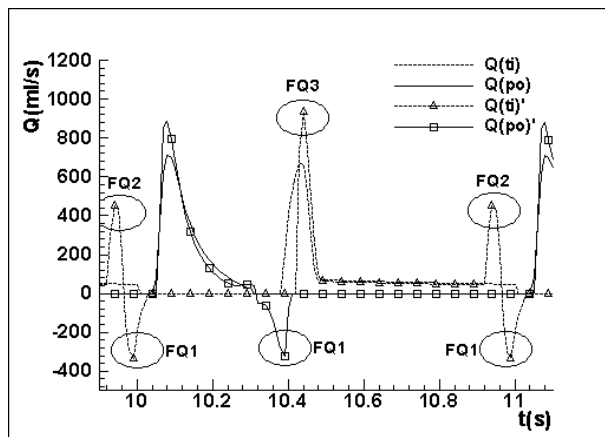
(b) Flow-rate, left heart



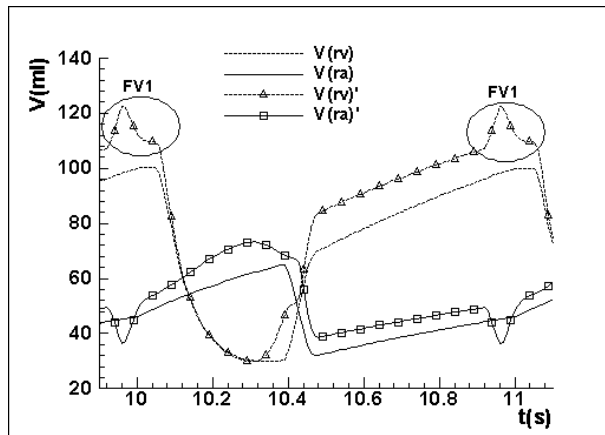
(c) Volume, left heart



(d) Pressure, right heart



(e) Flow-rate, right heart



(f) Volume, right heart

Figure 2-20 Response when all the features of atrial contraction, KG diaphragm motion and heart valve dynamics are considered

(Responses with a prime(') correspond to the condition when all the features are considered.)

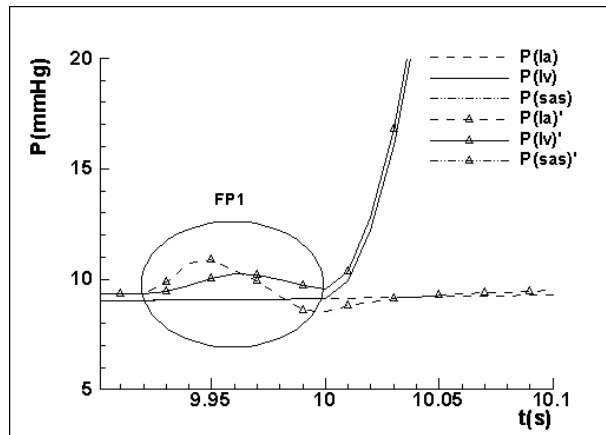


Figure 2-21 Phase lag between left atrial and left ventricular pressures in end diastole

(Responses with a prime(') correspond to the condition when all the features are considered.)

Figure 2-19 (a) and (b) compare the change of heart valve opening angles in the left and right heart when heart valve dynamics alone are modelled with that when all the features of atrial contraction, KG diaphragm motion and heart valve dynamics are considered. Generally the time periods taken for the valve opening and closing sequences are the same, but the exact instances for the opening and closing processes are changed due to the influence of atrial contraction and KG diaphragm motion. In the left heart, when all the features are considered the mitral valve closing process occurs about 0.02s earlier than when only the valve dynamics are considered, while the mitral valve opening does not change much. A close examination of the pressure change in Figure 2-20 (a) reveals that, in late diastole atrial contraction causes a local peak in left atrial pressure and a corresponding local peak in left ventricular pressure, but the local peak in the left ventricle has a phase lag compared to the local peak in the left atrium, as shown in Figure 2-21. Thus when left atrial pressure begins to drop at the late stage of atrial contraction, left ventricular pressure is still in the process of rising. This phase lag causes the left ventricular pressure to be temporarily greater than the left atrial pressure in late diastole, and this pressure difference drives the mitral valve to close. This situation is different from the former case when only valve dynamics were considered, in which mitral valve closing occurs in early systole under the contractile action of the left ventricle. When all the features are considered, the aortic valve opens about 0.01s earlier and closes 0.01s later than when only the valve dynamics are considered. This is also due to the influence of the KG diaphragm motion and atrial contraction, which improves the left ventricle filling and increases ventricular pressure

when compared with the case of when only the valve dynamics are considered. A similar situation also occurs in the right heart.

Figure 2-20 compares the pressure, flow-rate and volume changes during a typical heart cycle when the various features interact with each other with that in the simplified model. In the pressure response in Figure 2-20 (a) and (d), it is found that features FP1(*a* wave in atrial pressure waveform), FP3 (*v* wave in atrial pressure) and FP4 (dicrotic notch) are clearly demonstrated. These features require inclusion of atrial contraction and valve dynamics in the simulation. Feature FP2 of *c* wave is not obvious in the atrial pressure waveform, due to its minor physiological effect and due to neglecting leaflet elasticity in the valve model. The combined effect of atrial contraction, valve dynamics and KG diaphragm motion greatly decreases the peak left ventricular systolic pressure from 117.4mmHg to 102.7mmHg , thus decreasing the aortic pressure by about 20mmHg all over the heart cycle. The combined effect of these features does not change the peak right ventricular pressure much, while the pressure in the pulmonary artery is decreased by about $0.8 \sim 3.1\text{mmHg}$ in the diastolic phase. Left and right atrial pressures are slightly elevated in the heart cycle. Comparison of Figure 2-20 with Figure 2-14 and Figure 2-17 suggests that pressure changes are mainly due to the effect of heart valve dynamics. Pressure drops in the right heart are much smaller than that in the left heart. This is also due to the highly distensible blood vessels, and thus the greater compliance in the pulmonary loop, which buffers the pressure pulsation significantly.

All three features of FQ1 (regurgitant flow), FQ2 (*A* velocity effect in mitral/tricuspid flow) and FQ3 (*E* velocity effect in mitral/tricuspid flow) are simulated in the flow-rate response in Figure 2-20 (b) and (e). Compared to the simplified model, under the combined action of atrial contraction, KG diaphragm motion and heart valve dynamics, in both systemic and pulmonary loops the peak values of flow-rate through the heart valves enormously are increased. In aortic valve the value increases from 920.8ml/s to 1183.6ml/s ; in mitral valve it changes from 744.6ml/s to 851.4ml/s ; in pulmonary valve it increases from 695.5ml/s to 879.4ml/s ; and in tricuspid valve it changes from 665.5ml/s to 911.4ml/s . The *E/A* ratios are about 2 in both left and right heart. Regurgitant flows in the mitral and tricuspid valves begin from late diastole, almost immediately following the feature of FQ2 for *A* velocity, as compared to the

situation of happening to the early systole in the case when only valve dynamics are considered. The reason is still the phase lag between the peaks in atrial and ventricular pressures, as explained above.

Figure 2-20 (c) and (f) show that due to the combined action of atrial contraction, KG diaphragm motion and heart valve dynamics, the atrial volume is shifted upward slightly, except for a local trough in late diastole due to atrial contraction; while ventricular volume is prominently increased in the diastolic phase, and decreased in the systolic phase, thus producing an extra stroke volume of about 30% when compared to the simplified model. Feature FV1 corresponds to the step increase in the ventricular volume due to atrial contraction can be clearly observed in the volume response. However, due to regurgitant flow in the mitral and tricuspid valves caused by heart valve dynamics, the step volume increase is compromised in the late stage of diastole, as compared to the flat step volume increase in Figure 2-10 and Figure 2-14.

2.4 Discussion

Numerical modelling of the human cardiovascular system is an active research area due to its increasing use in physiological and pathological studies. Various models have been developed to address different aspects of cardiovascular dynamics. Most of these models concentrate on one detailed aspect of the overall system to suit specific application requirements, for instance, foetal circulation (Pennati *et al.* 1997a, Pennati *et al.* 1997b), response to orthostatic stress (Heldt *et al.* 2002), isocapnic hypoxia (Ursino and Magosso 2000a, Ursino and Magosso 2000b) etc. Although the above are useful for the specific applications, the model presented in this study takes a different approach and emphasizes dynamics within the four chambers of the heart. At the same time the proposed cardiac dynamics model developed can still be coupled to any model of the whole of the circulation loop. These circulation loop models can include simpler models of the systemic or pulmonary circulation loops, or in a more comprehensive model they can include local elaborate models of elements of the circulation loops such as renal flow, hepatic flow, cerebral flow etc. Specifically the cardiac dynamics model presented can be used to provide the input to the whole network of downstream blood vessels, which can be as simplified or as detailed as the specific study requires.

Previous cardiac models consider various features in cardiac dynamics, such as atrial contraction (Pennati *et al.* 1997a, Sun *et al.* 1997, Vollkron *et al.* 2002) and intra-

ventricular interaction (Chung *et al.* 1997, Olansen *et al.* 2000, Santamore and Burkhoff 1991, Sun *et al.* 1997), but do not include the combined effects of atrio-ventricular interaction and heart valve dynamics. Based on clinical MRI measurements, the present study takes into account the atrial and ventricular tissue stretching effect, and results in realistic description of the motion of the atrio-ventricular annulus fibrosus. Previous models of heart valve dynamics modelled the valve as a diode-resistance combination, or introduced concepts of time varying drag coefficient or dead space volume while used prescribed valve leaflet motion. The present study improves on previous models by directly considering the simplified blood-leaflet effect that governs the valve leaflet motion.

The combination of models in this study, including the combination of atrial contraction, atrio-ventricular interaction and heart valve leaflet dynamics successfully predicts a realistic description of key details of cardiac dynamics.

By comparing the simulation results with the conceptual drawing for cardiovascular dynamics extracted from textbooks, it is observed that main cardiac-flow dynamic features in the pressure changes with time, flow rate changes with time, and volume changes with time in the four chambers of the heart that were missing in previous work are realistically predicted in the current work. In the pressure response, features FP1, FP2 and FP3 for a , c and v waves in atrial pressure are revealed with the combination of models for atrial contraction, ventricular contraction, and atrio-ventricular interaction. These features are more prominent in the pulmonary loop than in the systemic loop due to the relative amplitude of the atrial pressure variation to ventricular pressure variation in the two loops. Feature FP4 for the dicrotic notch is also manifested with the improved heart valve dynamics model, which is missing in most previous models. In the flow rate response, the new heart valve dynamics model contributes to revealing feature FQ1 for regurgitant flow in the heart valves, which is also missing in most previous models. Features FQ2 for A velocity, FQ3 for E velocity and the E/A ratio in the mitral/tricuspid flow are also illustrated with the combined model for atrial contraction and atrio-ventricular interaction. Usually the above features are not mentioned in previous works. Modelling of heart valve dynamics also approximates aspects of the valve leaflet angular position, and through that of the valve opening and closing process, as illustrated in Figure 2-20. Details of feature FV1, some of which were observed in the MRI measurements, and others that appear in

physiology books, were simulated. Successful simulation of these features in the pressure, flow-rate and volume response has important physiological meaning, and may have implications for improvements in future clinical practice. Delicate changes in these features often herald the potential, or even the occurrence, of certain cardiovascular diseases. For example, certain changes in the features of FQ1, FQ2 and FQ3 may indicate heart valve stenosis or incompetence; and diminishing of feature FV1 may hint in atrial fibrillation. Some details of FV1 shown in the computations (Figure 2-20) are not evident in the measurements of Figure 2-3. Improvements in MRI, echocardiography, and other clinical techniques, and their companion software, may be required in order to clearly measure in clinical practice some features observed in the numerical results such as the computed details of FV1 in Figure 2-20. In turn these enhanced clinical measurements will provide data for calibration of the parameters of the numerical model, so that future numerical predictions simulate better the more-accurate future clinical measurements.

This chapter studies the individual relative contributions of atrio-ventricular interaction and heart valve dynamics on cardiovascular system dynamics. The models of atrio-ventricular interaction and heart valve dynamics help to reveal some characteristics in the cardiovascular response that were usually missing in previous papers. These new features and the effect of atrial contraction are then discussed, and their detailed contribution to the cardiovascular dynamics are examined one by one, based on comparison of pressure change with time, flow-rate change with time, and volume change with time as compared to the response from the simplified model (where these features were not included).

These comparisons showcase causes and effects of important details in the dynamic system response, such as the a and v waves in atrial pressure, dicrotic notch in aortic pressure, E/A velocity ratio in mitral flow, regurgitant flow through the heart valves, corresponding local variations in the volume changes in the four chambers of the heart, and their relative effects. Introducing the effects of each feature of the overall model consecutively contributes to better understanding of physiological as well as numerical aspects of the work, and their effect on overall system response. This is useful from the clinical as well as the modelling point of view.

The atrial contraction results confirm that atrial contraction promotes the ventricular filling process, thus leading to a prominent pressure increase in the left ventricle and

the aorta. The pressure elevation in the pulmonary circulation loop is not as prominent, due to the lower overall pressure and the great distensibility of the blood vessels in the pulmonary loop. KG diaphragm motion alone helps to increase the cardiac volumetric output while decreasing systolic ventricular pressure. When both atrial contraction and KG diaphragm motion are considered together, their combined effects on the pressure and flow-rate responses in the heart counteract each other, so that overall the combined beneficial result in atrio-ventricular interaction is that the volumetric cardiac output is improved by about 20% (compared with that in the simplified model). This supports the idea that KG diaphragm motion works as an auxiliary pumping mechanism (KG diaphragm pump) in the function of the heart. This combined effect has not been examined quantitatively and in this detail in prior work.

Considering heart valve dynamics alone reveals the significant interaction effects between valve leaflet motion and cardiac dynamics. The regurgitant flow in the valves decreases aortic pressure and systolic left ventricular pressure. The decrease in the right side of the heart is much smaller than in the left side due to the lower overall pressures in the pulmonary loop, and the great distensibility of pulmonary blood vessels. This suggests that valve dynamics has a great influence on the overall system response (again, from both the clinical and numerical points of view).

When all the effects of atrial contraction, KG diaphragm motion and valve dynamics are considered together in the simulation, the various factors interact with each other. The effects of atrial contraction and KG diaphragm motion on pressure and flow-rate responses counteract each other, but overall atrio-ventricular interaction results in increased volumetric cardiac output. If the model included ventricular contraction and valve dynamics but did not include the effect of atrio-ventricular interaction, then it would predict that regurgitant mitral and tricuspid valve flow would occur in early systole. Adding the atrio-ventricular interaction model causes a phase lag in the local difference between atrial and ventricular pressures in end diastole, resulting in regurgitant flow in the mitral and tricuspid valves near the end of the diastolic phase.

Comparing the results of the model containing individual features of the model with the results of the model containing all the features, illustrates which aspects of cardiovascular system response are caused by the individual model features. The combined effect of atrial contraction and KG diaphragm motion in atrio-ventricular interaction results in: features FP1, FP2 and FP3 for the a , c and v waves in atrial

pressure; feature FQ2 for A velocity; feature FQ3 for E velocity; and the E/A velocity ratio in mitral/tricuspid flows. The magnitude of features FP1, FP2 and FP3 is smaller in the pulmonary loop than in the systemic loop, but the change is more visible in the pulmonary loop traces, due to the overall lower values of pressure in the pulmonary loop.

The improved heart valve dynamics model illustrates feature FP4 for the aortic notch and feature FQ1 for regurgitant flow in the heart valves. The aortic notch is the result of the combined action of heart valve dynamics, blood inertia, and pulse wave reflection in the arteries. The heart valve dynamics model plays an important role in simulating this feature. In previous works that neglected valve dynamics modelling this feature is not manifested. Similarly, regurgitant valve flow results directly from the heart valve dynamics model, and it is missing in previous works that did not consider valve dynamics.

Modelling of heart valve dynamics also approximates aspects of the valve leaflet angular position, and through that of the valve opening and closing process, as illustrated in Figure 2-19.

The main limitation of the current model is that no neuro-regulation effect was considered. As introduced in the introduction chapter, in the human body the heart rate, the heart contractility, and the vessel tone, are under the regulation of sympathetic and parasympathetic nerves. In situations such as exercise condition or under emotional changes, the neuro-regulation effect can induce much change in the cardiovascular response. Some other non-linear effects and external interactions, such as interaction between the cardiovascular system and the respiratory system, the auto-regulation effect, venous collapse due to extra-luminal pressure, are all neglected in the current model. To achieve better simulation accuracy these factors will be properly modelled in the next stage of the modelling work. Since this is a lumped-parameter modelling, some cardiovascular features like pulse wave transmission and reflection cannot be captured by the model. To describe such features, the current model needs to be combined with higher order models (such as 1D and 3D models) to form a more comprehensive description of the cardiovascular dynamics.

2.5 Conclusions

In this chapter a new cardiovascular system model is developed to simulate human circulation dynamics. In the model, the heart is modelled as a four-chamber pump with variable elasticity.

As enhancement from previous models, new models for atrio-ventricular interaction motion and heart valve dynamics are developed. Based on MRI measurements of cardiac dynamics, motion of the atrio-ventricular annulus fibrosus, which is acting as a diaphragm pump called the KG diaphragm, is considered in the model, and a linear tissue stress--elasticity constitutive relation is assumed for the atrial and ventricular chambers. Motion of the atrio-ventricular interaction ring area (KG diaphragm) is modelled by considering the various factors of pressure difference across the diaphragm, frictional force, and tissue stress in the atrial and ventricular chambers. Based on previous CFD studies, heart valve dynamics is considered in the model. In modelling heart valve dynamics, the nonlinear pressure--flow-rate relation for flow through an orifice is used, and the valve leaflet motion is modelled based on Newton's second law by considering the flow-induced pressure difference across the valve and the frictional force from tissue movement. The systemic and pulmonary loops are each modelled as segments of aortic sinus/pulmonary artery sinus, artery, arteriole, capillary and vein, with the combined effects of flow resistance, blood vessel elasticity, and blood inertia modelled for each segment based on local flow characteristics.

This chapter also examines the individual contribution of each feature to cardiovascular system response, and then studies the integrated response as all features are considered together. Simulation results validate the great influence of heart valve dynamics on the cardiac response, and prove that the atrio-ventricular interaction acts as an auxiliary pumping mechanism. Certain important characteristics in cardiovascular response, such as the a and v waves in atrial pressure, dicrotic notch in aortic pressure, E/A ratio in mitral flow, regurgitant flow through heart valves etc., are successfully simulated. The study suggests that models for the heart valve dynamics and the atrio-ventricular interaction should be considered in the future cardiovascular studies.

Chapter 3 Computational Modelling and Evaluation of Cardiovascular Response under Pulsatile Impeller Pump Support²

This chapter presents a numerical simulation of cardiovascular response in the heart failure condition under the support of a Berlin Heart INCOR® impeller pump type ventricular assist device (VAD). To investigate the potential of using the Berlin Heart INCOR® impeller pump to produce physiologically meaningful arterial pulse pressure within the various physiological constraints, a series of VAD assisted cardiovascular cases are studied, in which the pulsation ratio and the phase shift of the VAD motion profile are systematically changed to observe the cardiovascular responses in each of the studied cases. An optimisation process is proposed, including the introduction of a cost function to balance the importance of the characteristic cardiovascular variables. Based on this cost function it is found that a pulsation ratio of 0.35 combined with a phase shift of 200° produces the optimal cardiovascular response, producing a maximal arterial pulse pressure of 12.6 mmHg without inducing regurgitant pump flow whilst keeping other characteristic cardiovascular variables within appropriate physiological ranges.

3.1 Introduction

Numerical simulation has been extensively applied to the study of cardiovascular dynamics in heart failure under support with a ventricular assist device (VAD), and this has greatly promoted the design and analysis of VADs to achieve optimised cardiovascular response. In terms of system-level cardiovascular dynamics, including the examination of perfusion efficiency under different VAD configurations, the most

² Adapted from:

- Shi Y., Brown A., Arndt A., Nuesser P., Lawford P., Hose R., Numerical Modelling and Evaluation of Cardiovascular Response under Pulsatile Impeller Pump Type VAD Support, *Journal of the Royal Society: Interface Focus*, 1(3), pp320-337, 2011
- Shi Y., Hose R., Lawford P., Numerical Modelling of Hemodynamics with Pulsatile Impeller Pump Support, *Annals of Biomedical Engineering*, 38(8), pp2621-2634, 2010

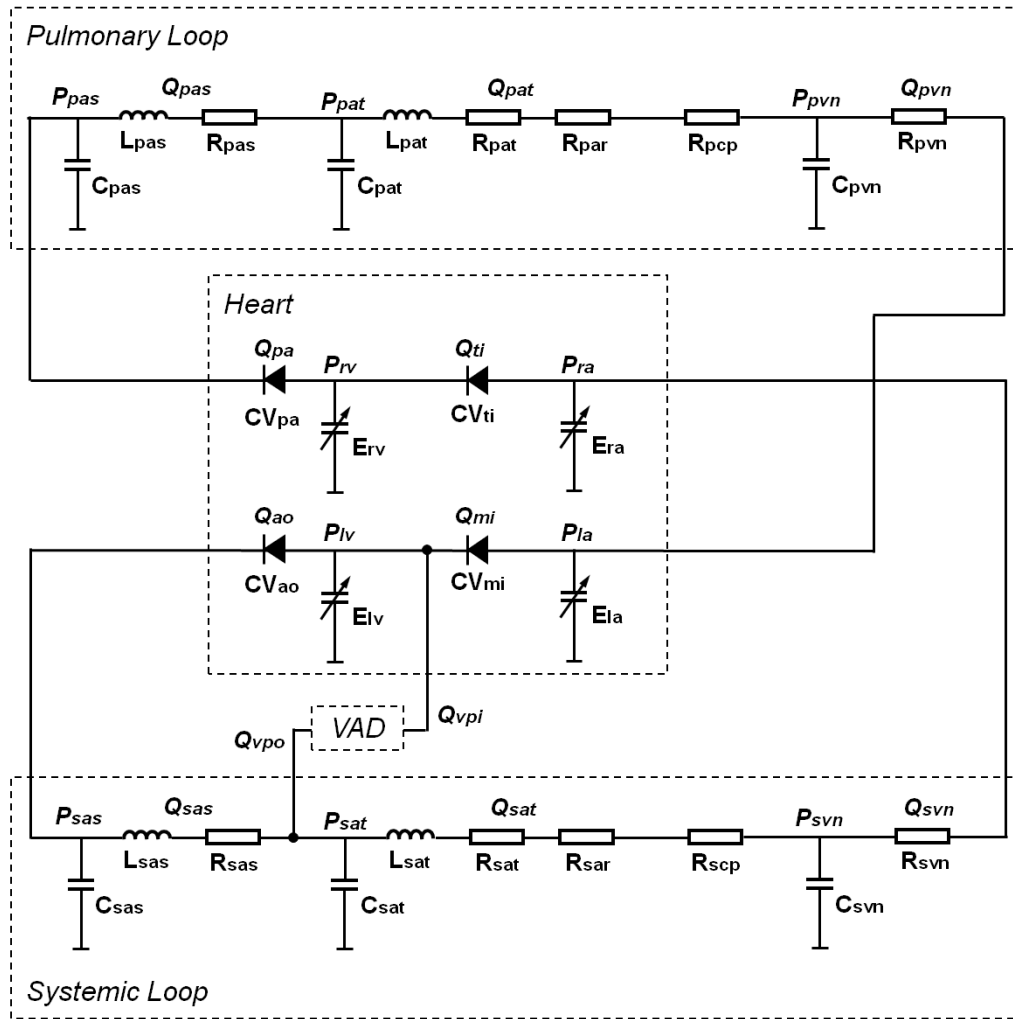
useful information has come from zero dimensional, lumped-parameter studies. Three dimensional computational fluid dynamics has its role in the detailed analysis of flow fields in the device itself, for example to evaluate blood damage and thrombosis potential, and in the future will be applied in models of the heart and vasculature to evaluate details of physiological flow fields under LVAD support (<http://www.euheart.eu>)

Currently two types of VAD design are widely used in treatment of end stage heart failure: impeller pumps and displacement pumps. Compared to displacement pumps, impeller pumps have the advantages of compactness, no valves, a simpler control aspect, lower power consumption and lower relative cost (Takatani 2001). However, most impeller type VADs are designed to work in a constant speed mode, and thus in principle produce non-pulsatile flow. It is widely recognised that pulsatile flow has an important effect on circulation physiology: it promotes kidney and liver perfusion, and promotes microcirculation at the cell level which is important in early treatment of acute heart failure (Sezai *et al.* 1999, Undar 2004). In the heart failure condition under impeller pump support, the diseased myocardium has some remaining contractility which can produce residual pulsatility in the blood flow, but such pulsatility is often negligible and does not have a physiological significance comparable to that of the healthy condition or of the condition of heart failure assisted with displacement pumps (Undar 2004). To enjoy the advantages of compact device design in the impeller pump VADs and the improved perfusion to peripheral organs with pulsatile blood flow, it has been proposed that the rotating speed of the impeller pump might be varied over the heart cycle (Choi *et al.* 2001, Gobel *et al.* 2001, Qian 1996, Vandenberghe *et al.* 2005). Several researchers have reported arterial pressure pulsation covering the physiological range of 80–120 *mmHg* without thrombus formation. Qian (Qian 1996) proposed the use of twisted impeller vanes to reduce the Reynolds shear stress minimizing the haemolysis within the pump, and thus claimed to have produced the first effective pulsatile centrifugal blood pump. Gobel *et al.* (Gobel *et al.* 2001) designed the Medos DeltaStream impeller pump and tested it under a sinusoidal speed variation of 3000–9500 *rpm*. The pump produced a pressure fluctuation between 80–120 *mmHg* with no thrombus formation in testing. Vandenberghe *et al.* compared the unloading effect of the Medos Micro microdiagonal rotary blood pump under both continuous and pulsatile modes (Vandenberghe *et al.* 2003), and also studied the haemodynamic modes

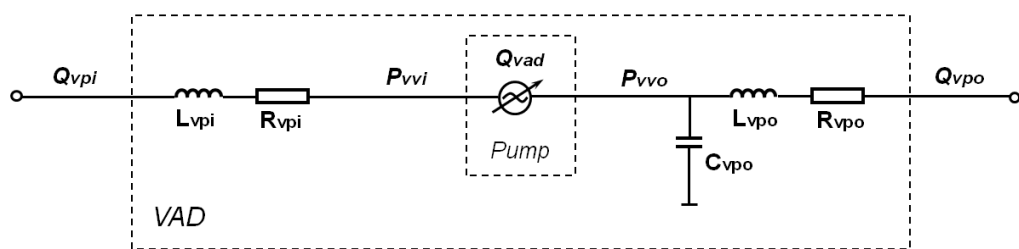
of ventricular assist with Medos DeltaStream rotary blood pump in continuous and pulsatile modes (Vandenberghe *et al.* 2005). In studies of VAD control strategy design, Giridharan *et al.* (Giridharan and Skliar 2003) and Ohuchi *et al.* (Ohuchi *et al.* 2004) modulated the speed of the rotary blood pump and produced pulsation of arterial pressure covering the physiological range. However, Shi *et al.* (Shi *et al.* 2010) carried out numerical evaluations in a HeartMate III impeller pump and warned that although modulating the pump rotating speed could produce physiological pressure pulsation, this control mechanism also induced strong regurgitant pump flow, which greatly reduced the pump efficiency. Since the cardiovascular response under VAD support depends on the interaction between the native circulation system and the VAD, and different VAD designs have different characteristics, more case studies are necessary and it is imperative to test other impeller pumps under similar situations before a concrete conclusion can be drawn.

To evaluate the performance of VAD support and the effect of VAD interaction with the native cardiovascular system, it is necessary to determine which quantitative physiological criteria, including cardiac output, pressures in various parts of the circulation system, balance of blood distribution between the systemic and the pulmonary circulation loops, metabolic requirements of peripheral organs, vital organs (such as brain, kidney) perfusion pressure, VAD energy consumption etc., should be used to compare cardiovascular response under different VAD control strategies. Inevitably those strategies that produce optimal performance against one of the physiological criteria offer degraded performance against others. In the majority of publications to date the focus has been on a subset of physiological criteria, neglecting the others. For example, cardiac output was the major concern in (Abe *et al.* 1998, Choi *et al.* 2001, He *et al.* 2005, Hsu 2004, Klute *et al.* 1992, Saito *et al.* 1999, Yoshizawa *et al.* 1992); left atrial pressure was the main target of VAD motion optimisation in (He *et al.* 2005, Kitamura 1990, McInnis *et al.* 1984, Olegario *et al.* 2003, Saito *et al.* 1999); left ventricular pressure was addressed in (Bullister *et al.* 2002); arterial pressure in (Barnea *et al.* 1992, Bullister *et al.* 2002, He *et al.* 2005, Kosaka *et al.* 2003, Wu *et al.* 2003); pressure difference across the VAD in (Waters *et al.* 1999, Wu *et al.* 2003); peripheral vascular resistance in (Abe *et al.* 1998, Saito *et al.* 1999); heart oxygen consumption in (Drzewiecki *et al.* 1990); and venous oxygen saturation in (Nakamura *et al.* 2000) etc. Also some VAD characteristic variables such as VAD pump flow

(Kosaka *et al.* 2003, Nakata *et al.* 1999) and VAD pump rpm (He *et al.* 2005, Ohuchi *et al.* 2004) have been included in evaluating the VAD support performance. Although each of these publications offers valuable insight into specific aspects of performance, it is apparent that there is a need for an overall physiological indicator (a cost function) that provides an indication of the extent to which the balance between the conflicting performance requirements is met. Wu *et al.* (Wu *et al.* 2003) used a weighted average of aortic pressure and pressure difference across the VAD in the design of a VAD controller. He *et al.* (He *et al.* 2005) designed specific member functions to calculate the effects of individual physiological variables including stroke volume, mean left atrial pressure, minimum aortic pressure, and mean pump rotation speed under different VAD motion conditions, and then computed the weighted average of these member functions to decide the overall quality of the VAD assisted cardiovascular response. Such a weighted average of physiological variables provides a better solution to address the contradictory requirements in the optimisation of VAD assisted cardiovascular response. In this chapter a more comprehensive physiological indicator cost function is introduced. The numerical model described in (Shi *et al.*) has been operated to study cardiovascular response in a heart failure condition under the support of a Berlin Heart INCOR® impeller pump, and to optimise a simple control algorithm against the proposed cost function.



(a) System configuration



(b) Model structure for the impeller pump

Figure 3-1 Illustration of cardiovascular system with impeller pump VAD

(Refer to the nomenclature table for detailed name of each compartment)

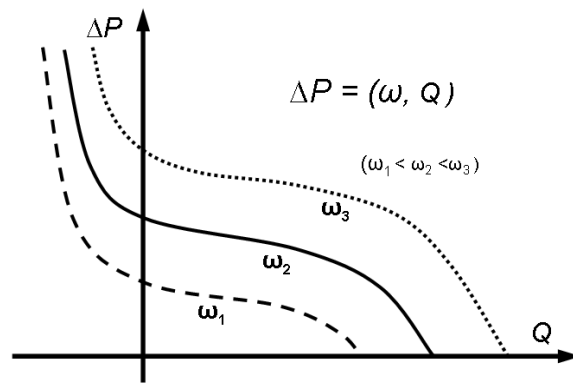


Figure 3-2 Conceptual drawing of pump characteristics for Berlin Heart INCOR® impeller pump

3.2 Materials and Methods

3.2.1 Numerical model of the System

Figure 3-1 shows a schematic of the whole system, based on that described by (Shi *et al.* 2010). The system comprises two parts: the native cardiovascular system and the impeller pump. The inlet conduit of the impeller pump is connected to the left ventricular apex to achieve improved unloading of the diseased ventricle. The outlet conduit of the pump is connected to the ascending aorta in order to minimise blood stasis in the aortic root.

A detailed zero-dimensional model of the native cardiovascular system has been described in (Shi and Korakianitis 2006). The system is modelled in three main parts: the heart, the systemic circulation loop and the pulmonary circulation loop. The heart is modelled as a four-chamber pump with variable elastance and four heart valves that control the direction of blood flow. The systemic and pulmonary circulation loops are separated into aortic sinus/pulmonary artery sinus, arterial, arteriolar, capillary and venous compartments. The local resistance to blood flow, elasticity of blood vessels, and inertia of blood are modelled in each compartment. The combined effect of venules, veins and vena cava is modelled as the venous compartment. The arterial compartment represents the general characteristics of the aorta, the main and smaller arteries. The aortic sinus compartment characterises the aortic root. The heart valve dynamics have also been modelled by combining pressure difference, frictional force and vortex effect on the valve leaflets.

The characteristics of the device are described by a relationship of the form $\Delta P = P(Q, \omega)$, based on the experimentally measured pressure-flow characteristic in the Berlin Heart INCOR® impeller pump. Figure 3-2 shows the conceptual drawing of the pump characteristics for the Berlin Heart INCOR® impeller pump.

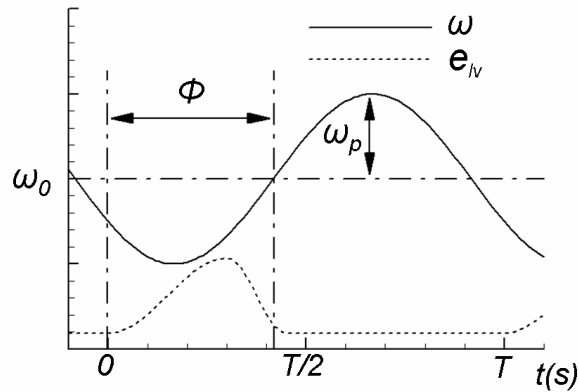


Figure 3-3 Legends for impeller pump speed change

(The two variables to be changed in the pump motion are the pulsation ratio ω_p/ω_0 and the phase shift ϕ .)

3.2.2 Strategy for the optimisation of pump motion

The primary variable of pump operation that can be controlled is its rotation speed. Although most commonly used in a constant speed mode, it is possible to vary the speed over the cardiac cycle. This study explores the optimisation of a two-parameter control algorithm, defined by the pulsation ratio (the amplitude of an imposed sinusoidal motion as a proportion of the necessary underlying constant component) and the phase of this imposed pulsation relative to the impaired contraction of the failing native heart. The control algorithm is described by the following equation:

$$\omega = \omega_0 + \omega_p \cdot \sin(2\pi t/T + \phi) \quad (3-1)$$

Although it is possible to prescribe any temporal expression for the impeller pump control (the rotation speed), in practice a smooth profile is best to reduce the impact and the effect of mechanical imbalance. A simple sinusoidal expression satisfies this constraint. The constant component of the VAD speed, ω_0 , determines the cardiac output in a heart cycle. In this study ω_0 is chosen to produce a cardiac output of about 70 ml/beat and an arterial pressure of $80\text{--}120 \text{ mmHg}$ under the simulated typical vascular impedance. The two control variables of pulsation ratio (defined as the ratio of pulsatile

to constant components in the pump speed, ω_p/ω_0) and phase shift ϕ can be varied individually in the corresponding ranges to obtain the optimal cardiac support. In this study the pulsation ratio is varied over a range of 0-0.8, in increments of 0.05. The upper limit of the pulsation ratio is chosen to avoid excessive regurgitant flow in the pump, which might happen at low VAD flows. The phase difference ϕ is changed over the range of 0–360°, in increments of 10°. Each combination of pulsation ratio and phase difference is examined to evaluate the cardiovascular performance. Figure 3-3 shows a typical temporal profile for the rotation speed of the impeller pump: the change of left ventricular elastance e_{lv} is also indicated to illustrate the phase relation between the pump motion and the native ventricular contraction.

3.2.3 Evaluation of cardiovascular performance

As discussed above, many studies have focused on one or two specific cardiovascular performance measures. (He *et al.* 2005) introduced the notion of a cost function, balancing competing and conflicting requirements to describe an overall performance index. In this study a new and more comprehensive cost function that includes a wider range of requirements ((He *et al.* 2005) included four parameters, whilst this study extends to eight) is introduced. Similar to (He *et al.* 2005), this study defines individual member functions that indicate the optimality of each individual performance parameter (such as cardiac output or left ventricular pressure). These individual contributors are multiplied to serve as the cost function that describes the overall performance of the system: the multiplication operation corresponds to the ‘and’ relation among the cardiovascular variables. Overall cardiovascular response should ideally satisfy all of these variable constraints. It is suggested that there is significant merit in the development of a single quantitative physiological performance index. Whilst subjectivity remains in the determination of both the member functions and the cost function, the optimisation process is formalised and clarified and it might be possible to achieve a community consensus on these basic building blocks.

Not all parameters have the same degree of importance and constraints on their inter-relations, and this should be reflected in their member functions. An acceptable cardiovascular response requires that the cardiac output, the left atrial/ventricular pressure, and the arterial pressure all lie within the normal ranges concurrently, whilst stroke volume and left ventricular volume are expected to lie outside the normal range

but not by too much. One of the questions in the current study was whether a physiologically meaningful arterial pressure pulsation could be produced without causing regurgitant pump flow. Thus the member functions are classified into two groups: a vital group and a non-vital group. The vital parameters should be maintained within the target ranges, within which their member functions are assigned a value of unity, and outside these ranges their member functions drop rapidly to zero, firstly to penalise and ultimately to exclude inappropriate modes of operation. For non-vital variables the maximum value of the membership function remains at unity but the minimum value is assigned a positive value even if the parameter lies outside the target ranges, so that these terms have less impact on the final overall performance index. The final performance index is expressed as:

$$I = f_1(CO) \cdot f_2(Q_{VAD}) \cdot f_3(\Delta P_{sat}) \cdot f_4(P_{la}) \cdot f_5(P_{lv}) \cdot f_6(P_{en}) \cdot f_7(V_{vlv}) \cdot f_8(SV) \quad (3-2)$$

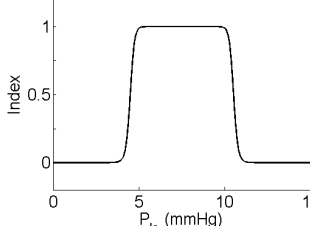
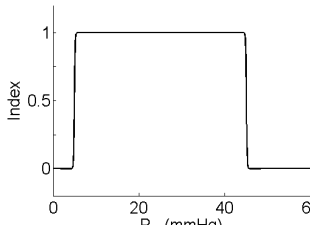
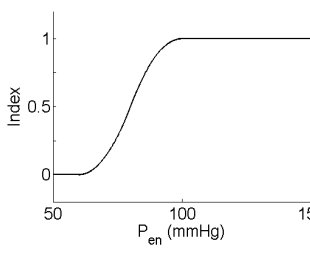
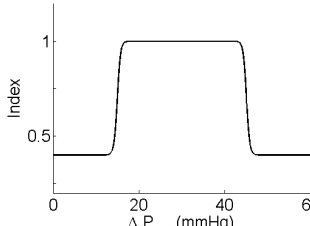
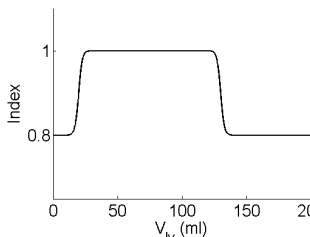
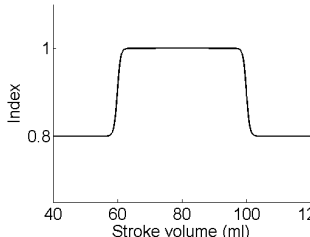
The definitions of the ranges and the forms of the functions are, of course, based on subjective judgement of the researcher. Cardiac output should meet the normal requirement of 70 ml/s in order to provide sufficient perfusion to the organs. Further increase in cardiac output might be advantageous to the cardiovascular response, but it is not necessary when not physiologically needed. The pump flow is mainly decided by the pump rotating speed applied as external control variable and the pressure difference across the pump. However, negative pump flow is often associated with impaired perfusion efficiency and increased blood cell damage and should be avoided. The VAD assisted left ventricular pressure should be maintained in the range of $5-55 \text{ mmHg}$. A smaller left ventricular pressure helps to pressure-unload the heart and thus facilitates the recovery of the myocardium; while too low ventricular pressure will induce collapsing of ventricular wall and needs to be avoided. The left atrial pressure preferably should be kept in the range of $5-10 \text{ mmHg}$, achieving a balance between minimizing the potential of pulmonary oedema and not causing atrial suction and thus stopping of flow to the VAD. The arterial pressure should be maintained in the normal range of $80-120 \text{ mmHg}$ and have the necessary pulsatility to minimize the vascular resistance and promote organ perfusion. Pulsatility of blood flow can be evaluated by the energy equivalent arterial pressure (defined as $\int_0^T P \cdot Q dt / \int_0^T Q dt$, which is a measure of the pulsatile energy delivered by the heart and/or VAD) (Shepard *et al.* 1966) and the arterial pulse pressure (i.e., the difference between the systolic and diastolic arterial

pressures during a cardiac cycle, $\Delta P = P_{es} - P_{ed}$) (Undar *et al.* 1999). The left ventricular volume should be decreased from the dilated condition to the normal range to volume-unload the heart chambers, and finally the stroke volume (approximately equals the volume difference of the left ventricle in a heart cycle) of the ventricle should be maximized within a reasonable range, in order to stimulate reverse remodelling of the diseased heart (Pieske 2004). It should be noted that the stroke volume may not necessarily equal to the cardiac output per heart cycle when the failing heart is supported with an impeller pump, due to the continuous flow nature of the pump. Some other physiological requirements proposed or used by previous researchers, such as balance of blood distribution between the systemic and the pulmonary circulation loops, metabolic requirement of peripheral organs, vital organs perfusion pressure, VAD energy consumption, heart oxygen consumption, and venous oxygen saturation, are too complex or difficult to evaluate, and they are not considered in the current study. Based on these considerations, a number of member functions are constructed (Shi *et al.*), with each corresponding to the individual physiological variables assessed. They are listed in Table 3-1.

Table 3-1. Physiological variables and the corresponding membership functions constructed in assess the cardiovascular response

(Those with a minimum index value of 0 belong to the vital group; those with a minimum index value of greater than 0 belong to the non-vital group)

Physiological variable	Membership function	Illustration of function
Cardiac output ($CO \geq 70 \text{ ml/s}$)	$f(CO) = \begin{cases} 0 & CO \leq 60 \\ 2 \left(\frac{CO - 60}{65 - 60} \right)^2 & 60 < CO \leq 65 \\ 2 \left(\frac{CO - 70}{70 - 65} \right)^2 & 65 < CO \leq 70 \\ 1 & CO > 70 \end{cases}$	
Minimum flow in the VAD ($Q_{VAD} \geq 10 \text{ ml/s}$)	$f(Q_{VAD}) = \begin{cases} 0 & Q_{VAD} \leq 2 \\ 2 \left(\frac{Q_{VAD} - 2}{6 - 2} \right)^2 & 2 < Q_{VAD} \leq 6 \\ 2 \left(\frac{Q_{VAD} - 6}{10 - 6} \right)^2 & 6 < Q_{VAD} \leq 10 \\ 1 & Q_{VAD} > 10 \end{cases}$	

<p>Left atrial pressure ($5\text{mmHg} \leq P_{la} \leq 10\text{mmHg}$)</p>	$f(P_{la}) = \frac{1}{1 + \left \frac{P_{la} - 7.5}{3} \right ^{24}}$	
<p>Left ventricular pressure ($5\text{mmHg} \leq P_{lv} \leq 55\text{mmHg}$)</p>	$f(P_{lv}) = \frac{1}{1 + \left \frac{P_{lv} - 25}{20} \right ^{240}}$	
<p>Energy equivalent arterial pressure ($P_{en} \geq 100\text{mmHg}$)</p>	$f(P_{en}) = \begin{cases} 0 & P_{en} \leq 60 \\ 2 \left(\frac{P_{en} - 60}{80 - 60} \right)^2 & 60 < P_{en} \leq 80 \\ 2 \left(\frac{P_{en} - 100}{100 - 80} \right)^2 & 80 < P_{en} \leq 100 \\ 1 & P_{en} > 100 \end{cases}$	
<p>Arterial pulse pressure ($15\text{mmHg} \leq \Delta P_{sat} \leq 45\text{mmHg}$)</p>	$f(\Delta P_{sat}) = 0.4 + \frac{0.6}{1 + \left \frac{\Delta P_{sat} - 30}{30} \right ^{40}}$	
<p>Left ventricular volume ($20\text{ml} \leq V_{lv} \leq 130\text{ml}$)</p>	$f(V_{lv}) = 0.8 + \frac{0.2}{1 + \left \frac{V_{lv} - 75}{55} \right ^{40}}$	
<p>Stroke volume ($60\text{ml} \leq SV \leq 100\text{ml}$)</p>	$f(SV) = 0.8 + \frac{0.2}{1 + \left \frac{SV - 80}{20} \right ^{40}}$	

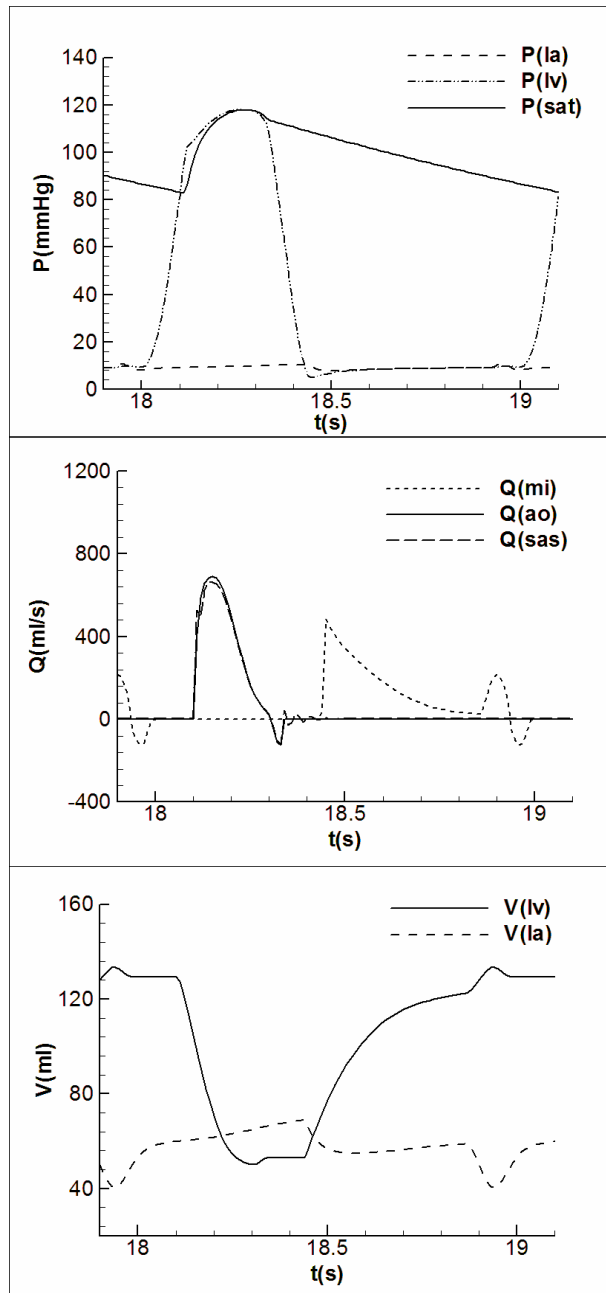
3.2.4 System Parameters

The values of the haemodynamic variables in the native cardiovascular model are the same as those used in (Korakianitis and Shi 2006c, Shi and Korakianitis 2006). Coefficients for the Berlin Heart INCOR® pump model and parameters for the inlet and outlet cannula are provided by the Berlin Heart GmbH. The heart period is set as 1s (corresponding to 60 beats per minute).

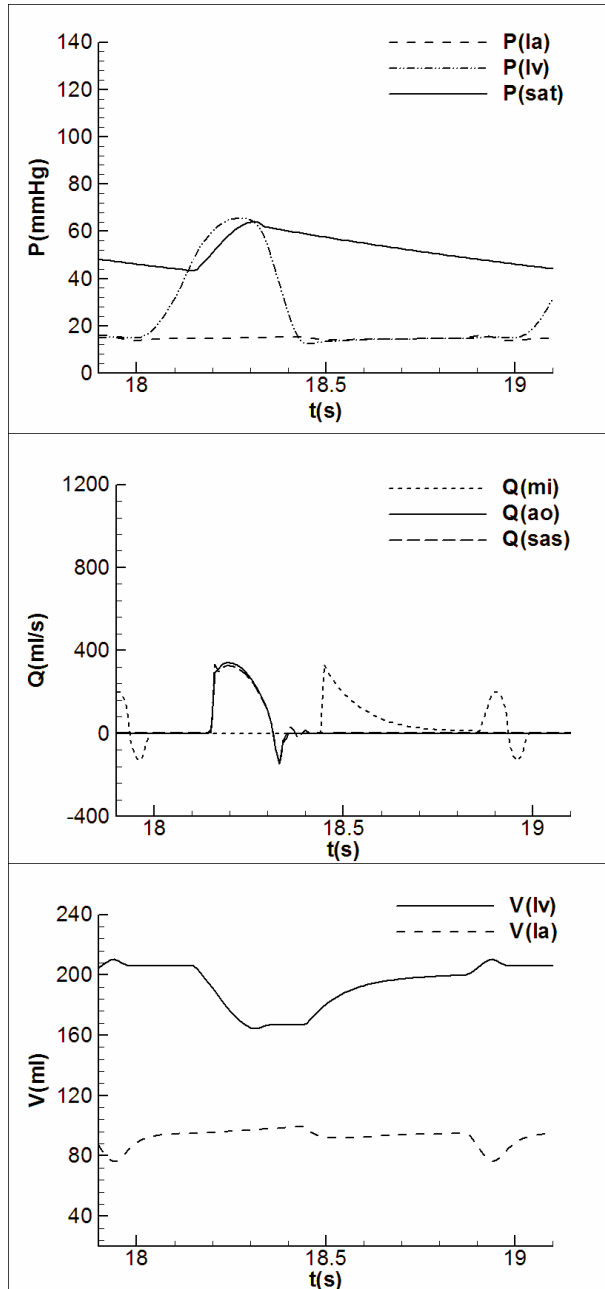
3.2.5 Procedure of numerical study

First the numerical model is tuned to simulate the cardiovascular response in healthy condition, to establish the baseline case for comparison with further cases. Then the left ventricular systolic elastance is reduced to one fifth of the normal value to simulate a typical heart failure condition. The regulatory effects of the sympathetic and parasympathetic nerves are not modelled, to facilitate direct comparison with the VAD-assisted system. Next in the numerical model the pump assistance is enabled, the pulsation ratio and the phase difference in the pump motion profile are both set to zero, and cardiovascular response for different pump speeds is examined to find the baseline constant pump speed that can produce a normal cardiac output. This value is then used as the constant component of the VAD speed, and the pulsation ratio and the phase difference are changed in increments over their full ranges to simulate the cardiovascular response under different combinations of these two control parameters. Of course it would be possible to run an optimisation routine directly to find the optimal solution of the cost function, but this would not characterise the solution space. For each case, the pressure, flow and volume changes are saved as data files. The data files are then read into MATLAB, the converged cardiac cycles identified, and the characteristic physiological variables extracted, including cardiac output, maximum and minimum values of left atrial/ventricular pressures, arterial pulse pressure, energy equivalent arterial pressure, maximum and minimum values of left ventricular volume, and stroke volume. These characteristic variables are then fed into the constructed membership functions to calculate the corresponding performance index for each of the simulated cases.

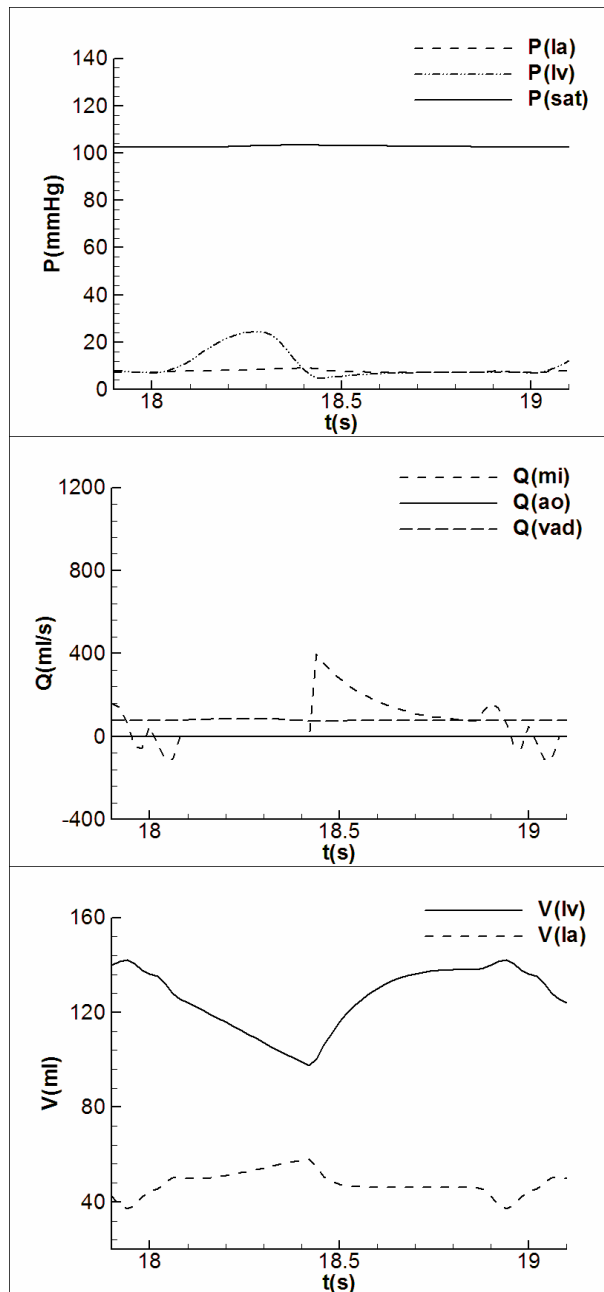
3.3 Results



(a) Healthy conditions



(b) Left ventricular failure without VAD support



(c) Heart failure with impeller pump VAD support}

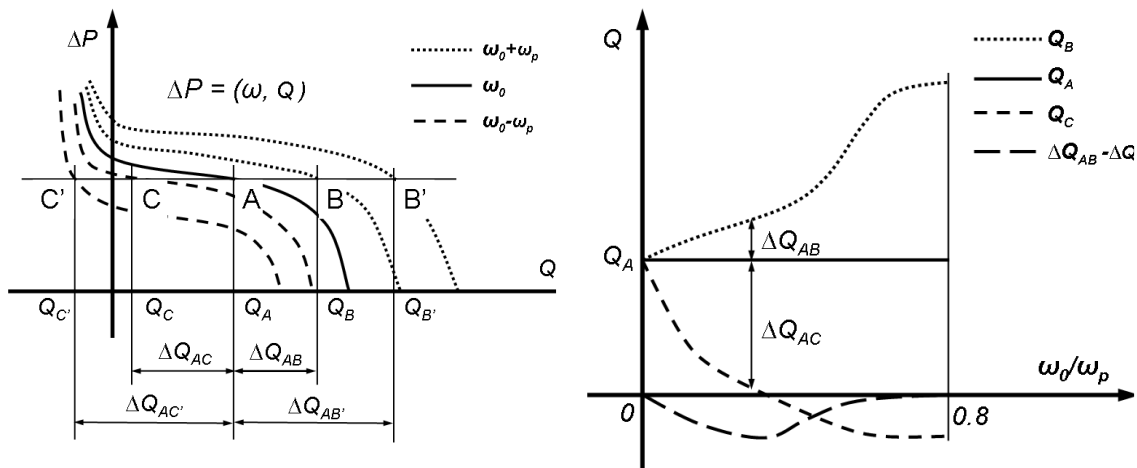
Figure 3-4 System response of cardiovascular model in different simulation cases

3.3.1 Cardiovascular Response in Healthy and Left Ventricular Failure Conditions and with Baseline Impeller Pump Support

Figure 3-4 (a) shows the simulation results for pressure, flow rate and volume changes in the systemic loop under the healthy condition. These results agree well with typical cardiovascular responses (Guyton 2006), with all pressure, flow rate, and volume parameters within the normal ranges. Figure 3-4 (b) illustrates the simulation results under a typical LV failure condition. Generally the response curves have the same

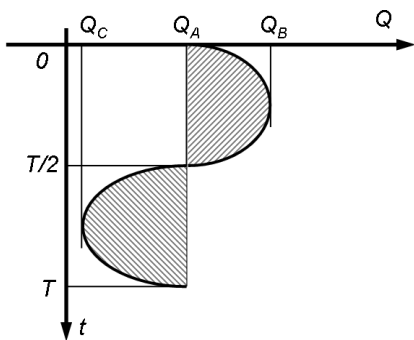
shapes as in the healthy condition but with altered variable values, corresponding to the impaired perfusion and the dilated left ventricular chamber in the heart failure condition. The cardiovascular response in the heart failure condition with Berlin Heart INCOR® support under baseline pump motion mode is shown in Figure 3-4 (c). Here a mean VAD flow-rate of 78 ml/s is chosen as the standard situation against which all other cases are compared. Generally the arterial pressure is restored to the normal range, and the ventricle is both pressure-unloaded and volume-unloaded from that of the heart failure condition to the healthy level in Figure 3-4 (a).

These simulation results also agree with previous validated data under the same conditions as reported in (Shi *et al.* 2010). These serve as the validation of the currently study.



(a) Shifting of working points with pulsation ratio

(c) Change of pump flow with pulsation ratio

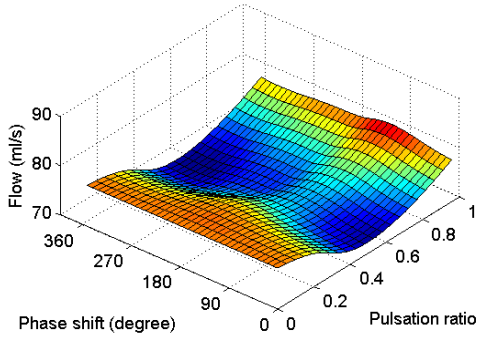
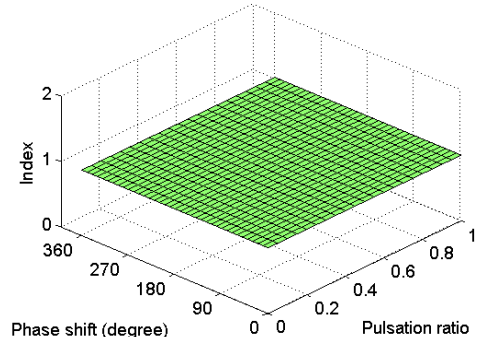
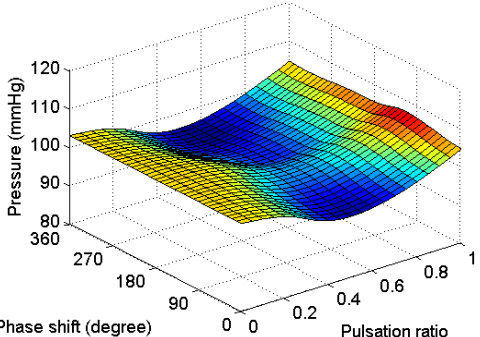
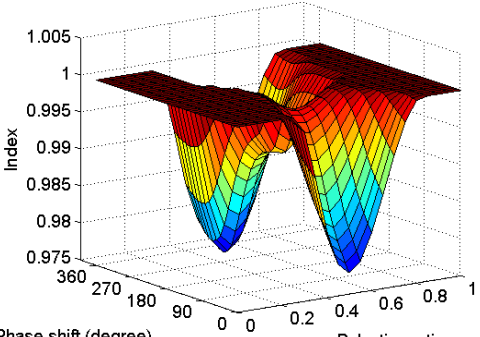
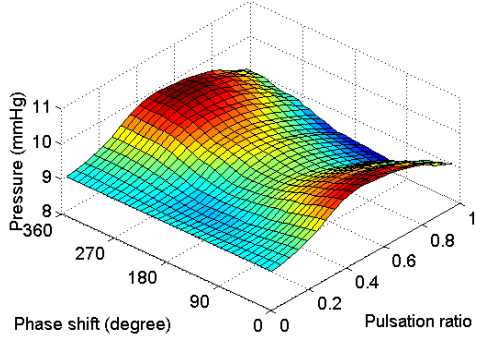
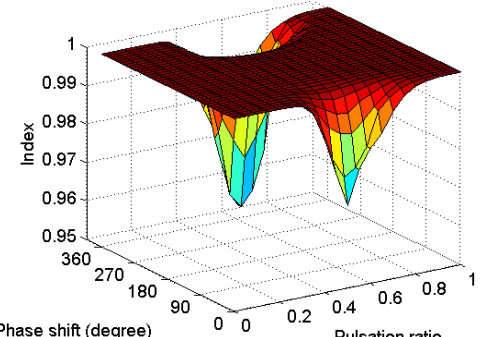


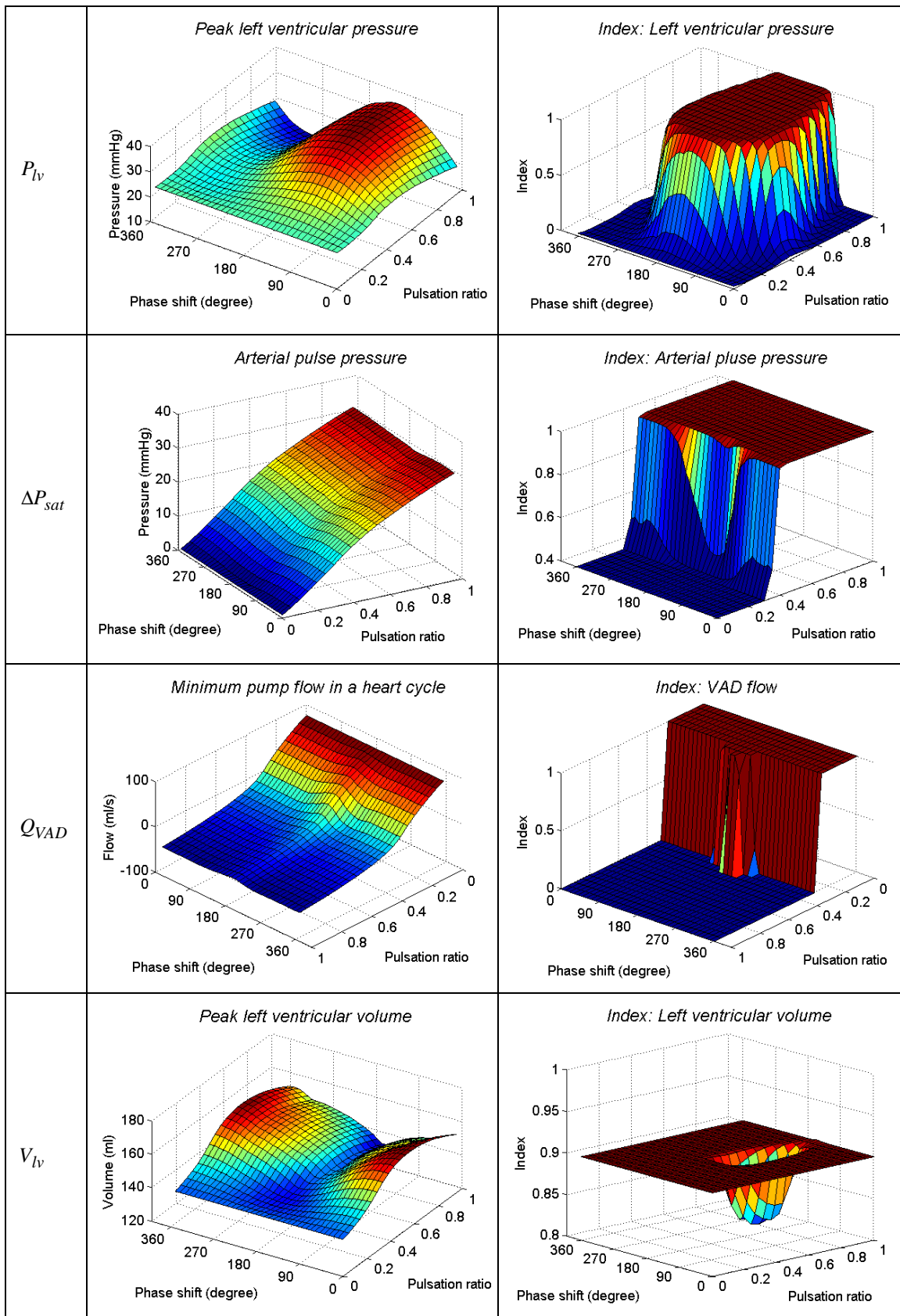
(b) Change of Q in a heart cycle with pulsation ratio

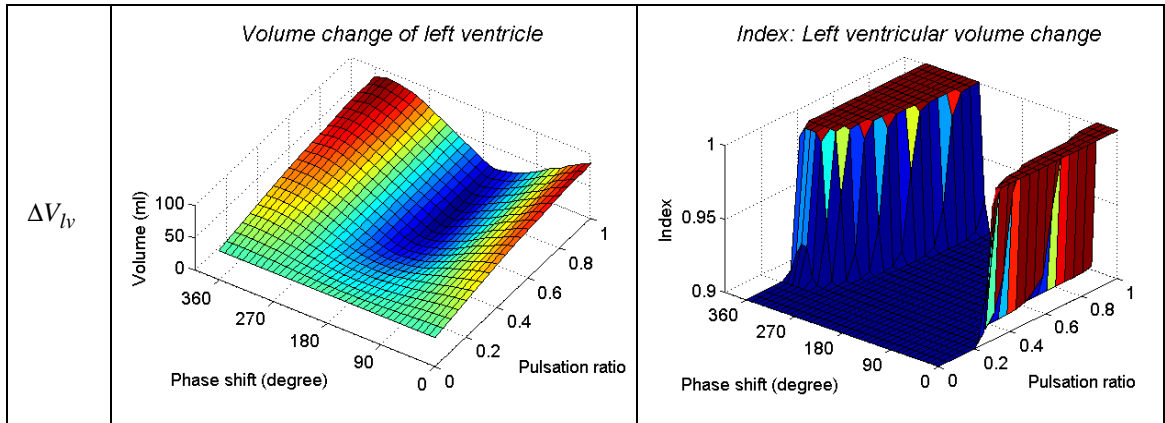
Figure 3-5 Illustration of change in cardiac output under different situations of pulsation ratio

(Variation of cardiac output is due to the different slopes of the pressure/flow curves in different flow ranges. Refer to the main text for detailed explanation.)

Table 3-2 Changes of cardiovascular variables and index values under different phase shift and pulsation ratio values

Variable	Variable plot	Variable index plot
CO	<p style="text-align: center;"><i>Cardiac output</i></p> 	<p style="text-align: center;"><i>Index: Cardiac output</i></p> 
$P_{sat,en}$	<p style="text-align: center;"><i>Energy equivalent arterial pressure</i></p> 	<p style="text-align: center;"><i>Index: Energy equivalent arterial pressure</i></p> 
P_{la}	<p style="text-align: center;"><i>Peak left atrial pressure</i></p> 	<p style="text-align: center;"><i>Index: Left atrial pressure</i></p> 





3.3.2 Searching for VAD motion to produce satisfactory cardiovascular response including arterial pressure pulsation

Following the procedure introduced at the end of the method section, different parameter combinations for the phase difference ϕ and pulsation ratio ω_p/ω_0 are applied in the VAD motion profile to simulate the assisted cardiovascular dynamics, and the corresponding response is evaluated using the membership functions and performance index developed. Table 3-2 illustrates the changes of characteristics cardiovascular variables as well as the index values of the each corresponding membership functions under the different ϕ and ω_p/ω_0 combinations.

In Table 3-2, the cardiac output changes in the range of 70-80 ml for the different cases. Although there is a small improvement of cardiac output at a ϕ value of around 120° , generally ϕ is not an important determinant of cardiac output. This is due to the counter-pulsation effect; a higher pump speed in early diastole instead of in systole delays the development of an arterial pressure peak until diastole. Also, with the remaining contractility in the diseased left ventricle, the peak in the left ventricular pressure occurs in mid-systole. Thus a ϕ value of 120° helps to produce a slightly higher pressure difference across the VAD in systole, which contributes to the slightly elevated pump flow and accordingly to the overall improved cardiac output in the case with a ϕ value of 120° . Note that the duration of systole is less than half of the heart period, as shown in Figure 3-3, and diastole starts at a phase of about 120° from the start of heart contraction, instead of 180° . Variation in pulsation ratio has a more prominent effect than the phase difference on the cardiac output. It is observed that

when either the minimum value of 0 or the maximum value of 1 is assigned to ω_p/ω_0 , the cardiac output will reach almost 78 ml, whilst between these two extreme conditions the cardiac output has a minimum, located at an ω_p/ω_0 of about 0.55. Shi *et al.*, (Shi *et al.* 2010), analysing a different pump, reported a similar decrease in cardiac output over the interval to 0.55, but did not see the recovery at the higher pulsation ratios. This recovery is attributable to the different slope in the pump characteristic curves, as illustrated in Figure 3-5 (a)-(c). As shown in Figure 3-5 (a), the pump P-Q curve in the second quadrant of the P-Q plane, i.e., the regurgitant pump flow region, has a much steeper slope than that in the first quadrant, i.e., the normal forward pump flow region. Also, in the first quadrant the P-Q curves have a steeper slope in the high flow range than in the low flow range. For a fixed pressure difference across the pump, suppose the constant pump rotating speed corresponds to the working point A and the modulated maximum and minimum pump speeds $\omega_0 \pm \omega_p$ during a heart cycle correspond to the pump working points of B and C individually, then the corresponding changes in pump flow due to pump speed modulation are ΔQ_{AB} and ΔQ_{AC} . As the pulsation ratio increases points B and C move to points B' and C'. A constant pump flow of Q_A will produce a cardiac output of $CO = Q_A \cdot T$, with T being the heart period. While with the pump speed modulation, the cardiac output is:

$$\begin{aligned}
 CO &= \int_0^{T/2} Q_B \cdot dt + \int_{T/2}^T Q_C \cdot dt = \int_0^{T/2} (Q_B + Q_A - Q_A) \cdot dt + \int_{T/2}^T (Q_C + Q_A - Q_A) \cdot dt \quad (3-3) \\
 &= Q_A \cdot T + \int_0^{T/2} \Delta Q_{AB} \cdot dt - \int_{T/2}^T \Delta Q_{AC} \cdot dt = Q_A \cdot T + \int_0^T (\Delta Q_{AB} - \Delta Q_{AC}) \cdot dt
 \end{aligned}$$

ΔQ_{AB} and ΔQ_{AC} are individually illustrated as shaded areas in Figure 3-5 (b). From the P-Q curves in Figure 3-5 (a), it is observed that as pulsation ratio changes, flows Q_A , Q_B and Q_C and flow difference $\Delta Q_{AB} - \Delta Q_{AC}$ generally follow the trend as shown in Figure 3-5 (c) due to the different slopes of the curves in different regions. The flow difference $\Delta Q_{AB} - \Delta Q_{AC}$ is zero at zero pulsation ratio. When the pulsation ratio increases, at first the relatively bigger slope in the P-Q curves between the flow range corresponding to points A and B compared to that corresponding to between points A and C produces a much smaller ΔQ_{AB} than ΔQ_{AC} , thus $\Delta Q_{AB} - \Delta Q_{AC} < 0$, and the overall cardiac output is falling rapidly with pulsation ratio increases. When the pulsation ratio increases further, point C moves to C', which is in a much steeper area of the P-Q curves, so that the difference between ΔQ_{AB} and ΔQ_{AC} begins to decrease,

although ΔQ_{AB} is still less than ΔQ_{AC} . When the pulsation ratio approaches 0.8, the difference between ΔQ_{AB} and ΔQ_{AC} becomes negligible and the drop in the cardiac output is decreasing to zero. Thus overall the cardiac output exhibits the form illustrated in Table 3-2. In summary, although the modulation of both amplitude ratio and phase produce changes in cardiac output, this parameter remains within the desired range over the whole of the operating space and so the membership function assumes a value of unity throughout.

The next two parameters investigated were the energy equivalent arterial pressure and the mean arterial pressure. In the low frequency range, both of these parameters are approximately proportional to the cardiac output. The energy equivalent arterial pressure is in the range of 95–106 mmHg. The index value for the energy equivalent arterial pressure is slightly smaller than 1 when ω_p/ω_0 is in the range of 0.3–0.8 but, as illustrated on Table 3-2, it is not significantly below its optimal range. Similar conclusions apply to the mean arterial pressure, not shown in the table.

Generally there is an inverse relationship between cardiac output and peak left atrial pressure; slightly more blood is accumulated in the left atrium when the cardiac output is low (ω_p/ω_0 in the range 0.3–0.9) and thus the peak left atrial pressure is higher. The model indicates that left atrial pressure generally lies in the target range of 5–10 mmHg and its contribution to the cost function remains close to unity, with a small drop off associated with a minor elevation of pressure over some of the solution space.

A single membership function for ventricular pressure is suggested, penalising excessively high or excessively low pressure at any point in the cardiac cycle. The maximum left ventricular pressure is of direct clinical interest because it is closely related to the peak stress level of the cardiac muscle. The minimum left ventricular pressure is also of interest in conditions of VAD support, because when it is too low there is a strong potential for collapse of the ventricular wall. This will adversely affect normal VAD function in the same manner as atrial suction. Generally the peak left ventricular pressure lies around the target level of 25 mmHg over the ω_p/ω_0 and ϕ ranges, except in two regions. The first corresponds to the situation of counter-pulsation in VAD assistance, for which $0.35 < \omega_p/\omega_0 \leq 1$ and $60^\circ < \phi < 210^\circ$, and the peak left ventricular pressure is as high as 40 mmHg. The second is related to the co-pulsation

mode of VAD assistance, for which $0.7 < \omega_p / \omega_0 \leq 1$ and $250^\circ < \phi < 360^\circ$, and the peak left ventricular pressure is about 12 mmHg . The minimum left ventricular pressure is also of interest in conditions of VAD support, because when it is too low then there is a strong potential for collapse of the ventricular wall, which will adversely affect normal VAD function in the same manner as in the atrial suction. In terms of minimum left ventricular pressure, the acceptable region is confined to about $0.2 < \omega_p / \omega_0 \leq 1$ and $60^\circ < \phi < 270^\circ$, as shown in the performance index plot for the membership function of the left ventricular pressure. The overall conclusion is that ventricular pressures are acceptable over most of the possible control spectrum. The unacceptable region is due to excessively low minimum left ventricular pressure ($< 5 \text{ mmHg}$), which may induce ventricular wall suction during VAD support.

Arterial pulse pressure increases almost linearly from $1-32 \text{ mmHg}$ when the pulsation ratio increase from 0 to 1. In this range, the pulsation ratio ω_p / ω_0 needs to be kept above 0.4 in order to produce the target minimum pressure pulsation of 15 mmHg (Undar *et al.* 1999). The phase shift has little influence on the arterial pressure pulsation, with only a small decrease in arterial pulse pressure when the phase shift is about 120° . Based on the form of the chosen membership function the contribution of arterial pressure pulse to the performance index exhibits a sharp change at the pulsation ratio of 0.4: below 0.4 the index value is zero, and above 0.4 it is 1.

In terms of pump flow, the critical issue is to avoid the development of regurgitant flow, which enormously decreases the pump efficiency and should be avoided. The plot for the minimum pump flow shows that the minimum pump flow exhibits a trend of quick dropping from about 75 ml/s to 0 ml/s when ω_p / ω_0 increase from 0 to 0.4; for further increasing in ω_p / ω_0 the minimum pump flow demonstrates a much slower dropping, and the value decreases from 0 ml/s to about -53 ml/s . Also the minimum pump flow seems not sensitive to the phase shift, with only a minor elevation exists near the region of 200° for the phase shift. The upper limit of the pump flow is always not a problem. Thus correspondingly the performance index plot for the membership function of VAD flow shows a steep variation at about 0.4 for ω_p / ω_0 .

The minimum ventricular volume computed under the envelope of present simulations remained within the normal range, and so this did not prove to be a critical parameter

under the conditions studied. In contrast, the peak volume did move into an unacceptable range, implying ventricular dilation, and so contributed to the optimisation under this envelope of operation. Under other conditions, for example if the rotation speed were set too high, the minimum volume might become a critical factor. The response surface for the peak left ventricular volume is similar in form to that for peak left atrial pressure. The model suggests that in most situations the peak left ventricular volume is above the ideal maximum ventricular volume of 130 ml , thus the performance index for the membership function of left ventricular volume shows a negative response. Since the left ventricular volume is classified as a less important physiological variable, its index value does not affect the overall performance index much. It should be noted that although the VAD assistance cannot fully restore the ventricular volume to the healthy condition of $20\text{-}130\text{ ml}$ range, this is the best that can be achieved in the current VAD application situation. In the current study the membership functions are all constructed based on the more stringent condition of a totally healthy condition, instead of based on the looser condition of VAD application practice.

The control of volume change of the left ventricle during a heart cycle is not strictly required as a criterion in the evaluation of VAD assisted cardiac response, but operation over a healthy range would be regarded as a positive feature. Generally increasing the pulsation ratio helps to produce elevated volume change. Phase shift also has strong influence on the left ventricular volume change. At a phase of about 150° the volume change in a heart cycle is minimised, and at about 330° it is maximised. The achievement of larger volume changes in the presence of a VAD is difficult, and for most of the operational range the stroke volume is too low to claim positive performance with respect to this parameter; only in two regions, one for $0.3 < \omega_p / \omega_0 \leq 1$ and $270^\circ < \phi < 360^\circ$ and the other for $0.3 < \omega_p / \omega_0 \leq 1$ and $0^\circ < \phi < 50^\circ$, does the ventricular volume change reach normal physiological levels.

The index values for the membership functions examined individually in the preceding text are combined using equation (3-2) to calculate the overall performance index, and Figure 3-6 shows the result as a function of the two control variables. It is observed that the performance index is 0 over most of the control range, meaning that the requirements for the characteristic cardiovascular variables are not satisfied in one way

or another. Only in a small region of $0.2 < \omega_p / \omega_0 \leq 0.4$ and $90^\circ < \phi < 270^\circ$ does the performance index rise to above 0, and the maximum value is 0.3, indicating that the conflicting requirements have made it impossible to find an operational condition in which all parameters lie within their individual optimal ranges. The peak performance index corresponds to the studied case of $\omega_p / \omega_0 = 0.35$ and $\phi = 200^\circ$. Figure 3-7 (a)–(c) shows the corresponding pressure, flow and volume changes in the studied case during one heart cycle. Generally the cardiovascular response for this case is acceptable, with the cardiac output, left atrial and ventricular pressures, mean artery pressure, VAD flow all in the normal healthy range. However, there are also deficiencies in the response. Firstly the amplitude of arterial pressure pulsation observed in Figure 3-7 (a) is 12.6 mmHg , which is slightly below the criterion of 15 mmHg in order to be classified as physiological meaningful. However, it is difficult to further increase the arterial pressure pulsation under all the constraints: increasing the pulsation ratio in VAD motion helps to produce elevated pulsation in arterial pressure, but note that the minimum pump flow is already near zero so far, as shown in Figure 3-7 (b), and any increasing in pulsation ratio will induce regurgitant pump flow. Also the left ventricular volume is still a bit higher than should be in healthy condition, and the left ventricular volume change is less than expected, meaning the ventricular muscle experiences little exercise and is less favourable when recovery of cardiac muscle is expected.

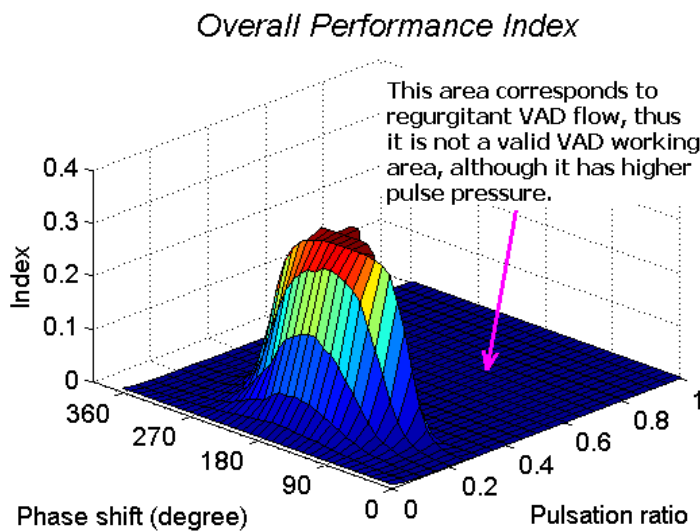


Figure 3-6 Performance indexes for the characteristic cardiovascular variables

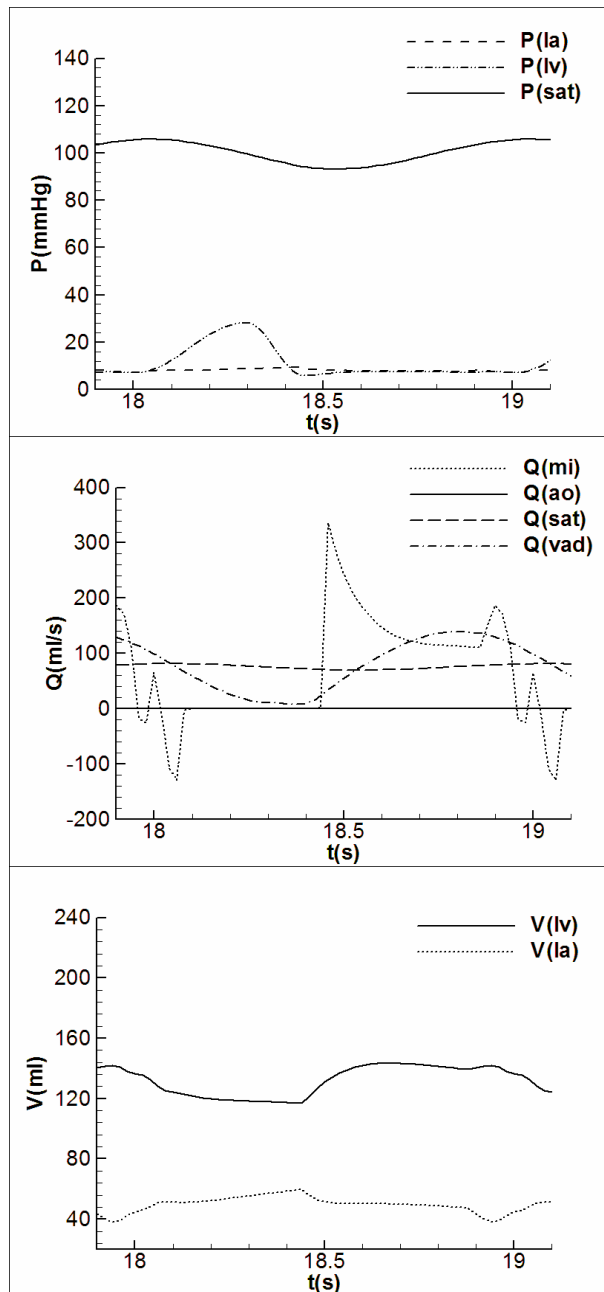


Figure 3-7 Cardiovascular response for the chosen optimal case (Phase shift = 200 degree, Pulsation ratio = 0.4)

(Although observable pulsation can be observed in the arterial pressure, the minimum pump flow is almost zero. Further modulation of pump speed will easily induce regurgitant pump flow, and thus should be avoided.)

3.4 Discussion

The modulation of the rotation speed of an impeller pump over the cardiac cycle to produce arterial pressure pulsation has been proposed for many years. A number of numerical simulation or experimental results have been published to advocate the

applicability of this technique (Choi *et al.* 2001, Gobel *et al.* 2001, Qian 1996, Shi *et al.* 2011a, Shi *et al.* 2011c, Vandenberghe *et al.* 2005). However results in the current study confirm those published earlier in the context of a different pump design (Shi *et al.* 2010): both revealed the development of strong regurgitant flow in the impeller pump when the pulsation ratio in the VAD motion profile is raised to the levels that might produce near-healthy arterial pressure pulsation. Regurgitant flow in the pump has several side-effects: firstly it greatly reduces the pump efficiency and thus increases the pump power consumption; secondly the regurgitant pump flow enormously increases the level of oscillatory shear index of blood flow in the VAD, which elevates the potential of blood cell damage; thirdly the regurgitant pump flow contributes to a unrealistically higher level of energy equivalent pressure due to the accompanying repeated direction changes of the blood flow in the VAD, although the main part of energy is wasted on the reversing of flow direction in the VAD, instead of being delivered to the perfusion of end organs. For this reason the regurgitant pump flow needs to be vigorously avoided in the VAD motion planning. In reviewing the previous work the regurgitant pump flow can be easily identified in those published data. Although the VAD devices used were different in those previous studies, few of them seem to have overcome the problem.

In the current study a formal optimisation procedure is developed, and a series of membership functions corresponding to fundamental characteristic cardiovascular variables are constructed to achieve accurate single evaluation criterion for VAD assisted cardiovascular response. It remains to establish a community consensus on the appropriate ranges and forms of the membership functions. With the currently chosen functions, a systematic investigation is carried out to cover the possible combinations of pulsation ratio and phase shift in VAD motion. The developed formalised procedure has the potential to be applied in serious VAD performance evaluations and motion optimisations.

In the current research the membership functions constructed to evaluate the characteristic cardiovascular variables are based on the idealised healthy condition, which is a quite stringent requirement for the cardiovascular response. In clinical practice with VAD support, it is always difficult to maintain every physiological variable within the idealised range. For example, in heart failure patients the impedance of the vascular network is often different from the healthy condition, and this poses

much difficulty in keeping both the cardiac output and the artery pressure exactly in the healthy ranges. Similarly the ventricular volume and stroke volume are difficult to maintain as well. Thus it is impossible to satisfy these membership functions concurrently in order to produce a overall performance index of 1. It would be of real value to the community to establish a more realistic set of membership functions, constructed to suit the practically achievable ranges of characteristic variables under VAD assistance.

In evaluating the level of pressure pulsation, the current study mainly adopted the rule of 15 mmHg arterial pulse pressure as suggested by Undar *et al.* (Undar *et al.* 1999). Undar *et al.* also proposed a more stringent criterion in which not only the pulse pressure was specified, but also the first derivative of aortic pressure, ejection time, stroke volume and pulse rate were requested in order to be qualified as a physiologically meaningful pulsatile flow (Undar *et al.* 1998). Actually both of these rules are empirically based and, given the importance of this parameter in driving the optimisation process, a more objective definition for the physiologically meaningful pulsatile flow, based on more comprehensive data from clinical measurements on organ perfusion conditions and the laboratory observations of cell and molecular level pathophysiological changes.

Several aspects of system characteristics affect the final cardiovascular response: the native cardiovascular system, the VAD performance, and the VAD motion profile. The current study uses a sinusoidal change of pump rotation speed for VAD motion profile, and the pulsation ratio and the phase shift are used as two parameters in the VAD control optimisation. It is possible to design more complex VAD motion profiles, such as triangle, square wave, or even more complex spline curves, and this may produce somewhat different cardiovascular response. However, this will not change the nature of the study. For example, the regurgitant pump flow will still develop when the pulsation ratio is high, and the cardiac output and the arterial pressure still can not be maintained exactly in the healthy range due to the change of vascular impedance in the diseased condition. As to the characteristics of the native cardiovascular system, due to the enormous difference in patient condition, usually only typical diseased case is studied, and patient-specific study is the task of a later stage when the numerical/experimental techniques have become fully matured. This may leave the gap for quantitative difference in comparison of results from different research groups, but

should not produce qualitative difference. The same rule also applies to the difference in VAD performance in facing the numerous VAD products from different manufacturers. Of course it is always cautious to investigate more VAD application cases before drawing the final conclusion.

For convenience of calculation and demonstration of results, the current study uses a heart rate of 60 beats/min, while in clinical situations patients often have a higher heart rate of 80-100 beats/min. Strictly speaking, the vasculature has a slightly smaller impedance in such frequency range as compared to the 60 beats/min situation, so the after-load to the pump will decrease slightly. At the same time the heart contractility generally remains about the same. Thus under the same pump speed variation pattern the pump working points will shift to the higher flow region (to the right in the pump pressure-flow curves in Figure 3-2) slightly. As a consequence, the pump flow and thus the aortic flow will increase slightly, while the arterial pulse pressure will exhibit a minor reduction because of the different slopes in the high and low flow regions of the pump pressure-flow characteristics. Generally, variation in the vascular impedance between the current assumed heart rate and the clinical patient heart rate is very small and thus the difference in heart rate will not cause appreciable changes to the current simulation results. However, in some other situations such as serious hypotension or hypertension, the vessel impedance will deviate substantially from the above simulated condition. Under hypertension, the stiffer and contracted vessels contribute to a much higher vessel impedance and greater after-load to the heart. With the preload to the ventricle/VAD maintained at a similar level to that in the systems analysed (preload is decided by the venous/atrial pressure), the pump working point will move towards the lower flow region (to the left in Figure 3-2). This induces a reduced pump flow and possibly higher arterial pressure pulsation. Under hypotension the situation will be just the opposite. Under both of these conditions the changes in impedance are sufficiently great to warrant the operation of the model to explore these envelopes, but this is beyond the scope of the current work.

3.5 Conclusions

This study reports on the development and application of a two-parameter control algorithm in the evaluation of cardiovascular response in a heart failure condition under the support of the Berlin Heart INCOR® impeller pump type VAD. A formal

procedure is developed based on the multiplication of a number of membership functions to provide a single physiological performance index (a cost function) to enable the optimisation of the control parameters. A parameter combination of 0.35 for the pulsation ratio and 200° for the phase shift in the VAD control produces the best cardiovascular response under the stated cost function. In particular it produces a maximum arterial pulse pressure of 12.6 mmHg without inducing regurgitant pump flow and whilst maintaining other characteristic cardiovascular variables within the corresponding physiological ranges. The membership functions themselves, and the way in which they are combined, are based on a subjective assessment of the appropriate physiological ranges and of the relative importance of each term. Although the ranges in the current study are based on published literature where available, it remains to establish a community consensus on the appropriate ranges and forms of the membership functions.

The focus of the current study is on proposition and demonstration of an approach to optimisation, with its application illustrated at one heart rate. Before practical implementation it is suggested that a whole envelope of simulations should be performed under a range of physiological states. Although this study focuses on optimisation under a rather narrow physiological envelope, representative of a rest condition, the methods could be applied to the development of a much more sophisticated control algorithm, based on adaptation to continuous monitoring of parameters such as heart rate. This level of control could yield the greatest benefit to the patient, but will require developments in monitoring technology as well as in optimisation and control.

Chapter 4 Physiological Control of an In-series Connected Pulsatile VAD: Numerical Simulation Study³

This chapter investigates VAD assisted cardiovascular dynamics under PID feedback control. Previously the author studied the cardiovascular responses under the support of an in-series connected reciprocating-valve VAD through numerical simulation, and no feedback control was applied in the VAD. This research explores the contribution of the VAD control on the circulatory dynamics assisted by the reciprocating-valve VAD, in response to the changing physiological conditions. The classical PID control algorithm is implemented to regulate the VAD stroke beat-to-beat, based on the error signal between the expected and the realistic mean aortic pressures. Simulation results show that under the PID VAD control, physiological variables such as left atrial, ventricular and systemic arterial pressures, cardiac output, and ventricular volumes are satisfactorily maintained in the physiological ranges. With the online PID feedback control, operation of the reciprocating-valve VAD can be satisfactorily regulated to accommodate metabolic requirements under various physiological conditions including normal resting and exercise situations.

4.1 Introduction

Since their first surgical implantation in the 1960s, ventricular assist devices (VADs) have greatly helped in the treatment of heart failure, either as a bridge to transplantation, or as a bridge to recovery, while lately there is also mention of permanent implantation (destination therapy) (Reul and Akdis 2000). Theoretically the VAD should adjust its rotating speed and/or stroke to produce tailored output to accommodate the physiological perfusion for individual patients under various physiological conditions. However, among the commercial VADs available none seems to have such a capability. In clinical practice usually the VAD rotating speed or the VAD stroke is adjusted by an experienced technician, or the patients are trained to adjust the VAD themselves until a comfortable perfusion level is achieved.

³ Adapted from: Shi Y., Shi Y., Korakianitis T., Physiological Control of an In-series Connected Pulsatile VAD: Numerical Simulation Study, *Computer Methods in Biomechanics and Biomedical Engineering*, 14(11), pp995-1007, 2011

In recent years the VAD control issue has received the attention of researchers, and various aspects of related problems are under investigation. In achieving VAD control the first requirement is to identify a physiological indicator which defines the desired perfusion condition. The VAD controller must adjust the VAD operation in order to match this physiological indicator, and in turn the combined native cardiovascular system and the VAD produce the desired perfusion condition to match the circulation requirements in the native healthy condition. This physiological indicator should satisfy the various physiological criteria, including the cardiac output, pressures in various parts of the circulation system, balance of blood distribution between the systemic and the pulmonary circulation loops, metabolic requirement of peripheral organs, vital organs (such as brain, kidney) perfusion pressure, VAD energy consumption etc. These requirements come from different aspects of circulation needs and usually contradict with each other (such as in diseased conditions the cardiac output and the arterial pressure cannot be maintained at the same time). Previous researchers proposed many physiological variables as the feedback signal in VAD control to address part of these requirements, such as: cardiac output (Abe *et al.* 1998, Choi *et al.* 2001, He *et al.* 2005, Hsu 2004, Klute *et al.* 1992, Saito *et al.* 1999, Yoshizawa *et al.* 1992); left atrial pressure (He *et al.* 2005, Kitamura 1990, McInnis *et al.* 1984, Olegario *et al.* 2003, Saito *et al.* 2002); left ventricular pressure (Bullister *et al.* 2002); arterial pressure (Barnea *et al.* 1992, Bullister *et al.* 2002, He *et al.* 2005, Kosaka *et al.* 2003, Wu *et al.* 2003); pressure difference across the VAD (Waters *et al.* 1999, Wu *et al.* 2003); peripheral vascular resistance (Abe *et al.* 1998, Saito *et al.* 1999); heart oxygen consumption (Drzewiecki *et al.* 1990); pulsatility gradient (Arndt *et al.* 2008); and venous oxygen saturation (Nakamura *et al.* 2000) etc. Also some VAD characteristic variables such as VAD pump flow (Kosaka *et al.* 2003, Nakata *et al.* 1999) and VAD pump rpm (He *et al.* 2005, Ohuchi *et al.* 2004) have been included in evaluating the VAD control performance. Some even used a weighted average value of several of these variables (He *et al.* 2005, Wu *et al.* 2003) or of the same variable in different instances (Barnea *et al.* 1992) as physiological indicator, in an effort to address several aspects of perfusion requirements at the same time. To avoid the possibility of thrombus formation and drift in measurement in long-term usage of transducers, some researchers (Ayre *et al.* 2000, Choi *et al.* 2001, Endo *et al.* 2000, Kitamura and Gross 1990, Nakata *et al.* 1999, Oshikawa *et al.* 2000, Saito *et al.* 1999, Tasch *et al.* 1990,

Waters *et al.* 1999) also attempted to use the VAD internal signals such as driving current/voltage, pump rotating speed, driving air pressure, piston position etc. as feedback signals in estimating the cardiac output, atrial pressure or ventricular pressure difference for VAD control purposes. However, it seems artificially constructed indicators cannot adequately address the diverse aspects of cardiovascular function requirements. (Giridharan and Skliar 2003) reviewed these proposed physiological indicators and compared their advantages and disadvantages as feedback signals in VAD control. Based on the comparison they proposed a new physiological indicator of pressure difference between the left ventricle and aorta for usage in VAD control. It is claimed that this physiological indicator is reliable and stable under various physiological situations and changes. Later on (Giridharan *et al.* 2004) revised the physiological indicator and used the pressure difference between the pulmonary vein and the aorta to replace the previously proposed one, in order to further improve the control system response.

Another important issue to be addressed in VAD control is the control algorithm. Different control algorithms, such as the classical proportion-integration-differentiation (PID) control, the modern state-space control including the optimal control, the latest nonlinear and fuzzy logic control etc., have been applied. Each of these control algorithms has its advantages and disadvantages in achieving various aspects of response performance and easiness of implementation. Previously numerous VAD control studies have chosen the PID control as the control algorithm (Giridharan and Skliar 2003, Giridharan *et al.* 2002, Kosaka *et al.* 2003, Olegario *et al.* 2003, Waters *et al.* 1999) due to its mature application in industrial practice. Modern linear feedback control (Kitamura and Gross 1990) and optimal control (Barnea *et al.* 1992, He *et al.* 2005, Klute *et al.* 1992) have also been applied to address the multiple physiological indicator requirements. In recent years fuzzy logic control has also been attempted in VAD control (Choi *et al.* 2001, Hsu 2004) to facilitate regulating the non-linear cardiovascular system without relying on detailed mathematical models of the system.

In achieving the desired VAD performance the controllers must be adapted to the detailed VAD types. Previously VAD controller designs have been implemented for the two traditional VAD types: impeller pumps (Choi *et al.* 2001, Giridharan and Skliar 2003, Giridharan *et al.* 2002, He *et al.* 2005, Kosaka *et al.* 2003, Olegario *et al.* 2003,

Waters *et al.* 1999) and displacement pumps (Drzewiecki *et al.* 1990, Hsu 2004, Kitamura 1990, Klute *et al.* 1992). The advantages and disadvantages of the two types of VADs, and correspondingly that of the non-pulsatile and pulsatile flows they produced, are still a matter of discussion (Saito *et al.* 2002, Undar 2004). In recent years several new kinds of pulsatile VADs have been proposed for in-parallel or in-series connection with the diseased ventricle, such as the artificial vasculature device (Giridharan *et al.* 2004) and the reciprocating-valve VAD (Korakianitis and Grandia 2003, Larson *et al.* 1999, Shi and Korakianitis 2006). In the in-parallel connection, the VAD is connected parallel with the native diseased ventricle, so that the VAD flow output and the native ventricular flow output combined to produce the total cardiac output; while in the in-series connection, the VAD is connected in-series with the native diseased ventricle thus the same amount of blood flows past the ventricle and the VAD. Previous numerical simulation studies (Shi and Korakianitis 2006, Shi *et al.* 2007) show that the reciprocating-valve VAD can produce superior hemodynamic support to the diseased heart with minimised power consumption, and has the potential to produce better physiological response, with relatively simple system structure in comparison to the two traditional types of VADs. At the same time, the in-series VAD connection has two important advantages over the parallel VAD connection configuration: it minimizes the damage to the cardiac muscle due to the unique VAD installation position; also it avoids the problem of stasis development and commissural fusion in the aortic valve (Shi *et al.* 2007). The in-series connected reciprocating-valve VAD has great potential in the VAD development.

This chapter is a pilot study on the control of the in-series connected reciprocating-valve VAD, in the hope of producing adapted VAD assistance action to suit the changing patient needs in different physiological conditions. In the previous numerical study of the fundamental cardiovascular system response (Shi and Korakianitis 2006, Shi *et al.* 2007) the VAD stroke was fixed at a prescribed value to maintain the basic cardiovascular perfusion requirement, and no VAD controller was included to address the physiological changes. The current research is a new contribution which studies the corresponding cardiovascular system response under heart failure conditions when a VAD controller adjusts the VAD stroke according to changes in physiological conditions. As a first instance in controller design for the reciprocating-valve VAD, the classical PID controller is adopted due to its proven merit in control performance and

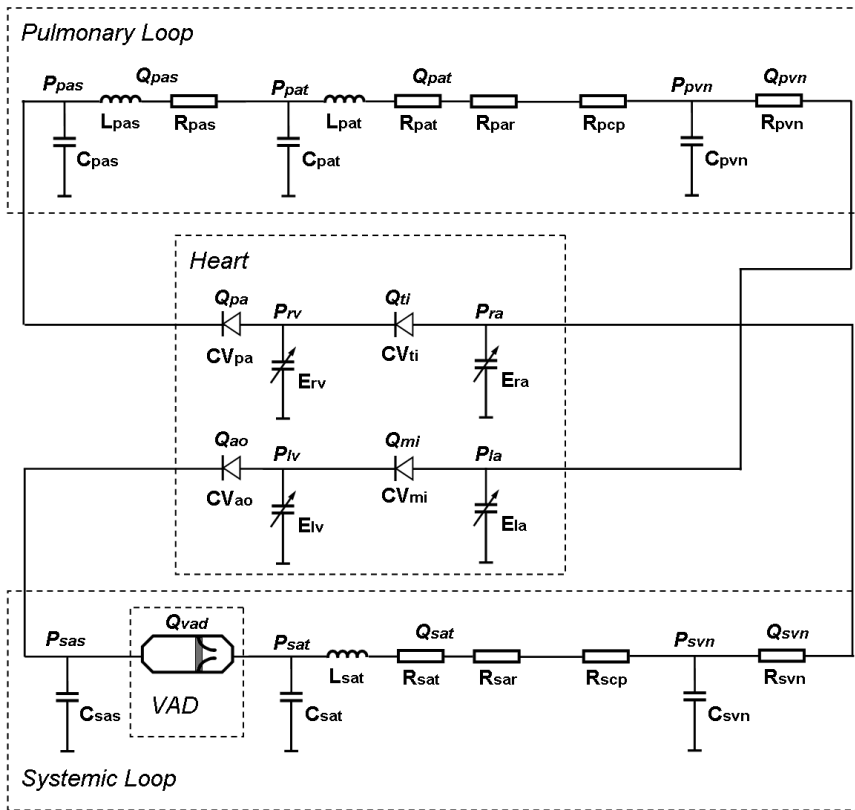
ease of implementation. Based on the system configuration, the VAD assisted aortic pressure is chosen as a concise feedback signal for VAD feedback control in the current chapter. The formulated VAD control system is then tested with the physiological transitions between normal resting and mild exercise conditions.

4.2 Materials and Methods

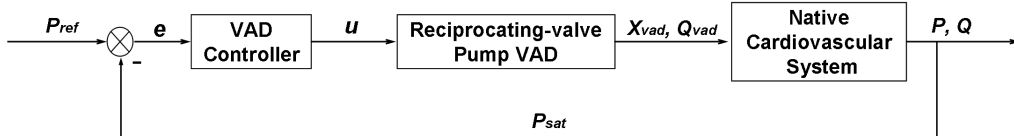
The numerical model comprises three parts: the native cardiovascular system; the reciprocating-valve VAD; and the PID VAD controller. Figure 4-1 (a) illustrates the hydraulic configuration of the system, and Figure 4-1 (b) shows the block diagram of the VAD control system.

4.2.1 Model of the Native Cardiovascular System

A detailed model for the native cardiovascular system has been introduced in the previous chapter. The system is modelled in three main parts: heart; systemic circulation loop; and pulmonary circulation loop. The heart is modelled as a four chamber pump with variable elastance and four heart valves that control the blood flow direction. The systemic and pulmonary circulation loops are each separated into aortic sinus/pulmonary artery sinus, artery, arteriole, capillary and vein segments. In every segment the individual component is modelled by considering the local resistance to blood flow, elasticity of blood vessels, and inertia of blood. The combined effect of venule, vein and vena cava is modelled as the vein segment. The artery segment represents the general characteristics of the aorta, the main and smaller arteries. The aortic sinus describes the general feature of blood vessel around the aortic root. The heart valve dynamic operation has also been specifically modelled by considering the various factors of pressure difference, frictional force, vortex effect etc. acted on the valve leaflets, which helps to give a more accurate description of the cardiac response. In the native cardiovascular model the neuro-regulation effect, including the sympathetic and parasympathetic nervous actions on the heart rate change and variations in unstressed venous volume, are neglected.



(a) Hydraulic configuration of the cardiovascular system (Refer to the nomenclature table in front pages for detailed name of each component.)



(b) Block diagram of the VAD control system

Figure 4-1 System configuration

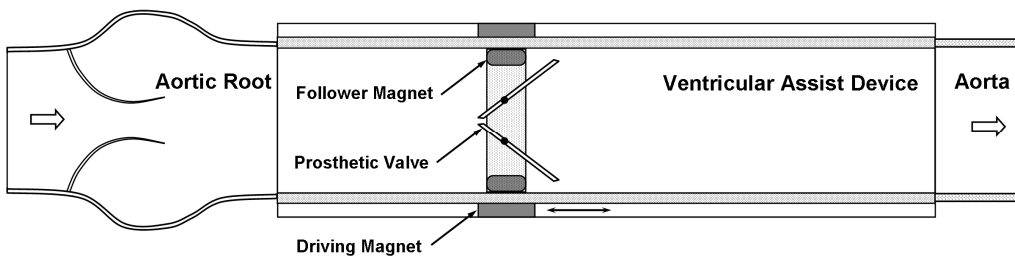
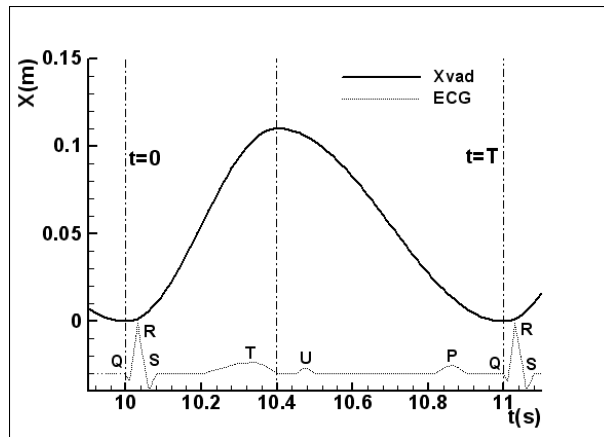
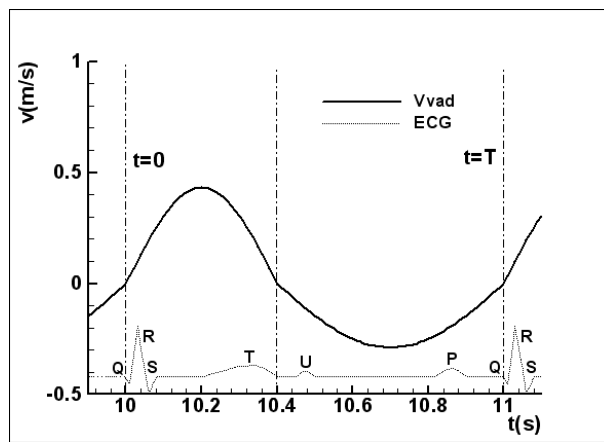


Figure 4-2 Schematic of the reciprocating valve pump type VAD



(a) Motion profiles of the LVAD



(b) Velocity profiles of the LVAD

Figure 4-3 Pumping action profiles of the LVAD

4.2.2 Model of Pulsatile VAD pumping action and motion

Traditional pulsatile VADs such as the intra-aortic balloon pump and in-parallel installations of impeller pumps and displacement pumps have been applied in clinical practice for many years, and numerous analysis have been carried out to study their performance. The model in this chapter concentrates on the in-series action of reciprocating-valve pulsatile-type VADs. These have various different implementations, as illustrated in (Korakianitis and Grandia 2003, Larson *et al.* 1999). Generally the reciprocating-valve VAD is connected in-series to the native diseased ventricle, and it is used to replace a segment of the ascending aorta. Figure 4-2 shows the schematic of the reciprocating-valve VAD in in-series configuration. In this design any type of prosthetic heart valve (mono-leaflet, bi-leaflet, PTFE membrane, bio-prosthetic etc.) is mounted on an annular magnet, and it is moved along the length of the VAD in response to the reciprocating motion of the driving magnet. The prosthetic

valve is closed and acts as a piston pump in one direction of motion along the length of the VAD, while it opens to let flow through the valve in the reverse direction of motion. The flow through the prosthetic valve in the VAD can be modelled by:

$$Q_{vad} = \begin{cases} A_{vad} \cdot \frac{dx}{dt} + CQ_{vad} \cdot AR_{vad} \cdot \sqrt{P_{sas} - P_{sat}} & P_{sas} \geq P_{sat} \\ A_{vad} \cdot \frac{dx}{dt} + CQ_{vad} \cdot AR_{vad} \cdot \sqrt{P_{sat} - P_{sas}} & P_{sas} < P_{sat} \end{cases} \quad (4-1)$$

When the VAD motion is properly designed, flow in the VAD chamber is continuous, so that $Q_{vad} = Q_{sas}$. The motion of the pumping action is specified by the VAD control algorithm. Various VAD motion profiles have been studied in (Shi and Korakianitis 2006). It was found that a revised sinusoidal wave shaped profile with skewed rising edge using Hermitian interpolation produces the optimal hemodynamic response. For simplicity a sinusoidal wave profile consisting of two segments of sine wave, as shown in Figure 4-3, is applied in the current research:

$$x(t) = \begin{cases} \frac{X_{vad}}{2} \cdot \left(1 - \cos \frac{\pi \cdot t}{T_{twe}} \right) & 0 < t < T_{twe} \\ \frac{X_{vad}}{2} \cdot \left(1 + \cos \frac{\pi \cdot (t - T_{twe})}{T - T_{twe}} \right) & T_{twe} < t < T \end{cases} \quad (4-2)$$

In the motion profile, the VAD stroke X_{vad} can be adjusted on a beat-to-beat basis to accommodate the physiological changes in the cardiovascular system.

4.2.3 Physiological Controller Design

Several factors affect the hemodynamic action of the reciprocating-valve VAD on the cardiovascular system: VAD stroke; VAD motion frequency; and VAD motion profile (including timing of VAD motion versus the native ventricular contraction). As concurrent regulation of all these factors will cause coupled effects to the control system, which easily induce stability and accuracy problems, a better and more practical approach is adopted in this study. The VAD motion is synchronized to the native heart rate, thus reaching a 1:1 ratio of motion pattern between the VAD motion and the native heart beating, which is the most efficient way for VAD functioning. The VAD motion profile is specified as the sinusoidal wave as discussed in the previous section. The VAD stroke is specifically controlled in this study. With VAD frequency

and motion profile being optimized as above, the controlled VAD stroke variation causes the least impact to system stability and accuracy.

In analysing the motion dynamics of the reciprocating-valve VAD, the time constants of the VAD electrical and mechanical parts are always much smaller than those of the hydraulic parts, which means that the electrical and mechanical parts can be considered as having ideal motion response in the VAD motion modelling. Thus in analysing the fluid-dynamic interaction between the in-series connected reciprocating-valve VAD and the native cardiovascular system, it is assumed that the VAD stroke in the heart cycle is proportional to the command voltage signal applied by the controller to the VAD motion driving mechanism ($X_{vad} = K_x \cdot u(t)$).

Previously various physiological indicators have been proposed as the controlled variable in VAD control. Among them some (such as cardiac output, left atrial/ventricular pressure, arterial pressure, pressure difference across the VAD, VAD pump flow and VAD pump rpm) can be easily measured using transducers, whereas others (including the peripheral vascular resistance, heart oxygen consumption, pulsatility gradient, and venous oxygen saturation) are much more difficult to measure due to the absence of suitable transducers or the complex algorithms concerned. A well designed VAD control system should achieve an optimal system performance within the constraint of hardware capabilities. For the reciprocating-valve VAD, this study aims to construct a VAD control system with maximally reduced hardware configuration. Based on the characteristics of the VAD motion, in the first instance the VAD assisted aortic pressure is chosen as the feedback signal in forming the control loop. Such choice of the feedback physiological index requires only one pressure sensor to be equipped at the outlet of the VAD, and the minimised VAD control system design is sufficient for the current conceptual analysis of the VAD motion dynamics. It is possible for more complex system hardware configurations to be adopted in the future to meet more advanced control performance requirements.

In view of the various control schemes available, the classical PID control is adopted due to its excellence in producing satisfactory system response and easy implementation. Specifically the incremental PID implementation is chosen because it does not need to save all the historical data during the algorithm calculation, thus

resulting in reduced memory requirement. For the incremental implementation of PID control, there are:

$$u(k) = K_p \cdot e(k) + K_i \cdot \sum_{i=1}^k e(i) + K_d \cdot [e(k) - e(k-1)] \quad (4-3)$$

$$u(k-1) = K_p \cdot e(k-1) + K_i \cdot \sum_{i=1}^{k-1} e(i) + K_d \cdot [e(k-1) - e(k-2)] \quad (4-4)$$

so:

$$\begin{aligned} \Delta u(k) &= u(k) - u(k-1) \\ &= K_p \cdot [e(k) - e(k-1)] + K_i \cdot e(k) \\ &\quad + K_d \cdot [e(k) - 2e(k-1) + e(k-2)] \\ &= (K_p + K_i + K_d)e(k) - (K_p + 2K_d)e(k-1) + K_d e(k-2) \end{aligned} \quad (4-5)$$

Thus the VAD stroke in every heart cycle is decided by:

$$X_{vad}(k) = K_x \cdot [u(k-1) + \Delta u(k)] \quad (4-6)$$

The error signal $e(k)$ is the deviation of the realistic VAD assisted aortic pressure from the expected value:

$$e(k) = P_{ref} - \bar{P}_{sat}(k) \quad (4-7)$$

where $\bar{P}_{sat}(k)$ is the mean value of the aortic pressure in the heart cycle k :

$$\bar{P}_{sat}(k) = \frac{1}{T} \int_{(k-1)T}^{kT} P_{sat} dt \quad (4-8)$$

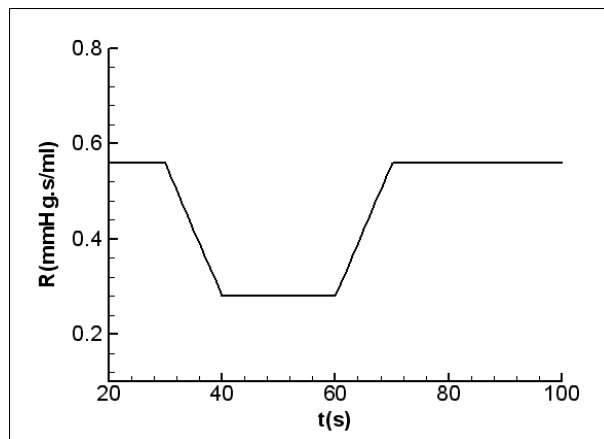


Figure 4-4 Change of arterial resistance in a simulated exercise condition

(Following previous researchers, transition between rest condition and exercise condition is represented by the change of the arteriole resistance, with exercise condition has half of the resistance value compared to the rest condition.)

4.2.4 Test Case of VAD Control

In physiological condition the various physiological variables including peripheral arteriole resistance, venous unstressed volume, heart rate etc. change under the regulation of the sympathetic and parasympathetic nervous. Previous researchers have developed mathematical models to describe such physiological changes in the healthy human subjects (Ursino 1998). However, it should be noted that in patients with heart failure, the baro-receptors have been subjected to abnormally high artery/venous pressures for a long time during the disease development, thus the sensitivity and the threshold values for the triggering of the baro-receptors have greatly deviated from those in the healthy condition. Such deviations have appreciably changed the response characteristics of the neuro-regulation mechanism under the pressure disturbances. Related research in this area is rare. Since direct extension of the previously developed neuro-regulation model such as (Ursino 1998) to cover the heart failure condition would induce unpredictable modelling errors, researchers (Choi *et al.* 2001, Giridharan and Skliar 2003) mostly chose to neglect the changes in the heart rate and venous unstressed volume, and directly prescribed the change of the peripheral arteriole resistance as the output of the neuro-regulation mechanism in the modelling of the diseased cardiovascular dynamics during exercise condition. This is not an ideal modelling, but it gives a partial description of the neuro-regulation effect in the analysis, and it is effective in the preliminary studies.

This simplified method is followed in the current study, and in modelling the physiological transition between the normal resting and exercise conditions for the test of VAD control performance, this study mainly considers the systemic arterioles (R_{sar}) as the cardiovascular effector of the neuro-regulation mechanism. The pre-defined change of the systemic arteriole resistance is applied to determine the contribution of VAD control on the cardiovascular responses. As a preliminary test of the VAD controller performance, a segmented slope change in peripheral arteriole resistance R_{sar} as illustrated in Figure 4-4 is specified to investigate the cardiovascular response under the VAD control action:

$$R_{sar} = \begin{cases} 0.56, & 0 \leq t \leq 30 \\ 0.28 \cdot [2 - 0.1(t - 30)], & 30 < t \leq 40 \\ 0.28, & 40 \leq t \leq 60 \\ 0.28 \cdot [1 + 0.1(t - 60)], & 60 < t \leq 70 \\ 0.56, & 70 < t \leq 100 \end{cases} \quad (4-9)$$

where $R_{sar} = 0.56 \text{ mmHg} \cdot \text{s/ml}$ corresponds to the arteriole resistance in the normal resting condition. In equation (4-9) it is assumed that in exercise condition the peripheral arteriole resistance reduces to half of the value for the normal resting condition, and the transition between normal resting and exercise conditions takes about 10s , which are reasonable approximations to the practical changes in the physiological conditions (Guyton 2006).

4.2.5 System Parameters

Table 4-1. VAD motion control parameters

Parameter	Value	Unit
K_p	0.25	V/mmHg
K_i	0.025	$V/(\text{mmHg} \cdot \text{s})$
K_d	0.005	$V \cdot \text{s}/\text{mmHg}$
K_x	0.02	m/V
P_{ref}	95.0	mmHg
T	1.0	s
T_{twb}	0.22	s
T_{twe}	0.42	s
T_{tww}	0.2	s
A_{vad}	0.0008	m^2
X_{vad}	0.126	m

Values for the hemodynamic variables in the native cardiovascular model are the same as those used in (Shi and Korakianitis 2006). In assigning values to the VAD motion, the sectional area of the cylinder is decided based on the human aortic geometry and

the VAD design. Based on this piston head area, the typical piston displacement is selected to produce the normal stroke volume. For the coefficients for the VAD dynamics, first the range of cardiac output with and without VAD support under normal, weakened and possible exercise conditions are identified, based on physiological text books (Guyton 2006) and clinical results (Elstad *et al.* 2002, Potapov *et al.* 2000, Simon *et al.* 2005). Then the coefficients for the equations describing the VAD dynamics are varied over a reasonable range to produce the compatible cardiac output changes in the different situations. The parameters for the PID controller in the VAD are decided by numerical experiments to find the optimized values that produce the desired cardiovascular response. The heart period is chosen to be 1 second in the simulations (60 beats per minute) to facilitate presentation and comparison of results. Other parameters such as the beginning and ending instances of the T wave in the ECG signal, the time step of simulation etc., were chosen based on general knowledge in physiological textbooks (Guyton 2006) and the simulation requirements. Table 4-1 shows values for these parameters.

4.2.6 Simulation Procedure

Based on the mathematical models described above, a program is developed in C language to simulate the cardiovascular dynamics under various healthy, diseased, and VAD supported conditions.

First the physiological variation in the peripheral vessel resistance is neglected and the VAD controller is excluded from the system model (i.e., equations (4-5), (4-6) and (4-9) are disabled), and the cardiac response for the healthy condition, for the heart failure conditions without VAD support, and for the heart failure conditions with VAD support but without VAD control are investigated. In simulating the native cardiovascular response under healthy and heart failure condition, equations (4-1) and (4-2) that describe the VAD motion dynamics are also disabled. For the healthy condition the left ventricular peak systolic elastance is kept at the normal value of 2.5 mmHg/ml , whereas for the situation of left ventricular failure without VAD support it is reduced to the much impaired value of 0.5 mmHg/ml . In simulating the heart failure condition with VAD support but without VAD control, the VAD flow and VAD motion profile described by equations (4-1) and (4-2) are applied to activate the reciprocating valve

pump in the numerical model, and the VAD stroke is fixed at a value of $X_{vad} = 0.126m$ to match the cardiac output requirement of $70ml$ in the simulated heart failure condition (This VAD stroke value can be changed to match other degrees of heart failure condition). In all the three cases, the peripheral arterial resistance is fixed at the normal value of $0.56mmHg \cdot s/ml$ to simulate the undisturbed circulation condition.

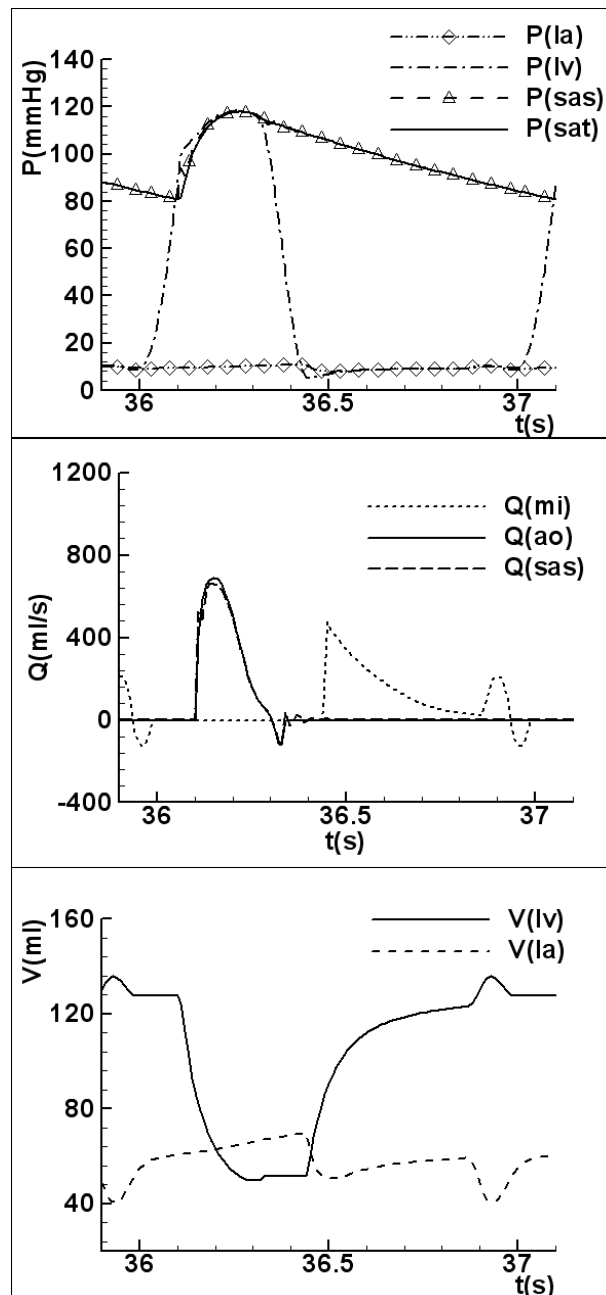
Next the VAD assisted cardiovascular responses under mild exercise condition, both with and without VAD control, are investigated. For this the VAD motion model (equations (4-1) and (4-2)) is enabled, and the slope change (equation (4-9)) as illustrated in Figure 4-4 is introduced in the peripheral arteriole resistance to mimic the neuro-regulated vessel change under the exercise condition. For the situation of VAD support without VAD control, the VAD stroke is still fixed at $X_{vad} = 0.126m$ as above. In simulating the automatic VAD adjustment to accommodate the physiological changes in the patient, the algorithm presented in equations (4-5) and (4-6) is implemented to form a feedback loop and regulate the VAD stroke based on the difference between the expected and the realistic mean aortic pressures in the systemic loop.

4.3 Results

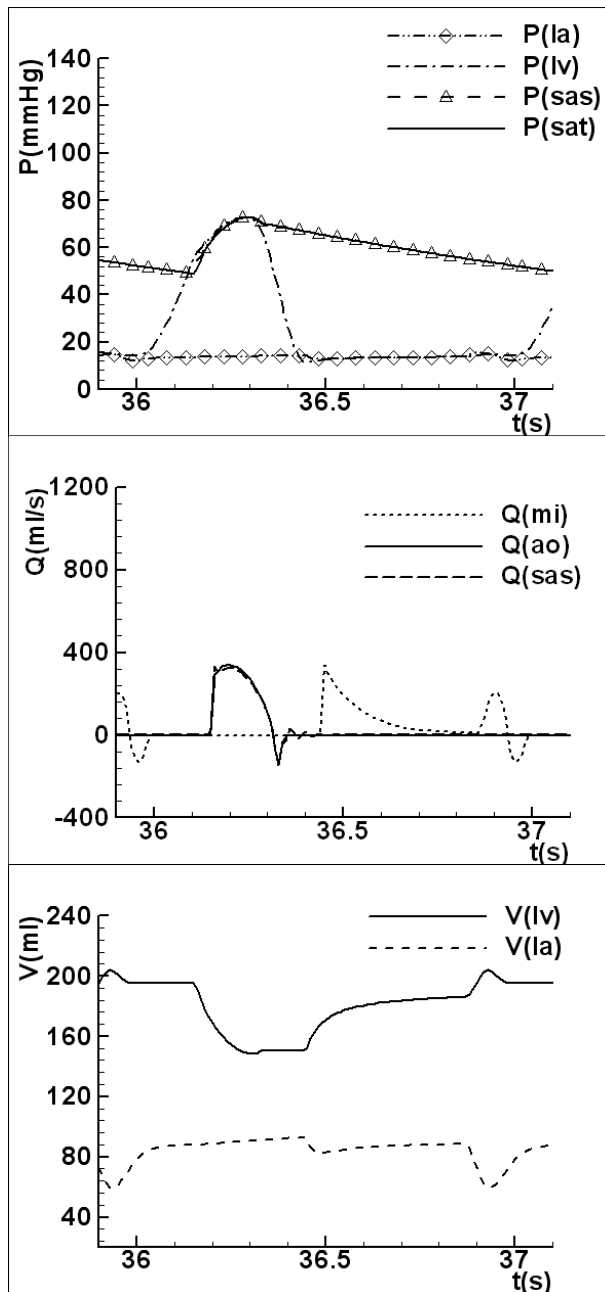
The simulation is carried out as described above, and the corresponding results are presented as following. In the simulations without VAD controller regulation and changes in peripheral arterial resistance, the system often reaches periodic solution after 10 to 15 heart cycles of calculation. The converged solution in the period from the 36th to 37th seconds is chosen in every simulated case for comparison of results in these cases. For reference the ECG signal is shown in some of the figures, to facilitate comparison and illustration of the timing in the cardiac cycle. Some characteristic variables, such as the VAD stroke, cardiac output and arterial pressure, are also compared for situations with and without VAD control, to illustrate the VAD control effect on the cardiovascular response.

4.3.1 Cardiovascular Response without VAD Control and Physiological Disturbance

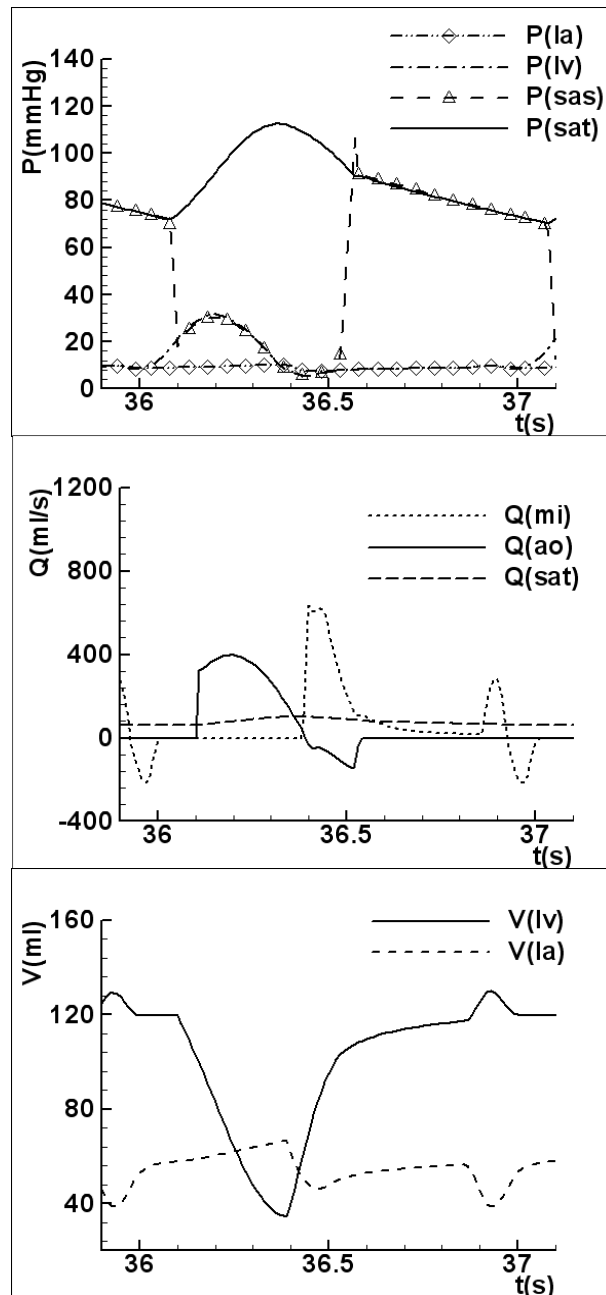
First the cardiovascular response under healthy and diseased conditions with/without VAD Support and neglecting the VAD controller and physiological disturbance is simulated. Figure 4-5 (a) to (c) illustrate the corresponding pressure, flow rate and volume changes in the systemic loop in the three simulated conditions of healthy, diseased without VAD support, and diseased with VAD support but without VAD control.



(a) Healthy condition



(b) Heart failure condition without VAD support



(c) Heart failure condition with VAD support, no VAD stroke control

Figure 4-5 System response of cardiovascular model with and without VAD support

Figure 4-5 (a) shows the simulated cardiovascular response under the healthy condition. The simulation results agree well with the typical drawings for cardiovascular response shown in textbooks such as (Guyton 2006). The left ventricular pressure is in the range of $0 \sim 120 \text{ mmHg}$ and the aortic pressure changes between $80 \sim 120 \text{ mmHg}$. Periodic peak flows exist in the mitral and aortic flows, which with forward and regurgitant flows reach an average flow-rate of about 5 l/min . The left

ventricular volume change is approximately from $50ml$ to $130ml$, with a stroke volume of $80ml$ and ejected volume of $70ml$.

Figure 4-5 (b) illustrates the results for the pathological condition of left ventricular failure without VAD support. Generally the computed cardiovascular response in the LV failure condition follows the same trend as that in the healthy condition, but the values for the physiological variables change greatly. Under the LV failure condition, the aortic pressure is reduced to the range of $46 \sim 68mmHg$ and the peak systolic left ventricular pressure is reduced from the normal value of $120mmHg$ to the current value of $68mmHg$. This greatly impaired perfusion condition will adversely affect the function of important organs in the cerebral, renal and hepatic sub-systems. The left atrial pressure is elevated to about $14mmHg$, almost increased 50% from the normal value of about $9mmHg$. The peak flow rates across the mitral and aortic valves are reduced to about 60% of the normal healthy values. In the volume response, there are prominent changes to chamber volumes in the heart. The left ventricular volume varies between $139ml$ and $192ml$, greatly elevated from the normal healthy range of $50 \sim 130ml$ and with a corresponding decrease in the difference between the minimum and maximum volumes. The left atrial volume is also increased, from the normal range of $40 \sim 68ml$ to the current range of $57 \sim 87ml$. These changes suggest that the ventricular volume difference has been reduced from the normal $80ml$ to the current value of $53ml$, with corresponding decrease in cardiac output, while at the same time prominent left heart dilation has developed.

Figure 4-5 (c) shows the corresponding results in LV failure condition with VAD support but without VAD control. Comparing Figure 4-5 (c) with (a) and (b) illustrates that VAD assistance greatly improves the cardiac function, and compensates the impaired cardiovascular response to almost matching that in the normal healthy condition. As shown in Figure 4-5 (c), the systemic arterial pressure under VAD support returns to the normal range of $80 \sim 120mmHg$, and the pressure in the left atrium drops back to the normal value of about $9mmHg$. The greatly dilated left heart chambers in the LV failure situation are satisfactorily remedied, and the compensated volume responses in the VAD assistance condition reasonably match the chamber volume in the normal healthy condition of Figure 4-5 (a). Besides successful compensation of pressure and volume response discussed above, other aspects of

pressure, flow rate, and volume response almost duplicate the native response in the healthy condition.

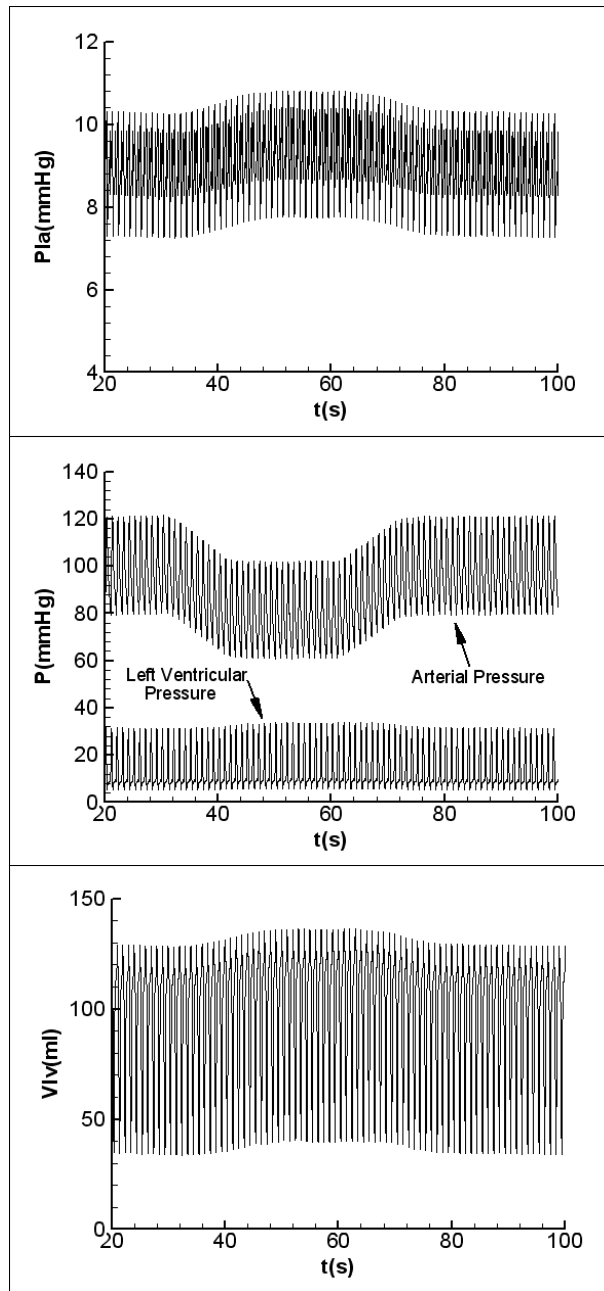


Figure 4-6 Cardiac response under arterial resistance change and without VAD control

(Without VAD control, the arterial pressure cannot be maintained in the physiological range during transition between rest and exercise conditions.)

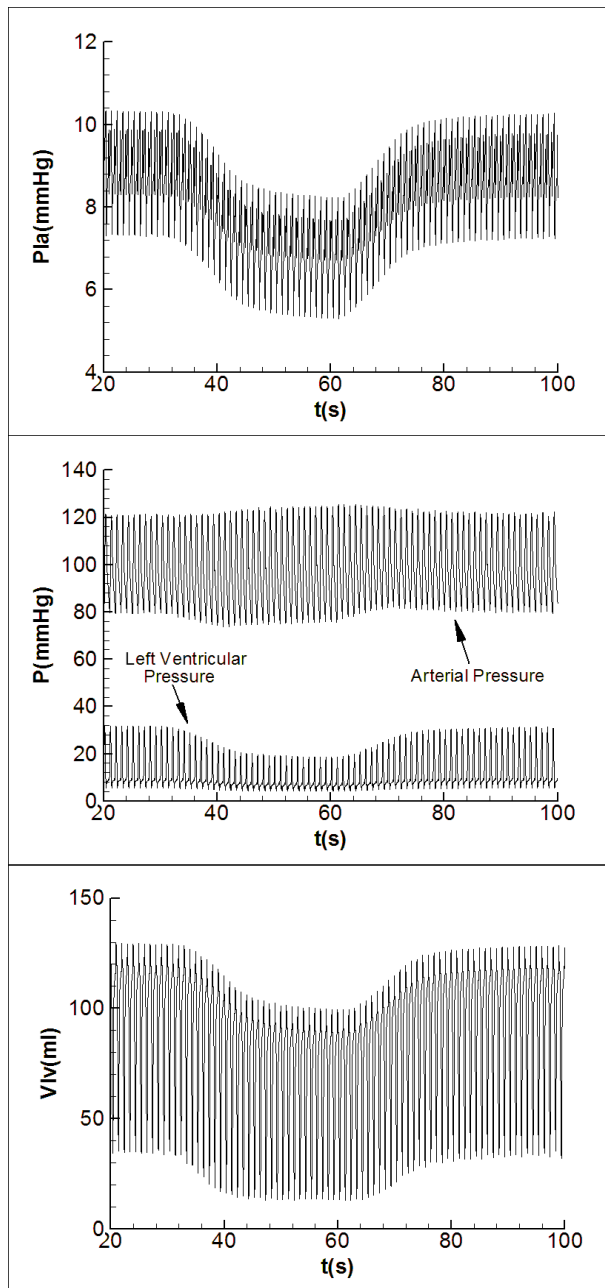


Figure 4-7 Cardiac response under arterial resistance change and with VAD control

(With VAD control, the arterial pressure is effectively maintained in the physiological range during transition between rest and exercise conditions.)

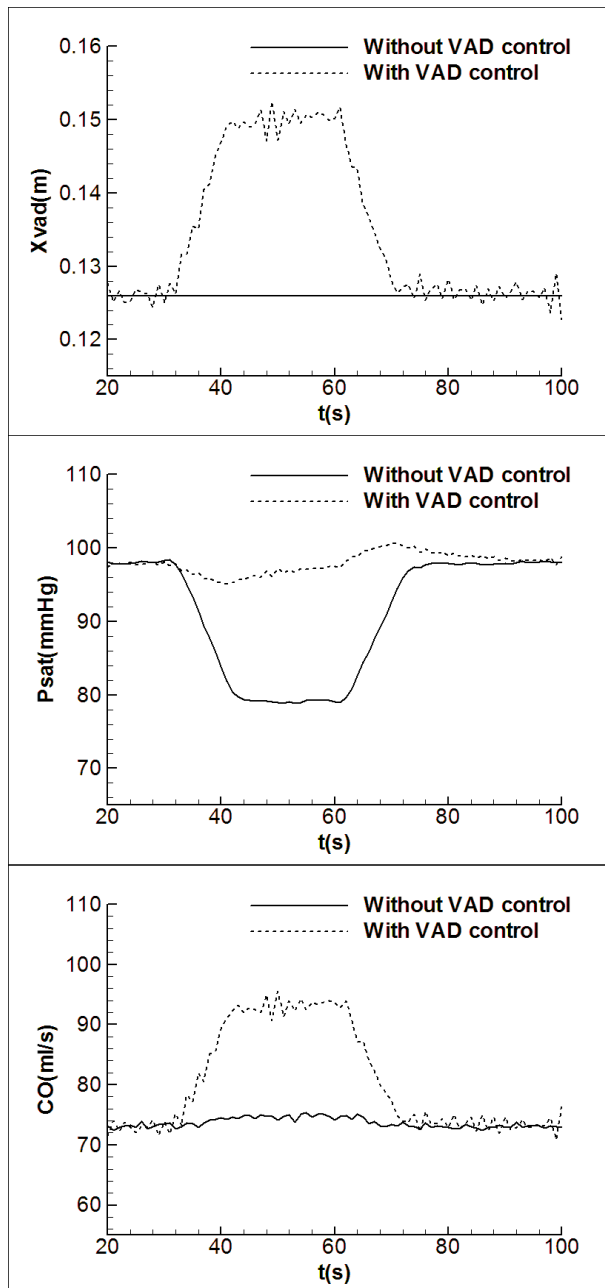


Figure 4-8 Comparison of VAD mean variables

(VAD control helps to maintain the arterial pressure in the physiological range, and at the same time produces increased cardiac output to suit the extra metabolic requirements in the exercise condition.)

4.3.2 Cardiovascular Response under VAD Control and Physiological Disturbance

Figure 4-6 shows the cardiac response under the simulated exercise condition without control in the VAD, and Figure 4-7 illustrates the cardiac response under the same exercise condition while the VAD control is activated. Figure 4-8 further compares the

changes of VAD stroke, mean aortic pressure, and the cardiac output under the two situations of with and without VAD control.

Comparison of Figure 4-6 and Figure 4-7 shows that during the beginning normal resting period ($t < 30s$) the cardiac response of left atrial pressure, left ventricular pressure, aortic pressure, and the left ventricular volume all maintain the stable changes. During the transition period of $t = 30 \sim 40s$ and the exercise period of $t = 40 \sim 60s$, the arteriole resistance is reduced from $R_{sar} = 0.56mmHg \cdot s/ml$ to half of that value. In the situation with VAD support but no VAD control, the left atrial and left ventricular pressures and the left ventricular volume are relatively stable. The aortic pressure drops from the normal range of about $80 \sim 120mmHg$ to about $60 \sim 100mmHg$. For the same period in the situation with VAD control, the left atrial pressure drops from the original range of about $7.2 \sim 10.4mmHg$ to about $5.2 \sim 8.8mmHg$; the peak left ventricular pressure drops from the original value of about $36mmHg$ to about $20mmHg$ and the left ventricular volume drops from the original range of about $45 \sim 130ml$ to about $15 \sim 110ml$. The aortic pressure is maintained in the previous normal range. During the transition period of from $t = 60 \sim 70s$ and later on for the physiological change of from mild exercise to normal resting conditions, all the physiological variables return to the normal ranges (those before the exercise started).

Figure 4-8 (a) to (c) show the comparisons of VAD stroke, mean aortic pressure, and cardiac output under the two situations of without and with VAD control. The cardiac output is defined as:

$$CO = \frac{1}{T} \int_0^T Q_{sar} dt \quad (4-10)$$

When the physiological condition changes from the normal resting ($t < 30s$) to the mild exercise ($40s < t \leq 60s$), in the case without VAD control the VAD stroke is fixed at $0.126m$, and the cardiac output is maintained at around $74ml/s$. The mean aortic pressure \bar{P}_{sar} drops from the normal value of about $98mmHg$ to the much lower value of about $80mmHg$. In the VAD control case the VAD stroke changes from around $0.126m$ to around $0.15m$, correspondingly the cardiac output is elevated to about $93ml/s$ to accommodate the increased metabolic requirement in the body. At the same

time the VAD control maintains the aortic pressure at around the prescribed value of 98mmHg . When the physiological condition changes back from mild exercise to normal resting, these physiological variables also return to the normal resting range.

Comparison of the physiological responses under the above two simulated situations suggest that by maintaining a constant aortic pressure through the PID feedback control, the VAD stroke output can be automatically adjusted to produce the required cardiac output to suit the changing peripheral metabolic requirement in the normal resting and exercise situations. Such ability is indispensable for the new generations of VAD in order to provide adapted physiological perfusion under changing conditions. VAD support without control lacks such a capability.

4.4 Discussion

This study presents a numerical investigation of the human cardiovascular dynamics under the PID controlled VAD support with an in-series connected reciprocating-valve VAD. The error signal between the expected and the realistic mean aortic pressure is used in forming the feedback loop. Simulation results show that the PID controller satisfactorily regulates the VAD stroke to accommodate different perfusion requirements under the test physiological conditions of normal resting and mild exercise situations. During transition from normal resting to mild exercise conditions, the systemic arteriole resistance is reduced to half the normal value, which produces the tendency for mean aortic pressure to drop. In this situation the VAD controller automatically maintains the aortic pressure by increasing the VAD stroke thus producing increased cardiac output to accommodate the elevated perfusion requirement for the exercise condition. When the physiological condition is returned from the exercise condition to normal resting, a reverse process in reducing the VAD stroke and cardiac output is induced by the VAD controller, following the corresponding change in the systemic resistance. Using the mean aortic pressure as the error signal helps to address the cardiac condition over a wide range of physiological conditions, thus the feedback control mechanism adopted in this study ensures that the VAD can automatically adjust its operation according to the physiological requirements under various changes, such as in exercise conditions, or in other situations of emotional changes, cardiac recovery etc. This capability is absent in the VADs without control. Simulation results suggest that the reciprocating-valve VAD has the potential to be

developed into a flexible pump to support the patients in response to various physiological changes, while follow-on *in vitro* and *in vivo* tests are needed to further validate the device.

In the simulation of transition between the normal resting and the mild exercise conditions, for the case of VAD assistance without VAD control, the VAD always maintains a constant cardiac output, thus when the peripheral arteriole resistance drops or increases, the aortic pressure also drops or increases. As a result, in the exercise condition the uncontrolled VAD not only fails to provide the increased cardiac output to satisfy the elevated metabolic requirement, but also produces a dropped mean aortic pressure that endangers the normal perfusion to the important peripheral organs. As a contrast, in the VAD assistance with VAD control, by maintaining a constant mean aortic pressure both of these two problems are solved. The rationale behind this is that, generally the arteriole resistance and the capillary resistance form the major part of the vessel resistance, thus the aortic pressure approximately equals the product of the cardiac output and the arteriole and capillary resistance ($\bar{P}_{sat}(k) = CO * (R_{sar} + R_{scp})$).

By maintaining a constant mean aortic pressure in the VAD control, decreasing of the arteriole resistance is directly mapped to the control strategy of increasing the VAD stroke and thus increasing the cardiac output, which satisfies the requirements for both the constant perfusion pressure and the increased flow output concurrently. Previous researchers have partially used the arterial pressure as physiological index in the VAD control, whereas their purposes were to assist the detection of ventricular collapse (Wu *et al.* 2003) or for the evaluation of coronary flow (Barnea *et al.* 1992). (Giridharan *et al.* 2002) and (Giridharan and Skliar 2003) adopted the pressure difference between the left ventricle and the aorta as the physiological index in controlling the rotating speed of a rotary pump type VAD, and later (Giridharan *et al.* 2004) revised it and used the pressure difference between the left atrium and the aorta as the physiological index. Since under rotary pump type VAD support the left atrial pressure is much smaller than the aortic pressure and the left atrial pressure is always relatively stable, generally using the pressure difference between the left atrium and the aorta as the physiological index has the same rationale as using the mean aortic pressure alone. Using the mean aortic pressure as the physiological index is easier to implement, and its validity has been proved in the current study.

VAD control not only provides adapted pressure and flow changes to suit the patient requirements in different physiological conditions, with the adapted perfusion it also allows the patients more freedom in having mild exercise, which not only improves the quality of the life but also induces some advantageous hemodynamic changes inside the patients. Using *in vivo* measurement and computational fluid dynamics simulation, (Taylor *et al.* 2002, Taylor *et al.* 1999) revealed that at resting condition, a region of flow recirculation and low wall shear stress often develops at mid diastole along the posterior wall of the infrarenal abdominal aorta. Such flow recirculation and low shear stress are thought to be responsible for the localisation of vascular disease in the infrarenal abdominal aorta. They further observed that under light to mild exercise conditions the recirculation and low shear stress zone disappears, and concluded that exercise could promote arterial health with the elimination of adverse hemodynamic conditions. Other studies (e.g., (Niebauer and Cooke 1996)) also suggested that increased shear stress under exercise condition helps to remove the lipid molecules from the vessel surface, increases nitric oxide and prostacyclin release, and inhibits atherosclerotic processes. In this sense VAD control is beneficial to the vessel health. However, it should be noted that increased cardiac output in exercise condition under VAD control also produces flow structure changes in the cardiovascular system and elevates the shear stress level in the vessels and the VAD, as compared to the condition without VAD control. The flow structure changes and elevated shear stress increase the potentials for haemolysis and thrombosis to develop in the vessels and the VAD. Although this can be partially addressed through VAD design optimisation, further investigation on VAD haemodynamics is indispensable.

The current study applies the PID control as the VAD control algorithms. It is noted that other more complex control algorithms such as optimal control, adaptive control etc. have been used by researchers in VAD control. These more sophisticated control algorithms were applied with the aim to improve the accuracy through further detailed system dynamics modelling. However, they always demand more expensive computational and hardware resources, and the inclusion of more complex system dynamics models may sometimes induce the stability problem. The current study stands on the safer and simpler end and chooses the concise and well-validated PID control algorithms for the VAD control. Industrial practice has proved that PID control is quite robust and can tolerate much of the environmental disturbances. To have

greater flexibility the current PID controller can be further improved into the non-linear intelligent PID controller when necessary, in which the controller parameters can be carefully adjusted online to suit more stringent physiological changes.

The current control loop needs a pressure transducer to be equipped at the outlet to record the pressure reading in the aorta. In recent years, sensor-less control methods are under development (Ayre *et al.* 2003, Ayre *et al.* 2000, Funakubo *et al.* 2002, Granegger *et al.* 2012, Kitamura *et al.* 2000, Lim *et al.* 2008, Ogawa *et al.* 2006, Tanaka *et al.* 2003, Tsukiya *et al.* 2001, Waters *et al.* 1999), in which only the VAD internal characteristic variables such as pump coil current/voltage and pump rotating speed etc. are sampled and used to re-construct the pressure (Ayre *et al.* 2000, Funakubo *et al.* 2002, Kitamura *et al.* 2000, Lim *et al.* 2008, Tanaka *et al.* 2003, Waters *et al.* 1999) and flow (Ayre *et al.* 2003, Ayre *et al.* 2000, Funakubo *et al.* 2002, Granegger *et al.* 2012, Kitamura *et al.* 2000, Lim *et al.* 2008, Ogawa *et al.* 2006, Tanaka *et al.* 2003, Tsukiya *et al.* 2001, Waters *et al.* 1999) as feedback signals, thus eliminating the use of physical transducers. This approach has the advantage of omitting the physiological transducers that are often unreliable in long term usage, but at the expense of reduced physical accuracy and more complex computational works, such as online identification of the system parameters. Following this idea the current research can be extended and the sensor-less implementation of the control loop can be explored to replace the physical pressure transducer with the online estimated pressure signal, possibly based on the build-in characteristic variable of VAD control voltage.

In a broader sense, VAD control concerns also the aspects of fault diagnosis in the VAD and detection of atrial suction/ventricular collapse etc., which are not only controller related but also depends on the VAD motion mechanism. As in most of preliminary designs for the VAD controller, these aspects are not included in the current study. However, they should be carefully considered in the formal VAD design, and the final VAD prototypes (comprising of both the VAD controller and the VAD motion mechanism) need to be critically tested against the above mentioned abnormal conditions.

4.5 Conclusions

This chapter investigates the VAD assisted cardiovascular dynamics under PID feedback control through numerical simulation. The in-series connected reciprocating-

valve type VAD located in the ascending aorta position is modelled. The classical PID control algorithm is implemented to regulate the VAD stroke on a beat-to-beat base based on the error signal of mean aortic pressure. With the online PID feedback control, the VAD can satisfactorily regulate its stroke to accommodate metabolic requirements under various physiological conditions, including normal resting and mild exercise situations.

Chapter 5 Numerical Simulation of Global Hydro-dynamics in a Pulsatile Bioreactor for Cardiovascular Tissue Engineering⁴

Previous numerical simulations of the hydro-dynamic response in the various bioreactor designs were mostly concentrated on the local flow field analysis using computational fluid dynamics, which cannot provide the global hydro-dynamics information to assist the bioreactor design. In this chapter a mathematical model is developed to simulate the global hydro-dynamic changes in a pulsatile bioreactor design by considering the flow resistance, the elasticity of the vessel and the inertial effect of the media fluid in different parts of the system. The developed model is used to study the system dynamic response in a typical pulsatile bioreactor design for the culturing of cardiovascular tissues. Simulation results reveal the detailed pressure and flow-rate changes in the different positions of the bioreactor, which are very useful for the evaluation of hydro-dynamic performance in the bioreactor designed. Typical pressure and flow-rate changes simulated agree well with the published experimental data, thus validates the mathematical model developed. The proposed mathematical model can be used for design optimization of other pulsatile bioreactors that work under different experimental conditions and have different system configurations.

5.1 Introduction

Design and construction of bioreactors are very important in tissue engineering research, because they directly provide the *ex vivo* environment for tissue regeneration. For this purpose various types of bioreactors have been designed to address the different tissue culturing requirements in previous studies. For the culturing of certain types of tissues such as the cardiovascular tissues, previous research has proved that *in vitro* environment of pulsatile pressure and shear stress can prominently improve the tissue formation and organization, and increase the mechanical strength of the tissue

1. ⁴ Adapted from: Shi Y., Numerical Simulation of Global Hydro-dynamics in a Pulsatile Bioreactor for Cardiovascular Tissue Engineering, *Journal of Biomechanics*, 41(3), pp953-959, 2008

cultured (Hoerstrup *et al.* 2001). Thus design of pulsatile bioreactors becomes an important task in providing the necessary condition for such tissue engineering studies.

In designing bioreactors of various configurations, numerical simulation can play an important role in predicting firstly the global dynamic response in the different parts of the bioreactors, and secondly the local hydro-dynamic changes in certain specific areas in the bioreactors such as around the tissue constructs. Such numerical simulation helps the designer to evaluate the performance of the bioreactor system design before the prototype bioreactor is constructed, thus greatly facilitates the design optimization, saves the design expense as well as speeds up the design process. In previous bioreactor research, numerous numerical simulations have been carried out to study the local media flow features around the tissue constructs using the computational fluid dynamics (CFD) method (Davidson *et al.* 2003, Dubey *et al.* 2006, Singh *et al.* 2007, Williams *et al.* 2002, Zeng *et al.* 2006). These CFD studies revealed the detailed pressure, velocity and shear stress distributions in the tissue culturing chambers of various bioreactor designs, which is very useful for the design optimization of the bioreactor internal geometric configurations. However, without the complimentary study of global hydro-dynamics analysis, such local CFD study in bioreactors is incomplete—a bioreactor design will not be accepted if its local flow field is optimized but the global hydro-dynamics does not meet the experiment requirements. Also without the global hydro-dynamics study to provide the accurate boundary conditions, in the local CFD calculations the designer would have to set the boundary conditions either based on his/her personal estimations or by searching the literatures for published data in previous similar bioreactor designs. For the simple bioreactor designs and when the media flow is steady, setting the boundary conditions based on estimation or previous data may introduce only limited errors; when the system configuration is complex or the media flow is unsteady, relying on estimation or previous data may introduce unexpected errors and thus produce totally artificial results. Thus the global hydro-dynamic study is a very important and necessary procedure in the design optimization of bioreactors. However, in the open literature no research has been done to study the global hydro-dynamic response in the bioreactors yet.

To fill this gap the current study proposes a mathematical model to analyse the global hydro-dynamic response in a typical pulsatile bioreactor design. The individual parts of

the bioreactor are modelled by considering the local media flow resistance, the elasticity of the vessel and the inertial effect of the media fluid. The different parts are then combined together to form the system model. The developed model is used to investigate the pressure and flow-rate changes in the different segments of a typical pulsatile bioreactor design, and satisfactory system response is obtained. The model can also be adapted to study the hydro-dynamic characteristics of broader ranges of pulsatile bioreactor designs that work under different operating conditions and have different system configurations.

5.2 Methods

5.2.1 Basic configuration of the pulsatile bioreactor

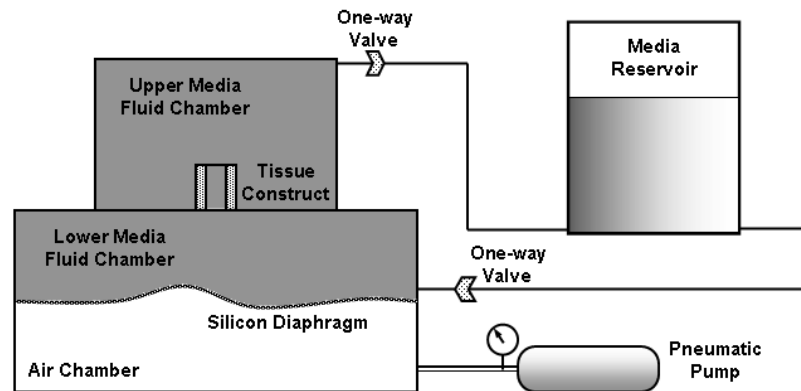


Figure 5-1 Schematics of the pulsatile bioreactor.

A typical pulsatile bioreactor design like those in previous studies (Narita *et al.* 2004, Sodian *et al.* 2002, Sodian *et al.* 2001) is adopted in this research. The bioreactor has two media flow chambers: a lower chamber and an upper chamber. The two chambers are connected by a constricted channel which is formed by the tissue construct. The detailed geometries for the two media chambers and the tissue construct can be optimized using CFD method in the follow-on studies, while in the current research they are assumed to have simple geometries and only the corresponding hydro-dynamic effects are considered, as discussed in the following sections. The lower and upper media chambers are connected to the media reservoir through an inlet valve and an outlet valve to keep the one-way flow direction. Silicon tubing is used for connecting the system parts together as well as to absorb the mechanical vibrations induced by fluid flow. To produce the pulsatile pressure and shear stress environment around the

tissue construct, an air chamber is equipped at the bottom of the lower media chamber in the bioreactor. A flexible silicon diaphragm separates the air chamber from the lower chamber of the bioreactor. The air chamber is connected to a pneumatic pump which produces varying pressure in the air chamber. Driven by the varying air pressure, the diaphragm moves up and down to produce the pulsatile flow into the lower media chamber. Figure 5-1 shows the schematics of the pulsatile bioreactor design.

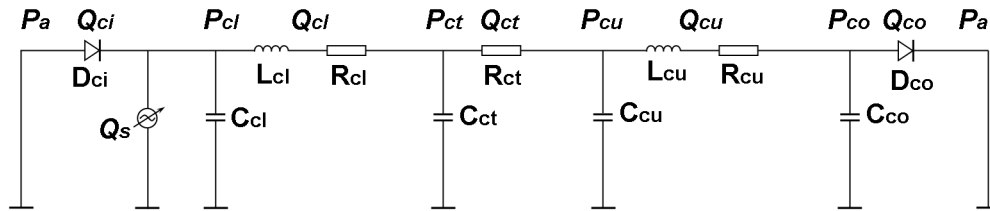


Figure 5-2 Equivalent circuit description of the hydro-dynamic characteristics for the pulsatile bioreactor

(Refer to the nomenclature table in the front pages for detailed name of each component.)

5.2.2 Numerical model of the pulsatile bioreactor

In modelling the global hydro-dynamics of the pulsatile bioreactor design, the concept of hydraulic-electric analogue is used in which the frictional loss, the elasticity of the vessel and the inertia of the fluid in the vessel are compared to the resistance R , capacitance C and inductance L in the electric circuit, while the pressure and flow-rate in the fluid flow are compared to the voltage and the electric current. The well-developed technique for analysing the electric circuits is then used to investigate the pressure and flow-rate changes in the different segments of the bioreactor. For different segments of the system, different combinations of R , C and L effect are used to describe the local dynamic characteristics, depending on the local flow features. Figure 5-2 shows the equivalent circuit description of the pulsatile bioreactor design illustrated in Figure 5-1.

5.2.2.1 Lower and upper media flow chambers

In the lower media flow chamber, the frictional loss comes from the secondary circulation flow accompanying the changing of the flow direction from the inlet valve to the tissue construct, the uneven driving action from the silicon diaphragm, and the restriction of flow through the tissue construct on the top of the lower media chamber. Vessel elasticity presents due to the deformation of the silicon diaphragm and the

silicon tubing that connecting the inlet one-way valve to the media chamber. The mass media fluid flows under pulsatile flow condition exhibits prominent inertial effect. To model these effects the full RCL combination is adopted. In the lower media chamber both the in-flow through the one-way inlet valve and the driving flow due to diaphragm motion contribute to the flow dynamics. Thus the pressure change in the lower media chambers follows the relation:

$$\frac{dP_{cl}}{dt} = \frac{Q_{ci} + Q_s - Q_{cl}}{C_{cl}} \quad (5-1)$$

and the flow-rate change is governed by:

$$\frac{dQ_{cl}}{dt} = \frac{P_{cl} - P_{ct} - \rho g \cdot h_{cl} - R_{cl} \cdot Q_{cl}}{L_{cl}} \quad (5-2)$$

where $\rho g \cdot h_{cl}$ is the pressure difference due to height of the lower media chamber.

Similarly in the upper media flow chamber there are:

$$\frac{dP_{cu}}{dt} = \frac{Q_{ct} - Q_{cu}}{C_{cu}} \quad (5-3)$$

and:

$$\frac{dQ_{cu}}{dt} = \frac{P_{cu} - P_{co} - \rho g \cdot h_{cu} - R_{cu} \cdot Q_{cu}}{L_{cu}} \quad (5-4)$$

where $\rho g \cdot h_{cu}$ considers the height effect of the upper media chamber.

5.2.2.2 Tissue construct

Tissue construct is the main focus of the biochemical study in the tissue culturing research. While from the hydro-dynamic sense, the tissue construct is an elastic tube and also serves as a restricting flow channel in the bioreactor. Due to the restricted flow area the resistance effect R in the tissue construct is more prominent than that in the lower and upper media chambers. The capacitance effect C comes from the elasticity of both the silicon seat of the scaffold and the scaffold itself. The fluid mass in the central channel of the tissue construct is minor compared with that in other parts of the system, thus the inertial effect L is neglected. The pressure change in the tissue construct is:

$$\frac{dP_{ct}}{dt} = \frac{Q_{cl} - Q_{ct}}{C_{ct}} \quad (5-5)$$

and the flow-rate change is governed by:

$$Q_{ct} = \frac{P_{ct} - P_{cu}}{R_{ct}} \quad (5-6)$$

5.2.2.3 Inlet and outlet valves

The inlet and outlet valves are modelled as orifices with varying openings, plus the elasticity of the silicon tubing that connects the valves. For the inlet valve, the elasticity of the silicon tubing has the same contribution to the fluid dynamics as that of the silicon diaphragm, thus it has been lumped into the general capacitance effect C_{cl} in the lower media chamber. For the outlet valve, the elasticity of the tubing affects the flow upstream to the valve and the influence is considered by:

$$\frac{dP_{co}}{dt} = \frac{Q_{cu} - Q_{co}}{C_{co}} \quad (5-7)$$

In modelling the orifice flow feature in the inlet valve, the flow-rate is described by:

$$Q_{ci} = CQ_{ci} \cdot \tau_{ci} \cdot \frac{P_a - \rho g \cdot h_s - P_{cl}}{\sqrt{|P_a - \rho g \cdot h_s - P_{cl}|}} \quad (5-8)$$

where h_s is the height of the air chamber and $\rho g \cdot h_s$ considers the height difference between the inlet valve position and the bottom of the media reservoir.

The valve opening τ_{ci} can be modelled by considering the detailed valve motion dynamics under various factors such as pressure difference and friction in the valve. For simplicity the current research models the valve as an ideal one without inertial effect and flow regurgitation, and there is:

$$\tau_{ci} = \begin{cases} 1 & P_a - \rho g \cdot h_s \geq P_{cl} \\ 0 & P_a - \rho g \cdot h_s < P_{cl} \end{cases} \quad (5-9)$$

Similarly for the outlet valve, there are:

$$Q_{co} = CQ_{co} \cdot \tau_{co} \cdot \frac{P_{co} - [P_a - \rho g \cdot (h_{cl} + h_{cu} + h_s)]}{\sqrt{|P_{co} - [P_a - \rho g \cdot (h_{cl} + h_{cu} + h_s)]|}} \quad (5-10)$$

and

$$\tau_{co} = \begin{cases} 1 & P_{co} \geq [P_a - \rho g \cdot (h_{cl} + h_{cu} + h_s)] \\ 0 & P_{co} < [P_a - \rho g \cdot (h_{cl} + h_{cu} + h_s)] \end{cases} \quad (5-11)$$

5.2.2.4 Air chamber

The air chamber is inflated and deflated by a pneumatic pump, which can be programmed to produce prescribed air pressure changes. The air pressure acts on the silicon diaphragm and drives the diaphragm motion, which then propels the fluid in the lower media chamber and produces the pulsatile flow in the bioreactor. According to its hydro-dynamic contribution, the air chamber can be modelled as a pressure modulated flow source.

In modelling the air chamber dynamics, for the first instance a sinusoidal air pressure change is assumed in the air chamber:

$$P_s = P_{s,0} + P_{s,a} \cdot \sin \frac{2\pi \cdot t}{T} \quad (5-12)$$

The silicon diaphragm is considered as an elastic rubber film. The diaphragm motion is governed by the force equilibrium under various effects including the pressure difference across the diaphragm, the elastic force, the frictional force and the acceleration related force:

$$m_s \cdot \frac{d^2 l}{dt^2} + k_f \cdot \frac{dl}{dt} + k_e \cdot l = (P_s - P_{cl}) \cdot A_s \quad (5-13)$$

The flow output from the air chamber is then calculated as:

$$Q_s = A_s \cdot \frac{dl}{dt} \quad (5-14)$$

5.2.3 Boundary conditions

Both the inlet and the outlet of the bioreactor are connected to the media reservoir, whose effect can be modelled as a constant pressure source:

$$P_a = P_{atm} + \rho g \cdot h_a \quad (5-15)$$

where P_{atm} is the atmospheric pressure and h_a is the height of media column in the media reservoir. The bottom of the bioreactor and the bottom of the media reservoir are in the same horizontal level, thus with reference to this common horizontal level, the silicon diaphragm and inlet valve have a height of h_s , the tissue construct $h_{cl} + h_s$, and the outlet valve $h_{cu} + h_{cl} + h_s$.

Table 5-1 Parameter settings for the bioreactor

Part	Parameter	Value	Unit
Upper media chamber	R_{cu}	0.05	$mmHg \cdot s/ml$
	C_{cu}	0.02	$ml/mmHg$
	L_{cu}	3.2e-4	$mmHg \cdot s^2/ml$
	h_{cu}	0.05	m
Tissue construct	R_{ct}	0.25	$mmHg \cdot s/ml$
	C_{ct}	0.005	$ml/mmHg$
Lower media chamber	R_{cl}	0.035	$mmHg \cdot s/ml$
	C_{cl}	0.05	$ml/mmHg$
	L_{cl}	5.2e-4	$mmHg \cdot s^2/ml$
	h_{cl}	0.1	m
Silicon diaphragm	m_s	6.8e-3	kg
	A_s	1.13e-2	m^2
	k_f	25.	$mmHg \cdot m \cdot s$
	k_e	1.5e4	$mmHg \cdot m$
Air chamber	h_s	0.02	m
	$P_{s,0}$	0.	$mmHg$
	$P_{s,a}$	100.	$mmHg$
Inlet valve	CQ_{ci}	250.	$ml/(s \cdot mmHg^{0.5})$
	C_{ci}	0.015	$ml/mmHg$
Outlet valve	CQ_{co}	250.	$ml/(s \cdot mmHg^{0.5})$
	C_{co}	0.015	$ml/mmHg$
Media reservoir	P_{atm}	0.	$mmHg$
	h_a	0.1	m
	ρ	1.e3	kg/m^3

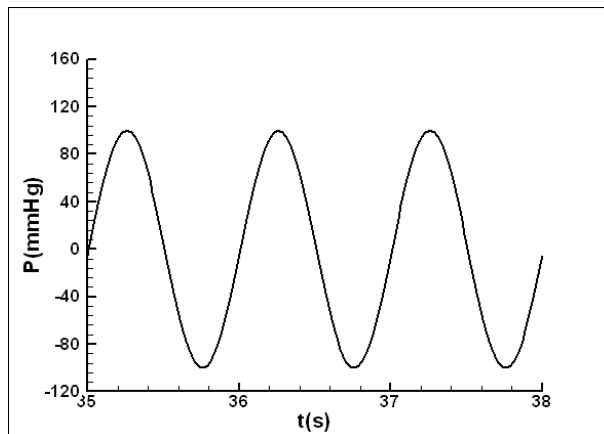
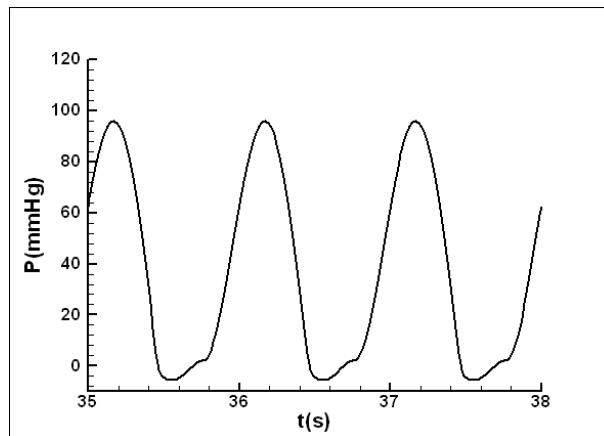


Figure 5-3 Driving pressure in the air chamber

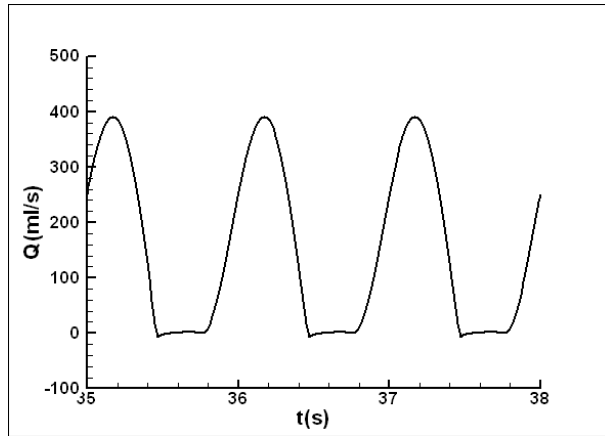
5.2.4 Parameter settings

In assigning values to the system parameters for the developed mathematical model, the bioreactor system configuration is compared with the designs of systemic flow test rigs

for cardiovascular research (Sharp and Dharmalingam 1999, Shi *et al.* 2004) and the numerical models for the human cardiovascular system (Shi and Korakianitis 2006, Ursino 1999) in the open literature. Parameters for the variables including resistance, capacitance and inductance for the lower and upper media chambers are scaled from these published data, while the values for the flow coefficients of the inlet and outlet valves are estimated by referring to the published data and considering the valve configurations and the diameters of the flow channels. Values for the height related variables including h_s , h_a , h_{cl} and h_{cu} are decided by the geometry of the current bioreactor design. For the silicon diaphragm, the area is calculated from the system geometry; the mass is calculated based on the area, thickness and estimated density of the silicon film; while the frictional coefficient is estimated by considering the realistic diaphragm motions. The amplitude of the pressure variation in the air chamber is set at 100 *mmHg*, as illustrated in Figure 5-3, so that the general system response produced in the bioreactor represents the typical physiological condition for the arterial vessels. The air chamber pressure can also be manipulated to provide different experimental conditions for different tissue culturing requirements. Table 5-1 illustrates the parameter settings in the simulation.

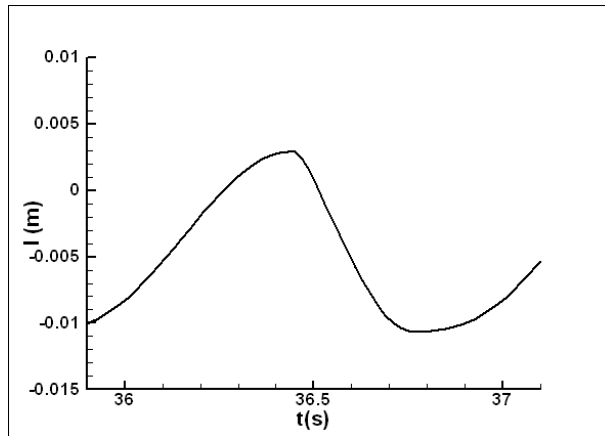


(a) Pressure

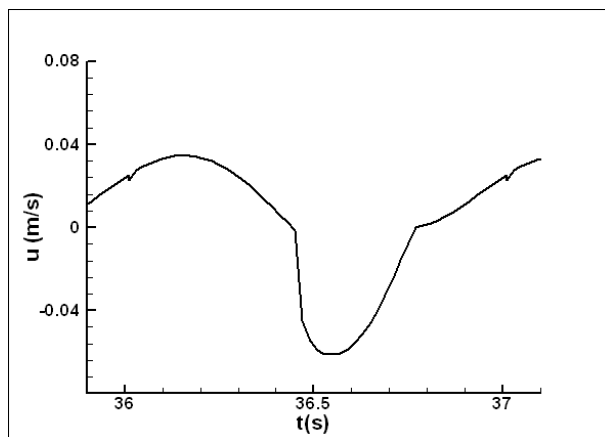


(b) Flow-rate

Figure 5-4 Simulated pressure and flow-rate changes generated in the tissue construct position

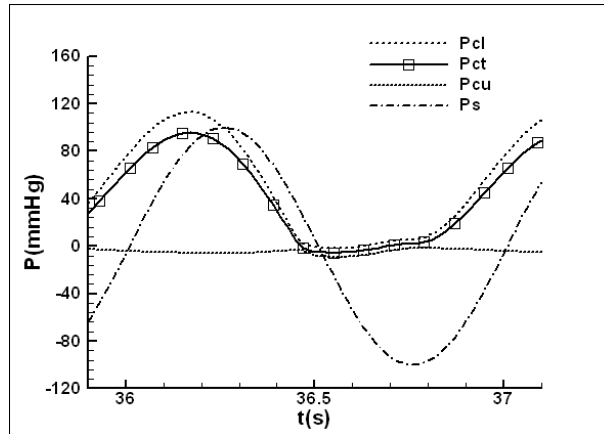


(a) Displacement

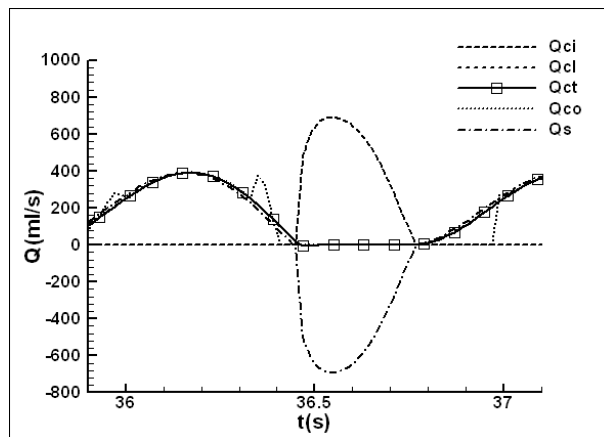


(b) Velocity

Figure 5-5 Simulated motion profile of the silicon diaphragm



(a) Pressure



(b) Flow-rate

Figure 5-6 Comparison of pressure and flow-rate changes in different positions of the system

5.3 Results and Discussion

Based on the mathematical model described above and the parameter settings, a computer program is developed in C language to simulate the hydro-dynamic changes in the pulsatile bioreactor design. The equations are solved using the classical Runge-Kutta method. For ease of comparison the period for the input air pressure is chosen as $1s$. The calculation converges to the periodic solution after about ten cycles. The typical converged results of the system dynamics are presented in the following figures. Figure 5-4 (a) and (b) illustrate the typical pressure and flow-rate changes produced at the tissue construct position. Figure 5-5 (a) and (b) show the displacement and velocity changes for the silicon diaphragm in an experimental cycle. Figure 5-6 (a) and (b) compare the pressure and flow-rate changes at different locations of the bioreactor in an experimental cycle.

From Figure 5-4 it is observed that the pressure and flow-rate changes produced at the tissue construct position lies in the normal physiological range for the cardiovascular tissues, as presented in the physiology textbooks such as (Guyton 2006) (0 ~ 120 mmHg for the general range of blood pressure. The detailed values for the pressure and the flow-rate change with the different positions of the tissue.) . These simulated results agree well with the waveform pattern in the experimental measurements in a similar bioreactor design by Sodian *et al.*(Sodian *et al.* 2002, Sodian *et al.* 2001), but have a broader range of pressure and flow-rate changes. In the current study, the simulated bioreactor design produces a pressure change of 0 ~ 120 mmHg and flow-rate change of 0 ~ 400 ml/s at a cycle period of 1 s ; while in Sodian *et al.*'s study, the bioreactor is designed to maintain a tissue culturing condition of -12 ~ 23 mmHg at 18 s cycle period to suit the requirements for the early stage of tissue regeneration. In this sense the current numerical simulation studies a more realistic physiological design of the bioreactor in cardiovascular tissue engineering. The numerical model can be easily adapted to simulate the dynamic response in the bioreactor system under other working conditions, such as the smaller range of pressure change at slower cycle period in Sodian *et al.* design (Sodian *et al.* 2001), or for different system configurations such as (Narita *et al.* 2004).

Figure 5-5 (a) and (b) present the displacement and velocity changes of the silicon diaphragm in an experimental cycle. It is observed that the diaphragm oscillates with an amplitude of 0.0065 m around its neutral position in the experimental cycle, while the neutral position is not exactly the zero displacement position. Instead, the neutral position for the diaphragm moves about 0.0035 m towards to air chamber direction. Several factors contribute to such an offset. Besides the stiffness of the silicon diaphragm, the weight of the media fluid in the lower and upper media fluid chambers and the fluid flow into the lower media fluid chamber through the inlet valve also affect the diaphragm offset value.

Figure 5-6 (a) and (b) compare the pressure and flow-rate changes in the different positions of the bioreactor during an experimental cycle. In Figure 5-6 (a) it is observed that generally pressures in the lower media chamber and in the tissue construct position (P_{cl} and P_{ct}) change in a half sinusoidal wave pattern under the combined influence of the sinusoidal driving air pressure P_s and the silicon diaphragm

action. During the increasing phase and the early half of the decreasing phase of P_s changing, P_{cl} and P_{ct} follow the same trend of changing as P_s . Under the combined influence of the supporting action of the silicon diaphragm and the additional flow from the inlet valve, P_{cl} and P_{ct} even exceed P_s during the increasing phase of the driving pressure. The peak values of P_{cl} and P_{ct} are mainly influenced by the resistance effect in the flow channel in the bioreactor. Bigger diameters of the flow channels correspond to smaller resistance effect in the system, thus producing smaller peak pressures of P_{cl} and P_{ct} under the same driving air pressure action, and *vice versa*. In the later half of the decreasing phase of the driving pressure changing, when P_s falls below a certain pressure value, P_{cl} and P_{ct} are clipped at their lower limit values and do not decrease further as the P_s falling. This is because that the silicon diaphragm begins to play the dominant role in such situation and stops the further downward motion of the media fluid in the lower media chamber. The lower limit values of P_{cl} and P_{ct} are strongly influenced by the elasticity of the silicon diaphragm. A softer silicon diaphragm allows P_{cl} and P_{ct} to follow the P_s changing further in the later half of the decreasing phase for the driving air pressure, thus produces smaller values of the lower limit pressures for P_{cl} and P_{ct} . Pressure in the upper media chamber maintains at a small value throughout the cycle.

In the flow-rate comparison in Figure 5-6 (b), it is observed that the flow-rate produced by the driving air pressure shows a pattern of skewed sinusoidal wave: the positive part is flattened to exhibit a smaller amplitude and longer duration when the air pressure needs to balance the combined action of the silicon diaphragm and the pressure in the media chamber, while the negative part is compressed to show a bigger amplitude and shorter duration when the air pressure is allowed to fall freely and the silicon diaphragm further assist such pressure dropping. Flow-rate changes in the lower media chamber (Q_{cl}), the tissue construct (Q_{ct}) and the outlet valve (Q_{co}) follow the positive half of the flow-rate change Q_s produced by the driving air pressure, while when Q_s becomes negative, Q_{cl} , Q_{ct} and Q_{co} maintain at zero. Flow-rate in the inlet valve Q_{ci} exhibits the opposite change: when Q_s is positive, Q_{ci} is maintained at zero; when Q_s is negative, the inlet valve opens and media fluid flows from the media reservoir into the lower media chamber to occupy the space vacated by the diaphragm motion, thus

Q_{ci} show the same pattern of changing as Q_s but with a different sign. The changing patterns of the flow-rates in the bioreactor are very similar to that in the cardiac chambers in human body.

Besides the above simulation results, the developed mathematical model can be further applied to study the system dynamics change when different values are assigned to the system variables, such as when the air chamber pressure is changed in other patterns and magnitudes, under other stiffness of the silicon diaphragm, other combinations of frictional lose, vessel elasticity and inertial effect under different bioreactor geometries. Such extension of research forms the fundamental optimization procedures in the bioreactor system design. This is a future work.

The simulation results in this research agree reasonably well with those published experimental data like (Sodian *et al.* 2001). This validates the current mathematical model and suggests that the developed model can be applied to predict the global hydro-dynamic characteristics of other similar pulsatile bioreactor designs. When combined with the CFD study which further reveals the velocity and shear stress distributions under the detailed geometry designs, it is believed that numerical simulation could play an important part in the evaluation of the hydro-dynamic characteristics of the bioreactor design even in the prototype design stage. This will provide a reliable and cost-effective way to assist and improve the future bioreactor design and analysis.

5.4 Conclusion

This research presents a mathematical model for the global hydro-dynamic study of the pulsatile bioreactor design. The developed model is then used to study the system dynamics in a typical pulsatile bioreactor design for the culturing of cardiovascular tissues. Simulation results reveal the detailed pressure and flow-rate changes in the different positions of the bioreactor. Typical pressure and flow-rate changes in the simulated system agree well with the published experimental data, thus validate the developed model. The current model has great potential to be extended for the design optimization of the pulsatile bioreactors.

Chapter 6 Conclusion and Future Works

Cardiovascular system is the vital system in maintaining the normal functioning of the human body. Due to the prevalence of the cardiovascular diseases in the UK society and the world alike, research into the cardiovascular physiology and pathology is an urgent task in the biomedical science and engineering. Mathematical modelling as a mature research tool has played an important part in the cardiovascular research. Among the mathematical models for the cardiovascular research, the lumped-parameter model predicts the pressure and flow changes in the cardiovascular organs, which are directly comparable to the clinical data and thus has the most straightforward clinical relevance.

6.1 Conclusions

The current thesis reports some selected studies from a series of coherent work that the author carried out previously on the lumped-parameter modelling, as detailed in the following:

1. A comprehensive review of the lumped-parameter cardiovascular modelling has been conducted, which covers the historical and concurrent models for the individual cardiovascular organs as well as the overall integrated system. Several non-linear effects in the modelling that affect the cardiovascular response are discussed. Sample parameter settings for the models and various model applications are summarised, and future directions for lumped parameter cardiovascular modelling are suggested.
2. An improved lumped-parameter cardiovascular model has been developed and presented. This improved model specifically includes the dynamic description of the atrial-ventricular septum and the heart valves, and thus can represent the important response features of the auxiliary pumping action of the atrial-ventricular septum and the three-stage leaflet motion in heart valve dynamics and, which are missing in previous models.
3. By integrating the VAD model into the developed cardiovascular model, a numerical study of the cardiovascular response under heart failure condition

supported with varying speed rotary pump type ventricular assist device has been conducted, using the Berlin Heart InCor pump as example. Results suggests that although by modulating the pump speed, the rotary pump can be manipulated to produce physiologically meaningful arterial pressure pulse, at the same time regurgitant flow develops in the pump which greatly deteriorates the pump efficiency, due to the intrinsic pump pressure-flow characteristic. A previous study using the HeartMate III pump has reached similar conclusion. To further evaluate the potential of generating pulsatile blood flow in rotary pumps by periodically varying the pump speed, it is necessary to extend the study to cover other pump products.

4. An incremental PID feedback control algorithm has been implemented in a new type of reciprocating-valve type VAD, to investigate the possibility of automatically producing tailored cardiac support to suit the needs in different physiological conditions in the heart failure patients. Results suggest that the VAD control algorithm can satisfactorily regulate the VAD motion to suite the transition between the rest and the mild exercise conditions.
5. The lumped-parameter modelling technique has been extended to the study of system response in a pulsatile bioreactor for cardiovascular tissue engineering applications. The lumped-parameter modelling technique has been proved to be also useful in the design optimise of the cardiovascular bioreactors.

The studies reported in this thesis suggest that lumped-parameter modelling as a mature research technique is highly effective in revealing the system level cardiovascular response under various healthy and diseased conditions. It is also an efficient research tool in the study of interaction between the human native circulatory system and the artificial cardiovascular organs, or for the design optimisation of in vitro/ex vivo experimental equipments for cardiovascular applications. This technique will continue to play important roles in the future cardiovascular dynamics studies.

6.2 Limitations of lumped-parameter modelling

Like any research technique, lumped-parameter modelling also has its deficiencies. Due to limitations in collecting invasive data from human and animal subjects, in many situations the model parameters need to be decided based on the limited number of experimental data obtainable. For such an under-constrained research question, it is

possible that multiple sets of parameter combinations are applicable to the model and they all can produce matching response to that observed clinically, and there is no easy way to decide which parameter set is the right one in the human/animal subject being studied. Further to this, cardiovascular response predicted by the lumped-parameter model is very sensitive to the model parameters used. Parameters chosen based on one physiological condition, when extrapolated to another condition without full validation, can produce wrong results even though the study is about the same human/animal subject. This uncertainty of model parameters and the sensitivity of modelling results demand special care in the study. In drawing important conclusions, validation and verification are often needed in interpreting the simulation results of lumped-parameter modelling.

Another deficiency of the lumped-parameter modelling is its limitation in simulating some important cardiovascular features, such as pulse wave propagation and shear stress induced damage to the vessel wall and blood cells, which often need to be studied with 1D or 3D models. Specifically, pulse wave dynamics reveals the travelling and reflection of pressure and flow waves in the vessel network, which helps to clarify the connections between the various pulse wave phenomena and the underlying pathological changes in the human body, and thus has important implications in clinical diagnosis. Pulse wave analysis demands the study of pressure and flow changes along the axial flow direction in the vessel network, which is best represented with 1D model in order to achieve a balance between the accuracy and the efficiency in the research. For such applications, the lumped-parameter model often needs to be integrated into the 1D or 3D model, in order to combine the advantages of both models.

6.3 On-going works

Lumped-parameter modelling has been applied extensively in biomedical as well as engineering research. Specifically as the extension of work reported in this thesis, I am working on the following modelling studies:

1. Modelling of the coronary circulation dynamics. Coronary flow uses 10% of the cardiac output to supply the blood perfusion to the heart. Coronary haemodynamics directly determines the cardiac physiology and pathology. Two unique effects strongly influence the coronary flow: the first one is the contraction and relaxation of the cardiac muscle during a heart cycle, which

directly influences the vessel calibre and tone and thus the flow features in the coronary vessels; the second one is the auto-regulation effect, in which the local biochemical mechanisms regulate the calibre of the small coronary arteries, thus to adapt the coronary flow to cater for the variations in myocardial oxidative metabolism. To study the coronary haemodynamics and its contribution to the overall circulatory dynamics, the author has built a complex circulatory model including the coronary vessels, as shown in Figure 6-1. This model has been applied for the simulation of typical coronary response, but needs further validation against clinical patient data.

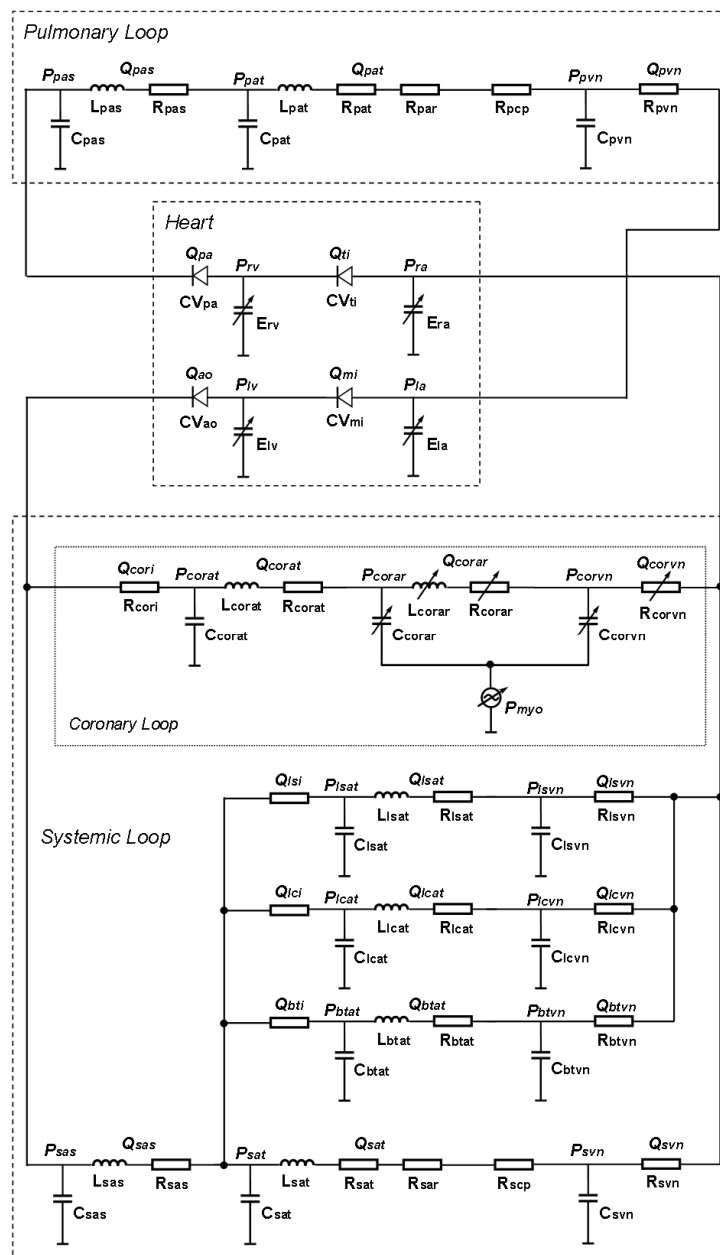


Figure 6-1 Circulatory model with coronary loop and several important branches

(Refer to the nomenclature table in front pages for detailed name of each component)

- Modelling of the cardiovascular response under pharmaceutical influence. Pharmacotherapy plays an important role in the clinical treatment of cardiovascular disease. Besides the cardiovascular modelling, lumped-parameter modelling has been extended to describe how the drug concentration varies in the body (called pharmaco-kinetic, or PK modelling), and how such variations influence key physiological variables (such as heart rate) in the human body (pharmaco-dynamic, or PD modelling). Historically the mathematical modelling of pharmaceutical and cardiovascular dynamics have been developed independent of each other. Currently I am developing an integrated pharmaceutical/cardiovascular model to study the cardiovascular response under pharmaceutical influence, as shown in Figure 6-2. Preliminary test has produced good agreement with typical clinical data reported in the open literature. Currently the model is under further refining and to be validated against wider ranges of pharmaceutical data. Once fully validated, this model can be applied in cardiovascular medicine to aid the clinical treatment and new drug design.

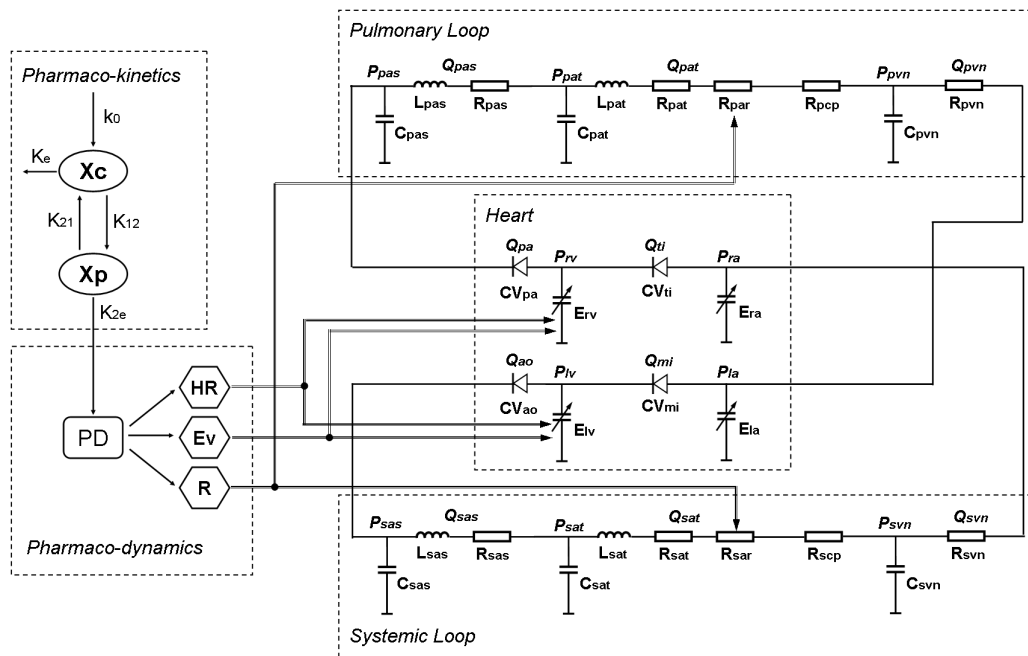


Figure 6-2 Schematic of the integrated cardiovascular/pharmaceutical model

(X_c and X_p : Drug concentration in central and peripheral compartments of the human body;
 PD: pharmaco-dynamic; HR: heart rate; E_v : cardiac contractility; R : vascular resistance.
 Refer to the nomenclature table in front pages for the meaning of other symbols)

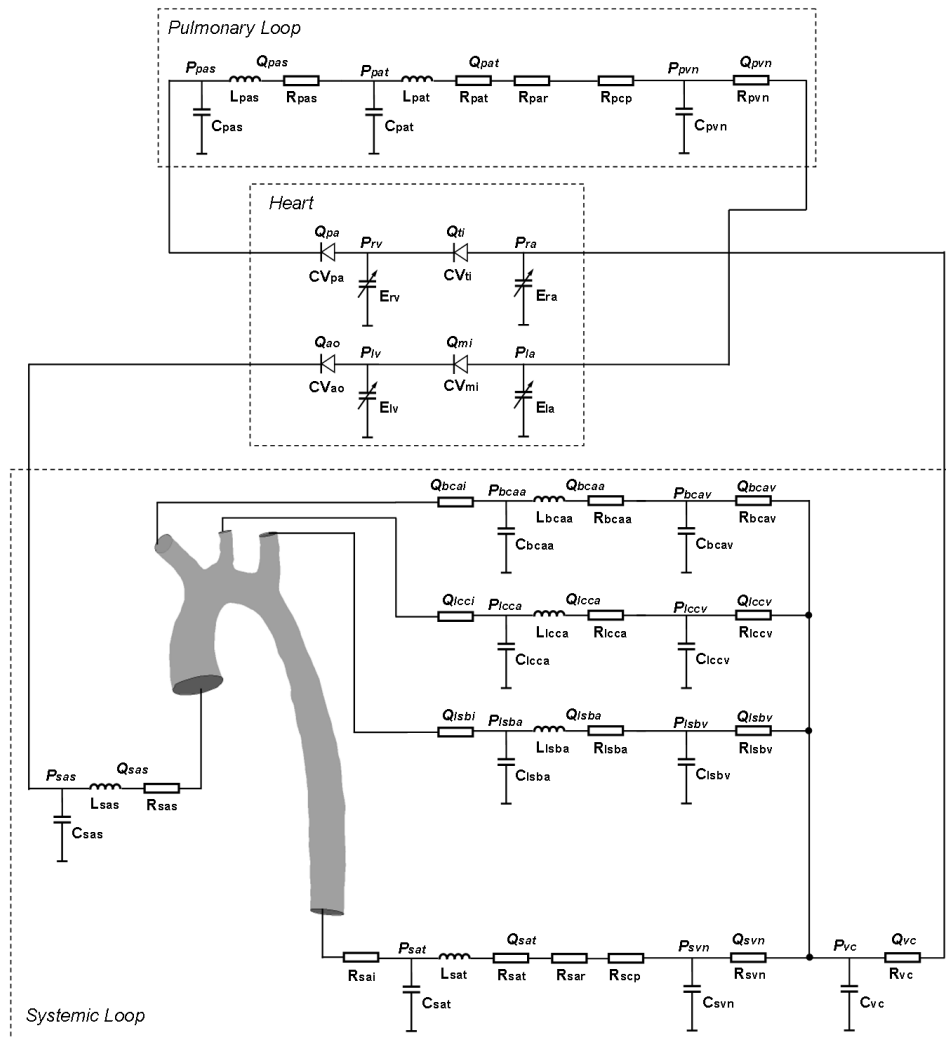


Figure 6-3 Coupled 0D/3D modelling, with 0D model providing the boundary conditions for the 3D CFD study

(bca: brachiocephalic vessel; lcc: left common carotid vessel; lsb: left subclavian vessel.

Refer to the nomenclature table in front pages for the meaning of other symbols)

3. Development of lumped-parameter models as boundary conditions for multi-scale modelling works. In traditional distributed-parameter models (i.e., 3D, 2D or 1D models), the boundary conditions to the computational domain are either idealised data or obtained from clinical measurements. Due to the environmental noise and the limitations in measurement technique, even the clinical measurement data often introduced much error in the calculation. For example, the distorted temporal synchronisation between the upstream and

downstream data will introduce artificial oscillations in the calculation. Chapter 2 has introduced the concurrent works on multi-scale modelling, in which the 0D model is used to provide the modelled physiological changes as the boundary condition for 3D/1D calculations. Figure 6-3 shows one of the multi-scale models that I am developing for the simulation of cardiovascular response in the aortic coarctation condition. Preliminary results suggest that such multi-scale model is very efficient in removing the artefacts in the traditional boundary conditions.

6.4 Future works

Chapter 2 has presented an in-depth review of the applications of the lumped-parameter modelling technique in the cardiovascular medicine, and suggested the directions for future effort. Specifically as the extension of work reported in this thesis, the following are the possible directions for further breakthroughs:

1. Models are developed to achieve specific research purposes in each individual studies, thus the complexity of the models should fit the purposes of the studies. An over-simplified model will produce inadequate accuracy in the study. However, this does not mean that more complex model will always produce more accurate results. For example, if the purpose of the study is to evaluate the short term assist action of a ventricular assist device on the failing heart, and the neuro-regulation effect does not need to be considered, then a single branch multiple-compartment model for the systemic vasculature, in which the vascular is divided into the aorta, artery, arteriole, capillary and vein segments, is sufficient to work as the after-load to the assisted heart. It is not necessary to model every artery and venous branches in this situation, since in an overly detailed vessel branch model the parameter setting becomes quite difficult. However, if the purpose of the study is to simulate the acceleration stress in flight training, then it is quite necessary to model the vessel branch for the lower extremity separately in order to include the effect of blood pooling, besides specifically coupling the neuro-regulation action in the cardiovascular model. There is no universally optimal model that suits every application. Researchers must decide what level of model sophistication is most suitable in their specific studies.

2. Since 0D model is a high level abstraction of the circulatory system and one model component often represents several complex anatomical structures, proper setting of model parameters is an important issue to be seriously addressed. This is still an area not sufficiently explored, with inconsistent model parameters being adopted among different researchers. Further effort in this direction is very necessary before a cardiovascular model can be considered as fully validated.
3. Previous studies have suggested a number of cardiovascular effects that need to be specially addressed in the 0D cardiovascular modelling, including ventricular interaction, effect of pericardial, atrial-ventricular interaction, auto-regulation in some local circulation loops, auxiliary pumping action to blood flow caused by peripheral muscle contraction, venous valve in some vessels such as in the lower extremity etc. Although intuitively correct, until now these effects have undergone very limited validations, due to the difficulty in isolating each of these effects from the overall cardiovascular response (which is often a coupled interaction among the different organs) as well as the restrictions in *in vivo* measurements. In the future effort should be made to further quantify the relative importance of each of these effects in the overall cardiovascular response, and to further study their underlying mechanism as well as to find proper parameter settings in their modelling.
4. The circulatory system does not work in isolation. It has close interaction with other systems such as the nervous system, respiratory system, and digestive system. Study of their coupled reactions, such as cardiovascular response under neuro-regulation and hormone control, coupled cardio-pulmonary response, simulation of coupled circulatory dynamics and transportation of nutrients/metabolic remaining, will bring the 0D cardiovascular modelling to a higher level, and such results will enormously improve our quantitative understanding of human physiology.
5. 0D cardiovascular models, especially the more complex ones, were often developed for research purposes. So far only concepts of vascular impedance is widely used to assist clinical diagnosis and treatment, and few integrated 0D model comprising the complete description of heart and vessels have seen use in clinical practice. With the success of 0D models in simulating cardiovascular

dynamics under various physiological and pathological conditions, it is time to work with the clinical community to personalise the 0D integrated models to achieve patient-specific modelling, and this will bring innovations to the cardiovascular clinical practice. To minimise the difficulty in parameter setting, models for patient-specific analysis may have reduced complexity as compared to those for research purposes.

6. With the development of computer hardware and numerical analysis techniques, higher dimensional haemodynamic analysis (2D and 3D) using computational fluid dynamics is no longer a prohibitive task. Thus to address the requirement of high accuracy and ability to simulate the interaction among cardiovascular organs concurrently, it is possible and necessary to couple the 0D models and the 1D/2D/3D models to build multi-dimensional models. Some successful applications have been produced in this direction. However, treatment of domain boundaries among the different dimensional models within an overall framework still needs further improvement. This includes not only the matching of mean pressure/flow values and their distribution information on the domain interfaces, but also the correct wave reflection description. Breakthroughs to be made on this issue will be enormously helpful to the improvement of simulation accuracy.

Bibliography

- Aarnoudse W., Fearon W. F., Manoharan G., Geven M., van de Vosse F., Rutten M., De Bruyne B. & Pijls N. H. 2004. Epicardial Stenosis Severity Does Not Affect Minimal Microcirculatory Resistance. *Circulation*, 110, 2137-2142.
- Aaronson P. I., Ward J. P. T., Wiener C. M., Schulman S. P. & Gill J., S. 1999. *The Cardiovascular System at a Glance*.
- Abe Y., Chinzei T., Mabuchi K., Snyder A. J., Isoyama T., Imanishi K., Yonezawa T., Matura H., Kouno A., Ono T., Atsumi K., Fujimasa I. & Imachi K. 1998. Physiological Control of a Total Artificial Heart: Conductance and Arterial Pressure Based Control. *J. Appl. Physiol.*, 84, 868-876.
- Alastruey J., Khir A. W., Matthys K. S., Segers P., Sherwin S. J., Verdonck P. R., Parker K. H. & Peiro J. 2011. Pulse Wave Propagation in a Model Human Arterial Network: Assessment of 1-D Visco-Elastic Simulations against in Vitro Measurements. *J Biomech*, 44, 2250-2258.
- Arndt A., Nusser P., Graichen K., Muller J. & Lampe B. 2008. Physiological Control of a Rotary Blood Pump with Selectable Therapeutic Options: Control of Pulsatility Gradient. *Artif Organs*, 32, 761-771.
- Avolio A. P. 1980. Multi-Branched Model of the Human Arterial System. *Med Biol Eng Comput*, 18, 709-718.
- Ayre P. J., Lovell N. H. & Woodard J. C. 2003. Non-Invasive Flow Estimation in an Implantable Rotary Blood Pump: A Study Considering Non-Pulsatile and Pulsatile Flows. *Physiol Meas*, 24, 1791-89.
- Ayre P. J., Vidakovic S. S., Tansley G. D., Watterson P. A. & Lovell N. H. 2000. Sensorless Flow and Head Estimation in the Ventriassist Rotary Blood Pump. *Artificial Organs*, 24, 585-588.
- Baccani B., Domenichini F., Pedrizzetti G. & Tonti G. 2002. Fluid Dynamics of the Ventricular Filling in Dilated Cardiomyopathy. *Journal of Biomechanics*, 35, 665-671.
- Bai J., Lu H., Zhang J., Zhao B. & Zhou X. 1998. Optimization and Mechanism of Step-Leap Respiration Exercise in Treating of Cor Pulmonale. *Comput Biol Med*, 28, 289-307.
- Barnea O. 1994. Mathematical Analysis of Coronary Autoregulation and Vascular Reserve in Closed-Loop Circulation. *Computer and Biomedical Research*, 27, 261-275.
- Barnea O., Moore T. W., Dubin S. & Jaron D. 1990. Cardiac Energy Considerations During Intraaortic Balloon Pumping. *IEEE Transactions on Biomedical Engineering*, 17, 170-181.
- Barnea O., Smith B. T., Dubin S., Moore T. W. & Jaron D. 1992. Optimal Controller for Intraaortic Balloon Pumping. *IEEE Transactions on Biomedical Engineering*, 39, 629-634.
- Barron V., Lyons E., Stenson-Cox C., McHugh P. E. & Pandit A. 2003. Bioreactors for Cardiovascular Cell and Tissue Growth: A Review. *Ann Biomed Eng*, 31, 1017-1030.

- Bassingthwaighte J., Hunter P. & Noble D. 2009. The Cardiac Physiome: Perspectives for the Future. *Exp Physiol*, 94, 597-605.
- Basu J. & Ludlow J. 2012. *Developments in Tissue Engineered and Regenerative Medicine Products: A Practical Approach*, Woodhead Publishing.
- Bellhouse B. J. 1972. *The Fluid Mechanics of Heart Valves*.
- Bergel D. H. 1972. *Cardiovascular Fluid Dynamics*.
- Berger D. S. & Li J., K. J. 1992. Temporal Relation between Left Ventricular and Arterial System Elastances. *IEEE Transactions on Biomedical Engineering*, 39, 404-410.
- Berne R. M. & Levy M. N. 1981. *Cardiovascular Physiology (Fourth Edition)*.
- Bessems D., Giannopapa C. G., Rutten M. C. & van de Vosse F. N. 2008. Experimental Validation of a Time-Domain-Based Wave Propagation Model of Blood Flow in Viscoelastic Vessels. *J Biomech*, 41, 284-291.
- Beyar R., Dong S. J., Smith E. R., Belenkie I. & Tyberg J. V. 1993. Ventricular Interaction and Septal Deformation: A Model Compared with Experimental Data. *Am J Physiol*, 265, H2044-H2056.
- Beyar R., Hausknecht M. J., Halperin H. R., Yin F. C. & Weisfeldt M. L. 1987. Interaction between Cardiac Chambers and Thoracic Pressure in Intact Circulation. *Am J Physiol*, 253, H1240-H1252.
- Biglino G., Kolyva C. & Khir A. W. 2012. Pressure-Wave Energy Relationship During Iabp Counterpulsation in a Mock Circulation: Changes with Angle and Assisting Frequency. *Int J Artif Organs*, 35, 15-24.
- Biglino G., Kolyva C., Whitehorne M., Pepper J. R. & Khir A. W. 2010. Variations in Aortic Pressure Affect the Mechanics of the Intra-Aortic Balloon: An in Vitro Investigation. *Artif Organs*, 34, 546-553.
- Biglino G., Whitehorne M., Pepper J. R. & Khir A. W. 2008. Pressure and Flow-Volume Distribution Associated with Intra-Aortic Balloon Inflation: An in Vitro Study. *Artif Organs*, 32, 19-27.
- Birks E. J., Tansley P. D., Hardy J., George R. S., Bowles C. T., Burke M., Banner N. R., Khaghani A. & Yacoub M. H. 2006. Left Ventricular Assist Device and Drug Therapy for the Reversal of Heart Failure. *New England Journal of Medicine*, 355, 1873-1884.
- Borlotti A., Khir A. W., Rietzschel E. R., De Buyzere M. L., Vermeersch S. & Segers P. 2012. Noninvasive Determination of Local Pulse Wave Velocity and Wave Intensity: Changes with Age and Gender in the Carotid and Femoral Arteries of Healthy Human. *J Appl Physiol*, 113, 727-735.
- Borlotti A., Vermeersch S., Rietzschel E., Segers P. & Khir A. W. 2010. A Comparison between Local Wave Speed in the Carotid and Femoral Arteries in Healthy Humans: Application of a New Method. *Conf Proc IEEE Eng Med Biol Soc*, 2010, 2857-2860.
- Boron W. F. & Boulpaep E. L. 2003. *Medical Physiology: A Cellular and Molecular Approach*.

- Bourque K., Gernes D. B., Loree H. M., Richardson J. S., Poirier V. L., Barletta N., Fleischli A., Foiera G., Gempp T. M., Schoeb R., Litwak K. N., Akimoto T., Watach M. J. & Litwak P. 2001. Heartmate Iii: Pump Design for a Centrifugal Lvad with a Magnetically Levitated Rotor. *ASAIO Journal*, 47, 401-405.
- Bovendeerd P. H., Borsje P., Arts T. & van De Vosse F. N. 2006. Dependence of Intramyocardial Pressure and Coronary Flow on Ventricular Loading and Contractility: A Model Study. *Ann Biomed Eng*, 34, 1833-1845.
- Bowman A. W., Frihauf P. A. & Kovacs S. J. 2004. Time-Varying Effective Mitral Valve Area: Prediction and Validation Using Cardiac Mri and Doppler Echocardiography in Normal Subjects. *Am J Physiol Heart Circ Physiol*, 287, H1650-H1657.
- Brown D. J. 1996. Input Impedance and Reflection Coefficient in Fractal-Like Models of Asymmetrically Branching Compliant Tubes. *IEEE Transaction on Biomedical Engineering*, 43, 715-722.
- Bullister E., Reich S. & Slueta J. 2002. Physiological Control Algorithms for Rotary Blood Pumps Using Pressure Sensor Input. *Artificial Organs*, 26, 931-938.
- Burattini R. & Campbell K. B. 2000. Physiological Relevance of Uniform Elastic Tube-Models to Infer Descending Aortic Wave Reflection: A Problem of Identifiability. *Ann Biomed Eng*, 28, 512-523.
- Burattini R. & Natalucci S. 1998. Complex and Frequency-Dependent Compliance of Viscoelastic Windkessel Resolves Contradictions in Elastic Windkessels. *Med Eng Phys*, 20, 502-514.
- Burkhoff D., Alexander J., Jr. & Schipke J. 1988. Assessment of Windkessel as a Model of Aortic Input Impedance. *Am J Physiol*, 255, H742-H753.
- Burkhoff D. & Tyberg J. V. 1993. Why Does Pulmonary Venous Pressure Rise after Onset of Lv Dysfunction: A Theoretical Analysis. *American Journal of Physiology(Heart Circ. Physiol.)*, 265, H1819-H1828.
- Cacciola G., Peters G. W. M. & Schreurs P. J. G. 2000. A Three-Dimensional Mechanical Analysis of a Stentless Fibre-Reinforced Aortic Valve Prosthesis. *Journal of Biomechanics*, 33, 521-530.
- Cappello A., Gnudi G. & Lamberti C. 1995. Identification of the Three-Element Windkessel Model Incorporating a Pressure-Dependent Compliance. *Ann Biomed Eng*, 23, 164-177.
- Casas F., Ahmed N. & Reeves A. 2007. Minimal Sensor Count Approach to Fuzzy Logic Rotary Blood Pump Flow Control. *ASAIO Journal*, 53, 140-146.
- Cavalcanti S. & Belardinelli E. 1996. Modeling of Cardiovascular Variability Using a Differential Delay Equation. *IEEE Trans Biomed Eng*, 43, 982-989.
- Cavalcanti S., Cavani S., Ciandrini A. & Avanzolini G. 2006. Mathematical Modeling of Arterial Pressure Response to Hemodialysis-Induced Hypovolemia. *Comput Biol Med*, 36, 128-144.
- Cavalcanti S. & Di Marco L. Y. 1999. Numerical Simulation of the Hemodynamic Response to Hemodialysis-Induced Hypovolemia. *Artif Organs*, 23, 1063-1073.
- Chen C.-H., Nevo E., Fetis B., Nakayama M., Kass D. A., Pak P. H. & Maughan W. L. 1997. Comparison of Continuous Left Ventricular Volumes by Transthoracic

Two-Dimensional Digital Echo Quantification with Simultaneous Conductance Catheter Measurements in Patients with Cardiac Diseases. *American Journal of Cardiology*, 80, 756-761.

- Chen H. C. & Hu Y. C. 2006. Bioreactors for Tissue Engineering. *Biotechnol Lett*, 28, 1415-1423.
- Chen S., Zhang S., Gong Y., Dai K., Sui M., Yu Y. & Ning G. 2008. The Role of the Autonomic Nervous System in Hypertension: A Bond Graph Model Study. *Physiol Meas*, 29, 473-495.
- Choi S., Antaki J. F., Boston J. R. & Thomas D. 2001. A Sensorless Approach to Control of a Turbodynamic Left Ventricular Assist System. *IEEE Transactions on Control Systems Technology*, 9, 473-482.
- Chou N. K., Wang S. S., Lin Y. H., Shyu J. J., Hsieh K. H., Jan G. J. & Chu S. H. 2001. Development of a Totally Implantable Pulsatile Centrifugal Pump as a Ventricular Assist Device. *Artif Organs*, 25, 603-606.
- Chow G., Roberts I. G., Edwards A. D., Lloyd-Thomas A., Wade A., Elliott M. J. & Kirkham F. J. 1997. The Relation between Pump Flow Rate and Pulsatility on Cerebral Hemodynamics During Pediatric Cardiopulmonary Bypass. *The Journal of Thoracic and Cardiovascular Surgery*, 114, 568-577.
- Chung D. C., Niranjan S. C., Clark J. W., Bidani A. J., Johnston W. E., Zwischenberger J. B. & Traber D. L. 1997. A Dynamic Model of Ventricular Interaction and Pericardial Influence. *American Journal of Physiology(Heart Circ. Physiol.)*, 272, H2942-H2962.
- Cohen A., Guyon P., Johnson N., Chauvel C., Logeart D., Costagliola D. & Valty J. 1995. Hemodynamic Criteria for Diagnosis of Right Ventricular Ischemia Associated with Inferior Wall Left Ventricular Acute Myocardial Infarction. *American Journal of Cardiology*, 76, 220-225.
- Cornelissen A. J., Dankelman J., VanBavel E. & Spaan J. A. 2002. Balance between Myogenic, Flow-Dependent, and Metabolic Flow Control in Coronary Arterial Tree: A Model Study. *Am J Physiol Heart Circ Physiol*, 282, H2224-H2237.
- Cornelissen A. J., Dankelman J., VanBavel E., Stassen H. G. & Spaan J. A. 2000. Myogenic Reactivity and Resistance Distribution in the Coronary Arterial Tree: A Model Study. *Am J Physiol Heart Circ Physiol*, 278, H1490-H1499.
- Cox L. G., Loerakker S., Rutten M. C., de Mol B. A. & van de Vosse F. N. 2009. A Mathematical Model to Evaluate Control Strategies for Mechanical Circulatory Support. *Artif Organs*, 33, 593-603.
- Davidson K. M., Sushil S., Eggleton C. D. & Marten M. R. 2003. Using Computational Fluid Dynamics Software to Estimate Circulation Time Distributions in Bioreactors. *Biotechnol Prog*, 19, 1480-1486.
- de Hart J., Baaijens F. P. T., Peters G. W. M. & Schreurs P. J. G. 2003a. A Computational Fluid-Structure Interaction Analysis of a Fiber-Reinforced Stentless Aortic Valve. *Journal of Biomechanics*, 36, 699-712.
- de Hart J., Peters G. W. M., Schreurs P. J. G. & Baaijens F. P. T. 2000. A Two-Dimensional Fluid-Structure Model of the Aortic Valve. *Journal of Biomechanics*, 33, 1079-1088.

- de Hart J., Peters G. W. M., Schreurs P. J. G. & Baaijens F. P. T. 2003b. A Three-Dimensional Computational Analysis of Fluid-Structure Interaction in the Aortic Valve. *Journal of Biomechanics*, 36, 103-112.
- de Lazzari C., Darowski M., Ferrari G., Pisanelli D. M. & Tosti G. 2006. Modelling in the Study of Interaction of Hemopump Device and Artificial Ventilation. *Comput Biol Med*, 36, 1235-1251.
- de Lazzari C., Mimmo F., R., Tosti G. & Ambrosi D. 1994. A Desk-Top Computer Model of the Circulatory System for Heart Assistance Simulation: Effect of an Lvad on Energetic Relationships inside the Left Ventricle. *Medical Engineering and Physics*, 16, 97-103.
- Deswysen B., Charlier A. A. & Gevers M. 1980. Quantitative Evaluation of the Systemic Arterial Bed by Parameter Estimation of a Simple Model. *Med Biol Eng Comput*, 18, 153-166.
- Diaz-Zuccarini V. & LeFevre J. 2007. An Energetically Coherent Lumped Parameter Model of the Left Ventricle Specially Developed for Educational Purposes. *Comput Biol Med*, 37, 774-784.
- Drzewiecki G., M., Pilla J. & Welkowitz W. 1990. Design and Control of the Atrio-Aortic Left Ventricular Assist Device Based on O₂ Consumption. *IEEE Transactions on Biomedical Engineering*, 37, 128-137.
- Drzewiecki G., Wang J. J., Li J. K. J., Kedem J. & Weiss H. 1996. Modeling of Mechanical Dysfunction in Regional Stunned Myocardium of the Left Ventricle. *IEEE Transaction on Biomedical Engineering*, 43, 1151-1163.
- Dubey H., Das S. K. & Panda T. 2006. Numerical Simulation of a Fully Baffled Biological Reactor: The Differential Circumferential Averaging Mixing Plane Approach. *Biotechnol Bioeng*, 95, 754-766.
- Ei-Banayosy A., Arusoglu L., Kizner L., Fey O., Minami K. & Krfer R. 2000. Complications of Circulatory Assist. *Perfusion*, 15, 327-331.
- Einav S., Aharoni S. & Manoach M. 1988. Exponentially Tapered Transmission Line Model of the Arterial System. *IEEE Transaction on Biomedical Engineering*, 35, 333-339.
- Elstad M., Toska K. & Walle L. 2002. Model Simulations of Cardiovascular Changes at the Onset of Moderate Exercise in Humans. *Journal of Physiology*, 543, 719-728.
- Endo G., Araki K., Oshikawa M., Kojima K., Saitoh T., Nakamura K. & Onitsuka T. 2000. Control Strategy for Biventricular Assistance with Mixed-Flow Pumps. *Artificial Organs*, 24, 594-599.
- Enriquez-Sarano M., Bailey K. R., Seward J. B., Tajik A. J., Krohn M. J. & Mays J. M. 1993. Quantitative Doppler Assessment of Valvular Regurgitation. *Circulation*, 87, 841-848.
- Ferrari G., Khir A. W., Fresiello L., Di Molfetta A. & Kozarski M. 2011. Hybrid Model Analysis of Intra-Aortic Balloon Pump Performance as a Function of Ventricular and Circulatory Parameters. *Artif Organs*, 35, 902-911.
- Ferrari G., Kozarski M., Fresiello L., Molfetta A. D., Zielinski K., Gorczynska K., Palko K. J. & Darowski M. 2013. Continuous-Flow Pump Model Study: The

- Effect on Pump Performance of Pump Characteristics and Cardiovascular Conditions. *J Artif Organs*, Preprint.
- Fisher J. P., Mikos A. G., Bronzino J. D. & Peterson D. R. 2013. *Tissue Engineering: Principles and Practices*, CRC Press.
- Fogliardi R., Di Donfrancesco M. & Burattini R. 1996. Comparison of Linear and Nonlinear Formulations of the Three-Element Windkessel Model. *Am J Physiol*, 271, H2661-H2668.
- Formaggia L., Gerbeau J. F., Nobile F. & Quarteroni A. 2001. On the Coupling of 3d and 1d Navier-Stokes Equations for Flow Problems in Compliant Vessels. *Computer Methods in Applied Mechanics and Engineering*, 191, 561-582.
- Formaggia L., Lamponi D., Tuveri M. & Veneziani A. 2006. Numerical Modeling of 1d Arterial Networks Coupled with a Lumped Parameters Description of the Heart. *Comput Methods Biomech Biomed Engin*, 9, 273-288.
- Formaggia L., Nobile F., Quarteroni A. & Veneziani A. 1999. Multiscale Modelling of the Circulatory System: A Preliminary Analysis. *Computing and Visualization in Science*, 2, 75-83.
- Formaggia L., Quarteroni Alfio, and Veneziani Alessandro 2009. Multiscale Models of the Vascular System. In: Formaggia L., Quarteroni Alfio, and Veneziani Alessandro (ed.) *Cardiovascular Mathematics: Modeling and Simulation of the Circulatory System*. Milano: Springer-Verlag Italia.
- Formaggia L. & Veneziani A. 2003. Reduced and Multiscale Models for the Human Cardiovascular System. Politecnico di Milano.
- Frasch H. F., Kresh J. Y. & Noordergraaf A. 1996. Two-Port Analysis of Microcirculation: An Extension of Windkessel. *Am J Physiol*, 270, H376-H385.
- Frazier O. H., Myers T., J., Westaby S. & Gregoric I., D. 2004. Clinical Experience with an Implantable, Intracardiac, Continuous Flow Circulatory Support Device: Physiologic Implications and Their Relationship to Patient Selection. *The Annals of Thoracic Surgery*, 77, 133-142.
- Fresiello L., Khir A. W., Di Molletta A., Kozarski M. & Ferrari G. 2013. Effects of Intra-Aortic Balloon Pump Timing on Baroreflex Activities in a Closed-Loop Cardiovascular Hybrid Model. *Artif Organs*, 37, 237-247.
- Funakubo A., Ahmed S., Sakuma I. & Fukui Y. 2002. Flow Rate and Pressure Head Estimation in a Centrifugal Blood Pump. *Artif Organs*, 26, 985-990.
- Fung Y. C. 1984. *Biodynamics: Circulation*.
- Fung Y. C. 1993. *Biomechanics: Mechanical Properties of Living Tissues*.
- Geven M. C., Bohte V. N., Aarnoudse W. H., van den Berg P. M., Rutten M. C., Pijls N. H. & van de Vosse F. N. 2004. A Physiologically Representative in Vitro Model of the Coronary Circulation. *Physiol Meas*, 25, 891-904.
- Giridharan G., Ewart D. L., Pantalos G. M., Gillars K. J., Litwak K. N., Gary L. A. & Koenig S. C. 2004. Left Ventricular and Myocardial Perfusion Responses to Volume Unloading and Afterload Reduction in a Computer Simulation. *ASAIO Journal*, 50, 512-518.

- Giridharan G. & Skliar M. 2002. Nonlinear Controller for Ventricular Assist Devices. *Artificial Organs*, 26, 980-984.
- Giridharan G. & Skliar M. 2003. Control Strategy for Maintaining Physiological Perfusion with Rotary Blood Pumps. *Artificial Organs*, 27, 639-648.
- Giridharan G., Skliar M., Olsen D. B. & Pantalos G. M. 2002. Modeling and Control of a Brushless Dc Axial Flow Ventricular Assist Device. *ASAIO Journal*, 48, 272-289.
- Gobel C., Arvand A., Eilers R., Marseille O., Bals C., Meyns B., Flameng W., Rau G. & Reul H. 2001. Development of the Medos/Hia Deltastream Extracorporeal Rotary Blood Pump. *Artif Organs*, 25, 358-365.
- Granegger M., Moscato F., Casas F., Wieselthaler G. & Schima H. 2012. Development of a Pump Flow Estimator for Rotary Blood Pumps to Enhance Monitoring of Ventricular Function. *Artif Organs*, 36, 691-699.
- Granet I. 1996. *Fluid Mechanics*.
- Grant B. J. & Paradowski L. J. 1987. Characterization of Pulmonary Arterial Input Impedance with Lumped Parameter Models. *Am J Physiol*, 252, H585-H593.
- Grasman J., Brascamp J. W., Van Leeuwen J. L. & Van Putten B. 2003. The Multifractal Structure of Arterial Trees. *Journal of Theoretical Biology*, 220, 75-82.
- Green J. F. & Miller N. C. 1973. A Model Describing the Response of the Circulatory System to Acceleration Stress. *Ann Biomed Eng*, 1, 455-467.
- Guyton A. C. 1986. *Textbook of Medical Physiology*.
- Guyton A. C. 2006. *Textbook of Medical Physiology*, Elsevier Inc.
- Guyton A. C., Coleman T. G. & Granger H. J. 1972. Circulation: Overall Regulation. *Annu Rev Physiol*, 34, 13-46.
- He P., Bai J. & Xia D. D. 2005. Optimum Control of the Hemopump as a Left-Ventricular Assist Device. *Medical & Biological Engineering & Computing*, 43, 136-141.
- Heldt T., Shim E. B., Kamm R. D. & Mark R. G. 2002. Computational Modeling of Cardiovascular Response to Orthostatic Stress. *Journal of Applied Physiology*, 92, 1239-1254.
- Hoerstrup S. P., Zund G., Sodian R., Schnell A. M., Grunenfelder J. & Turina M. I. 2001. Tissue Engineering of Small Caliber Vascular Grafts. *Eur J Cardiothorac Surg*, 20, 164-169.
- Hollander E. H., Dobson G. M., Wang J. J., Parker K. H. & Tyberg J. V. 2004. Direct and Series Transmission of Left Atrial Pressure Perturbations to the Pulmonary Artery: A Study Using Wave-Intensity Analysis. *Am J Physiol Heart Circ Physiol*, 286, H267-H275.
- Hose D. R., Narracott A. J., Penrose J. M., Baguley D., Jones I. P. & Lawford P. V. 2006. Fundamental Mechanics of Aortic Heart Valve Closure. *J Biomech*, 39, 958-967.
- Hsu C.-H. 2004. Fuzzy Logic Automatic Control of the Phoenix-7 Total Artificial Heart. *Journal of Artificial Organs*, 7, 69-76.

- Huberts W., Bosboom E. M. & van de Vosse F. N. 2009. A Lumped Model for Blood Flow and Pressure in the Systemic Arteries Based on an Approximate Velocity Profile Function. *Math Biosci Eng*, 6, 27-40.
- Isoyama T., Abe Y., Chinzei T., Mochizuki S., Karita T., Saito I., Ono T., Kouno A., Baba K. & Imachi K. 2000. Using One Rotary Blood Pump to Produce Separate Pulsatile Circulations in the Upper and Lower Halves of the Body. *Artif Organs*, 24, 680-682.
- Jager G. N., Westerhof N. & Noordergraaf A. 1965. Oscillatory Flow Impedance in Electrical Analog of Arterial System: Representation of Sleeve Effect and Non-Newtonian Properties of Blood. *Circ Res*, 16, 121-133.
- Jeays A. D., Lawford P. V., Gillott R., Spencer P. A., Bardhan K. D. & Hose D. R. 2007. A Framework for the Modeling of Gut Blood Flow Regulation and Postprandial Hyperaemia. *World J Gastroenterol*, 13, 1393-1398.
- John L. R. 2004. Forward Electrical Transmission Line Model of the Human Arterial System. *Med Biol Eng Comput*, 42, 312-321.
- Khair A. W. 2010. What Is It with Patient's Posture During Intra Aortic Balloon Pump Therapy? *Artif Organs*, 34, 1077-1081.
- Khair A. W. 2011. Left Ventricular Temporary Assistance: By Blood Propelling or Counterpulsating? *Artif Organs*, 35, 840-842.
- Khair A. W., O'Brien A., Gibbs J. S. & Parker K. H. 2001. Determination of Wave Speed and Wave Separation in the Arteries. *J Biomech*, 34, 1145-1155.
- Khair A. W. & Parker K. H. 2002. Measurements of Wave Speed and Reflected Waves in Elastic Tubes and Bifurcations. *J Biomech*, 35, 775-783.
- Khair A. W. & Parker K. H. 2005. Wave Intensity in the Ascending Aorta: Effects of Arterial Occlusion. *J Biomech*, 38, 647-655.
- Khair A. W., Price S., Hale C., Young D. A., Parker K. H. & Pepper J. R. 2005. Intra-Aortic Balloon Pumping: Does Posture Matter? *Artif Organs*, 29, 36-40.
- Khair A. W., Price S., Henein M. Y., Parker K. H. & Pepper J. R. 2003. Intra-Aortic Balloon Pumping: Effects on Left Ventricular Diastolic Function. *Eur J Cardiothorac Surg*, 24, 277-282.
- Khair A. W., Swalen M. J., Feng J. & Parker K. H. 2007. Simultaneous Determination of Wave Speed and Arrival Time of Reflected Waves Using the Pressure-Velocity Loop. *Med Biol Eng Comput*, 45, 1201-1210.
- Khair A. W., Swalen M. J., Segers P., Verdonck P. & Pepper J. R. 2006. Hemodynamics of a Pulsatile Left Ventricular Assist Device Driven by a Counterpulsation Pump in a Mock Circulation. *Artif Organs*, 30, 308-312.
- Khair A. W., Zambanini A. & Parker K. H. 2004. Local and Regional Wave Speed in the Aorta: Effects of Arterial Occlusion. *Med Eng Phys*, 26, 23-29.
- Kilner P. J., Yang G.-Z., Wilkes A. J., Mohladdin R. H., Firmin D. N. & Yacoub M. H. 2000. Asymmetric Redirection of Flow through the Heart. *Nature*, 404, 759-761.
- Kim H. J., Vignon-Clementel I. E., Figueroa C. A., LaDisa J. F., Jansen K. E., Feinstein J. A. & Taylor C. A. 2009. On Coupling a Lumped Parameter Heart

- Model and a Three-Dimensional Finite Element Aorta Model. *Ann Biomed Eng*, 37, 2153-2169.
- Kiris C., Kwak D., Rogers S. & Chang I. D. 1997. Computational Approach for Probing the Flow through Artificial Heart Devices. *Journal of Biomechanics*, 119, 452-460.
- Kitamura T. 1990. Left Atrial Pressure Controller Design for an Artificial Heart. *IEEE Transactions on Biomedical Engineering*, 37, 164-169.
- Kitamura T. & Gross D. R. 1990. On-Line Pressure for a Left Heart Assist Device. *IEEE Transactions on Biomedical Engineering*, 37, 968-974.
- Kitamura T., Matsushima Y., Tokuyama T., Kono S., Nishimura K., Komeda M., Yanai M., Kijima T. & Nojiri C. 2000. Physical Model-Based Indirect Measurements of Blood Pressure and Flow Using a Centrifugal Pump. *Artificial Organs*, 24, 589-593.
- Klute G. K., Tasch U. & Geselowitz D. B. 1992. An Optimal Controller for an Electric Ventricular Assist Device: Theory, Implementation and Testing. *IEEE Transactions on Biomedical Engineering*, 39, 394-403.
- Koenig S. C., Pantalos G. M., Gillars K. J., Ewart D. L., Litwak K. N. & Etoch S. W. 2004. Hemodynamic and Pressure-Volume Responses to Continuous and Pulsatile Ventricular Assist in an Adult Mock Circulation. *ASAIO Journal*, 50, 15-24.
- Kolyva C., Spaan J. A., Piek J. J. & Siebes M. 2008. Windkesselness of Coronary Arteries Hampers Assessment of Human Coronary Wave Speed by Single-Point Technique. *Am J Physiol Heart Circ Physiol*, 295, H482-H490.
- Korakianitis T. 2003. *RE: Motion of Kg Diaphragm*. Type to Shi Y.
- Korakianitis T. & Grandia L. 2003. *Optimized Pulsatile Flow Ventricular Assistance Device and Total Artificial Heart*.
- Korakianitis T. & Shi Y. 2006a. A Concentrated Parameter Model for the Human Cardiovascular System Including Heart Valve Dynamics and Atrioventricular Interaction. *Med Eng Phys*, 28, 613-628.
- Korakianitis T. & Shi Y. 2006b. Effects of Atrial Contraction, Atrioventricular Interaction and Heart Valve Dynamics on Human Cardiovascular System Response. *Med Eng Phys*, 28, 762-779.
- Korakianitis T. & Shi Y. 2006c. Numerical Simulation of Cardiovascular Dynamics with Healthy and Diseased Heart Valves. *Journal of Biomechanics*, 39, 1964-1982.
- Korakianitis T. & Shi Y. 2007. Numerical Comparison of Hemodynamics with Atrium to Aorta and Ventricular Apex to Aorta Vad Support. *ASAIO J*, 53, 537-548.
- Kosaka R., Yanagi K., Sato T., Ishitoya H., Motomura T., Kawahito S., Mikami M., Linneweber J., Nonaka K., Takano T., Glueck J., Sanki Y. & Nose Y. 2003. Operating Point Control System for a Continuous Flow Artificial Heart: In Vitro Study. *ASAIO Journal*, 49, 259-264.
- Kresh J. Y., Brockman S. K. & Noordergraaf A. 1990. Theoretical and Experimental Analysis of Right Ventricular Bypass and Univentricular Circulatory Support. *IEEE Trans Biomed Eng*, 37, 121-127.

- Kroon W., Huberts W., Bosboom M. & van de Vosse F. 2012. A Numerical Method of Reduced Complexity for Simulating Vascular Hemodynamics Using Coupled 0d Lumped and 1d Wave Propagation Models. *Comput Math Methods Med*, 2012, 156094.
- Lai Y. G., Chandran K. B. & Lemmon J. 2002. A Numerical Simulation of Mechanical Heart Valve Closure Fluid Dynamics. *Journal of Biomechanics*, 35, 881-892.
- Landes G. 1943. Einige Untersuchungen an Elektrischen Analogieschaltungen Zum Kreislaufsystem. *Z. Biol.*, 101, 418-429.
- Larson C. O., Smith J. S., Chapman J. H., Slimon S. A., Trahan J. D., Brozek R. J., Franco A., McGarvey J. J., Rosen M. E. & Pasque M. K. 1999. *Reciprocating Pumps and Linear Motor Arrangement*.
- Leefe S. E. & Gentle C. R. 1995. A Review of the in Vitro Evaluation of Conduit-Mounted Cardiac Valve Prosthesis. *Medical Engineering & Physics*, 17, 497-506.
- Lerma C., Minzoni A., Infante O. & Jose M. V. 2004. A Mathematical Analysis for the Cardiovascular Control Adaptations in Chronic Renal Failure. *Artif Organs*, 28, 398-409.
- Levick J. R. 2003. *An Introduction to Cardiovascular Physiology*, Arnold.
- Leyh R. G., Schmidtke C., Sievers H. H. & Yacoub M. H. 1999. Opening and Closing Characteristics of the Aortic Valve after Different Types of Valve-Preserving Surgery. *Circulation*, 100, 2153-2160.
- Li J. K.-J. 2000. *The Arterial Circulation: Physical Principles and Clinical Applications*, Humana Press Inc.
- Li J. K. J., Cui T. & Drzewiecki G., M. 1990. A Nonlinear Model of the Arterial System Incorporating a Pressure-Dependent Compliance. *IEEE Transactions on Biomedical Engineering*, 37, 673-678.
- Li Y., Borlotti A., Parker K. H. & Khir A. W. 2011. Variation of Wave Speed Determined by the Pu-Loop with Proximity to a Reflection Site. *Conf Proc IEEE Eng Med Biol Soc*, 2011, 199-202.
- Li Y. & Khir A. W. 2011. Experimental Validation of Non-Invasive and Fluid Density Independent Methods for the Determination of Local Wave Speed and Arrival Time of Reflected Wave. *J Biomech*, 44, 1393-1399.
- Liang F. Y., Takagi S., Himeno R. & Liu H. 2009. Biomechanical Characterization of Ventricular-Arterial Coupling During Aging: A Multi-Scale Model Study. *J Biomech*, 42, 692-704.
- Lim E., Karantonis D. M., Reizes J. A., Cloherty S. L., Mason D. G. & Lovell N. H. 2008. Noninvasive Average Flow and Differential Pressure Estimation for an Implantable Rotary Blood Pump Using Dimensional Analysis. *IEEE Trans Biomed Eng*, 55, 2094-2101.
- Liu Z., Brin K. P. & Yin F. C. 1986. Estimation of Total Arterial Compliance: An Improved Method and Evaluation of Current Methods. *Am J Physiol*, 251, H588-H600.
- Lodi C. A. & Ursino M. 1999. Hemodynamic Effect of Cerebral Vasospasm in Humans: A Modeling Study. *Ann Biomed Eng*, 27, 257-273.

- Loerakker S., Cox L. G., van Heijst G. J., de Mol B. A. & van de Vosse F. N. 2008. Influence of Dilated Cardiomyopathy and a Left Ventricular Assist Device on Vortex Dynamics in the Left Ventricle. *Comput Methods Biomech Biomed Engin*, 11, 649-660.
- Lu K., Clark J. W. J., GhorBel F. H., Ware D. L. & Bidani A. 2001. A Human Cardiopulmonary System Model Applied to the Analysis of the Valsalva Maneuver. *American Journal of Physiology(Heart Circ. Physiol.)*, 281, H2661-H2679.
- Lucas C. L., Wilcox B. R., Ha B. & Henry G. W. 1988. Comparison of Time Domain Algorithms for Estimating Aortic Characteristic Impedance in Humans. *IEEE Trans Biomed Eng*, 35, 62-68.
- Magosso E., Cavalcanti S. & Ursino M. 2002. Theoretical Analysis of Rest and Exercise Hemodynamics in Patients with Total Cavopulmonary Connection. *Am J Physiol Heart Circ Physiol*, 282, H1018-H1034.
- Magosso E. & Ursino M. 2001. A Mathematical Model of Co2 Effect on Cardiovascular Regulation. *Am J Physiol Heart Circ Physiol*, 281, H2036-H2052.
- Mahmood A. K., Courtney J. M., Westaby S., Akdis M. & Reul H. 2000. Critical Review of Current Left Ventricular Assist Devices. *Perfusion*, 15, 399-420.
- Makhijani V. B., Siegel J. M. J. & Hwang N. H. C. 1996a. Numerical Study of Squeeze-Flow in Tilting Disc Mechanical Heart Valves. *Journal of Heart Valve Disease*, 5, 97-103.
- Makhijani V. B., Siegel J. M. J. & Singhal A. K. 1996b. Coupled Fluid-Structure Analysis of Bi-Leaflet Mitral Mechanical Heart Valve Dynamics. *Advances in Bioengineering ASME*, BED-Vol. 33.
- Makhijani V. B., Yang H. Q., Dionne P. J. & Thubrikar M. J. 1997. Three Dimensional Coupled Fluid-Structure Simulation of Pericardial Bio-Prosthetic Aortic Valve Function. *ASAIO Journal*, 48, M387-M392.
- Manor D., Beyar R. & Sideman S. 1994. Pressure-Flow Characteristics of the Coronary Collaterals: A Model Study. *Am J Physiol*, 266, H310-H318.
- Marieb E. N. 2003. *Human Anatomy & Physiology*, Benjamin Cummings.
- Martin I., Wendt D. & Heberer M. 2004. The Role of Bioreactors in Tissue Engineering. *Trends Biotechnol*, 22, 80-86.
- Martin Y. & Vermette P. 2005. Bioreactors for Tissue Mass Culture: Design, Characterization, and Recent Advances. *Biomaterials*, 26, 7481-7503.
- Matthys K. S., Alastruey J., Peiro J., Khir A. W., Segers P., Verdonck P. R., Parker K. H. & Sherwin S. J. 2007. Pulse Wave Propagation in a Model Human Arterial Network: Assessment of 1-D Numerical Simulations against in Vitro Measurements. *J Biomech*, 40, 3476-3486.
- Maughan W. L., Sunagawa K. & Sagawa K. 1987. Ventricular Systolic Interdependence: Volume Elastance Model in Isolated Canine Hearts. *Am J Physiol*, 253, H1381-H1390.

- McIlroy M. & Targett R. C. 1988. A Model of the Systemic Arterial Bed Showing Ventricular Systemic Arterial Coupling. *American Journal of Physiology(Heart Circ. Physiol.)*, 254, H609-H616.
- McInnis B. C., Lu P. C. & Wang J. C. 1984. *Control Strategies for Artificial Hearts and Assist Devices*, Los Angeles, CA.
- McQueen D. M., Peskin C. S. & Yellin E. L. 1982. Fluid Dynamics of the Mitral Valve: Physiological Aspects of a Mathematical Model. *Am J Physiol*, 242, H1095-H1110.
- Melchior F. M., Srinivasan R. S. & Charles J., B. 1992. Mathematical Modeling of Human Cardiovascular System for Simulation of Orthostatic Response. *American Journal of Physiology(Heart Circ. Physiol.)*, 262, H1920-H1933.
- Merkx M. A., Bode A. S., Huberts W., Oliván Bescos J., Tordoir J. H., Breeuwer M., van de Vosse F. N. & Bosboom E. M. 2013. Assisting Vascular Access Surgery Planning for Hemodialysis by Using Mr, Image Segmentation Techniques, and Computer Simulations. *Med Biol Eng Comput*, (Preprint).
- Migliavacca F., Balossino R., Pennati G., Dubini G., Hsia T. Y., de Leval M. R. & Bove E. L. 2006. Multiscale Modelling in Biofluidynamics: Application to Reconstructive Paediatric Cardiac Surgery. *J Biomech*, 39, 1010-1020.
- Migliavacca F., Pennati G., Dubini G., Fumero R., Pietrabissa R., Urcelay G., Bove E. L., Hsia T. Y. & de Leval M. R. 2001. Modeling of the Norwood Circulation: Effects of Shunt Size, Vascular Resistances, and Heart Rate. *Am J Physiol Heart Circ Physiol*, 280, H2076-H2086.
- Milisic V. & Quarteroni A. 2004. Analysis of Lumped Parameter Models for Blood Flow Simulations and Their Relation with 1d Models. *ESAIM-Mathematical Modelling and Numerical Analysis*, 38, 613-632.
- Mulder G. 2011. *Patient Specific Modelling of the Cerebral Arterial Tree for Aneurysm Risk Assessment*. PhD, Eindhoven University of Technology.
- Mulder G., Bogaerds A. C., Rongen P. & van de Vosse F. N. 2011. The Influence of Contrast Agent Injection on Physiological Flow in the Circle of Willis. *Med Eng Phys*, 33, 195-203.
- Myers L. J. & Capper W. L. 2002. A Transmission Line Model of the Human Foetal Circulation System. *Medical Engineering & Physics*, 24, 285-294.
- Mynard J. P. & Nithiarasu P. 2008. A 1d Arterial Blood Flow Model Incorporating Ventricular Pressure, Aortic Valve and Regional Coronary Flow Using the Locally Conservative Galerkin Method. *Communications in Numerical Methods in Engineering*, 24, 367-417.
- Nageh M. F., Kopelen H. A., Zoghbi W. A., Quiones M. A. & Nahueh S. F. 1999. Estimation of Mean Right Atrial Pressure Using Tissue Doppler Imaging. *The American Journal of Cardiology*, 84, 1448-1451.
- Nakamura M., Homma A., Tatsumi E., Uesho K., Taenaka Y., Masuzawa T., Nakamura T., Zhang B., Kakuta Y., Imada K., Nakatani T. & Takano H. 2000. Mixed Venous Oxygen Saturation as a Promising Parameter for Physiological Control of Total Artificial Heart. *ASAIO Journal*, 46, 761-766.

- Nakata K., Ohtsuka G., Ypshikawa M., Takano T., Glueck J., Fujisawa A., Makinouchi K., Yokokawa M. & Nose Y. 1999. A New Control Method That Estimates the Backflow in a Centrifugal Pump. *Artificial Organs*, 23, 538-541.
- Narita Y., Hata K., Kagami H., Usui A., Ueda M. & Ueda Y. 2004. Novel Pulse Duplicating Bioreactor System for Tissue-Engineered Vascular Construct. *Tissue Eng*, 10, 1224-1233.
- Nichols W. W. & O'Rourke M. F. 1990. *McDonald's Blood Flow in Arteries: Theoretical, Experimental and Clinical Principles [Third Edition]*.
- Niebauer J. & Cooke J. P. 1996. Cardiovascular Effects of Exercise: Role of Endothelial Shear Stress. *J Am Coll Cardiol*, 28, 1652-1660.
- Noordergraaf A. 1978. *Circulatory System Dynamics*.
- Noordergraaf A., Verdouw D. & Boom H. B. 1963. The Use of an Analog Computer in a Circulation Model. *Prog Cardiovasc Dis*, 5, 419-439.
- O'Rourke M. F. & Avolio A. P. 1980. Pulsatile Flow and Pressure in Human Systemic Arteries. Studies in Man and in a Multibranched Model of the Human Systemic Arterial Tree. *Circ Res*, 46, 363-372.
- Ogawa D., Yoshizawa M., Tanaka A., Abe K., Olegario P., Motomura T., Okubo H., Oda T., Okahisa T., Igo S. R. & Nose Y. 2006. Indirect Flow Rate Estimation of the Nedo Pi Gyro Pump for Chronic Bvad Experiments. *ASAIO J*, 52, 266-271.
- Ohuchi K., Kikugawa D., Takahashi K., Uemura M., Nakamura M., Murakami T., Sakamoto T. & Takatani S. 2004. Control Strategy for Rotary Blood Pumps. *Artificial Organs*, 28, 717-727.
- Olansen J. B., Clark J. W., Khoury D., Ghorbel F. & Bidani A. 2000. A Closed-Loop Model of the Canina Cardiovascular System That Includes Ventricular Interaction. *Computer and Biomedical Research*, 33, 260-295.
- Olegario P. S., Yoshizawa M., Tanaka A., Abe K., Takeda H., Yambe T. & Nitta S.-i. 2003. Outflow Control for Avoiding Atrial Suction in a Continuous Flow Total Artificial Heart. *Artificial Organs*, 27, 92-98.
- Olufsen M. S. 1999. Structured Tree Outflow Condition for Blood Flow in Larger Systemic Arteries. *Am J Physiol*, 276, H257-H268.
- Oshikawa M., Araki K., Endo G., Anai H. & Sato M. 2000. Sensorless Controlling Method for a Continuous Flow Left Ventricular Assist Device. *Artificial Organs*, 24, 600-605.
- Ottesen J. T. & Danielsen M. 2003. Modelling Ventricular Contraction with Heart Rate Changes. *Journal of Theoretical Biology*, 222, 337-346.
- Pekkan K., Frakes D., de Zelicourt D., Lucas C. W., Parks W. J. & Yoganathan A. P. 2005. Coupling Pediatric Ventricle Assist Devices to the Fontan Circulation: Simulation with a Lumped-Parameter Model. *ASAIO Journal*, 51, 618-628.
- Pennati G., Bellotti M. & Fumerco R. 1997a. Mathematical Modelling of the Human Foetal Cardiovascular System Based on Doppler Ultrasound Data. *Medical Engineering & Physics*, 19, 327-335.
- Pennati G., Migliavacca F., Dubini G., Pietrabissa R. & de Leval M. R. 1997b. A Mathematical Model of Circulation in the Presence of the Bidirectional

- Cavopulmonary Anastomosis in Children with a Univentricular Heart. *Medical Engineering & Physics*, 19, 223-234.
- Perloff J. K. 2000. *Physical Examination of the Heart and Circulation*, W.B. Saunders Company.
- Peterson K., Ozawa E. T., Pantalos G. M. & Sharp M. K. 2002. Numerical Simulation of the Influence of Gravity and Posture on Cardiac Performance. *Ann Biomed Eng*, 30, 247-259.
- Pieske B. 2004. Reverse Remodeling in Heart Failure--Fact or Fiction? *European Heart Journal Supplements*, 6(Supplement D), D66-D78.
- Pontrelli G. 2004. A Multiscale Approach for Modelling Wave Propagation in an Arterial Segment. *Comput Methods Biomech Biomed Engin*, 7, 79-89.
- Portner R., Nagel-Heyer S., Goepfert C., Adamietz P. & Meenen N. M. 2005. Bioreactor Design for Tissue Engineering. *J Biosci Bioeng*, 100, 235-245.
- Potapov E. V., Loebe M., Nasser B. A., Sinawski H., Koster A., Kuppe H., Noon G. P., DeBakey M. E. & Hetzer R. 2000. Pulsatile Flow in Patients with a Novel Nonpulsatile Implantable Ventricular Assist Device. *Circulation*, 102(Suppl III), III-183--III-187.
- Power H. M. 1979. *Models of Electrical and Mechanical Activity in the Heart*.
- Qian K. X. 1996. Pulsatile Impeller Heart: A Viable Alternative to a Problematic Diaphragm Heart. *Med Eng Phys*, 18, 57-66.
- Qian K. X., Zeng P., Ru W. M., Yuan H. Y., Feng Z. G. & Li I. 2000. How to Produce a Pulsatile Flow with Low Haemolysis? *J Med Eng Technol*, 24, 227-229.
- Quarteroni A. 2001. Modeling the Cardiovascular System---a Mathematical Adventure: Part I & II. *SIAM News*, 34, 1-3.
- Quick C. M., Berger D. S. & Noordergraaf A. 1998. Apparent Arterial Compliance. *Am J Physiol*, 274, H1393-H1403.
- Quick C. M., Berger D. S., Stewart R. H., Laine G. A., Hartley C. J. & Noordergraaf A. 2006. Resolving the Hemodynamic Inverse Problem. *IEEE Trans Biomed Eng*, 53, 361-368.
- Reul H. M. & Akdis M. 2000. Blood Pumps for Circulation Support. *Perfusion*, 15, 295-311.
- Reymond P., Merenda F., Perren F., Rufenacht D. & Stergiopoulos N. 2009. Validation of a One-Dimensional Model of the Systemic Arterial Tree. *Am J Physiol Heart Circ Physiol*, 297, H208-H222.
- Roditi G. 2004. *RE: Mri Measurement of Cardiac Motion*. Type to Korakianitis T. & Yubing S.
- Rose W. C. & Shoukas A. A. 1993. Two-Port Analysis of Systemic Venous and Arterial Impedances. *Am J Physiol*, 265, H1577-H1587.
- Saito I., Chinzei T., Abe Y., Ishimaru M., Shuichi M. O., Ono T., Isoyama T., Iwasaki K., Kouno A., Baba A., Ozeki T., Takiura K., Tohyama T., Nakagawa H. & Imachi K. 1999. Progress in the Control System of the Undulation Pump Total Artificial Heart. *Artificial Organs*, 27, 27-33.

- Saito S., Westaby S., Piggot D., Dudnikov S., Robson D., Catarino~Pedro A., Clelland C. & Nojiri C. 2002. End-Organ Function During Chronic Nonpulsatile Circulation. *The Annals of Thoracic Surgery*, 74, 1080-1085.
- Santamore W. P. & Burkhoff D. 1991. Hemodynamic Consequences of Ventricular Interaction as Assessed by Model Analysis. *American Journal of Physiology(Heart Circ. Physiol.)*, 260, H146-H157.
- Santamore W. P., Shaffer T. & Papa L. 1990. Theoretical Model of Ventricular Interdependence: Pericardial Effects. *Am J Physiol*, 259, H181-H189.
- Schampaert S., Rutten M. C., van T. Veer M., van Nunen L. X., Tonino P. A., Pijls N. H. & van de Vosse F. N. 2013a. Modeling the Interaction between the Intra-Aortic Balloon Pump and the Cardiovascular System: The Effect of Timing. *ASAIO J*, 59, 30-36.
- Schampaert S., van T. Veer M., Rutten M. C., van Tuijl S., de Hart J., van de Vosse F. N. & Pijls N. H. 2013b. Autoregulation of Coronary Blood Flow in the Isolated Beating Pig Heart. *Artif Organs*, (Preprint).
- Schampaert S., van T. Veer M., van de Vosse F. N., Pijls N. H., de Mol B. A. & Rutten M. C. 2011. In Vitro Comparison of Support Capabilities of Intra-Aortic Balloon Pump and Impella 2.5 Left Percutaneous. *Artif Organs*, 35, 893-901.
- Segers P., Rietzschel E. R., De Buyzere M. L., Stergiopoulos N., Westerhof N., Van Bortel L. M., Gillebert T. & Verdonck P. R. 2008. Three- and Four-Element Windkessel Models: Assessment of Their Fitting Performance in a Large Cohort of Healthy Middle-Aged Individuals. *Proc Inst Mech Eng [H]*, 222, 417-428.
- Segers P. & Verdonck P. 2000. Role of Tapering in Aortic Wave Reflection: Hydraulic and Mathematical Model Study. *J Biomech*, 33, 299-306.
- Sezai A., Shiono M., Orime Y., Nakata K.-u., Hata M., Iida M., Kashiwazaki S., Kinoshita J., Nemoto M., Koujima T., Furuichi M., Eda K., Hirose H., Yoshino T., Saitoh A., Tanguchi Y. & Sezai Y. 1999. Major Organ Function under Mechanical Support: Comparative Studies of Pulsatile and Nonpulsatile Circulation. *Artificial Organs*, 23, 280-285.
- Sharp M. K. & Dharmalingam R. K. 1999. Development of a Hydraulic Model of the Human Systemic Circulation. *ASAIO Journal*, 45, 334-338.
- Sharp M. K., Pantalos G. M., Minich L., Tani L. Y., McGough E. C. & Hawkins J. A. 2000. Aortic Input Impedance in Infants and Children. *J Appl Physiol*, 88, 2227-2239.
- Sheng C., Sarwal S. N., Watts K. C. & Marble A. E. 1995. Computational Simulation of Blood Flow in Human Systemic Circulation Incorporating an External Force Field. *Med Biol Eng Comput*, 33, 8-17.
- Shepard R., Simpson D. C. & Sharp J. 1966. Energy Equivalent Pressure. *Arch Surg*, 93, 730-740.
- Sherwin S. J., V. F., J. P. & K. P. 2003. One-Dimensional Modelling of a Vascular Network in Space-Time Variables. *Journal of Engineering Mathematics*, 47, 217-250.

- Shi Y. 2008. Numerical Simulation of Global Hydro-Dynamics in a Pulsatile Bioreactor for Cardiovascular Tissue Engineering. *J Biomech*, 41, 953-959.
- Shi Y., Brown A. G., Lawford P. V., Arndt A., Nuesser P. & Hose D. R. 2011a. Computational Modelling and Evaluation of Cardiovascular Response under Pulsatile Impeller Pump Support. *Interface Focus*, 1, 320-337.
- Shi Y. & Hose R. 2009. *Cellml Implementation of a Group of Lumped-Parameter Cardiovascular Models*. [Online]. Available: http://models.cellml.org/cardiovascular_circulation.
- Shi Y. & Korakianitis T. 2006. Numerical Simulation of Cardiovascular Dynamics with Left Heart Failure and in-Series Pulsatile Ventricular Assist Device. *Artif Organs*, 30, 929-948.
- Shi Y., Korakianitis T. & Bowles C. 2007. Numerical Simulation of Cardiovascular Dynamics with Different Types of Vad Assistance. *J Biomech*, 40, 2919-2933.
- Shi Y., Lawford P. & Hose R. 2011b. Review of Zero-D and 1-D Models of Blood Flow in the Cardiovascular System. *Biomed Eng Online*, 10, 33.
- Shi Y., Lawford P. V. & Hose D. R. 2010. Numerical Modeling of Hemodynamics with Pulsatile Impeller Pump Support. *Ann Biomed Eng*, 38, 2621-2634.
- Shi Y., Shi Y. & Korakianitis T. 2011c. Physiological Control of an in-Series Connected Pulsatile Vad: Numerical Simulation Study. *Comput Methods Biomech Biomed Engin*, 14, 995-1007.
- Shi Y., Yeo T. J. & Zhao Y. 2004. Numerical Simulation of a Systemic Flow Test Rig. *ASAIO J*, 50, 54-64.
- Shi Y., Zhao Y., Yeo J. H. & Hwang N. H. C. 2003. Numerical Simulation of Opening Process in a Bileaflet Mechanical Heart Valve under Pulsatile Flow Condition. *Journal of Heart Valve Disease*, 12, 245-256.
- Simon M. A., Kormos R. L., Murali S., Nair P., Heffernan M., Gorcsan J., Winowich S. & McNamara D. M. 2005. Myocardial Recovery Using Ventricular Assist Device: Prevalence, Clinical Characteristics, and Outcomes. *Circulation*, 112(Suppl I), I-32--I-36.
- Singh H., Ang E. S., Lim T. T. & Hutmacher D. W. 2007. Flow Modeling in a Novel Non-Perfusion Conical Bioreactor. *Biotechnol Bioeng*, 97, 1291-1299.
- Slinker B. K., Chagas A. C. & Glantz S. A. 1987. Chronic Pressure Overload Hypertrophy Decreases Direct Ventricular Interaction. *Am J Physiol*, 253, H347-H357.
- Slinker B. K. & Glantz S. A. 1986. End-Systolic and End-Diastolic Ventricular Interaction. *Am J Physiol*, 251, H1062-H1075.
- Smith N. P., Dickerson D. P., Crampin E. J. & Hunter P. J. 2004. Multiscale Computational Modelling of the Heart. *Acta Numerica*, 13, 371-431.
- Smith N. P., Pullan A. J. & Hunter P. J. 2002. An Anatomically Based Model of Transient Coronary Blood Flow in the Heart. *SIAM Journal on Applied mathematics*, 62, 990-1018.
- Snyder M. F. & Rideout V. C. 1969. Computer Simulation Studies of the Venous Circulation. *IEEE Trans Biomed Eng*, 16, 325-334.

- Sodian R., Lemke T., Fritsche C., Hoerstrup S. P., Fu P., Potapov E. V., Hausmann H. & Hetzer R. 2002. Tissue-Engineering Bioreactors: A New Combined Cell-Seeding and Perfusion System for Vascular Tissue Engineering. *Tissue Eng*, 8, 863-870.
- Sodian R., Lemke T., Loebe M., Hoerstrup S. P., Potapov E. V., Hausmann H., Meyer R. & Hetzer R. 2001. New Pulsatile Bioreactor for Fabrication of Tissue-Engineered Patches. *J Biomed Mater Res*, 58, 401-405.
- Sohn D.-W., Chai I.-H., Lee D.-J., Kim H.-C., Kim H.-S., Oh B. H., Lee M.-M., Park Y.-B., Choi Y.-S., Seo J.-D. & Lee Y.-W. 1997. Assessment of Mitral Annulus Velocity by Doppler Tissue Imaging in the Evaluation of Left Ventricular Diastolic Function. *Journal for American College of Cardiology*, 30, 474-480.
- Spaan J. A., Breuls N. P. & Laird J. D. 1981. Diastolic-Systolic Coronary Flow Differences Are Caused by Intramyocardial Pump Action in the Anesthetized Dog. *Circ Res*, 49, 584-593.
- Stergiopoulos N., Meister J. J. & Westerhof N. 1995. Evaluation of Methods for Estimation of Total Arterial Compliance. *Am J Physiol*, 268, H1540-H1548.
- Stergiopoulos N., Westerhof B. E. & Westerhof N. 1998. Physical Basis of Pressure Transfer from Periphery to Aorta: A Model-Based Study. *Am J Physiol*, 274, H1386-H1392.
- Stergiopoulos N., Westerhof B. E. & Westerhof N. 1999. Total Arterial Inertance as the Fourth Element of the Windkessel Model. *Am J Physiol*, 276, H81-H88.
- Stevenson L. W. & Rose E. A. 2003. Left Ventricular Assist Devices: Bridges to Transplantation, Recovery, and Destination for Whom? *Circulation*, 108, 3059-3063.
- Suga H., Sagawa K. & Shoukas A., A. 1973. Load Independence of the Instantaneous Pressure-Volume Ratio of the Canine Left Ventricle and Effects of Epinephrine and Heart Rate on the Ratio. *Circulation Research*, XXXII, 314-322.
- Sun Y., Beshara M., Lucariello R. J. & Chiaramida-Salvatore A. 1997. A Comprehensive Model for Right-Left Heart Interaction under the Influence of Pericardium and Baroreflex. *American Journal of Physiology(Heart Circ. Physiol.)*, 272, H1499-H1515.
- Sun Y. H., Anderson T. J., Parker K. H. & Tyberg J. V. 2000. Wave-Intensity Analysis: A New Approach to Coronary Hemodynamics. *J Appl Physiol*, 89, 1636-1644.
- Swalen M. J. & Khir A. W. 2009. Resolving the Time Lag between Pressure and Flow for the Determination of Local Wave Speed in Elastic Tubes and Arteries. *J Biomech*, 42, 1574-1577.
- Takatani S. 2001. Can Rotary Blood Pumps Replace Pulsatile Devices? *Artif Organs*, 25, 671-674.
- Tanaka A., Yoshizawa M., Abe K., Takeda H., Yambe T. & Nitta S. 2003. In Vivo Test of Pressure Head and Flow Rate Estimation in a Continuous-Flow Artificial Heart. *Artif Organs*, 27, 99-103.
- Tasch U., Koontz J. W., Ignatoshi M. A. & Geselowitz D. B. 1990. An Adaptive Pressure Observer for the Penn State Electric Ventricular Assist Device. *IEEE Transactions on Biomedical Engineering*, 37, 374-383.

- Taylor C. A., Cheng C. P., Espinosa L. A., Tang B. T., Parker D. & Herfkens R. J. 2002. In Vivo Quantification of Blood Flow and Wall Shear Stress in the Human Abdominal Aorta During Lower Limb Exercise. *Ann Biomed Eng*, 30, 402-408.
- Taylor C. A., Hughes T. J. & Zarins C. K. 1999. Effect of Exercise on Hemodynamic Conditions in the Abdominal Aorta. *J Vasc Surg*, 29, 1077-1089.
- Taylor C. A., Kim K. J. & S. C. J. 2010. *Patient-Specific Hemodynamics of the Cardiovascular System, Us 2010/0241404 A1, United States Patent*.
- Taylor C. A., Zarins C. K. & Hughes T. J. R. 2001. *Method for Predictive Modeling for Planning Medical Interventions and Simulating Physiological Conditions, Us 6,236,878 B1, United States Patent*.
- Thomas J. D., Zhou J., Greenberg N., Bibawy G., McCarthy P., M. & van der Voort P. M. 1997. Physical and Physiological Determinants of Pulmonary Venous Flow: Numerical Analysis. *American Journal of Physiology(Heart Circ. Physiol.)*, 272, H2453-H2465.
- Timmis A. D., Nathan A. W. & Sullivan I. D. 1997. *Essential Cardiology (Third Edition)*.
- Toorop G. P., Westerhof N. & Elzinga G. 1987. Beat-to-Beat Estimation of Peripheral Resistance and Arterial Compliance During Pressure Transients. *Am J Physiol*, 252, H1275-H1283.
- Tsukiya T., Taenaka Y., Nishinaka T., Oshikawa M., Ohnishi H., Tatsumi E., Takano H., Konishi Y., Ito K. & Shimada M. 2001. Application of Indirect Flow Rate Measurement Using Motor Driving Signals to a Centrifugal Blood Pump with an Integrated Motor. *Artif Organs*, 25, 692-696.
- Tuzun E., Rutten M., Dat M., van de Vosse F., Kadipasaoglu C. & de Mol B. 2011. Continuous-Flow Cardiac Assistance: Effects on Aortic Valve Function in a Mock Loop. *J Surg Res*, 171, 443-447.
- UK National Statistics. 2013. *Health Care Personnel, Finance and Performance* [Online]. Available: <http://www.statistics.gov.uk/hub/health-social-care/health-care-system/health-care-personnel-finance-and-performance>.
- Undar A. 2003. Fundamentals of Pulsatile Versus Nonpulsatile Flow During Chronic Support. *ASAIO Journal*, 49, 139-140.
- Undar A. 2004. Myths and Truths of Pulsatile and Nonpulsatile Perfusion During Acute and Chronic Cardiac Support. *Artificial Organs*, 28, 439-443.
- Undar A., Frazier O. H. & Fraser C. D., Jr. 1999. Defining Pulsatile Perfusion: Quantification in Terms of Energy Equivalent Pressure. *Artif Organs*, 23, 712-716.
- Undar A., Lodge A. J., Daggett C. W., Runge T. M., Ungerleider R. M. & Calhoun J. H. 1998. The Type of Aortic Cannula and Membrane Oxygenator Affect the Pulsatile Waveform Morphology Produced by a Neonate-Infant Cardiopulmonary Bypass System in Vivo. *Artif Organs*, 22, 681-686.
- Ursino M. 1991. A Mathematical Model of Overall Cerebral Blood Flow Regulation in the Rat. *IEEE Transactions on Biomedical Engineering*, 38, 795-807.

- Ursino M. 1998. Interaction between Carotid Baroregulation and the Pulsating Heart: A Mathematical Model. *American Journal of Physiology(Heart Circ. Physiol.)*, 275, H1733-H1747.
- Ursino M. 1999. A Mathematical Model of the Carotid Baroregulation in Pulsating Conditions. *IEEE Transactions on Biomedical Engineering*, 46, 382-392.
- Ursino M., Fiorenzi A. & Belardinelli E. 1996. The Role of Pressure Pulsatility in the Carotid Baroreflex Control: A Computer Simulation Study. *Computers in Biology and Medicine*, 26, 297-314.
- Ursino M. & Giulioni M. 2003. Quantitive Assessment of Cerebral Autoregulation from Transcranial Doppler Pulsatility: A Computer Simulation Study. *Medical Engineering & Physics*, 25, 655-666.
- Ursino M., Iezzi M. & Stocchetti N. 1995. Intracranial Pressure Dynamics in Patients with Acute Brain Damage: A Critical Analysis with the Aid of a Mathematical Model. *IEEE Transactions on Biomedical Engineering*, 42, 529-540.
- Ursino M. & Magosso E. 2000a. Acute Cardiovascular Response to Isocapnic Hypoxia. I. A Mathematical Model. *American Journal of Physiology(Heart Circ. Physiol.)*, 279, H149-H156.
- Ursino M. & Magosso E. 2000b. Acute Cardiovascular Response to Isocapnic Hypoxia. Ii. Model Validation. *American Journal of Physiology(Heart Circ. Physiol.)*, 279, H166-H175.
- Ursino M. & Magosso E. 2003. Role of Short-Term Cardiovascular Regulation in Heart Period Variability: A Model Study. *American Journal of Physiology(Heart Circ. Physiol.)*, 284, H1479-H1493.
- Ursino M., Minassian A. T., Lodi C. A. & Beydon L. 2000. Cerebral Hemodynamics During Arterial and Co2 Pressure Changes: In Vivo Prediction by a Mathematical Model. *American Journal of Physiology(Heart Circ. Physiol.)*, 279, H2439-H2455.
- van de Vosse F. N. 2003. Mathematical Modelling of the Cardiovascular System. *Journal of Engineering Mathematics*, 47, 175-183.
- van de Vosse F. N. & Stergiopoulos N. 2011. Pulse Wave Propagation in the Arterial Tree. *Annu. Rev. Fluid Mech.*, 43, 467-499.
- van T. Veer M., Geven M. C., Rutten M. C., van der Horst A., Aarnoudse W. H., Pijls N. H. & van de Vosse F. N. 2009. Continuous Infusion Thermodilution for Assessment of Coronary Flow: Theoretical Background and in Vitro Validation. *Med Eng Phys*, 31, 688-694.
- Vandenbergh S., Segers P., Antaki J. F., Meyns B. & Verdonck P. R. 2005. Hemodynamic Modes of Ventricular Assist with a Rotary Blood Pump: Continuous, Pulsatile, and Failure. *ASAIO J*, 51, 711-718.
- Vandenbergh S., Segers P., Meyns B. & Verdonck P. 2003. Unloading Effect of a Rotary Blood Pump Assesed by Mathematical Modeling. *Artificial Organs*, 27, 1094-1101.
- Vandenbergh S., Segers P., Meyns B. & Verdonck P. R. 2002. Effect of Rotary Blood Pump Failure on Left Ventricular Energetics Assessed by Mathematical Modeling. *Artificial Organs*, 26, 1032-1039.

- Vandenberghe S., Segers P., Steendijk P., Meyns B., Dion R. A., Antaki J. F. & Verdonck P. 2006. Modeling Ventricular Function During Cardiac Assist: Does Time-Varying Elastance Work? *ASAIO J*, 52, 4-8.
- Verberne H. J., Meuwissen M., Chamuleau S. A., Verhoeff B. J., van Eck-Smit B. L., Spaan J. A., Piek J. J. & Siebes M. 2007. Effect of Simultaneous Intracoronary Guidewires on the Predictive Accuracy of Functional Parameters of Coronary Lesion Severity. *Am J Physiol Heart Circ Physiol*, 292, H2349-H2355.
- Vollkron M., Shima H., Huber L. & Wieselthaler G. 2002. Interaction of the Cardiovascular System with an Implanted Rotary Assist Device: Simulation Study with a Refined Computer Model. *Artificial Organs*, 26, 349-359.
- Wan J., Steele B., Spicer S. A., Strohsand S., Feijoo G. R., Hughes T. J. & Taylor C. A. 2002. A One-Dimensional Finite Element Method for Simulation-Based Medical Planning for Cardiovascular Disease. *Comput Methods Biomech Biomed Engin*, 5, 195-206.
- Wang J. J. & Parker K. H. 2004. Wave Propagation in a Model of the Arterial Circulation. *J Biomech*, 37, 457-470.
- Watanabe H., Sugiura S., Kafuku H. & Hisada T. 2004. Multiphysics Simulation of Left Ventricular Filling Dynamics Using Fluid-Structure Interaction Finite Element Method. *Biophys J*, 87, 2074-2085.
- Waters T., Allaire P., Tao G., Adams M., Bearson G., Wei N., Hilton E., Baloh M., Olsen D. & Khanwilkar P. 1999. Motor Feedback Physiological Control for a Continuous Flow Ventricular Assist Device. *Artificial Organs*, 23, 480-486.
- Werner J., Bohringer D. & Hexamer M. 2002. Simulation and Prediction of Cardiotherapeutical Phenomena from a Pulsatile Model Coupled to the Guyton Circulation Model. *IEEE Transaction on Biomedical Engineering*, 49, 430-439.
- Wesseling K. H., Jansen J. R., Settels J. J. & Schreuder J. J. 1993. Computation of Aortic Flow from Pressure in Humans Using a Nonlinear, Three-Element Model. *J Appl Physiol*, 74, 2566-2573.
- West J. B. 1990. *Best and Taylor's Physiological Basis of Medical Practice (Twelfth Edition)*.
- Westerhof N., Bosman F., De Vries C. J. & Noordergraaf A. 1969. Analog Studies of the Human Systemic Arterial Tree. *J Biomech*, 2, 121-143.
- Westerhof N., Elzinga G. & Sipkema P. 1971. An Artificial Arterial System for Pumping Hearts. *J Appl Physiol*, 31, 776-781.
- Westerhof N., Lankhaar J. W. & Westerhof B. E. 2009. The Arterial Windkessel. *Med Biol Eng Comput*, 47, 131-141.
- Williams K. A., Saini S. & Wick T. M. 2002. Computational Fluid Dynamics Modeling of Steady-State Momentum and Mass Transport in a Bioreactor for Cartilage Tissue Engineering. *Biotechnol Prog*, 18, 951-963.
- Womersley J. R. 1955. Method for the Calculation of Velocity, Rate of Flow and Viscous Drag in Arteries When the Pressure Gradient Is Known. *J Physiol*, 127, 553-563.
- Womersley J. R. 1957. Oscillatory Flow in Arteries: The Constrained Elastic Tube as a Model of Arterial Flow and Pulse Transmission. *Phys Med Biol*, 2, 178-187.

- Wu Y., Allaire P., Tao G., Wood H., Olsen D. & Tribble C. 2003. An Advanced Physiological Controller Design for a Left Ventricular Assist Device to Prevent Left Ventricular Collapse. *Artificial Organs*, 27, 926-930.
- Yacoub M. H., Kilner P. J., Birks E. J. & Misfeldn M. 1996. The Aortic Outflow and Root: A Tale of Dynamism and Crosstalk. *Annals Thoracic Surgury*, 68, S37-S43.
- Yaku H., Goto Y., Futaki S., Ohgoshi Y., Kawaguchi O. & Sugu H. 1991. Multicompartment Model for Mechanics and Energetics of Fibrillating Ventricle. *American Journal of Physiology(Heart Circ. Physiol.)*, 260, H292-H299.
- Yoshigi M. & Keller B. B. 1997. Characterization of Embryonic Aortic Impedance with Lumped Parameter Models. *Am J Physiol*, 273, H19-H27.
- Yoshizawa M., Takeda H., Watanabe T., Miura M., Yambe T., Katahira Y. & Nitta S.-i. 1992. An Automatic Control Algorithm for the Optimal Driving of the Ventricular-Assist Device. *IEEE Transactions on Biomedical Engineering*, 39, 243-251.
- Zacek M. & Krause E. 1996. Numerical Simulation of the Blood Flow in the Human Cardiovascular System. *J Biomech*, 29, 13-20.
- Zeng Y., Lee T. S., Yu P., Roy P. & Low H. T. 2006. Mass Transport and Shear Stress in a Microchannel Bioreactor: Numerical Simulation and Dynamic Similarity. *J Biomech Eng*, 128, 185-193.
- Zervides C., Narracott A. J., Lawford P. V. & Hose D. R. 2008. The Role of Venous Valves in Pressure Shielding. *Biomed Eng Online*, 7, 8.